CAMPYLOBACTER JEJUNI KDO8PS: A METAL-DEPENDENT KDO8PS

CHARACTERIZATION OF THE METAL-DEPENDENT KDO8P SYNTHASE FROM CAMPYLOBACTER JEJUNI AND INHIBITION BY KDO8P OXIME, A NOVEL SLOW-BINDING INHIBITOR

By

Simanga R. Gama, B. Sc.

A Thesis

Submitted to the School of Graduate Studies

in Partial Fulfillment of the Requirements

for the Degree

Doctor of Philosophy

McMaster University

DOCTOR OF PHILOSOPHY
(Chemical Biology Graduate Program)

McMaster University
Hamilton, Ontario

TITLE: Characterization of the metal-dependent KDO8P Synthase from *Campylobacter jejuni* and inhibition by KDO8P oxime, a novel slow-binding inhibitor

AUTHOR: Simanga R. Gama, B.Sc. (Hons.)

SUPERVISOR: Dr. Paul J. Berti

NUMBER OF PAGES: xvii, 218

Lay Abstract

The relentless increase in global antibiotic resistance is, regrettably, not matched with an increase in new effective antibiotics. New antimicrobial drug discovery strategies are desperately needed. Enzymes are key targets for drug design because they catalyze the majority of biological processes. In this project we sought to study and inhibit the activity of KDO8P synthase (KDO8PS) from *Campylobacter jejuni*, a common cause of food poisoning. KDO8P synthase is a critical enzyme involved in the lipopolysaccharide (LPS) biosynthesis in Gram-negative bacteria. The LPS acts as a permeability barrier and is crucial for bacterial pathogenicity/virulence. We found that *C. jejuni* KDO8PS is potently inhibited by KDO8P oxime, a novel inhibitor of KDO8PS. This inhibitor presents a unique opportunity to study these enzymes and a platform from which antibiotics against Gram-negative bacteria can be developed.

Abstract

Antibiotic resistance is a worldwide threat to human health yet fewer new antibiotics are being approved. New antimicrobial drugs are urgently required. 3-Deoxy-D-*manno*-2-octulosonate-8-phosphate synthase (KDO8PS) is a target for antimicrobial drug design. KDO8PS catalyzes the condensation of D-arabinose-5 phosphate (A5P) with phosphoenolpyruvate (PEP) to produce KDO8P. KDO8PS catalyzes the first committed step in the lipopolysaccharides (LPS) biosynthesis pathway in Gram-negative bacteria and is critical for bacterial pathogenicity/virulence. We have characterized KDO8PS from *Campylobacter jejuni* (cjKDO8PS), a new metal-dependent KDO8P synthase (KDO8PS). cjKDO8PS is a tetramer in solution and optimally active at pH 7.5 and 60 °C. We have kinetically established that cjKDO8PS follows a rapid equilibrium sequential ordered ter ter kinetic mechanism, where Mn^{2+} binds first, followed by PEP, then A5P. Pi dissociates first, before KDO8P, then Mn^{2+}. cjKDO8PS was inhibited by KDO8P oxime, a novel slow tight-binding inhibitor. KDO8P oxime is a competitive inhibitor with respect to PEP and A5P, but uncompetitive with respect to Mn^{2+}, with $K_i = 10 \pm 1$ μM and an ultimate $K_i^* = 0.28 \pm 0.10$ μM. KDO8P oxime has a residence time (t_R) of 5 days on the enzyme, a parameter that is highly correlated to *in vivo* efficacy. Crystallization conditions for the cjKDO8PS·Mn^{2+}·KDO8P oxime complex have been found and can be optimized to obtain a crystal structure that shows how KDO8P oxime interacts with the active sites.

Acknowledgements

I would like to take this opportunity to thank my supervisor, Dr. Paul Berti, for affording me this great opportunity to conduct research in his lab. Your vast knowledge, creativity, guidance, support and patience have helped me to achieve my dream. Thank you.

I would also like to thank my supervisory committee, Dr. Russell Bishop and Dr. Fred Capretta, for their support and guidance throughout my graduate career.

I would also like to express my sincere gratitude to my family for being with me in every step of the way. Thank you for your support and understanding.

I would like to thank all former and current Berti lab members, Maren Heimhalt, Naresh Balachandran, Vincent Azhikannickal, Rasa Bakhtiari, Lisset Llano, Vladimir Popović, Fred To, Jennifer Wild, Kelvin Tsao, Peter Kim, Jenny Zheng, Funing Lin, Shivneet Gill, Jacob Pierscianowski, Elizabeth Curiel-Tejeda, Hanna Zhao, Meiko Peng, Bryanna Tibensky, Dhruv Patel and Shahbano Syed. It has been an honour working with you.

I would like to thank the collaborators that have contributed to this project. Dr. José Carlos Bozelli Junior and Dr. Richard Epand (Laboratory of Membrane Biophysics, McMaster University) for allowing us to use your ITC instrument and for your help and advice with the ITC experiments. Dr. Murray Junop (Western University) for your help with crystallization. Dr. Alba Guarné (McMaster

University) for allowing us to use your crystallization facility and additive screens.

I would like to also thank Dr. Naresh Balachandran who produced the plasmids for *N*-terminally His-tagged and wild type cjKDO8PS and Dr. Martin Young (National Research Council of Canada) for the generous gift of the *C*-terminally tagged cjKDO8PS. Maren Heimhalt who produced phosphoenolpyruvate synthase used to synthesize [1-^{14}C]PEP. I would like thank Dr. Hilary Jenkins for her help with NMR experiments for KDO8P oxime.

Finally, I would like to thank Tammy Feher, Administrative Coordinator in the Chemical Biology Graduate Program, for your assistance.

Table of Contents

List of Figures

List of Tables

List of Abbreviations

A5P	arabinose-5-phosphate
[^{33}P]A5P	^{33}P-radiolabelled A5P
ATP	adenosine triphosphate
[γ-^{33}P]ATP	ATP radiolabelled with ^{33}P at the terminal (γ) phosphate group
BSA	Bovine serum albumin
BTP	Bis-tris propane
^{13}C-NMR	Carbon-13 nuclear magnetic resonance
CAPS	*N*-cyclohexyl-3-aminopropanesulfonic acid
CMP-KDO	cytidine monophosphate-3-deoxy-D-*manno*-oct-2-ulosonic acid
*cj*KDO8PS	*Campylobacter jejuni* KDO8P synthase
*cj*KDO8PS$_{H6}$	*N*-terminally His$_6$-tagged *C. jejuni* KDO8P synthase
*cj*KDO8PS$_{wt}$	wild type *C. jejuni* KDO8P synthase
cpm	counts per min of radiation
COSY	homonuclear correlation spectroscopy
DAHP	3-deoxy-D- *arabino*-heptulosonate-7-phosphate
DAHPS	DAHP synthase
DAHPS(Phe)	DAHP synthase (phenylalanine-sensitive isozyme)
[1−^{14}C]DAHP oxime	^{14}C- radiolabelled DAHP oxime at carbon atom number 1
EDTA	ethylenediaminetetraacetic acid
E	free enzyme
E·I	enzyme·inhibitor complex
$[E]_0$	initial enzyme concentration
E4P	erythrose-4-phosphate
ESI-MS	electrospray ionization mass spectrometry
GBS	Guillain–Barré syndrome
^{1}H-NMR	proton nuclear magnetic resonance
HRMS	High resolution mass spectrometry
I	inhibitor
IPTG	isopropyl β-D-1-thiogalactopyranoside
ITC	isothermal titration calorimetry
K_M	Michaelis-Menten constant
K_d	equilibrium ligand dissociation constant
K_i	inhibition constant
K_M(1s)	Michaelis-Menten constant for single substrate enzymes
K_M(re)	Michaelis-Menten constant under rapid equilibrium assumption
K_M(ss)	Michaelis-Menten constant under steady state approximation
k_{obs}	is rate of the onset of slow-binding inhibition
k_{off}	rate constant for dissociation of inhibitor from enzyme
k_{on}	rate constant for binding of inhibitor to enzyme
K_s	equilibrium dissociation constant for substrate(s)
KDO	3-deoxy-D-*manno*-octulosonic acid

KDO8P	3-deoxy-D-*manno*-2-octulosonate 8-phosphate
[1−^{14}C]pyruvate	^{14}C- radiolabeled DAHP at carbon atom number 1
KDO8PS	KDO8P synthase
LPS	lipopolysaccharides
LB	Luria broth
ManNAc	*N*-acetylmannosamine
MES	2-(N-morpholino)ethanesulfonic acid
NeuNAc	*N*-acetylneuraminic acid
NeuB	*N*-acetylneuraminic acid synthase
NMR	nuclear magnetic resonance
^{31}P-NMR	Phosphorus-31 nuclear magnetic resonance
PEP	phosphoenolpyruvate
[1−^{14}C]PEP	^{14}C- radiolabelled DAHP at carbon atom number 1
PMSF	phenylmethylsulfonyl fluoride
ppsA	phosphoenolpyruvate synthase
[1−^{14}C]pyruvate	^{14}C- radiolabelled DAHP at carbon atom number 1
Rib5P	ribulose-5-phosphate
R5P	ribose-5-phosphate
S	substrate
SDS-PAGE	sodium dodecyl sulfate polyacrylamide-gel electrophoresis
SS_{rel}	residual sum of squares
TCEP	tris(2-carboxyethyl)phosphine
TEV	Tobacco Etch Virus
THI	tetrahedral intermediate
Tris	tris(hydroxymethyl)amino methane
UDEFT-^{13}C NMR	uniform driven equilibrium fourier transform ^{13}C-NMR

Standard amino acid nomenclature:

A	Ala	Alanine
C	Cys	Cysteine
D	Asp	Aspartic acid
E	Glu	Glutamic acid
F	Phe	Phenylalanine
G	Gly	Glycine
H	His	Histidine
I	Ile	Isoleucine
K	Lys	Lysine
L	Leu	Leucine
M	Met	Methionine
N	Asn	Asparagine
P	Pro	Proline
Q	Gln	Glutamine
R	Arg	Arginine
S	Ser	Serine
T	Thr	Threonine
V	Val	Valine
W	Trp	Tryptophan
Y	Tyr	Tyrosine

Declaration of Academic Achievement

I, Simanga Richard Gama, declare that I am the sole author of this thesis. I have obtained all the reported data except as noted below. To deduce the kinetic mechanism of *C. jejuni* KDO8PS and the mode of inhibition by KDO8P oxime with respect to manganese, my supervisor, Dr. Paul Berti, performed the data simulations using Dynafit. The recombinant vector bearing a TEV-cleavable *N*-terminal His_6 tag and the wildtype vector for KDO8PS were prepared in our lab by Dr. Naresh Balachandran. All figures used from other sources have been appropriately cited. My supervisor, Dr. Berti, and my supervisory committee members, Dr. Russell Bishop and Dr. Fred Capretta, have guided and supported me throughout this project.

1. Introduction

1.1. Overview

This dissertation reports the characterization of *Campylobacter jejuni* 3-deoxy-D-manno-2-octulosonate-8-phospahte (KDO8P) synthase, a new addition to the metal-dependent Class II KDO8P synthase (KDO8PS) family. KDO8PS is a member of the NeuB superfamily of α-carboxyketose synthases.[1,2] These enzymes have been identified as potential antimicrobial targets because they are essential for bacterial survival and are not present in mammals. We fully characterised the kinetic mechanism of *C. jejuni* KDO8PS (cjKDO8PS) with respect to the order of substrate binding. We used an oxime-based inhibitor, KDO8P oxime, as a mechanistic probe to further characterize catalysis by *C. jejuni* KDO8PS (cjKDO8PS). The oxime-based inhibitor builds the platform from which more potent inhibitors could be optimized into new antibiotics. Characterizing KDO8PS with respect to its inhibition by KDO8P oxime required that we explore its catalytic mechanism, kinetics and thermodynamic analyses of inhibitor binding to cjKDO8PS.

1.2. Antibiotic Resistance

Antibiotic resistance is a global threat to human health requiring urgent attention.[3] This relentless emergence of antimicrobial resistance has an impact on

patients' health, and on the cost of healthcare worldwide. The Centers for Disease Control and Prevention reported that in the United States alone 2 million people become infected with bacteria that are resistant to antibiotics, and at least 23,000 people die each year as a direct result of these infections.[4] The World Health Organization (WHO) states that treatment failure to third-generation cephalosporins, the antibiotics of last resort for the treatment of gonorrhea, has been confirmed in Austria, Australia, Canada, France, Japan, Norway, Slovenia, South Africa, Sweden and the United Kingdom. An estimated 106 million people are infected with gonorrhea every year,[5] and this is just information from countries where it is easy to obtain data. It could be the same or worse with other countries, especially less developed countries where data is sparse. *Klebsiella pneumonia*, a common intestinal bacterium and a major cause of hospital-acquired infections, is resistant to treatment by the last resort antibiotic, carbapenem.[3] According to WHO, this trend is spreading to all regions of the world. The emergence of the extensively drug-resistant tuberculosis (XDR-TB), which is almost completely fatal within a few weeks,[5] is of greater concern.

The rapidity of the rise of antibiotic resistance is made worse by the misuse of antibiotics. Antibiotics are among the most commonly prescribed drugs in human medicine, yet up to 50% of those prescriptions are not needed.[4] Antibiotics are also used in food-producing animals to prevent, control and treat diseases in animals.[6,7] Antibiotic treatment of livestock infections in itself is not a problem; however, increasing the growth rate of livestock by treating healthy

livestock with sub-clinical doses of antibiotics too low to treat infections leads to antibiotic resistance.

Bacterial resistance mechanisms are classified into four basic types, namely: (a) enzymatic inactivation/modification, (b) decreased uptake, (c) altered target sites and (d) 'bypass' pathways.[8] (a) A classic example is the β-lactamase cleavage of four-membered β lactam ring in penicillins and cephalosporins, rendering them inactive. (b) Some resistant bacteria prevent the antibiotic from entering the cell. For example, *Pseudomonas aeruginosa* resistant to β-lactam antibiotic imipenem lack the specific D2 porin that allows the antibiotic to enter the cell.[8] Tetracycline resistant Gram-negative bacteria bear an energy-driven transport pump encoded by *tet*(A) that accelerates drug efflux.[9] (c) Penicillin-resistant strains of *Neisseria gonorrhoeae* produce altered forms of penicillin-binding proteins (PBPs) with decreased affinity for the antibiotic.[10] For example, in methicillin-resistant *Staphylococcus aureus* (MRSA), a proline-to-leucine mutation at position 458 of the native protein PBP 2 reduced its affinity for ceftizoxime, a β-lactam antibiotic.[11] (d) The "bypass" pathway resistance mechanism involves the expression of an alternative target protein that is resistant to the antibiotic. This mechanism is evident in MRSA where an acquired gene, *mec*A, expresses alternative penicillin binding protein (PBP2a) resistant to β-lactams.[12,13]

Antibiotic-resistant bacteria, particularly the "ESKAPE" pathogens (*Enterococcus faecium*, *Staphylococcus aureus*, *Klebsiella pneumoniae*,

Acinetobacter baumannii, *Pseudomonas aeruginosa*, and *Enterobacter* species) are deadly, causing infections ranging from urinary tract infections (UTI) to life-threatening pneumonias and bloodstream infections.[14,15] Despite the ever-increasing number of multi-resistant Gram-negative strains, there are very few new antibiotic alternatives. In fact, the number of new antibiotics developed and approved declined during the 1983 – 2012 period, presumably due to reduced economic incentives and extensive regulatory requirements.[16–18] Antibiotic development is not an economically attractive investment for the pharmaceutical industry because they are used for short periods and are curative. They are therefore not as profitable as drugs for chronic diseases such as those for diabetes, cancer, asthma, etc.[16] According to the Infectious Diseases Society of America (IDSA) only 2 new antibiotics against Gram-negative bacteria were developed between 2009 and 2013 (Figure 1.1).[19] IDSA's 10 × 20 initiative is a global antibacterial drug research and development enterprise, aimed at developing 10 new antibiotics by 2020.[19] The jump in new antibiotics approval between 2013 and 2017 could be viewed as a positive response to this initiative.

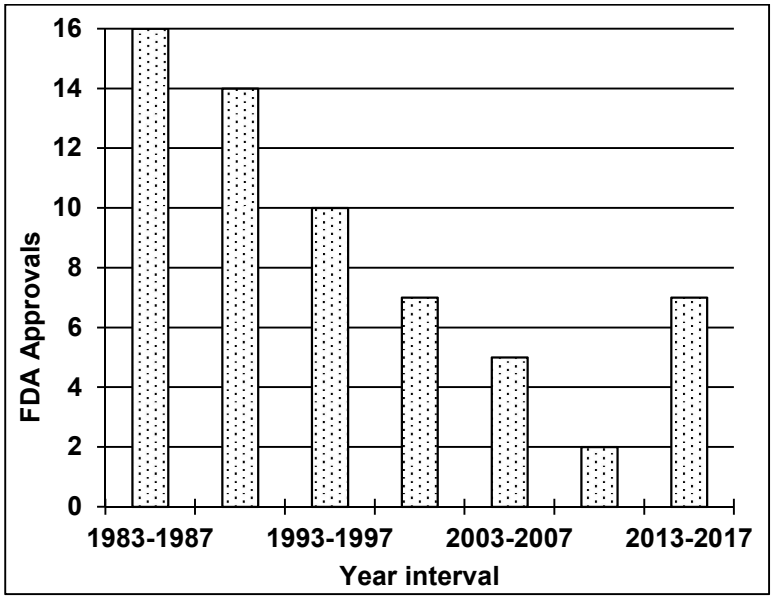

Figure 1.1. Novel antibacterial drugs approved by the FDA from 1983 to 2017.

The data from 1983 to 2012 is from reference [19], while the data between 2013 and 2017 is from the FDA' s Center for Drug Evaluation and Research (CDER) website: https://www.fda.gov/Drugs/DevelopmentApprovalProcess/DrugInnovation/default.htm and the FDA's Orange Book[20]

1.3. The Lipopolysaccharide biosynthesis

The lipopolysaccharide (LPS) is the major component of the outer leaflet of the outer membrane in Gram-negative bacteria; it is largely responsible for structural integrity of the bacteria (Figure 1.2).[21] LPS is an effective permeability barrier against large hydrophobic molecules and host cellular defensive responses.[22] The LPS plays a role in host-bacterium interactions such as adhesion, colonization and virulence. [23] An LpxC inhibitor that affect lipid A biosynthesis did not inhibit *Acinetobacter baumannii* (*A. baumannii*) growth but reduced its virulence in mice by blocking sepsis activation and by enhancing opsonophagocytic killing of the bacteria.[24] LPS is composed of Lipid A, the inner

and outer cores, and the O-antigen repeat. Lipid A is the hydrophobic component, consisting of fatty acid tails anchoring the LPS to the outer membrane of bacterial cell.[21] The inner core consists of two KDO residues and two heptose sugars connecting Lipid A to the outer core. The outer core contains variable types of sugars (heptose, galactose, glucose, etc.) and it provides the attachment site for the O-antigen repeat. The O-antigen component extends to the extracellular space and helps bacteria resist antibiotics and the complement system.[21] It also defines the antigenic specificity in an organism. The Lipid A-KDO domain is the minimal LPS component required for the growth of *Escherichia coli* in vitro.[21,25] Complete synthesis of Lipid A does not occur without the KDO domain.[26,27] A nonconditional *E. coli* K-12 suppressor strain KPM22 that lacks KDO was found to be viable, although it was susceptible to large, hydrophobic antibiotics largely due to the decreased barrier of lipid A.[22] LpxC inhibitor PF-5081090 was found to inhibit lipid A biosynthesis in *A. baumannii* resulting in significant increase in cell permeability and increased susceptibility to several antibiotics, such as rifampicin, vancomycin, azithromycin, imipenem and amikacin.[28] Inhibitors that block LPS biosynthesis have the potential to treat multidrug resistant bacterial infections since they can potentiate the entry of other co-administered drugs.

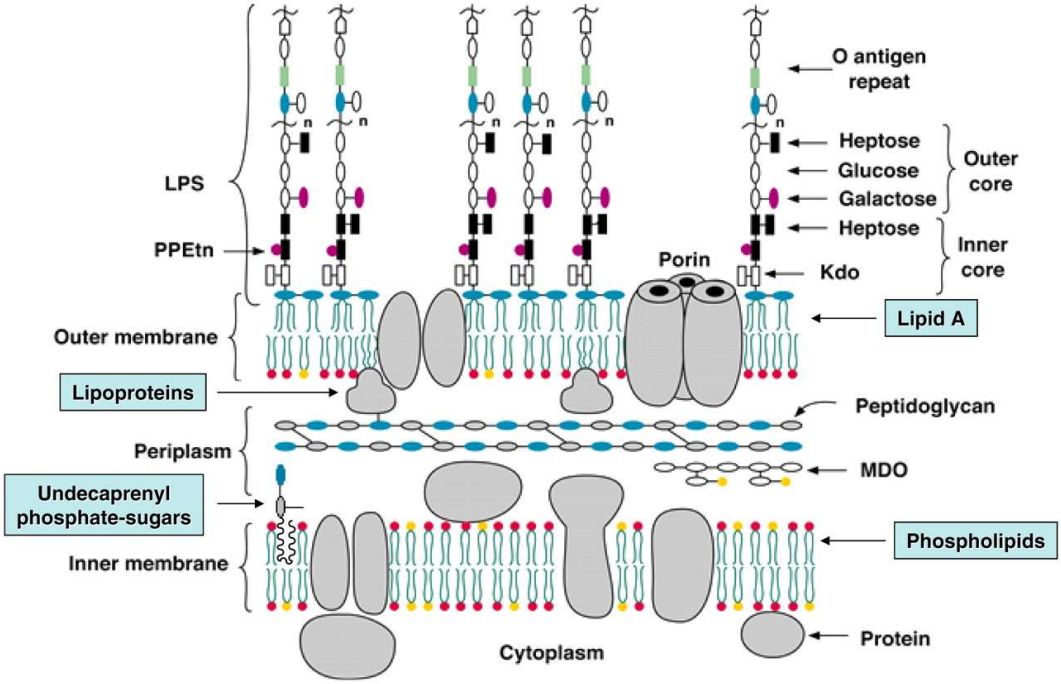

Figure 1.2. Model of the inner and outer membranes of *E. coli* K-12.

The KDO-lipid A regions of LPS are required for the growth of *E. coli* and most other Gram-negative bacteria. This figure was taken from Raetz and Whitfield.[26]

The KDO-Lipid A biosynthetic pathway (Figure 1.3) is found only in Gram-negative bacteria and some plants. For this reason, it has become a target for new antimicrobial drug development. It begins with the isomerization of D-ribulose 5-phosphate (Rib5P) into arabinose-5 phosphate (A5P), catalyzed by A5P isomerase.[29] The aldol-like condensation of A5P with phosphoenolpyruvate (PEP) is catalyzed by KDO8P synthase (KDO8PS) to produce KDO8P and an inorganic phosphate (Pi).[30] KDO8P is dephosphorylated by KDO8P phosphatase to KDO. KDO is modified to CMP-KDO, catalyzed by CMP-KDO synthase. KDO transferase uses CMP-KDO to incorporate KDO into lipid A.[31] Several

more steps leads to the Lipid A-KDO moiety linking the outer cell membrane with the extracellular portion of the LPS.

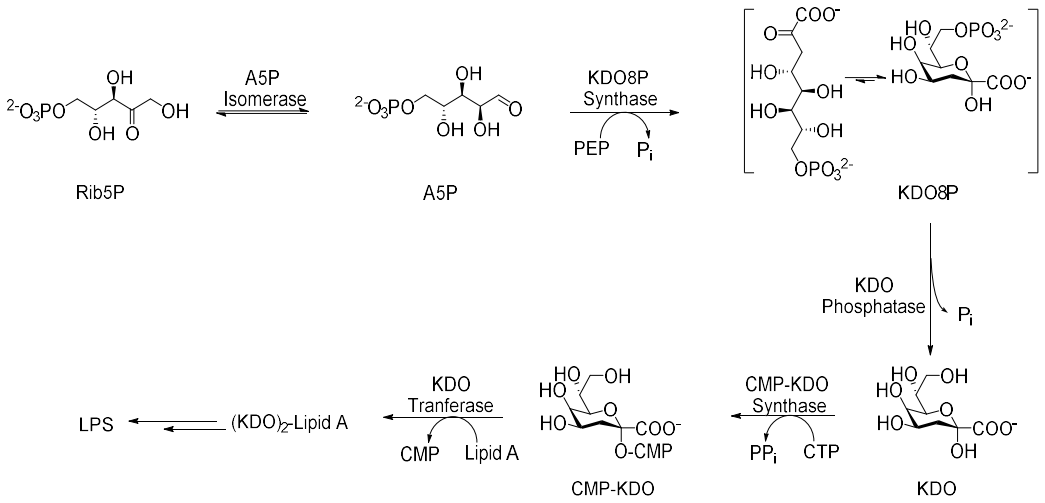

Figure 1.3. The KDO-Lipid A biosynthetic pathway.

Several inhibitors have been developed against the KDO biosynthetic pathway. A5P isomerase inhibitors include Rib5P analogues with IC_{50} values in the higher micromolar to millimolar range.[32] KDO analogues against CMP-KDO synthase have also been developed with 2-deoxy-β-KDO having a K_i = 3.9 μM.[33] KDO analogues with peptides attached at position 8, presumed to target CMP-KDO synthase, led to inhibition of LPS synthesis and accumulation of lipid A precursor, resulting in cell growth inhibition and perturbation of outer membrane structure and function.[34]

KDO8PS is the other identified target in the Gram-negative KDO-Lipid A pathway. It is a member of the NeuB superfamily of α-carboxyketose synthases[1,2] which combine PEP and an aldose to form α-carboxyketose product (Figure 1.4).

A mutant of *Salmonella typhimurium* KDO8PS that leads to a temperature-dependent decrease in A5P affinity caused cell growth inhibition at high temperatures.[35,36] An inhibitor of KDO8PS believed to mimic the tetrahedral intermediate (Figure 1.13) has been found to inhibit Gram-negative bacterial growth.[37]

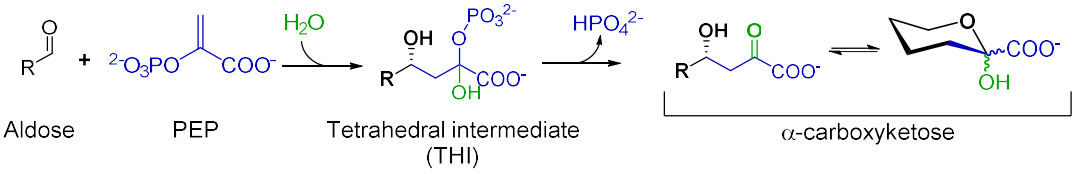

Aldose	α-Carboxyketose product	Occurrence
A5P (arabinose-5-phosphate)	KDO8P (2-keto-3-deoxy-8-phospho-D-*manno*octulosonate)	lipopolysaccharides (LPS) in all Gram-negative bacteria
E4P (erythrose-4-phosphate)	DAHP (3-deoxy-D-*arabino*-heptulosonate 7-phosphate)	shikimate pathway in all bacteria, plants, and some fungi
ManNAc (*N*-acetylmannosamine)	NeuNAc (*N*-acteylneuraminic acid)	neuro-invasive bacteria

Figure 1.4. α-Carboxyketose synthase reactions.
(top) The generic α-carboxyketose reaction uses PEP and an aldose to produce a 6- to 9-carbon sugar. (bottom) The three most important α-carboxyketose synthases' reactions. KDO8PS catalyzes the reaction of PEP with A5P to produce KDO8P. The related α-carboxyketose synthases DAHP synthase and NeuB use erythrose-4-phosphate and *N*-acetylmannosamine as the aldose substrates.

1.4. KDO8PS

1.4.1. Quaternary and crystal structures

All bacterial KDO8PSs are homotetramers with monomeric molecular weight of approximately 30 – 40 kDa.[38–41] The quaternary structure of the homotetramer is essentially a dimer-of-dimers, with a tight interface between the subunits within each dimer, and a looser interface between each dimer (Figure 1.5, top). Each monomer is composed of a TIM $(\beta/\alpha)_8$ barrel (Figure 1.5, top) with the active sites located near the dimer interface. Some examples include the well-studied metal-independent KDO8PS from *E. coli* and the metal-dependent *Aquifex aeolicus* KDO8PS.[39] *Arabidopsis thaliana* KDO8PS, a plant KDO8PS, is a dimer in solution.[42] *A. aeolicus*, a thermophilic KDO8PS that is optimally active at 95 °C, was used to form crystal complexes where all substrates were bound at 4 °C, at which temperature the enzyme is not active.[40] In that study, PEP was bound to all four active sites while A5P was bound in only two, leading to the half-of-sites reactivity hypothesis. When only PEP was bound, the extended active site loop 7 (L7) was disordered, whereas when both A5P and PEP were bound L7 was ordered and sealed off the active site from bulk solvent (Figure 1.5, bottom panel, b).[40] Residues that bind A5P's 5-phosphate group are from this loop, and presumably loop closure is triggered by A5P binding via these residues. The Arg106 sidechain is extended from one subunit to the next, and has been proposed to be involved in regulating loop closure. The *A. aeolicus* KDO8PS R106G

mutant showed that the L7 loop was disordered even when both PEP and A5P were bound, indicating the importance of this residue in L7 closure and opening.[43]

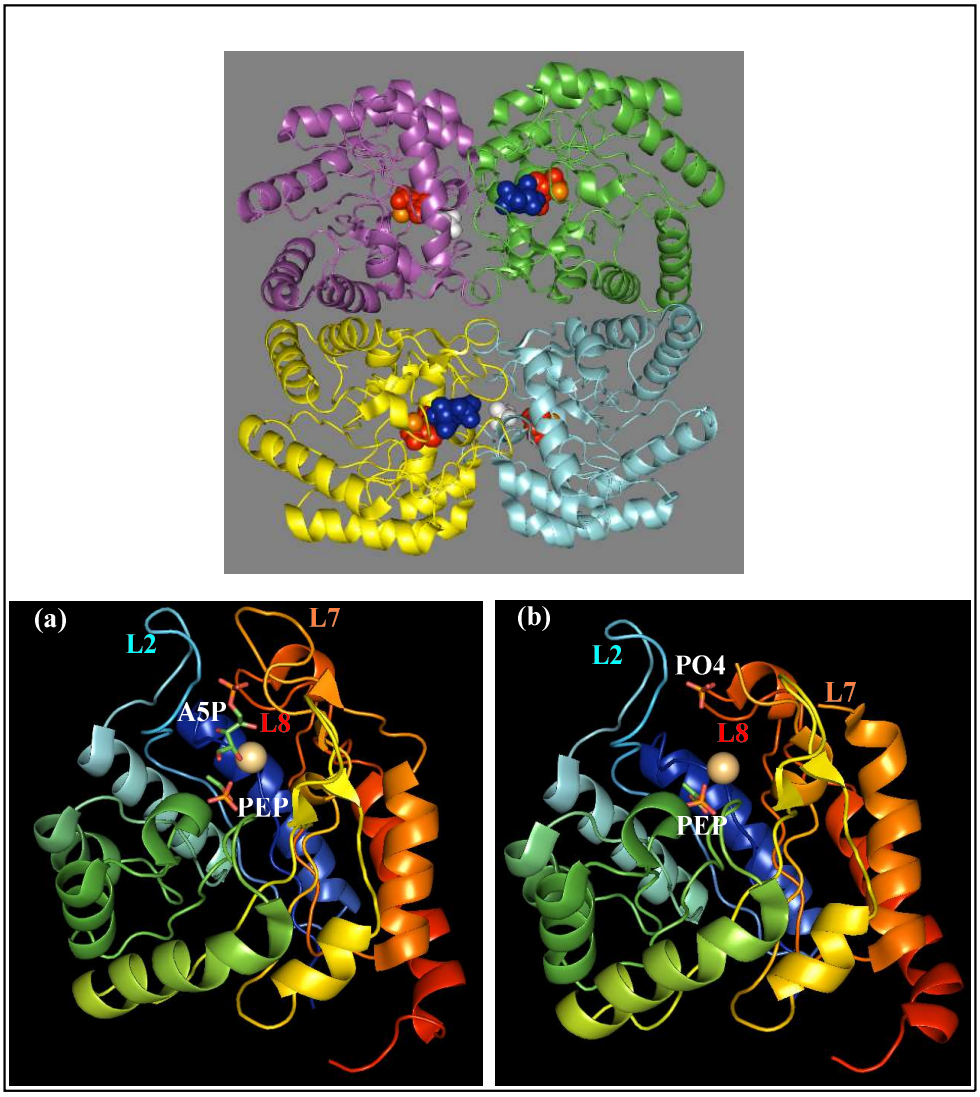

Figure 1.5. Oligomeric structure of bacterial KDO8PSs.

(top) The cartoon structure of *A. aeolicus* KDO8PS with bound PEP (red), A5P (blue), Cd^{2+} (gold) and phosphate (white). (bottom) The L7 loop was ordered when both PEP and A5P were bound in subunit A (panel a) and disordered when only PEP was bound in subunit B (panel b). The L7 (orange), L2 (cyan) and L8 (red) loops are labelled. The structure PDBID:1FWW[40] is shown.

1.4.2. Metal ion dependence

KDO8PSs are divided into two classes, based on their need for a divalent metal ion. [30,38,44] Class I KDO8PSs are metal ion independent, including KDO8PSs from *E. coli*,[30] *Neisseria meningitidis*[45] and the plant *A. thaliana*,[42] among others. These enzymes are not inactivated by metal chelators like EDTA. Class II KDO8PSs, on the other hand, require a metal ion for activity, and they are inactivated by EDTA and other chelators. Addition of divalent metal ions activate Class II KDO8PSs. Class II KDO8PSs include those from *A. aeolicus*,[39] *Acidithiobacillus ferrooxidans*,[46] *Aquifex pyrophilus*[47] and *Helicobacter pylori*.[48] The metal-dependent class II KDO8PSs are believed to have diverged from the absolutely metal-dependent type Iβ 3-deoxy-D-*arabino*-heptulosonate 7-phosphate (DAHP) synthases (DAHPS, see below).[38] Another hypothesis is that both type Iβ DAHPSs and class II KDO8PSs originated from a common ancestral metal-dependent protein.[38,49–51] The class I KDO8PSs are thought to have branched relatively recently from the class II KDO8PSs.

Structural alignments of the metal-binding residues in *E. coli* DAHPS (which is metal-dependent), metal-dependent *A. aeolicus* KDO8PS (aaKDO8PS), and metal-independent *E. coli* KDO8PS (ecKDO8PS) showed that at least two out of four metal binding residues, a His and Glu, are conserved in all three enzymes (Figure 1.6).[52] A metal-binding Asp residue, D326 in ecDAHPS and D233 in aaKDO8PS, is also Asp in ecKDO8PS, D251, but its density was not visible in the crystal structure. A Cys residue that also binds with the metal ion, C61 in

DAHPS and C11 in aaKDO8PS is replaced with an Asn residue, N26, in ecKDO8PS. Metal-dependent KDO8PSs have been converted to metal independent enzymes and vice versa, by mutating this residue.[52–54] For example, the C11N mutation in aaKDO8PS produced a mutant that did not bind metal, was not activated by metal ions nor inactivated by EDTA, and its kinetic parameters were similar to metal-independent ecKDO8PS.[54] The equivalent C11N mutation in *A. pyrophilus* (apKDO8PS) produced a mutant that had only 7-fold lower activity than wild type in the presence of Cd^{2+}, and treatment with metal chelators did not affect activity.[53] In the same study, the N26C mutation of ecKDO8PS produced an enzyme that had similar metal-dependent properties as wild type apKDO8PS. Conversely, the equivalent C31N mutation in *Pyrococcus furiosus* DAHPS (pfDAHPS) produced an enzyme that was inactive with or without EDTA or Mn^{2+}.[55] The fact that metal-dependent KDO8PSs can be converted to metal-independent enzymes by substituting C11 (or equivalent) to N indicates that the cysteine at this position plays a role in metal binding and that the metal ion has a different role in KDO8PS, where it is dispensable, compared with DAHPS, where it is not.

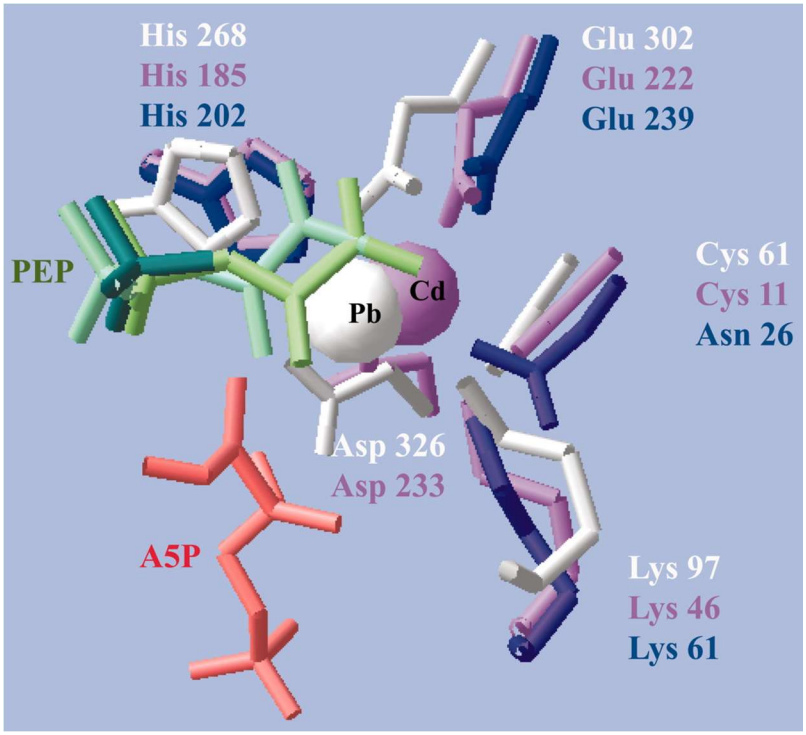

Figure 1.6. Metal binding residues in KDO8PS and DAHPS.

Structural alignment of the metal-binding residues of ecDAHPS (white), aaKDO8PS (lilac) and the equivalent residues of ecKDO8PS (purple). The equivalent residue to D326/D233 is D251 in ecKDO8PS, but it was disordered in the crystal structure. This figure was taken directly from Oliynyk et al.[52] with permission of the publisher.

Although DAHPS and KDOPS catalyse a similar reaction, there are some differences with respect to the role of the metal ion. In KDO8PS the metal ion is dispensable while in DAHPS it is not.[52–54] This is presumably because in DAHPS the metal is involved in catalysis by directly interacting with E4P carbonyl oxygen, polarizing it and activating the carbonyl carbon to be more electrophilic, favouring a nucleophilic attack from PEP.[55] In KDO8PS, the metal ion does not interact with the carbonyl oxygen in A5P, but rather interacts with C2 hydroxyl oxygen via a water molecule.[40,56] This role can be easily fulfilled by an asparagine

sidechain in non-metal dependent KDOPSs. DAHPS does not have a strict requirement for a hydroxyl at C2 of the aldose sugar, while KDO8PS does, and it must have the opposite stereochemistry to DAHPS. The replacement of ecDAHPS residues R165 by F103 in aaKDO8PS also plays a role in substrate specificity. F103 makes the PEP phosphate binding site relatively hydrophobic compared to DAHPS's. This allows the aldehyde to bind differently and PEP to bind to KDO8PS in the dianionic form rather than trianionic.[55] In this way the PEP phosphate would H-bond A5P's aldehyde oxygen. In DAHPS, the E4P's carbonyl oxygen is pointed towards the metal ion, in the opposite direction from the aldehyde oxygen of A5P in aaKDO8PS. It has been proposed that E4P's aldehyde oxygen displaces a metal-bound water and become polarized by the metal.[57] KDO8PS does not form a strong carbonyl oxygen···metal ion interaction as in ecDAHPS. Instead, the A5P carbonyl group is positioned by an interaction between A5P's C2 hydroxyl group and a metal-bound water molecule, or Asn in metal-independent enzymes. The C2 hydroxyl is more important for KDO8PS that it is for DAHPS since KDO8PS cannot use E4P, R5P or other alternative substrates which lack a C2 hydroxyl group and/or have the wrong C2 configuration.[55,58] DAHPS, on the other hand, can tolerate the five-carbon phosphorylated sugars, A5P, R5P, 2-deoxyR5P as well as four-carbon phosphorylated sugars 2-deoxyE4P and D-threose 4-phosphate (T4P) as alternative substrates.[55,59,60]

1.5. KDO8PS Homologues

KDO8PS is a member of the NeuB superfamily of α-carboxyketose synthases (Figure 1.4). Other major members of the family are DAHPS and NeuB, which use the erythrose-4-phosphate and *N*-acetylmannosamine to form DAHP and NeuNAc, respectively.[1,30,61,62] Since KDO8PS and DAHPS are essential for bacterial viability/pathogenicity and NeuB is essential for evasion of the immune system, and none are found in animals, they have been identified as targets for antibiotic drug development.

1.5.1. DAHPS

3-Deoxy-D-arabino-heptulosonate 7-phosphate synthase (DAHPS) catalyzes the first step in the shikimate biosynthetic pathway (Figure 1.7). It uses PEP and E4P to produce DAHP and Pi.[63] DAHP is converted through several steps into chorismate, a precursor for the biosynthesis of the aromatic amino acids tryptophan, phenylalanine and tyrosine, and other secondary metabolites[64] in bacteria, plants and some fungi.[65,66] Many DAHPS isozymes are subject to feedback inhibition by Trp, Phe and Tyr. Since DAHPS controls the carbon flow in this pathway, its inhibition would block the shikimate pathway and inhibit bacterial growth.[37] Despite the importance of DAHPS in the shikimate pathway, no antibiotics that target DAHPS have been developed yet.

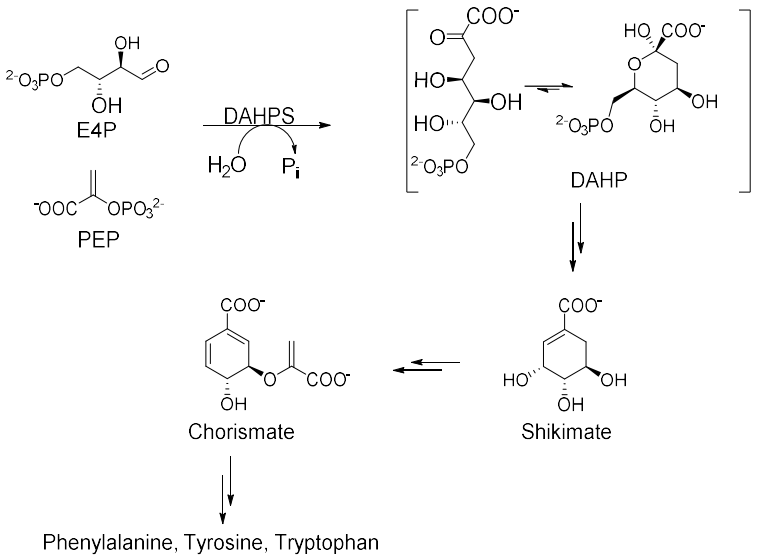

Figure 1.7. DAHP synthesis by DAHPS.

DAHPS and KDO8PS are homologous; that is, they share a common ancestor; however, the sequence identities are only on the order of ≈25%, and there are many differences in their behaviours.[49,50,67] For example, DAHPSs are regulated by different shikimate pathway products in different organisms, including, for example, the aromatic amino acids, or chorismic acid. In contrast, there is no known regulation of KDO8PSs. All DAHPSs are metal dependent while both metal-independent (Class I) and metal-dependent (Class II) KDO8PSs exist. Metal-dependent KDO8PSs have been successfully engineered to be metal-independent,[53,54,68] but the equivalent mutation in *P. furiosus* DAHPS resulted in a complete loss of activity, suggesting that metal-dependence is indispensable for DAHPS catalysis.[55] Although bacterial KDO8PSs are all homotetramers,[30,47,48,69,70] DAHPSs exist as homodimers and homotetramers in bacteria.[71–74]

1.5.2. NeuNAc synthase (NeuB)

NeuB catalyses the synthesis of *N*-acetylneuraminic acid (NeuNAc) from PEP and *N*-acetylmannosamine (ManNAc).[62] NeuNAc is an acetylated form of neuraminic acid, or sialic acid. Sialic acid itself does not occur in nature, but its derivatives make up a family of 9-carbon polyhydroxylated α-keto acids that have a variety of roles.[75] In animals, sialic acids are found at the terminal positions of cell surface glycoconjugates.[76] Their functions include cell recognition, adhesion and immune response.[76–78] Some neuroinvasive bacterial strains such as *C. jejuni*, *E. coli K1* and *N. meningitidis* use NeuNAc-containing oligo- or polysaccharides to mimic mammalian cells' surfaces and hence evade the immune system.[76,79] NeuNAc is synthesized by different pathways in bacteria and mammals, making inhibition of bacterial NeuNAc synthases an antimicrobial target.[75] NeuB-catalyzed NeuNAc synthesis in bacteria uses ManNAc directly to make NeuNAc, while the analogous reaction in mammals uses MacNAc-6-phosphate as a substrate to synthesize NeuNAc-9-phosphate, which is then dephosphorylated to yield NeuNAc. This difference in the biosynthetic pathways can be exploited in designing antimicrobial inhibitors that target only bacterial NeuNAc synthesis.

NeuB exists pre-dominantly as a homodimer[80,81] although pH-induced dimer of dimers have been detected using electrospray ionization mass spectrometry.[82] The TIM barrel $(\beta/\alpha)_8$ that is characteristic of α-carboxyketose synthases is housed in the *N*-terminal domain. The *N*-terminal domain is connected by a 10-amino acid linker to the *C*-terminal, which has high sequence

similarity with ice-binding type III antifreeze protein.[80] In the homodimer, the antifreeze domain of one monomer overlaps the TIM barrel of the other monomer (Figure 1.8). This completes and seals off the active site. NeuBs require a metal ion for activity.[83] The ManNAc carbonyl group is believed to coordinate with the metal ion and become activated by this interaction during catalysis. The metal ion in this case is likely to play both structural and catalytic roles in NeuB.

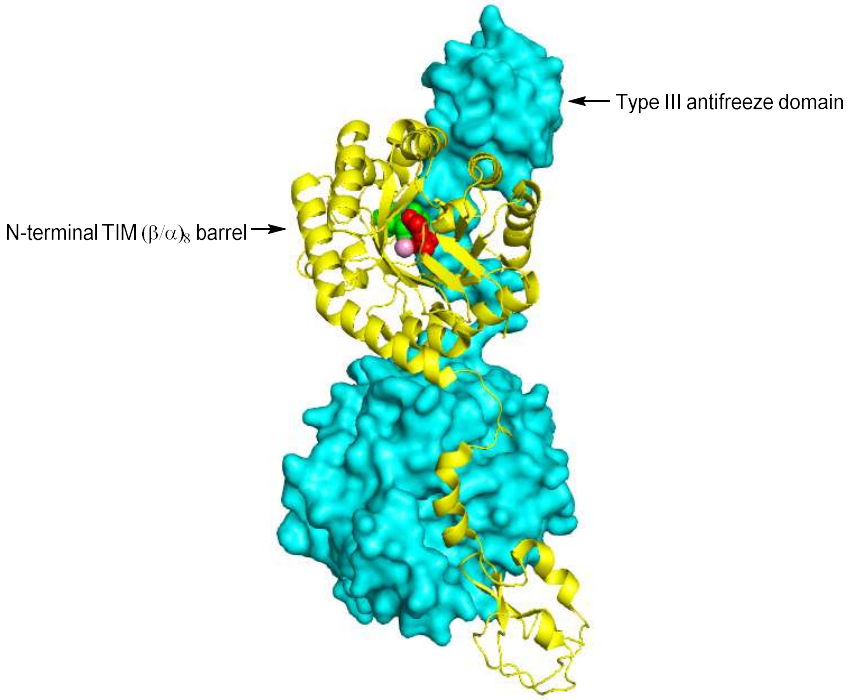

Figure 1.8. Crystal structure of *N. meningitidis* NeuB.

The NeuB dimer (PDBID: 1XUZ)[80] is comprised of swapped monomers where the *N*-terminal TIM barrel containing the active site is overlapped by the *C*-terminal antifreeze-like domain of the second monomer. Bound Mn^{2+}, rManNAc and PEP are shown in pink, green and red, respectively. rManNAc is reduced ManNAc, where the aldehyde functionality has been reduced to a primary alcohol. The asymmetric unit of 1XUZ contains one monomer; the homodimer was generated using the symmetry generation tool in Pymol.[84]

1.6. Reaction mechanism

The exact catalytic mechanisms employed by α-carboxyketose synthases remain unclear. Previous studies on KDO8PS showed that the ketose product is formed via an acyclic tetrahedral intermediate (THI), but the initial reaction pathway(s) leading to the THI is not clearly understood.[85,86] Anionic and cationic mechanisms that could lead to a tetrahedral intermediate (THI) have been proposed (Figure 1.9). [55,57,61,86–90] In the anionic path a nucleophilic attack on C2 of PEP by water or hydroxide anion forms a carbanion intermediate at C3. Nucleophilic attack on the C1 carbonyl group of A5P by C3 of PEP leads to the THI.[61,86,87] In the cationic path, C3 of PEP attacks the C1 carbonyl carbon of A5P, leading to a presumed oxacarbenium ion intermediate. Nucleophilic addition of water or hydroxide anion at C2 forms the THI.[55,88–90] Evidence for THI formation includes the fact that it has been detected by mass spectrometry in the KDO8PS reaction.[91] Also, using PEP ^{18}O-labelled at the bridging oxygen led to ^{18}O-labelled Pi as a product in the DAHPS[61], KDO8PS[86] and NeuB[80] catalyzed reactions. This demonstrated that phosphate departure occurred via C−O bond cleavage, which can only plausibly occur through THI formation and breakdown. The THI was also reported to have been detected by X-ray crystallography of a mutant KDO8PS, though the electron density was not unambiguous.[68] The THI breaks down through phosphate departure via C–O bond cleavage at the C2 centre, leading to KDO8P and Pi as products. In both pathways, the aldehydic carbonyl needs to be

protonated or activated by a metal ion. This protonation is likely carried out by the highly conserved Lys residue in the substrate selecting KANRS motif in KDO8PS.[45,92] Clark and Berti[93] showed that a nucleophilic attack on C2 of PEP would require prior activation of the C3 of PEP. Thus, the anionic mechanism is unlikely. The anionic and cationic mechanisms represent the two extremes of stepwise mechanisms in which a discrete intermediate is formed. It is also possible that the reaction intermediates are very unstable, and THI formation proceeds through a concerted reaction mechanism, rather than a step-wise reaction mechanism. Computational studies on the KDO8PS reaction suggested that the above stepwise mechanisms are not favourable and that the lowest energy transition state for THI formation would have the $C3^{PEP}$–$C1^{A5P}$ bond largely formed prior to C–O bond formation from water attack.[90]

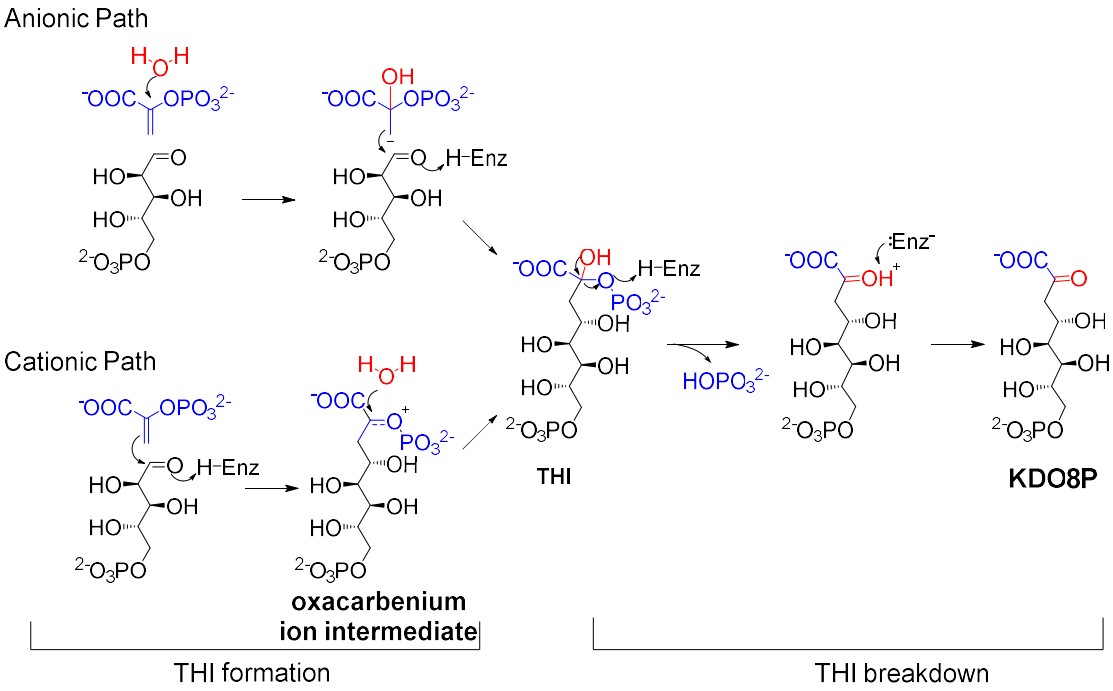

Figure 1.9. Proposed catalytic mechanism of KDO8PS.
Enz-H and :Enz denote protonating and deprotonating residues, respectively.

The second step of the reaction involves THI breakdown to form the final products, KDO8P and Pi. This step has been less studied, presumably because it was presumed that THI formation was more energetically demanding, and therefore a more important target for inhibitor design. However, the linear free energy relationship (LFER) analysis of DAHP oxime that showed that it is a transition state mimic also implied that the first irreversible step of the DAHPS reaction is THI breakdown.[94] THI breakdown involves departure of the phosphate group, which must be catalyzed by protonation of the phosphate group's bridging oxygen.[95] This leads to formation of an oxacarbenium ion intermediate whose protonated carbonyl oxygen must be deprotonated to yield the final product. It is

also possible that, like THI formation, THI breakdown is concerted, with phosphate departure and oxygen deprotonation being concerted.

1.7. Kinetic mechanism

1.7.1. A note on the nomenclature of kinetic mechanisms

The terminology of kinetic mechanisms is explained here, to clarify the meaning of the terms used.[96] In this study, wildtype cjKDO8PS (cjKDO8PS$_{wt}$) was shown to follow a *"rapid equilibrium sequential ordered ter ter kinetic mechanism*". The terms describing this kinetic mechanism are explained in reverse order. "Kinetic mechanism" refers to the microscopic rate constants and equilibrium constants that describe the steps in the reaction, as distinct from a chemical mechanism that shows "arrow pushing" to detail the chemical processes involved in each step. For example, the first step of any enzymatic reaction is substrate binding, E + S ⇌ E·S, with binding described by the microscopic rate constants k_1 and k_{-1}, or the equilibrium constant K_s. "Ter ter" means that there are three substrates and three products. As described below, the essential divalent metal ion that is required for activity is treated as a substrate (and product), even though it is, strictly, an essential activator. Previous studies on KDO8PS only considered PEP and A5P as substrates and KDO8P and Pi as products.[40,43,97] Those studies therefore referred to KDO8PS as having a "bi bi" kinetic mechanism. "Ordered" means that the substrates must bind in a specific order (A,

then B, then C), and the products dissociate in a specific order (P, then Q, then A). This is in contrast to some enzymes where substrate binding is random and can occur in any order. "Sequential" refers to the fact that all of the substrates bind before any of the products dissociate. This is in contrast to a "ping pong" kinetic mechanism, where the first product dissociates before the last substrate binds. "Rapid equilibrium" refers to the fact that all the substrate-binding steps are fast and in equilibrium with each other. This is in contrast to the steady state approximation, which assumes that d[ES]/dt = 0 (or d[EABC]/dt = 0 in the case of a ter ter mechanism). In the absence of specific experimental evidence demonstrating a rapid equilibrium kinetic mechanism, the steady state approximation must be used. It is a safer assumption to make as it does not depend on substrate binding being rapid compared to catalysis, but leads to more complicated kinetic expressions. It is preferable, if it can be shown to be true experimentally, to use the rapid equilibrium assumption. Therefore, a rapid equilibrium sequential ordered ter ter kinetic mechanism means that all three substrates bind rapidly and in the order A, B, C, before the chemical steps of the reaction occur, releasing the products P, Q, then A.

1.7.2. Order of substrate binding

The inhibitory profiles of ribulose-5-phosphate (Rib5P), KDO8P and Pi against ecKDO8PS were used to investigate the order of substrate binding.[97] Rib5P, an analogue of A5P, was found to be uncompetitive with respect to PEP

but competitive with respect to A5P indicating that both A5P and Rib5P bind to the same form of enzyme, the KDO8PS·PEP complex. In that study, it was also found that KDO8P was a competitive inhibitor with respect to PEP but noncompetitive with respect A5P, whereas Pi was noncompetitive with respect to both A5P and PEP. This further suggested that KDO8P is released after Pi dissociation from the active site. Thus, in KDO8PSs the proposed order of substrate binding is PEP, then A5P. Product dissociation was proposed to start with Pi release, followed by KDO8P. These studies did not consider the binding of the essential metal ion as part of the kinetic mechanism. Thus, the kinetic mechanism was sequential ordered bi bi. The rapid equilibrium assumption has generally been used, though there is no specific evidence to support it. Structural studies support this model in that the active site of KDO8PS is shaped like a funnel, with PEP binding at the bottom, followed by A5P at the top (Figure 1.5, bottom, panel A).[40] In *A. aeolicus* KDO8PS crystal structure, A5P and PEP bound in active sites on only one face of the enzyme, suggesting the possibility of alternate face catalysis, where only one face of the enzyme is catalytically active, while products are released from the other face.[40] In DAHPS, substrate binding is ordered, with PEP binding before E4P.[72,98] In most kinetic studies the metal ion is considered a cofactor and, since it is not consumed during the reaction, it is neglected in substrate binding studies. Recently, DAHP oxime, a transition state mimic inhibitor of DAHPS, has been found to be competitive with respect to Mn^{2+} and PEP at neutral pH.[98] This warranted that the metal be treated as a

substrate in determining the inhibitory constant, K_i. In that study, it was clear that substrate binding favoured the route where the metal, Mn^{2+}, binds first followed by PEP and E4P in a rapid equilibrium manner. That is, it followed a rapid equilibrium sequential ordered ter ter kinetic mechanism. Kinetic analysis of cjKDO8PS$_{wt}$ indicated that Mn^{2+} binds first followed by PEP then A5P in an ordered mechanism (see Chapter 2). In aaKDO8PS, Cd^{2+} binding in one site appeared to have induced structural changes that prevented A5P binding to the other site. All these point to the importance of considering the metal ion in catalytic studies, especially when characterizing inhibition.

1.8. Inhibitors

Chemical Biology research often employs small molecules to probe and manipulate biological systems. Inhibitors are one of the probes used to study biological functions and the probes could be developed into therapeutic agents. Enzyme inhibitors constitutes almost half of the drugs in clinical use.[99,100] The portion of the human genome that encodes for disease-associated targets is dominated by enzymes.[100] Enzyme inhibitors can be classified into non-reversible and reversible inhibitors.[100–102] Irreversible inhibitors form covalent bonds with the target enzyme whereas reversible inhibitor binding can be achieved via non-covalent interactions, such as hydrophobic and electrostatic attractions, and hydrogen bonding. Reversible inhibitors, which act by modulating enzyme activity, are categorized by their mode of inhibition: competitive, noncompetitive

or uncompetitive with respect to the substrate(s) (Figure 1.10).[100] Competitive inhibitors, in the strictest definition, exhibit mutually exclusive binding with respect to the substrate. If the inhibitor and substrate occupy the same physical space in the active site, then their binding is necessarily mutually exclusive, and therefore competitive. Because the substrate and inhibitor compete with each other for the binding site, inhibition can be relieved by increasing the substrate concentration. It is also possible, however, for an inhibitor and substrate to exhibit mutually exclusive binding without occupying the same physical space; this is the case with the DAHPS inhibitor DAHP oxime, and the essential metal ion, Mn^{2+}.[98] They bind competitively even though they do not occupy the same physical space in the enzyme. Competitive inhibitors are characterized by their effects of increasing the apparent K_M value for the substrate, but not affecting k_{cat}. A noncompetitive inhibitor (I) can either bind equally to free enzyme (E) to form E·I or to the enzyme-substrate complex (E·S) to form E·S·I, and thus cannot be outcompeted by increasing substrate concentration. Noncompetitive inhibitors decrease the apparent k_{cat} value without changing K_M. Uncompetitive inhibitors bind only to the E·S complex, resulting to a decrease in both k_{cat} and the apparent K_M (or apparent substrate affinity).

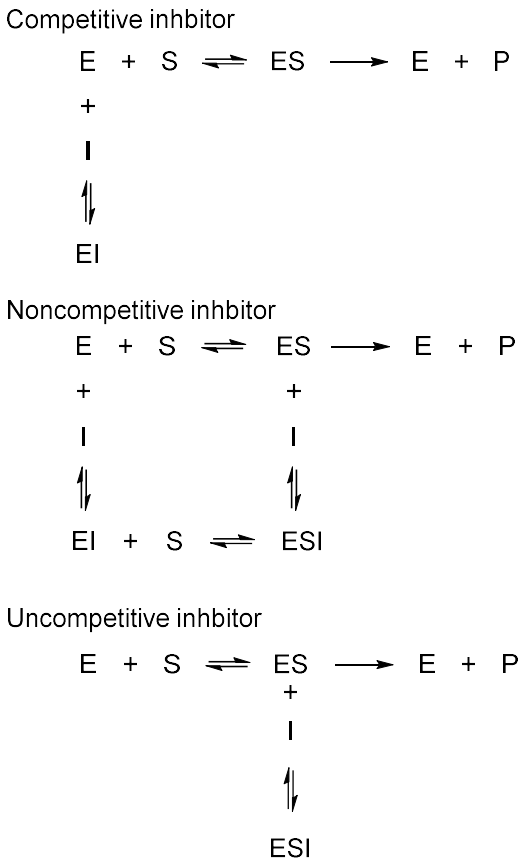

Figure 1.10. Modes of binding of reversible inhibitors.

E = enzyme, S = substrate, I = inhibitor, P = product.

Enzymes can enhance reaction rates by up to 10^{19}-fold compared to noncatalyzed reactions.[101,103] Enzymes accomplish this through various methods such as; approximation of reactive functionalities of molecules and enzyme functional groups, covalent catalysis, acid/base catalysis, and conformational distortion catalysis.[100,101] For enzymes to be able to enhance reaction rates, they must bind the high energy transition state with higher affinity than the ground state substrate. The estimated dissociation constants for transition states, $K_d^{\ddagger}$, can be estimated, and are typically in the range of 10^{-9} to 10^{-24} M, while substrate

dissociation constants for most enzymes are in the range 10^{-3} to 10^{-6} M.[100] Therefore, an excellent inhibitor should have a transition state-like character with potency typically in the nanomolar range or lower. For example, inhibitors that were designed to mimic substrate, products and transition state-like intermediates were developed for cytidine deaminase (Figure 1.11). This enzyme converts cytidine to uridine through a transition state with an sp^3-hybridized reactive carbon atom.[100] The inhibitors against this enzyme that mimicked the substrate, product and transition state had K_i values of 3×10^{-5} M, 2.5×10^{-3} M and 1.2×10^{-12} M, respectively.[104] The $K_d^{\ddagger}$ for the transition state for the cytidine deaminase reaction is estimated at 1.1×10^{-16} M,[105] thus the transition state mimic inhibitor, though close, does not perfectly mimic the inherently unstable transition state.

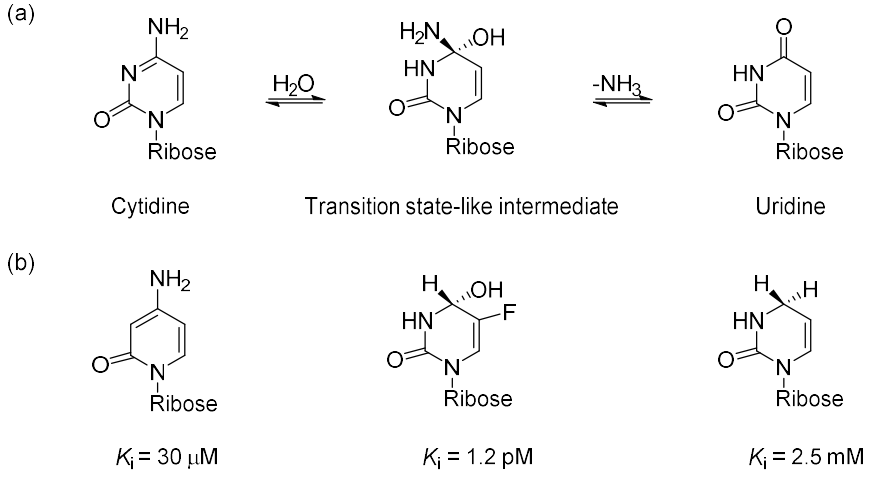

Figure 1.11. Cytidine deaminase catalyzed conversion of cytidine to uridine. (a) cytidine conversion to uridine via a transition state-like intermediate. (b) Cytidine deaminase inhibitors designed to mimic the substrate, transition state-like intermediate and product states of the enzymatic reaction. The figure is based on Copeland.[100]

Transition states are short-lived (approximately 10^{-13} s) and, as a result, they are difficult to study.[106] The transition states for α-carboxyketose synthesis are not yet known. The THI of KDO8P synthesis has recently been directly identified with time resolved electrospray ionization mass spectrometry (ESI-MS) in a millisecond time-scale.[91] The THI has also been identified by X-ray crystallography.[68] Potential energy surfaces (PESs) for a C11N mutant of *A. aeolicus* KDO8PS (an effectively metal-independent mutant of *A. aeolicus* KDO8PS) were computationally generated based on the mutant crystal structure where both A5P and PEP are bound.[90] The KDO8PS reaction favoured a concerted reaction between PEP, A5P, and water in which C−C bond formation between C3 of PEP and C1 of A5P is far advanced over C−O bond formation between C2 of PEP and the water nucleophile. Because C−C bond formation was advanced, the proposed transition state had oxacarbenium ion-like character, with a partial positive charge present at C2 of PEP. However, this study considered only the first step of the reaction, THI formation. That is, the THI was the product of the computational reaction, and the relative importance of THI formation and breakdown was not considered, nor was the mechanism of THI breakdown.[90] While the majority of inhibitors designed to inhibit α-carboxyketose synthases have targeted either the THI or the oxacarbenium ion(-like) intermediate/transition state of THI formation, the transition state of THI breakdown is also a target for inhibitor design.

1.9. Slow-binding inhibitors

The textbook view of noncovalent inhibitors binding to the target enzyme involves rapid binding that can be characterized simply by the inhibitor's dissociation constant, K_i. In reality, a large number of inhibitors, particularly tight-binding inhibitors and transition state mimics, display slow-binding inhibition, and exert their effects in a time-dependent fashion.[100] Given the ubiquity of slow-binding inhibition, especially in transition state mimics, the origin of slow-binding has been proposed to be related to the fact that enzymes must undergo conformational changes as they proceed from substrate binding to tighter binding of the transition state. Enzymes have evolved to achieve this quickly in the real reaction, but because transition state mimics are never perfect, they impair the conformational change step in some way, leading to inhibitors where the ultimate affinity is achieved on a minutes to hours timescale.[107] Consequently, transition state mimics are often slow-binding inhbitors.[108]

Slow-binding inhibitors can be classified into three kinetic mechanisms (Figure 1.12). In mechanism A, the E·I complex is formed in a single-step binding mechanism in which the association (k_3) or dissociation rate constants (k_4), or both, are slow. In mechanism B, there is initial rapid equilibrium binding to form a relatively weakly bound E·I complex. This is followed by a slow isomerization of the enzyme (k_5) to form a tighter E*·I complex with an even slower reverse isomerization rate (k_6). Isomerization here refers to the conformational change of

the enzyme's active site to form the more tightly bound E*·I complex. In mechanism C, there is rapid reversible E·I complex formation, followed by an irreversible, generally covalent, step that modifies the enzyme with an affinity label or a mechanism-based inhibitor (E-I).

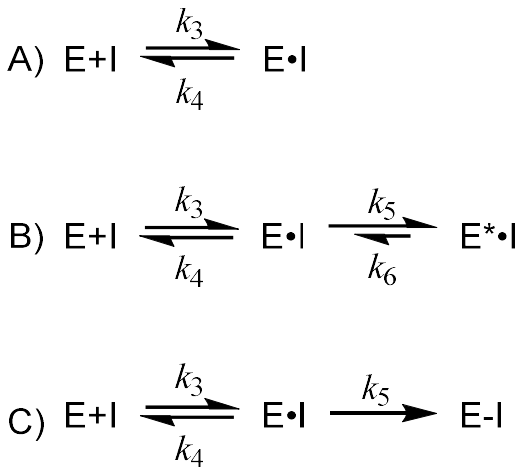

Figure 1.12. Mechanisms of slow-binding inhibition.

The ultimate affinity of slow-binding inhibitors that follow mechanism B is largely dictated by the E*·I since the off-rate, k_6, can be slow enough that its measurement could take hours to days. Therefore, fast-binding experiments that are done in minutes can underestimate the true inhibitor affinity, and experiments aimed at characterizing slow-binding inhibitors need to consider the isomerization step.

The attractiveness of slow-binding inhibition is not the slow-binding itself, but the fact that slow-binding inhibition necessarily also requires slow dissociation, which is where the real power of slow-binding inhibitors comes

from. Recent investigations and reviews have demonstrated a positive correlation between inhibitor residence time ($t_R = 1/k_6$) and *in vivo* efficacy.[109–112] This occurs because inhibitor concentrations in the body can fall quickly after initial injection/ingestion as it is metabolized or excreted, which leads to short periods when the inhibitor is at a therapeutic concentration. If an inhibitor is slow-dissociating, then it will continue to exert its therapeutic effect even after the bulk of it has been metabolized/excreted.

Inhibitor binding kinetics can be influenced by various molecular determinants.[113] For example, ligand binding via a hydrogen bond that is shielded from water by surrounding hydrophobic regions leads to a more kinetically stable complex than in non-shielded ligand-receptor hydrogen bond interactions. Conformational fluctuations, especially of the active site, can also affect ligand binding kinetics. For example, the slow off-rate of an inhibitor of *Mycobacterium tuberculosis* enoyl-ACP reductase is associated with the ordering of the active site loops.[112] In aaKDO8PS the active site loops switch from an open conformation, where only PEP is bound, to a closed conformation where both PEP and A5P are bound (Figure 1.5). This feature could be exploited in designing an inhibitor that has a long residence time. For instance, an inhibitor that extends from the PEP to the A5P binding subsites, making key contacts with the L7 loop involved in loop ordering might lead to a longer residence time.

1.10. KDO8PS inhibitors

KDO8PS is involved in a key step of LPS biosynthesis, and therefore, is a target of novel antimicrobial drug design. Several KDO8PS inhibitors have been designed to mimic the intermediates or transition states (Figure 1.13).

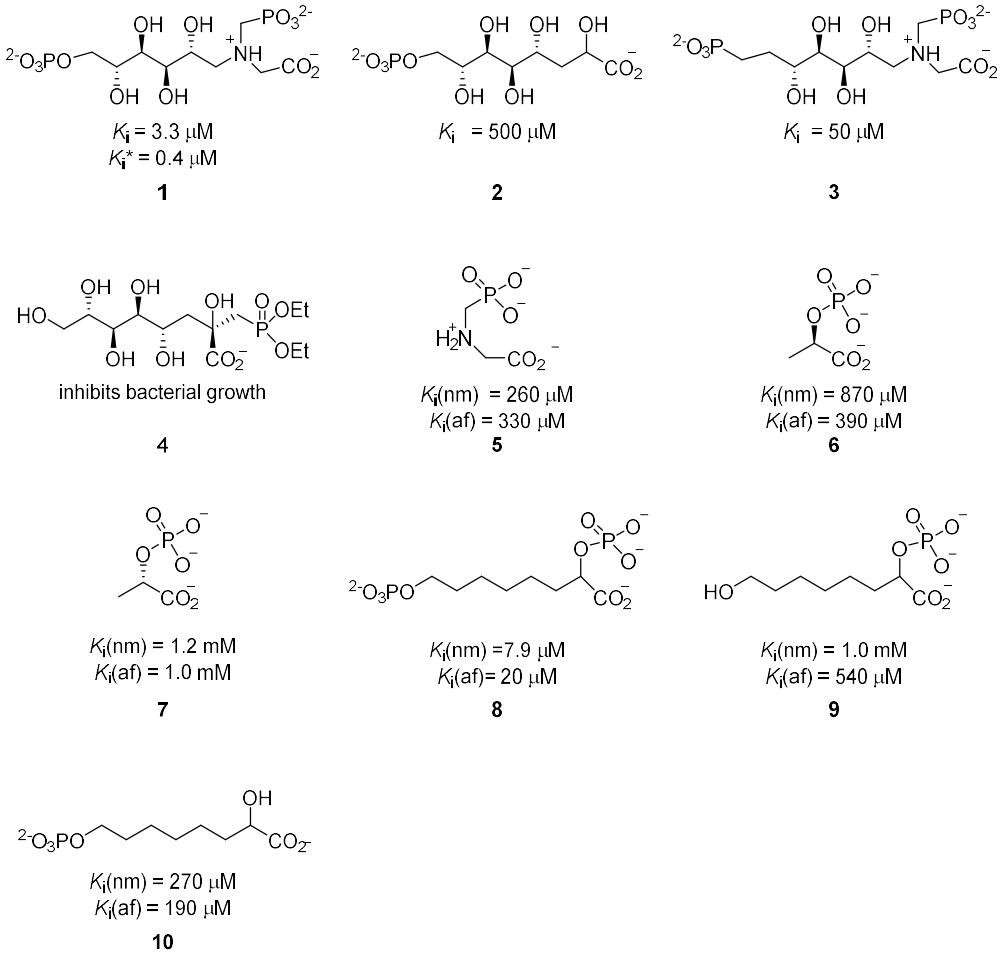

Figure 1.13. Reported KDO8PS inhibitors.

K_i and K_i^* are fast- and slow-binding binding inhibition constants, respectively. Compounds **5** – **10** were tested against metal-independent *N. meningitidis* KDO8PS *(nm)* and metal-dependent A. *ferrooxidans* KDO8PS *(af)*.

Compound **1** has an aminophosphonate group designed to mimic the oxacarbenium ion intermediate character through the positive charge on the nitrogen. It was a competitive inhibitor of ecKDO8PS with respect to PEP, with a K_i = 3.3 μM under fast-binding conditions,[114] and K_i^* = 0.4 μM[115] under slow-binding conditions. It did not halt bacterial growth, presumably due to its negatively charged phosphate group preventing it from crossing the cell membranes. The primary phosphate group is also susceptible to bacterial phosphatase hydrolysis.[116] Compound **2** was designed to mimic the acyclic KDO8P intermediate and had K_i = 500 μM.[115] Compound **3** is a derivative of **1** where the primary phosphate was replaced by a phosphonate group. This led to a 15-fold increase in K_i, to 50 μM, and no inhibition of bacterial growth.[116] Compound **4** inhibited Gram-negative bacterial growth, though no K_i was reported.[37] Inhibitors **5** to **10** were tested against metal-independent *N. meningitidis* KDO8PS (nmKDO8PS) and metal-dependent *A. ferrooxidans* KDO8PS (afKDO8PS), and all were competitive with respect to PEP.[117] Inhibitor **5** is the 'PEP moiety' of inhibitor **1**. Compound **6** and **7** were designed to mimic some aspect of the THI, and, being fragments, had poor potency. Compound **8** was designed to mimic the THI and it contained phosphate groups corresponding to the PEP and A5P phosphate groups, linked via an eight-carbon chain. This gave lower K_i values, 7.9 and 20 μM against nmKDO8PS and afKDO8PS, respectively. Compound **9** was used to probe the importance of the A5P-derived phosphate group and, relative to compound **8**, showed a 127- and 27-fold increase in K_i

against nmKDO8PS and afKDO8PS, respectively. Compound **10** was used to investigate the importance of the PEP derived phosphate group, and showed a 34- and 10-fold increase in K_i. Thus, it appears that the A5P-derived phosphate group was important in binding affinity.

1.11. DAHPS and NeuB Inhibitors

Similar inhibitor design strategies have been utilized to develop inhibitors of KDO8PS, DAHPS and NeuB (Figure 1.14).

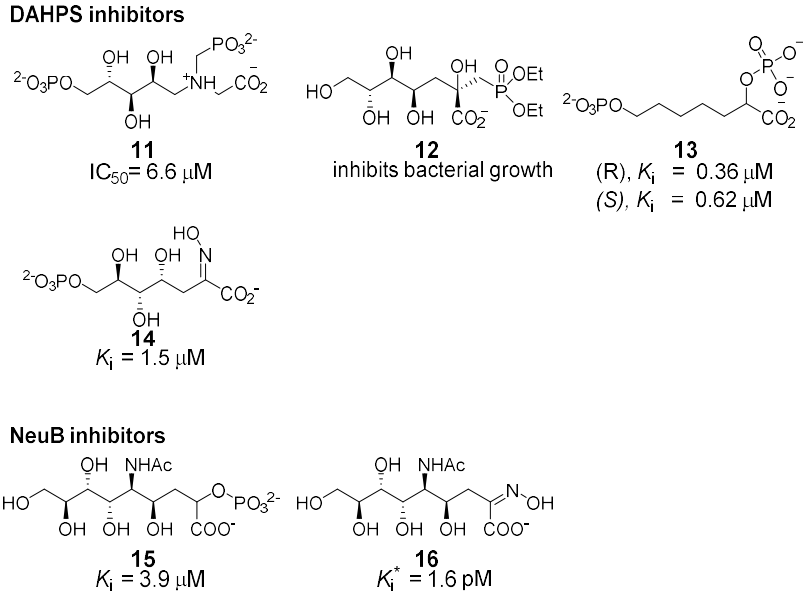

Figure 1.14. Inhibitors of DAHPS and NeuB.

Like compound **1**, **11** has been proposed to mimic the oxacarbenium ion intermediate with respect to the positive charge at the nitrogen atom. It is also a slow-binding inhibitor with IC_{50} = 6.6 μM.[118] Compound **12,** which was designed to mimic the THI, inhibited bacterial growth in cultures of *E. coli*, *Yersinia*

enterocolitica, *Pseudomonas aeruginosa*, *Staphylococcus aureus* and *Bacillus subtilis*, though no K_i values were reported.[37] Compound **13**, a presumed THI mimic, was the most potent among the DAHPS inhibitors with K_i in the nanomolar range.[119] This inhibitor is over 10-fold more potent than the corresponding compound **8** against KDO8PS. Recently, an oxime-based inhibitor of DAHPS, DAHP oxime, **14**, has been developed.[98] The DAHPS·**14** crystal structure revealed that the oxime group, combined with two crystallographic waters, was bound at the same location in the catalytic center as the phosphate group of PEP and the THI. DAHP oxime showed residual activity in rate assays and displayed half-of-sites inhibitor binding in the crystal structure, with the inhibitor bound to only 2 of the 4 subunits in the homotetrameric protein. DAHP oxime is a slow-binding inhibitor with a K_i = 1.5 μM and a residence time, t_R, of 83 min.[98,120] The IC_{50} for slow-binding inhibition was 9 μM, higher than K_i. This was an indication that binding to all four subunits was necessary for slow-binding inhibition to occur. DAHP oxime was shown by LFER analysis to be a transition state mimic.[94] Presumably it mimics the transition state for phosphate departure from the THI, with the oxime nitrogen atom hydrogen bonding to the K186 sidechain, the residue that is presumed to act as a general catalyst in phosphate group departure.[95,121] For NeuB, the THI mimic **15** had a lower K_i than the similar THI mimic inhibitor **13** against DAHPS.[122] NeuNAc oxime **16** showed slow-binding inhibition with a binding half-life of 2.5 h and K_i^* of 1.6 pM.[123] This is the most potent inhibitor known against NeuB. Given the similarities in reaction

mechanisms and inhibition profiles of the three α-carboxyketose synthase family of enzymes, inhibitor design strategy for one enzyme can be translated to the other two. An antimicrobial agent that target all three enzymes would be very effective against bacterial infections.

1.12. Project object

It has been established that the α-carboxyketose synthases family's structural and catalytic properties are similar. It is possible, therefore, for an inhibitory motif against one enzyme to be applied to the inhibition of the other two. Transition state mimic inhibitors are often slow-binding inhibitors. DAHP oxime, **14**, is a slow-binding inhibitor with K_i = 1.5 μM and a residence time of 83 min. DAHP oxime mimics a transition state, presumably that for phosphate group departure from the THI (Figure 1.15). NeuNAc oxime, **16**, is also a very potent slow-binding inhibitor of NeuB. The oxime-based inhibitor design is a novel strategy against the α-carboxyketose synthases family of enzymes. Since DAHP oxime and NeuNAc oxime inhibitors are potent against DAHPS and NeuB, respectively, we propose that a similar inhibitor KDO8P oxime, **17** (Figure 1.15) would be potent against KD8PS.

This dissertation reports the characterization of a new Class II KDO8PS from *C. jejuni.* We employed traditional protein expression and protein purification protocols to obtain transform and express the *kdsA* from *C. jejuni* in an *E. coli* expression system. We used nickel immobilized metal affinity

chromatography to purify the polyhistidine-tagged enzyme, cjKDO8PS$_{H6}$, and traditional chromatographic methods, namely anion exchange, hydrophobic interaction and size exclusion chromatography to purify the wild type enzyme, cjKDO8PS$_{wt}$. Kinetic assay methods were utilized to characterize activity. We took advantage of Dynafit Software[124] to fit the kinetic data for cjKDO8PS$_{wt}$, which made it possible to determine microscopic rate constants involved in substrate binding. This made it possible to establish whether the kinetics follow rapid equilibrium or steady state assumptions. We were also able to deduce the order of substrate binding, especially for the metal ion (Mn^{2+}). Metal ions have previously been overlooked in kinetic mechanism studies of metal-dependent KDO8PSs. We also used kinetic assays to characterize inhibition of cjKDO8PS by KDO8P oxime both in the fast-binding phase and slow-binding phase. To supplement the kinetic data, we also employed isothermal titration calorimetry (ITC) to study substrate and KDO8P oxime binding to cjKDO8PS$_{H6}$. We attempted to crystallize cjKDO8PS in complex with various ligands including KDO8P oxime. We also attempted to radioactively track KDO8P oxime binding to cjKDO8PS in a bid to further confirm the kinetically determined residence time of KDO8P oxime on the target.

We showed that cjKDO8PS is a metal-dependent homotetramer that is optimally active at pH 7.5 at 60 °C. We demonstrated that cjKDO8PS$_{wt}$ follows a rapid equilibrium sequential ordered ter ter kinetic mechanism, where the metal

binds first, followed by PEP, then A5P. We also showed that KDO8P oxime is a potent slow-binding inhibitor of cjKDO8PS.

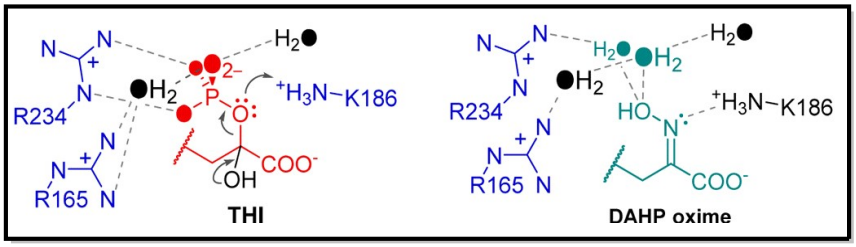

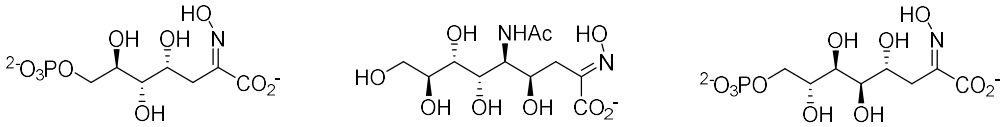

DAHP oxime
14

NeuNAc oxime
16

KDO8P oxime
17

Figure 1.15. Oxime inhibitors of DAHPS, NeuB and KDO8PS.

The boxed figure was modified from Balachandran et al.[94] and represents the proposed mechanism of phosphate group departure from the THI (left) and DAHP oxime active site interactions in DAHPS (right). These are based on the crystal structures of DAHP oxime[98] and PEP[125] bound in the active site.

2. Characterization of *C. jejuni* KDO8PS

2.1. Introduction

Campylobacter jejuni, a microaerophilic Gram-negative bacterium, is one of the most common causes of acute gastroenteritis.[126] This gastrointestinal illness is characterized by diarrhea, fever, and abdominal cramps. It is often self-limiting, requiring no antibiotic treatment; however, some patients can be severely affected. For example, in developing countries, *Campylobacter* species are an important cause of childhood morbidity caused by diarrheal illness.[127] *Campylobacter* infections can also be serious for immune-suppressed patients.[128] *C. jejuni* infection has been linked to serious post-infection complications such as the Guillain-Barré syndrome (GBS), a demyelinating disease affecting the peripheral nervous system.[126,127] *C. jejuni* lipooligosaccharides (LOS) mimic gangliosides prevalent on nerve cells. As a result, antibodies against *C. jejuni* LOS cross-react with gangliosides in nerve cells, triggering GBS, which may manifest as muscle weakness or even paralysis.[129,130] Given these serious post-infection diseases, the emergence of antibiotic resistant strains of *C. jejuni* is of great concern. In many regions, *C. jejuni* is resistant to fluoroquinolones.[128] *C. jejuni* KDO8PS (cjKDO8PS) is characterized here for the first time, and confirmed as metal-dependent (Class II) enzyme. cjKDO8PS, like other KDO8PSs, is a potential target in the design of novel antibiotics.

2.2. Experimental

All chemicals and materials were obtained from Sigma-Aldrich, unless specified.

2.2.1. Cloning and expression

Histidine-tagged C. jejuni KDO8PS (cjKDO8PS$_{H6}$)

The *C. jejuni* KDO8PS *kdsA* plasmid bearing a *C*-terminal His$_6$ tag was a generous gift from Dr. Martin Young (National Research Council of Canada). From this, the recombinant pET300/NT-DEST destination vector bearing a TEV-cleavable *N*-terminal His$_6$ tag was prepared by Dr. Naresh Balachandran according to procedure in reference [120]. The DNA and amino acid sequence bearing the *N*-terminal His$_6$ tag and the TEV recognition sequence ENLYFQG is shown (Figure 2.1).

```
atgcatcatcatcatcatcacatcacaagtttgtacaaaaaagcaggcttcgaaaacctg
 M  H  H  H  H  H  H  I  T  S  L  Y  K  K  A  G  F  E  N  L

tattttcagggcatgaaaaaaatgatactcattgctggtccttgcgtgatagaaagcaaa
 Y  F  Q  G  M  K  K  M  I  L  I  A  G  P  C  V  I  E  S  K

gatttgatttttaaagttgctgaacagttaaaaaattttaatgaaaatccaaatatagaa
 D  L  I  F  K  V  A  E  Q  L  K  N  F  N  E  N  P  N  I  E

ttttatttcaaatcaagttttgataaggccaatcgcacaagtattaattcttttcgaggt
 F  Y  F  K  S  S  F  D  K  A  N  R  T  S  I  N  S  F  R  G

cctggtcttgaagaaggattaaaaattttacaaagcgtaaaagatgaatttggtatgaaa
 P  G  L  E  E  G  L  K  I  L  Q  S  V  K  D  E  F  G  M  K

atcttaaccgatatacacgaaagcaatcaagcaaaccctgtaagtgaagtagctgatgtc
 I  L  T  D  I  H  E  S  N  Q  A  N  P  V  S  E  V  A  D  V

ttgcaaattcctgctttttatgtcgtcaaaccgatttacttgtagccgcagcaaaaact
 L  Q  I  P  A  F  L  C  R  Q  T  D  L  L  V  A  A  A  K  T

aaggcaaaaattaatatcaaaaaaggacaatttttaaacccaagcgatatcaaatacagc
 K  A  K  I  N  I  K  K  G  Q  F  L  N  P  S  D  I  K  Y  S

gttaaaaaagttctacaaacccgtggtatagaagatgaaggctatgaagctgctcaaaga
 V  K  K  V  L  Q  T  R  G  I  E  D  E  G  Y  E  A  A  Q  R

aatggtgtttttgtagctgaaagaggggctagctttggctatggaaatttagtagtagat
 N  G  V  F  V  A  E  R  G  A  S  F  G  Y  G  N  L  V  V  D

atgcgttctttagttatcatgcgtgaatttgctccagttatttttgatgctacccatagc
 M  R  S  L  V  I  M  R  E  F  A  P  V  I  F  D  A  T  H  S

gtacaaatgccaggggctgcaggtggaagtagcggagggaaaagcgaatttgtagaacct
 V  Q  M  P  G  A  A  G  G  S  S  G  G  K  S  E  F  V  E  P

ttagcaagagcggcagcagccgtaggcatagatggctttttctttgaaacacatattaat
 L  A  R  A  A  A  A  V  G  I  D  G  F  F  F  E  T  H  I  N

ccttgcgaggctttatgcgatggacctaatatgcttaatcttacacgccttaaaaattgc
 P  C  E  A  L  C  D  G  P  N  M  L  N  L  T  R  L  K  N  C

 gttaatacattactagaaatacaaaatatcataaaggaaaacaaataa
  V  N  T  L  L  E  I  Q  N  I  I  K  E  N  K  -
```

Figure 2.1. Sequence of His_6-tagged *C. jejuni* KDO8PS ($cjKDO8PS_{H6}$).

The *N*-terminal hexahistidine tag is shown in blue text. TEV protease recognizes the ENLYFQG recognition site (red text) and cleaves at the Gln↑Gly (Q↑G) bond (underlined).

E. coli BL21 (DE3) cells (200 µL) were transformed with 1 µL of plasmid (0.23 ng) using the heat shock method.[131] The transformed cells were incubated on ice for 5 min, followed by incubation at 42 °C for 2 min, and back on ice for 5 min. Luria-Broth (LB) media (900 µL) was added to the transformed cells, and they were incubated at 37 °C for 1 h. The cells were plated on an LB-agar plate containing 100 µg/mL ampicillin. A single colony was used to inoculate 50 mL of LB media containing 100 µg/mL ampicillin, and the starter culture was shaken at 37 °C for 15 h. This culture was used to inoculate 1 L of LB media and grown to OD_{600} = 0.6, at which point protein expression was induced with 1 mM isopropyl β-D-1-thiogalactopyranoside (IPTG), and incubated at 37 °C for 4 h. The cells were harvested by centrifugation at 5000 × g for 20 min, and stored at -80 °C until purification.

Thawed cells were lysed and homogenized using a cell disrupter (Constant Systems Ltd. UK) set at 30 kpsi. Cell debris was separated from the supernatant by centrifugation at 10 000 × g for 30 min at 4 °C. Protease inhibitor cocktail (Sigma-Aldrich) was added to the cell homogenate at 1 mL per 20 g (wet weight). The cell homogenate was filtered through a 0.45 µm cut-off Acrodisc Syringe Filters (Pall Life Sciences). cjKDO8PS$_{H6}$ was purified on a 1 mL nickel-charged Chelating-Sepharose column (GE Healthcare). The column was charged by passing 10 column volumes of 100 mM nickel sulphate, followed by washing with 10 column volumes of water. After pre-equilibrating the column with buffer A (50 mM Tris·Cl, pH 7.5, 100 mM KCl, 25 mM imidazole) the cell homogenate

was loaded. cjKDO8PS$_{H6}$ was eluted with buffer B (50 mM Tris·Cl, pH 7.5, 100 mM KCl, 500 mM imidazole). SDS-PAGE analysis revealed that pure cjKDO8PS$_{H6}$ was eluted in 80% buffer B.

The purified protein was dialyzed against 3 × 1 L of buffer C (50 mM Tris·Cl pH 7.5, 150 mM KCl, 10% glycerol, 1 mM EDTA) to lower the imidazole concentration and remove divalent metal ions. The protein was exchanged into storage buffer D (50 mM Tris·Cl, pH 7.5, 150 mM KCl, 5% glycerol, 1 mM tris(2-carboxyethyl)phosphine(TCEP)) previously treated with 0.05 g/mL of the sodium form of Chelex 100 (Sigma-Aldrich) to remove metals. Purified protein was concentrated, flash-frozen in dry ice/ethanol bath and stored at -80 °C in 100 µL aliquots. Protein concentration was determined from A_{280}, using ε_{280} = 9738 $M^{-1}cm^{-1}$.[132]

Wild type C. jejuni KDO8PS (cjKDO8PS$_{wt}$)

To create a more soluble enzyme form for crystallization, the histidine tag needed to be removed with TEV protease. Cleavage experiments were not successful under a variety of conditions, even at very high TEV protease concentrations. The wildtype cjKDO8PS (cjKDO8PS$_{wt}$) plasmid was produced in our lab by Dr. Naresh Balachandran by introducing a TAA stop codon into the *C*-terminal His$_6$ tagged plasmid obtained from Dr. Martin Young (National Research Council of Canada) using QuikChange mutagenesis, as described previously (Figure 2.2).[98]

```
atgaaaaaaatgatactcattgctggtccttgcgtgatagaaagcaaagatttgatttttt
 M  K  K  M  I  L  I  A  G  P  C  V  I  E  S  K  D  L  I  F
aaagttgctgaacagttaaaaaatttttaatgaaaatccaaatatagaattttatttcaaa
 K  V  A  E  Q  L  K  N  F  N  E  N  P  N  I  E  F  Y  F  K
tcaagttttgataaggccaatcgcacaagtattaattcttttcgaggtcctggtcttgaa
 S  S  F  D  K  A  N  R  T  S  I  N  S  F  R  G  P  G  L  E
gaaggattaaaaattttacaaagcgtaaaagatgaatttggtatgaaaatcttaaccgat
 E  G  L  K  I  L  Q  S  V  K  D  E  F  G  M  K  I  L  T  D
atacacgaaagcaatcaagcaaaccctgtaagtgaagtagctgatgtcttgcaaattcct
 I  H  E  S  N  Q  A  N  P  V  S  E  V  A  D  V  L  Q  I  P
gctttttatgtcgtcaaaccgatttacttgtagccgcagcaaaaactaaggcaaaaatt
 A  F  L  C  R  Q  T  D  L  L  V  A  A  A  K  T  K  A  K  I
aatatcaaaaaaggacaatttttaaacccaagcgatatcaaatacagcgttaaaaaagtt
 N  I  K  K  G  Q  F  L  N  P  S  D  I  K  Y  S  V  K  K  V
ctacaaacccgtggtatagaagatgaaggctatgaagctgctcaaagaaatggtgttttt
 L  Q  T  R  G  I  E  D  E  G  Y  E  A  A  Q  R  N  G  V  F
gtagctgaaagaggggctagctttggctatggaaatttagtagtagatatgcgttcttta
 V  A  E  R  G  A  S  F  G  Y  G  N  L  V  V  D  M  R  S  L
gttatcatgcgtgaatttgctccagttatttttgatgctacccatagcgtacaaatgcca
 V  I  M  R  E  F  A  P  V  I  F  D  A  T  H  S  V  Q  M  P
ggggctgcaggtggaagtagcggagggaaaagcgaatttgtagaacctttagcaagagcg
 G  A  A  G  G  S  S  G  G  K  S  E  F  V  E  P  L  A  R  A
gcagcagccgtaggcatagatggctttttctttgaaacacatattaatccttgcgaggct
 A  A  A  V  G  I  D  G  F  F  F  E  T  H  I  N  P  C  E  A
ttatgcgatggacctaatatgcttaatcttacacgccttaaaaattgcgttaatacatta
 L  C  D  G  P  N  M  L  N  L  T  R  L  K  N  C  V  N  T  L
ctagaaatacaaaatatcataaaggaaaacaaataa
 L  E  I  Q  N  I  I  K  E  N  K  -
```

Figure 2.2. Sequence of wildtype *C. jejuni* KDO8PS (cjKDO8PS$_{wt}$).

The *C*-terminal hexa-histidine tag was removed by introducing a stop codon, TAA (green text) before the His$_6$-tag sequence.

cjKDO8PS$_{wt}$ was expressed as described for cjKDO8PS$_{H6}$.

A four-step purification method for cjKDO8PS$_{wt}$ was developed. The cell pellet was suspended in buffer E (50 mM Tris·Cl, pH 7.0) and the cells were lysed as described above. To the filtered supernatant, ammonium sulphate was gradually added to 60% saturation. The mixture was stirred at 4° C for 1 h, at which time the precipitate containing impurities was removed by centrifugation at 10 000 × g at 4 °C for 20 min. The supernatant was filtered through a 0.45 μm cut-off Acrodisc syringe filter. Ammonium sulphate was gradually added to 80%

saturation and stirred at 4 °C for 1 h. The cjKDO8PS$_{wt}$-containing precipitate was harvested by centrifugation as above, dissolved in a minimal volume of buffer F (50 mM Tris·Cl, pH 7.00, 1 M ammonium sulphate) and loaded onto a Phenyl-Sepharose Fast Flow XK 16/20 column (GE Healthcare) pre-equilibrated with buffer F. The bound protein was washed with 10 column volumes with buffer F, then eluted by decreasing the ammonium sulphate concentration (1 – 0 M) over 12 column volumes, i.e. 100 % buffer F to 100 % buffer E. cjKDO8PS$_{wt}$ eluted at 30% buffer F (300 mM ammonium sulphate), was dialyzed into anion exchange chromatography buffer G (50 mM Tris·Cl, pH 8.5) and loaded onto a preparative Q-Sepharose Fast Flow XK 16/20 column (GE Healthcare) pre-equilibrated with buffer G. The column was washed with 5 column volumes of buffer G, then the protein was eluted with a gradient of 0 – 50% buffer H (50 mM Tris·Cl, pH 8.5, 1 M NaCl). cjKDO8PS$_{wt}$ eluted at 30% buffer H. The pooled protein fractions were dialyzed against buffer G for size exclusion chromatography. The protein was loaded onto a Superose 12 10/300 GL (GE Healthcare Life Sciences) column, and eluted at 1 mL/min in buffer G. Based on SDS-PAGE analysis, pure cjKDO8PS$_{wt}$ was obtained as the higher molecular weight species (Figure 2.4). The pure fractions were dialyzed against buffer I (50 mM Tris-HCl, pH 7.5, 50 mM KCl, 5% glycerol, 1 mM TCEP, 5 mM EDTA) to remove contaminating metal ions. cjKDO8PS$_{wt}$ was finally exchanged into storage buffer J (50 mM Tris·Cl, pH 7.5,

100 mM KCl, 5% glycerol, 1 mM TCEP). Protein concentration was determined from A_{280}, using $\varepsilon_{280} = 6886\ M^{-1}cm^{-1}$ in storage buffer.[132]

2.2.2. A5P synthesis

A5P synthesis was modified from the method of Bednarski and co-workers.[133] The reaction mix consisted of 100 mM PEP, as a potassium salt (Sigma-Aldrich) or tri-ammonium salt (Bio Basic Inc), 400 mM D-arabinose (Sigma-Aldrich), 28 mM KCl, 300 mM $MgSO_4$, 31 mM β-mercaptoethanol, and 12 mM ATP dissolved in 50 mM Tris·Cl, pH 7.6 buffer. The pH of the solution was adjusted to pH 7.6 with a few drops of 10 M KOH. The enzymes; *Saccharomyces cerevisiae* hexokinase (1000 U, 0.1 U/μL) and rabbit muscle pyruvate kinase (250 U, 0.025 U/μL) were added to the reaction mixture. The reaction was incubated at room temperature and reaction progress was monitored by ^{31}P NMR spectroscopy. The reaction was complete after 12 -14 days (Figure S10.4).

A5P was purified with anion exchange chromatography using Q-Sepharose Fast Flow XK 16/20 column pre-equilibrated with 100 mM ammonium formate in 10 mM ammonium bicarbonate, pH 6.2. A5P was eluted by increasing the ammonium formate concentration (100 – 800 mM) over 30 column volumes, with A5P eluting at 300 mM ammonium formate. A5P-containing fractions were pooled and lyophilized before being loaded onto a cation exchange SP-Sepharose High Performance preparative column to remove ammonium ions that would

otherwise have caramelized the A5P product. A5P was eluted with 7 column volumes of water. The A5P concentration was determined by measuring the release of Pi via KDO8P synthesis using cjKDO8PS$_{H6}$ and excess PEP, and also by using alkaline phosphatase-catalyzed phosphate hydrolysis. It was routinely stored at -20°C.

2.2.3. Kinetic parameters for C. jejuni KDO8PS

General assay conditions

Initial velocities to determine the kinetic parameters k_{cat}, $K_{M,A5P}$, $K_{M,PEP}$ and $K_{M,Mn}$ for cjKDO8PS$_{H6}$ and cjKDO8PS$_{wt}$ were generally determined with two substrates' concentrations being held constant and the third being varied. Assays were conducted in reaction buffer (50 mM BTP·Cl, pH 7.5, 150 mM KCl, 1% glycerol, 100 μM TCEP). After incubating the reaction mixture for 2 min at 37 °C, the reaction was initiated by adding the enzyme, typically at 200 nM. The reaction progress was monitored for 3 -7 min by following inorganic phosphate (Pi) production using the Malachite Green/ammonium molybdate assay.[134] For cjKDO8PS$_{H6}$, the fixed substrate concentrations were 1000 μM $MnCl_2$, 500 to 1000 μM PEP, and 200 to 500 μM A5P, depending on the experiment. The kinetic experiments for cjKDO8PS$_{wt}$ were performed in the same manner as for the cjKDO8PS$_{H6}$, except in some experiments the fixed A5P concentration was

increased to 1000 μM. The enzyme concentration in the reaction mix was 200 to 250 nM.

Data fitting

The initial velocity data were fitted initially to the "random A" and ordered mechanisms with the steady state approximation (Figure 2.5) using the software package Dynafit (see the Supporting Information, Table S10.1). These analyses were done by Dr. Berti. Initial velocities are only weakly dependent on the absolute values of the association rate constants (k_1, k_2, etc.) unless they are significantly slower than the diffusion rate limit. Initial velocities, however, are dependent on the ratios of association and dissociation (k_{-1}/k_1, k_{-2}/k_2, etc.) rate constants. The fitting approach was to first scan sets of rate constants, and using the residual sum of squares, select the best sets for further optimization. The association rate constants (k_1, k_2, etc) were then fixed while the dissociation rate constants, plus k_4 (the rate constant for the irreversible chemical step), were optimized. For the "random A" mechanism, 7×10^4 sets of initial estimates were scanned, with association rate constants ranging from 10^3 μM^{-1} s^{-1} (the diffusion rate limit) to 0.01 μM^{-1} s^{-1}. Based on the 100 best sets of initial estimates, a further 1.2×10^5 sets of initial estimates were scanned. The top 500 initial estimates were optimized. Only 6 sets of initial estimates could be fully optimized. The failure of other initial estimates to fully converge was likely a reflection of the fact that the "random A" kinetic mechanism was not correct and resulted in poorly defined

fitted parameters. For the ordered steady-state mechanism, a scan of 4050 sets of initial estimates was enough, and the top 500 was optimized, and the best solutions were selected for further analysis.

Under the rapid equilibrium assumption, eq. **2.1** was used to fit k_{cat} values. To lower the standard errors by, presumably, reducing the covariance between individual K_M values, equation **2.2** was used to fit the specificity constant $k_{cat}/(K_{M,Mn}\,K_{M,PEP}\,K_{M,A5P})$ (fitted as a single parameter) and individual K_M values.

$$\frac{v_0}{[E]_0} = \frac{k_{cat}\dfrac{[Mn][PEP][A5P]}{K_{M,Mn}K_{M,PEP}K_{M,A5P}}}{1+\dfrac{[Mn]}{K_{M,Mn}}+\dfrac{[Mn][PEP]}{K_{M,Mn}K_{M,PEP}}+\dfrac{[Mn][PEP][A5P]}{K_{M,Mn}K_{M,PEP}K_{M,A5P}}} \tag{2.1}$$

$$\frac{v_0}{[E]_0} = \frac{\left(\dfrac{k_{cat}}{K_{M,Mn}K_{M,PEP}K_{M,A5P}}\right)[Mn][PEP][A5P]}{1+\dfrac{[Mn]}{K_{M,Mn}}+\dfrac{[Mn][PEP]}{K_{M,Mn}K_{M,PEP}}+\dfrac{[Mn][PEP][A5P]}{K_{M,Mn}K_{M,PEP}K_{M,A5P}}} \tag{2.2}$$

In order to compare the kinetic parameters determined in this study with literature values, which typically use only the single substrate Michaelis-Menten equation, k_{cat} and K_M values were also fitted to the single substrate Michaelis-Menten equation, eq. **2.3**.

$$\frac{v_0}{[E]_0} = \frac{k_{cat}[S]}{[S]+K_M} \tag{**2.3**}$$

2.2.4. Optimum pH and temperature

cjKDO8PS$_{H6}$'s activity was tested at 37 °C over the pH range 5 to 11. Reactions were carried out in a reaction mixture containing 50 mM buffer, 100 mM KCl, 1 mM $MnCl_2$, 200 μM A5P, and 500 μM PEP. The buffers were; 2-(*N*-morpholino)ethanesulfonic acid (MES, pH 5 - 6), bis-tris propane (BTP, pH 5 - 9), and *N*-cyclohexyl-3-aminopropanesulfonic acid (CAPS, pH 9.5 - 11). The reaction mix was incubated for 2 min at 37 °C, then the reaction started by adding 56 nM enzyme. An pH profile was generated by fitting data into eq. **2.4**, a modified version of the equation used by Jiang et al.[135]

$$\frac{v_0}{[\mathrm{E}]_0} = \frac{k_{\mathrm{cat}} \times 10^{\mathrm{p}K\mathrm{a} - \mathrm{pH}}}{10^{\mathrm{p}K\mathrm{a} - \mathrm{pH}} + 1} \tag{2.4}$$

where pK_a is for the basic descending limb. Because the enzyme denatured at pH < 6.5 (see below), only the basic limb of the pH profile could be fitted. The temperature dependence of activity from 25 – 75 °C for cjKDO8PS$_{H6}$ were tested using 50 mM BTP·Cl, pH 7.5 as the buffer.

2.3. Results

2.3.1. Purification

Histidine tagged C. jejuni KDO8PS ($cjKDO8PS_{H6}$)

$cjKDO8PS_{H6}$ was successfully purified using a Ni^{2+}-loaded chelating-Sepharose column, using step elution with 400 mM imidazole. The purified protein was pure by SDS-PAGE (Figure 2.3), and was stable at concentrations between 30 - 100 µM in the presence of 5% glycerol. The enzyme was stable for two weeks at 4 °C and for months at -80 °C.

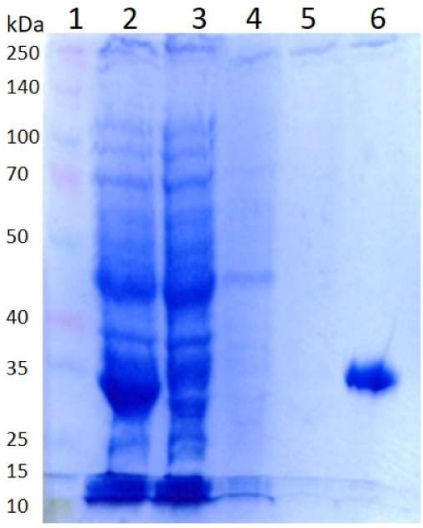

Figure 2.3. 4-13% SDS-PAGE gel of $cjKDO8PS_{H6}$.
Lanes: 1) Molecular weight standards ladder; 2) lysate; 3) column flow-through; 4) buffer A wash; 5) 10 % buffer B wash; 6) Pure fraction eluted at 80 % buffer B.

Wild type C. jejuni KDO8PS ($cjKDO8PS_{wt}$)

$cjKDO8PS_{wt}$ was purified using the traditional methods for untagged proteins. This included ammonium sulphate fractionation, hydrophobic interaction

chromatography (Figure S10.1), anion exchange chromatography (Figure S10.2), and size exclusion chromatography (Figure S10.3). The enzyme was fairly stable through all these steps. Highly concentrated fractions of cjKDO8PS$_{wt}$ and cjKDO8PS$_{H6}$ had a pinkish-red colour, likely due to iron bound to KDO8PS.[51] The purity by SDS-PAGE of enzyme fractions at each purification steps are shown in Figure 2.4. Purification yield and activity at each step is presented in Table 2.1.

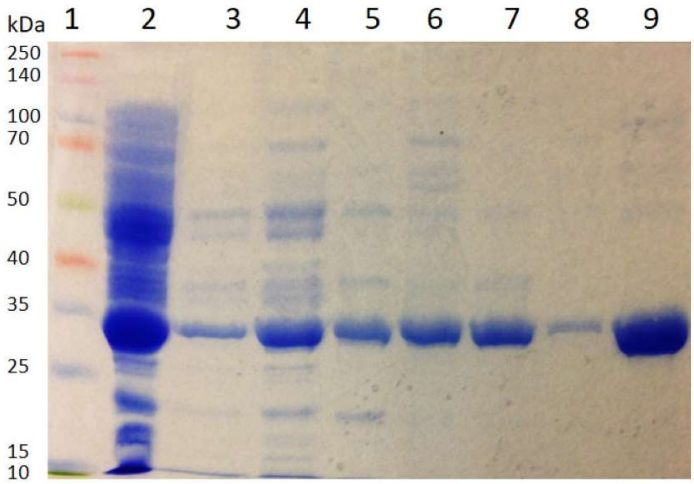

Figure 2.4. 4-13% SDS-PAGE gel of cjKDO8PS$_{wt}$.

Lanes: 1) Molecular weight standards ladder; 2) cell lysate; 3) 0 - 60% $(NH_4)_2SO_4$ fractionation supernatant; 4) 60 - 80% $(NH_4)_2SO_4$ fractionation pellet; 5) Phenyl Sepharose fraction; 6) Q-Sepharose anion exchange purification; 7 & 8) Size exclusion chromatography (tetrameric peak) for assays; 9) Size exclusion chromatography (high molecular weight peak) for crystallography.

Table 2.1. Purification of wildtype cjKDO8PS.

The purification involved ammonium sulphate precipitation, hydrophobic interaction chromatography on Phenyl-Sepharose, anion exchange chromatography on Q-Sepharose, and size exclusion chromatography on Superose 12.

Fraction	Amount of protein (mg)	Yield (%)	Specific activity (s^{-1})[a]	Purification (fold)
Cell lysate	166	100	1.1	1
60 % ammonium sulphate fractionation	50	30	2.1	2
80 % ammonium sulphate fractionation	34	20	3.1	3
Hydrophobic Chromatography	18	11	5	5
Anion Exchange Chromatography	13	8	4	4
Size exclusion Chromatography	5	6	2.1[b]	2

[a] Specific activity was measured with the Malachite green/ammonium molybdate assay and the concentration of the enzyme was measured with the Pierce™ BCA Protein Assay Kit (Thermo Scientific).

[b] The size exclusion fraction rate is 2-fold lower that the in the two preceding steps, presumably because the purification protocol is lengthy and this might lead to reduced stability. The protein is effectively pure enough for assay after the hydrophobic interaction step, but for crystallography it needed further purification.

2.3.2. cjKDO8PS$_{wt}$ kinetic mechanism: Order of binding.

Previous studies of KDO8PS from other bacteria showed an ordered sequential bi bi kinetic mechanism in which the substrate PEP binds before A5P and the product Pi dissociates before KDO8P.[40,43,97] However, these studies did not examine the place of metal binding in the kinetic mechanism. Therefore, the first question about the kinetic mechanism that must be answered is whether metal ion binding is random or ordered. Once the orderedness of the kinetic mechanism is established, it also possible to test whether the steady state approximation (i.e.,

d[EABC]/dt = 0) is required, or if the rapid equilibrium assumption is sufficient. Our group recently addressed the same questions with the homologous enzyme *E. coli* DAHPS, and showed that metal ion binding was ordered, occurring before PEP binding, and that the rapid equilibrium assumption was sufficient to model the reaction.[98] The orderedness of sequential ter ter mechanisms can be determined from the substrate concentration dependence only,[96] unlike sequential bi bi mechanisms, which also require product concentrations (which act as inhibitors) to be varied. The kinetic mechanism was first examined for cjKDO8PS$_{wt}$. The strategy for determining the kinetic mechanism was to first fit the experimental initial velocities with the fewest possible assumptions, that is, random order of metal binding ("random A" kinetic mechanism) and the steady state approximation. Once the data was fitted to that model, it was examined to see which simplifications (ordered metal binding, rapid equilibrium assumption) were supported by the data. The "random A" model (Figure 2.5, black + blue pathways), which allowed metal binding to occur at any step before catalysis, was created. The chemical step and all product release steps were combined into one constant, k_4, since the KDO8PS reaction is irreversible after the chemical steps.[86] The enzymology software package Dynafit was used to fit the experimental data.[124] When using the steady state approximation to fit experimental initial velocities, Dynafit automatically derives the rate equations for the kinetic mechanism under investigation using the King-Altman method,[124] then fits the kinetic constants to the model.

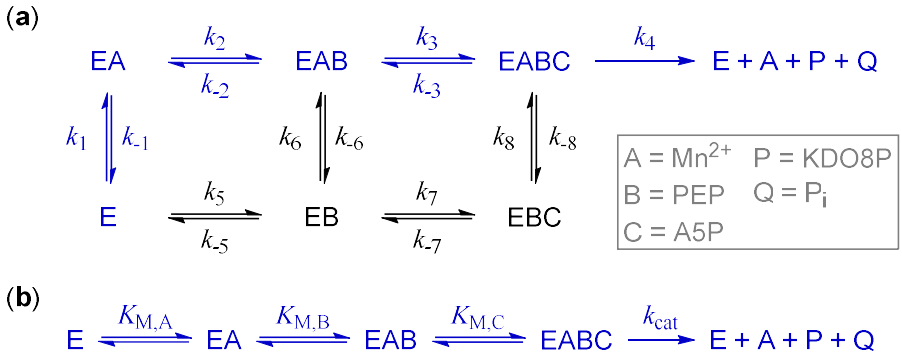

Figure 2.5. cjKDO8PS sequential ter ter kinetic mechanism.

(a) Under steady state kinetic mechanism assumption PEP binds first then A5P. Mn^{2+} binding can be ordered (blue) or random (black). (b) Rapid equilibrium ordered kinetic mechanism.

Data fitting for $cjKDO8PS_{wt}$ was done in two stages in order to account for the fact that the association rate constants (k_1, k_2, k_3…) are often so fast that they are not well defined by the initial velocities. That is, calculated initial velocities are not strongly dependent on the absolute values of the association rate constants, but rather depend sensitively on the ratios of association to dissociation rate constants (k_{-1}/k_1, k_{-2}/k_2, k_{-3}/k_3, etc.). Thus, the first stage of fitting was to scan the initial estimates and select those that gave the lowest residual errors. The association rate constants were then fixed while the dissociation rate constants (k_{-1}, k_{-2}, k_{-3}, etc.) and k_4 were optimized. For the "random A" mechanism, 7×10^4 sets of initial estimates were scanned, with association rate constants ranging from the diffusion rate limit, 10^3 μM^{-1} s^{-1}, to 0.01 μM^{-1} s^{-1}. Based on the 100 best sets of initial estimates, a further 1.2×10^5 set of initial estimates over a narrower range were scanned. The top 500 initial estimates were then optimized. Only 6 sets of initial estimates out of 500 fully converged (Table S10.2). The failure of most

initial estimates to fully converge was likely a reflection of the fact that if, in reality, the kinetic mechanism is ordered, then the rate constants in the non-ordered part of the kinetic mechanism (black type in Figure 2.5a) will not be defined by the experimental data, leading to a convergence failure in the fitting algorithm.

The six sets of converged parameters for the steady state "random A" kinetic mechanism were not well defined for many of the parameters, as might be expected when fitting too many parameters to the data. The % coefficient of variation (%CV) values were large. %CV is the standard deviation of each fitted parameter, expressed as a percent of the parameter's value. The average %CV for each set of fitted parameters was > 10^4%. These large %CV values presumably reflect the large covariance between fitted parameters, plus the fact that, because the kinetic mechanism is adequately modelled by the ordered mechanism (see below), large variations in the parameters in the off-pathway part of the mechanism (Figure 2.5a, black type) had little or no effect on the calculated initial velocities, meaning that their %CV values were extremely large.

In every case $K_{d,A}$ (k_{-1}/k_1), the equilibrium dissociation constant for Mn^{2+} binding to the free enzyme, was lower than $K_{d,B}$ (k_{-5}/k_5), the equilibrium dissociation constant for PEP binding, though in some cases by only a factor of 1.6. More importantly, though, k_1 was 100- to 1000-fold higher than k_5. That implies that PEP binding to free enzyme is vanishingly slow compared to Mn^{2+} binding, and therefore that the only kinetically significant pathway is ordered

binding, with Mn^{2+} binding to free enzyme before PEP binds to the E·Mn^{2+} complex (Figure 2.5a, blue pathway).

Given the evidence that the sequential ordered pathway is sufficient to explain the experimental data, the initial velocities were then fitted to the sequential ordered ter ter kinetic mechanism while retaining the steady state approximation. Because of the smaller number of microscopic rate constants to be fitted, a scan of 4050 sets of initial estimates was sufficient, followed by optimization of the top 500 (Table S10.3). From these optimizations, those with the lowest residual sum of squares (SS_{rel}) were selected for further analysis. The residual sum of squares reflects the differences between the experimental and fitted data points, and SS_{rel} is normalized to the lowest sum of squares observed among the optimizations. That is, $SS_{rel} = 1$, by definition, is for the "best" optimization (Table S10.3). The range of SS_{rel} values among the top 100 optimizations was small, ranging from 1.00 to 1.35, versus $SS_{rel} = 6.4$ for the 500^{th} best optimization. While SS_{rel} is useful as a rough guide for selecting optimized parameters, the %CV values are more important.[124] By this criterion, solution set #4 had both the lowest average and lowest maximal %CV, and was selected as the best values for the sequential ordered steady state ter ter kinetic mechanism (Table 2.2).

Comparing the fits to the "random A" and ordered mechanisms strongly supports the ordered binding mechanism where Mn^{2+} binds first, then PEP,

followed, in turn, by A5P. This does not absolutely preclude any contribution from the "random A" pathway; it only shows that the experimental data were adequately modelled by the ordered kinetic mechanism. If there is a contribution from the "random A" pathway, it is modest compared to the ordered pathway. This also does not preclude ligand binding off the ordered pathway. Specifically, ITC titrations show that A5P can bind to free enzyme in the absence of Mn^{2+} and PEP (Section 3.3).

2.3.3. Steady state versus rapid equilibrium model

Having established that the initial velocity data for cjKDO8PS$_{wt}$ is adequately explained with an ordered steady state mechanism instead of the "random A" mechanism, the next question is whether it is possible to further simplify the mechanism by making the rapid equilibrium assumption. That is, instead of assuming that d[EABC]/dt = 0, assume that substrate binding is in equilibrium in each step (Figure 2.5b). For this to be true, substrate association and dissociation must be fast relative to k_{cat}. If the rapid equilibrium assumption is true, then following conditions will be observed in the steady state kinetic parameters: (1) $K_{M,A}(ss) << K_{i,A}(ss)$, (2) $K_{M,B}(ss) << K_{i,B}(ss)$ and (3) the dissociation rate constants are much greater than k_{cat}.[96] The steady state kinetic parameters for cjKDO8PS$_{wt}$ matched these criteria (Table 2.2), with $K_{i,A}(ss)/K_{M,A}(ss) = 560$, and $K_{i,B}(ss)/ K_{M,B}(ss) = 240$. The dissociation rate constants for A and B ($k_{-1} = 80\ s^{-1}$, $k_{-2} = 660\ s^{-1}$) were much greater than $k_{cat}(ss)$

= 2.4 s^{-1}. C's dissociation rate constant, k_{-3} = 21 000 s^{-1}, was also much greater than k_{cat}(ss), though the rapid equilibrium assumption does not require that k_{-3} >> k_{cat}(ss).[96] Taken together, the fitted steady state kinetic parameters demonstrated that the rapid equilibrium kinetic assumption was valid for cjKDO8PS$_{wt}$.

Once the rapid equilibrium assumption is made, it becomes possible to use analytical expressions to fit the kinetic parameters directly to equations **2.1** and **2.2** using nonlinear least squares regression, as implemented in the software package Grafit (Table 2.2). Equations **2.1** and **2.2** are identical, except that in eq. **2.2** the specificity constant $k_{cat}/(K_{M,Mn}K_{M,PEP}K_{M,A5P})$ was fitted as a single parameter, rather than fitting k_{cat} and the individual K_M values separately (though the individual K_M values were still fitted in the denominator). Fitting the specificity constant as a single parameter lowered the standard errors without changing the fitted values by (presumably) reducing the covariance between individual K_M values. The fitted kinetic constants matched the experimental data well (Figure 2.6).

2.3.4. Single substrate Michaelis-Menten kinetic parameters

The initial velocities were also fitted to the single substrate Michaelis-Menten equation (eq. **2.3**) for each substrate (Table 2.2). This equation is not appropriate for the KDO8PS reaction, but because it has often been used

(incorrectly) in the literature, it is useful for comparison to other reported kinetic constants.

Table 2.2. cjKDO8PS$_{wt}$ kinetic constants for a sequential ordered ter ter mechanism.

Constant[a]	Value
Steady State[b]	
k_{cat}(ss)	2.4 ± 0.1 s^{-1}
$K_{M,Mn}$(ss)	0.20 ± 0.01 μM
$K_{M,PEP}$(ss)	2.4 ± 0.1 μM
$K_{M,A5P}$(ss)	21 ± 13 μM
$K_{i,Mn}$(ss)	130 ± 70 μM
$K_{i,PEP}$(ss)	580 ± 450 μM
Rapid Equilibrium [c]	
k_{cat}(re)	2.4 ± 0.1 s^{-1}
$K_{M,Mn}$(re)	130 ± 30 μM
$K_{M,PEP}$(re)	650 ± 140 μM
$K_{M,A5P}$(re)	21 ± 4 μM
$k_{cat}/(K_{M,Mn}K_{M,PEP}K_{M,A5P})$	(1.4 ± 0.2) × 10^{12} M^{-3} s^{-1}
Single Substrate [d]	
k_{cat}(1s)	2.1 ± 0.3 s^{-1}[e]
$K_{M,Mn}$(1s)	16 ± 3 μM
$K_{M,PEP}$(1s)	48 ± 7 μM
$K_{M,A5P}$(1s)	36 ± 6 μM

[a] Description (ss) indicates steady state approximation, (re) indicates rapid equilibrium assumption (eq. **2.1**), and (1s) indicates single substrate Michaelis−Menten equation (eq. **2.3**).

[b] Fitted to the ordered kinetic mechanism (Figure 2.5a) with the steady state approximation, using Dynafit (Courtesy of Dr. Berti),[124] with the King−Altman parameters derived from the fitted microscopic rate constants (Table S10.3).

[c] Fitted to eq. **2.1** using GraFit,[136] where the kinetic parameters obtained using Dynafit were used as initial guesses and optimized on GraFit.

[d] Fitted to the single substrate Michaelis−Menten equation (eq. **2.3**).

[e] Average of independent k_{cat} values for each substrate.

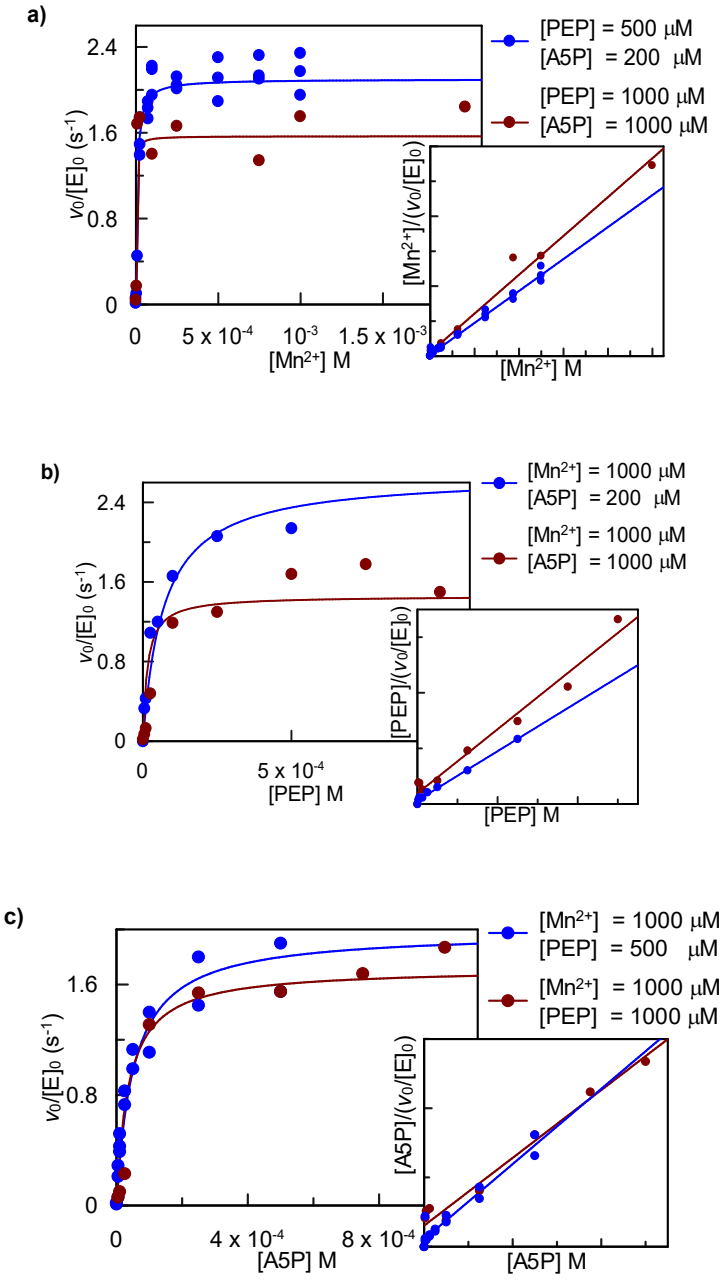

Figure 2.6. Kinetic constants for cjKDO8PS$_{wt}$ rapid equilibrium ordered sequential ter ter kinetic mechanism.

Initial velocity vs. [substrate] for: a) Mn^{2+}, b) PEP, and c) A5P. The curves represent the experimental data fitted to eq. **2.1.** Each colour coded curve represents data obtained where the concentrations of two of the substrates were fixed at two different concentrations (see legend). The inset graphs are Hanes plots, [S]/(v_0/[E]$_0$) vs. [S].

2.3.5. cjKDO8PS$_{H6}$ kinetic parameters.

Based on the cjKDO8PS$_{wt}$ results, the initial velocity data for cjKDO8PS$_{H6}$ were fitted to equations **2.1** and **2.2** (Table 2.3, Figure 2.7).

Table 2.3. cjKDO8PS$_{H6}$ kinetic constants for a sequential ordered ter ter mechanism.

Constant[a]	Value
Rapid Equilibrium [a]	
k_{cat}(re)	1.2 ± 0.1 s^{-1}
$K_{M,Mn}$(re)	6.4 ± 1.5 μM
$K_{M,PEP}$(re)	899 ± 75 μM
$K_{M,A5P}$(re)	14 ± 1 μM
$k_{cat}/(K_{M,Mn}K_{M,PEP}K_{M,A5P})$	(1.4 ± 0.1) × 10^{13} M^{-3} s^{-1}
Single Substrate [b]	
k_{cat}(1s)	1.2 ± 0.1 s^{-1} [c]
$K_{M,Mn}$(1s)	2.8 ± 0.5 μM
$K_{M,PEP}$(1s)	86 ± 16 μM
$K_{M,A5P}$(1s)	19 ± 6 μM

[a] (re) indicates rapid equilibrium assumption (eq. **2.1, 2.2**) fitted to the ordered kinetic mechanism (Figure 2.5a) with the rapid equilibrium assumption, using GraFit.[136]

[b] (1s) indicates fitting to the single substrate Michaelis−Menten equation (eq. **2.3**).

[c] Average of independent k_{cat} values for each substrate.

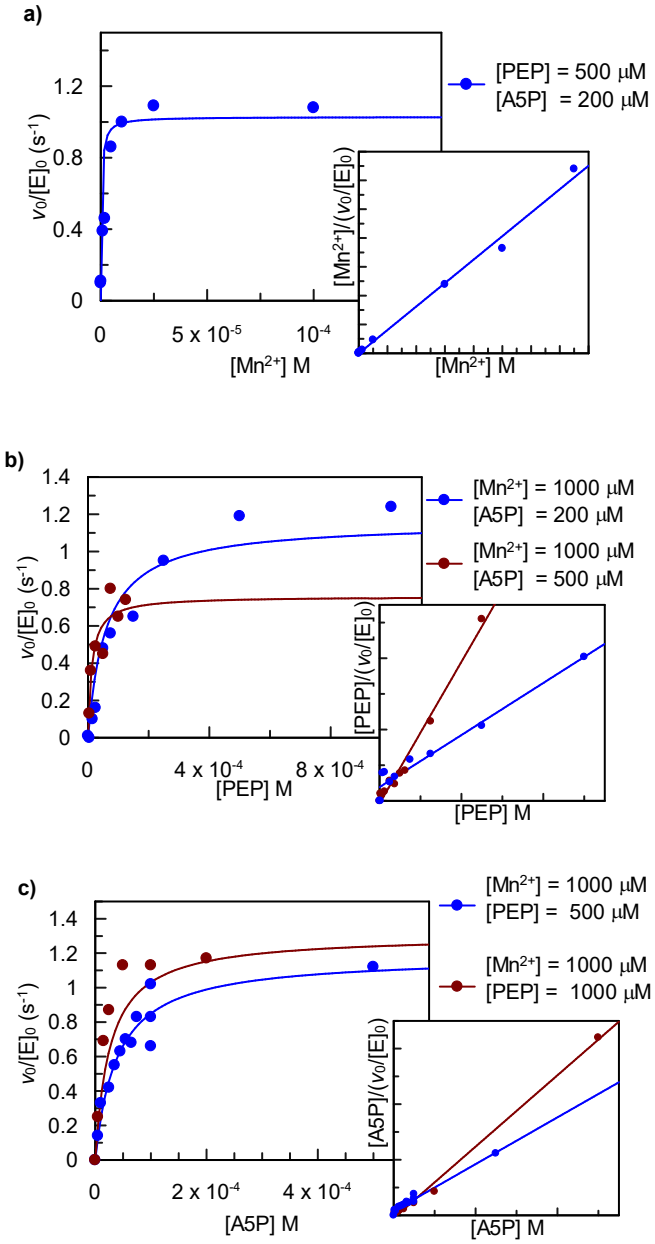

Figure 2.7. Kinetic constants for cjKDO8PS$_{H6}$ with a rapid equilibrium ordered sequential ter ter kinetic mechanism.

Initial velocity vs. [substrate]: a) Mn^{2+}, b) PEP, and c) A5P. The curves represents the experimental data fitted to eq. **2.1**, **2.2**. Each colour coded curve represents data obtained where the concentrations of two of the substrates were fixed at two different concentrations (see legend).

2.3.6. pH dependence

A pH profile of cjKDO8PS$_{H6}$ activity was generated from pH 5 to 11 using K·MES, BTP·Cl and CAPS·Cl for the pH ranges; 5 - 6, 5 - 9 and 9.5 - 11, respectively. The pH profile was determined at saturating substrate concentrations at pH 7. Thus, at pH 7 the rate was determined by k_{cat}. At high pH values, if the K_M values increased enough that the substrate concentrations were no longer saturating, then the decrease in observed rates may be due to some combination of decreased k_{cat} and/or increased K_M. Since our goal was to find out the conditions where the enzyme was most active, there was no need to distinguish between changes in k_{cat} and K_M. The pH optimum curve follows typical bell-shaped curve yielding an optimum pH in the range 7 − 8 (Figure 2.8a). There was a sharp drop in activity below pH 6.5 (red data points) which was a reflection of enzyme denaturation, rather than the enzyme's protonation state. This was shown using a Selwyn plot[137] to detect enzyme inactivation. In a Selwyn plot, the product concentration, [P], is plotted as a function of $[E]_0$×time, and the reaction is run at different $[E]_0$'s. If there is no time-dependent enzyme inactivation, then reactions at different enzyme concentrations will give superimposable plots of [P] versus $[E]_0$×time. However, if there is time-dependent enzyme inactivation, then the effects of inactivation will be larger for lower $[E]_0$ reactions, which take longer to reach a given [P] value, and the plots will not be superimposable. At pH 6.0, there was clearly time-dependent enzyme inactivation, as reaction curves run at 50 to 400 nM cjKDO8PS$_{H6}$ were not superimposable (Figure 2.8b). The half-life of

enzyme inactivation was obtained by fitting the data to a reaction progress curve eq. **2.5**:

$$[\mathrm{P}] = \left(\frac{v_i - v_f}{k}\right) * (1 - e^{-k*\mathrm{Et}}) + \mathrm{offset} \quad (2.5)$$

where [P] is the reaction product concentration ($[P_i]$), v_i and v_f are initial and final velocities, respectively; k is the inactivation rate constant, Et denotes $[E]_0 \times$ time, and offset represents the upper limit of product concentration. The rate constant for inactivation of 100 nM cjKDO8PS$_{H6}$ was 0.0093 ± 0.0004 s^{-1}, which corresponds to an inactivation half-life ($t_{1/2} = 0.693/k$) of 75 ± 3 s.

The basic limb had a fitted pK_a value of 9.8 ± 0.1 obtained from fitting the activity data to eq. **2.4**. A pK_a value of 9.8 is closest to the unperturbed pK_a values of the Lys (10.6) or Tyr (10.5) sidechains, and significantly above Cys (8.3) or His (6.5). The residue K120 in cjKDO8PS (Figure 2.13) is aligned with K124 and K186, residues that are proposed to act as a general acid catalyst in promoting phosphate group departure during breakdown of the tetrahedral intermediate in *A. aeolicus* KDO8PS[138] and in DAHPS[98], so it is a good candidate for the residue responsible for the pH dependence of cjKDO8PS$_{H6}$'s activity. Substrate ionizations are not likely to contribute to the basic limb of the pH profile since the most basic pK_a in PEP and A5P will be the second ionization of the phosphate groups, which typically have pK_a values of 5.7 to 6.8.[95]

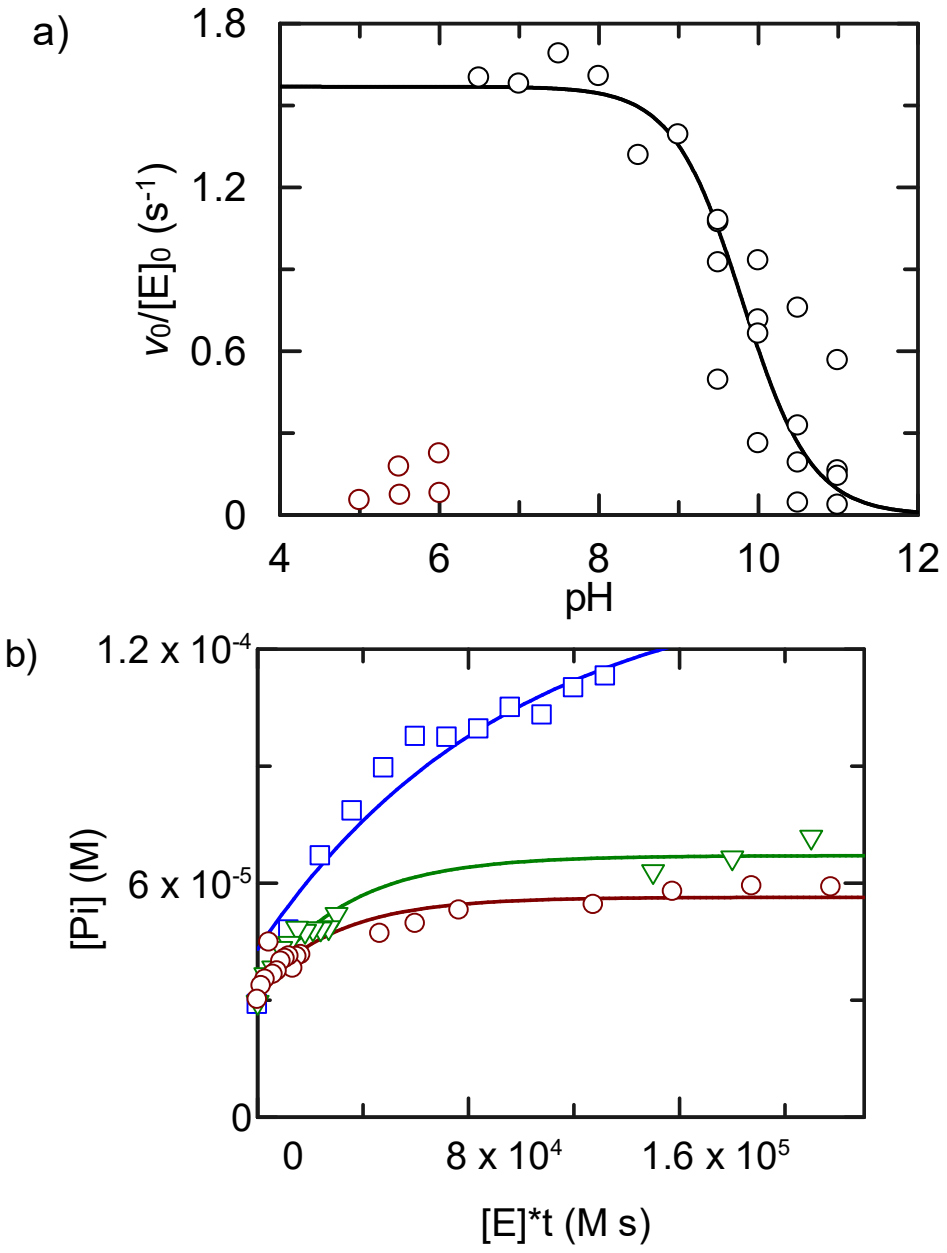

Figure 2.8. pH optimum investigation of cjKDO8PS$_{H6}$.

(a) pH profile of cjKDO8PS$_{H6}$ activity. The buffers used were; K·MES (pH 5 - 6), (BTP·Cl (pH 5 - 9) and CAPS·Cl (pH 9.5 -11). The basic limb had pK_a = 9.8 ± 0.1. (b) A Selwyn plot to test for enzyme denaturation during the assay at pH 6.0. cjKDO8PS$_{H6}$ inactivation was concentration-dependent: 400 nM (blue), 100 nM (green), 50 nM (maroon). Reaction conditions: 1 mM $MnCl_2$, 500 µM PEP, 400 µM A5P, in reaction buffer containing 50 mM BTP·Cl, pH 6.0, at 37 °C.

2.3.7. Temperature dependence

A temperature profile for cjKDO8PS$_{H6}$ activity was generated using BTP·Cl buffer at pH 7.5 (Figure 2.8a). There was an exponential increase in rate for every 10 °C increase in temperature, but the rate dropped drastically at higher temperatures. This profile is consistent with most enzyme temperature profiles. cjKDO8PS$_{H6}$ was optimally active at 60 - 65 °C. Plotting ln(k_{cat}) vs. 1/T according to the Arrhenius equation[96] gave an energy of activation of 20 ± 1 kcal mol^{-1} (Figure 2.9a, inset). This value is in good agreement with an energy of activation of 15 kcal mo1^{-1} reported for *E. coli* KDO8PS[30] and of 13.3 kcal mol^{-1} for *A. aeolicus* KDO8PS[69], and presumably relates to the energy of hydrolysis of PEP.[30]

The half-life of inactivation at 53 °C was obtained by fitting the [P] as a function of time in the presence of 100 nM cjKDO8PS$_{H6}$ (eq. **2.5**, Figure 2.9b). The PEP, A5P and Mn^{2+} concentrations were kept at 500 μM, 400 μM and 1 mM, respectively. The inactivation constant was (100 ± 7) × 10^{-5} s^{-1} which corresponds to an inactivation half-life ($t_{1/2} = 0.693/k$) of 12 ± 1 min.

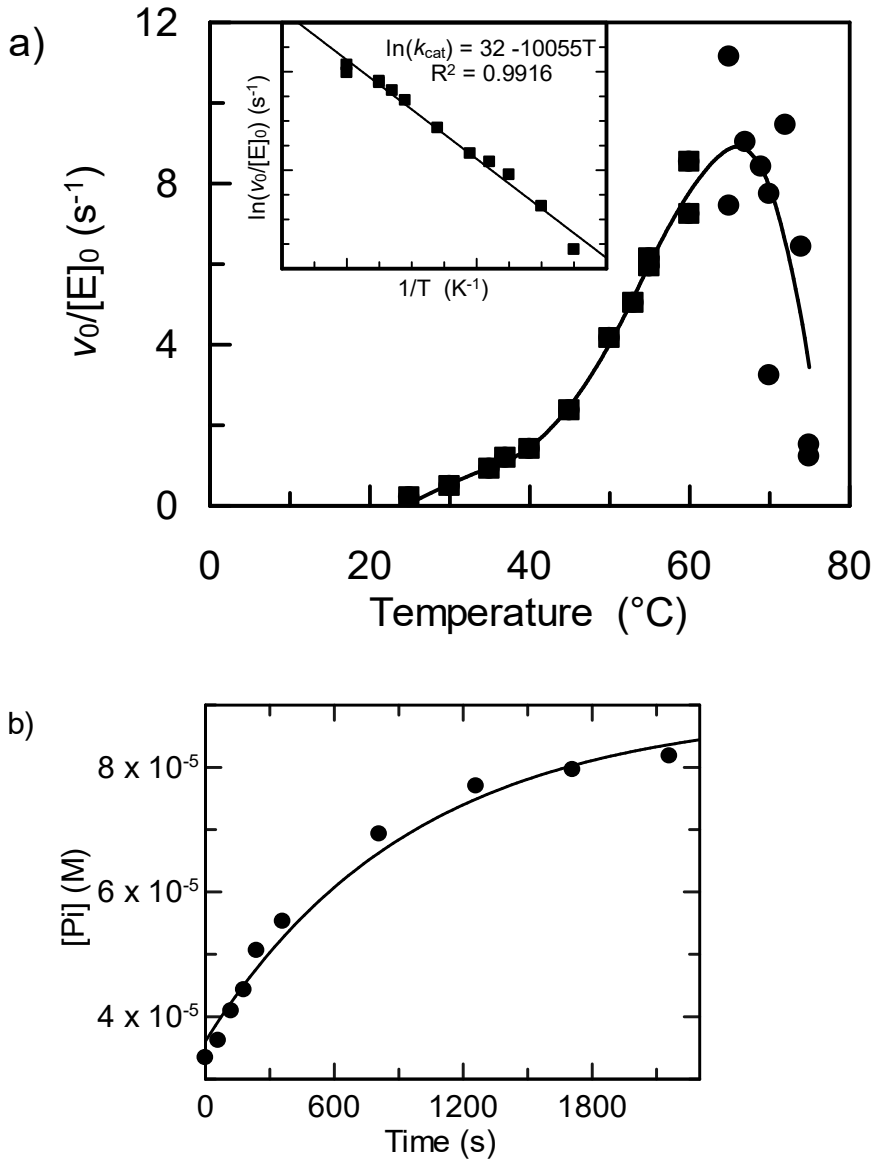

Figure 2.9. Temperature optimum investigation of cjKDO8PS$_{H6}$.

(a) Optimum temperature activity profile of cjKDO8PS$_{H6}$. Enzyme activity was assayed in 50 mM BTP·Cl pH 7.5 using the general assay conditions. cjKDO8PS$_{H6}$ was optimally active at 60 – 65 °C. The solid line was not a fit of the data but it is meant to guide the eye to the data trend. The inset is plot of ln(k_{cat}) versus 1/T for the ascending limb of the temperature optimum profile (squares). The slope of the linear curve was used to estimate the energy of activation E_a by the Arrhenius equation.[96] (b) Thermo-inactivation assay was done at 53 ° C where PEP, A5P and Mn^{2+} concentrations were kept at 500 µM, 400 µM and 1 mM, respectively. The half-life of thermo-inactivation was 12 ± 1 min.

2.3.8. Metal dependence

Unlike DAHPS and NeuB, which are both obligatorily metal-dependent, KDO8PSs occur in both metal-independent (Class I) and metal-dependent (Class II) forms. Amino acid sequence alignment of the β_1 strand and $\beta_1\alpha_1$ loop of KDO8PS and DAH7PS leads to the prediction that cjKDO8PS would be a metal-dependent enzyme due to the presence of the metal-binding Cys residue, C8 which corresponds to C11 in metal-dependent aaKDOPS.[52] As such, cjKDO8PS$_{H6}$ and cjKDO8PS$_{wt}$ were characterized with respect to metal dependence. Metal dependence was tested using the general enzyme assay conditions, i.e. using reaction buffer 50 mM BTP·Cl, pH 7.5, 150 mM KCl, 1% glycerol, 200 μM A5P, and 500 μM PEP. Both enzymes were extensively demetallated with 10 mM EDTA overnight, before rate assays. With cjKDO8PS$_{H6}$ divalent metal ions were tested at 1 mM at room temperature. Control assays with no added metal or 1 mM EDTA were also conducted. With cjKDO8PS$_{wt}$ the concentrations were 1 mM for Mn^{2+}, Ni^{2+} and Cd^{2+}, 200 μM Co^{2+} and Cu^{2+}, and 2 mM Mg^{2+}, and the assays were conducted at 37 °C. The activities are reported relative to that with Mn^{2+}. In the presence of 1 mM EDTA there is no activity, confirming that both cjKDO8PS$_{H6}$ and cjKDO8PS$_{wt}$ are metal-dependent. Activity was restored in the presence of divalent metals in the order (from highest to lowest): $Co^{2+} > Ni^{2+} \approx Fe^{2+} > Mn^{2+} > Mg^{2+} \approx Ca^{2+} \approx Cd^{2+} > Zn^{2+}$ for cjKDO8PS$_{H6}$ (Figure 2.10, top). For cjKDO8PS$_{wt}$ the order of activity was: $Mn^{2+} \approx Co^{2+} \approx Ni^{2+} > Mg^{2+} > Cu^{2+}$ (Figure

2.10, bottom). For cjKDO8PS$_{H6}$ there was no activity with Zn^{2+} and Cu^{2+} at 1 mM concentrations whereas with cjKDO8PS$_{wt}$, Cu^{2+} activation was observed at 200 μM. Both cjKDO8PS$_{H6}$ and cjKDO8PS$_{wt}$ had a pinkish-red colour during purification which was removed during dialysis with EDTA. This is likely due to bound endogenous metal, presumably Fe^{2+} given the colour and the fact that Fe^{2+} is one of the metal ions that gave the highest activity for cjKDO8PS$_{H6}$, suggesting it could be the endogenous metal ion used in vivo. *A. aeolicus* KDO8PS[51] and *A. pyrophilus* KDO8PS[47] are metal-dependent enzymes that have been purified with bound iron and zinc, and possess a pinkish colour. Reactivation of cjKDO8PS with Zn^{2+} and Cu^{2+} is likely concentration dependent, such that at 1 mM Cu^{2+}, cjKDO8PS$_{H6}$ was inactivated while at 200 μM Cu^{2+} cjKDO8PS$_{wt}$ was activated. Mn^{2+} was used for all assays because it was more stable in the assay conditions and was less inhibitory at higher concentrations.

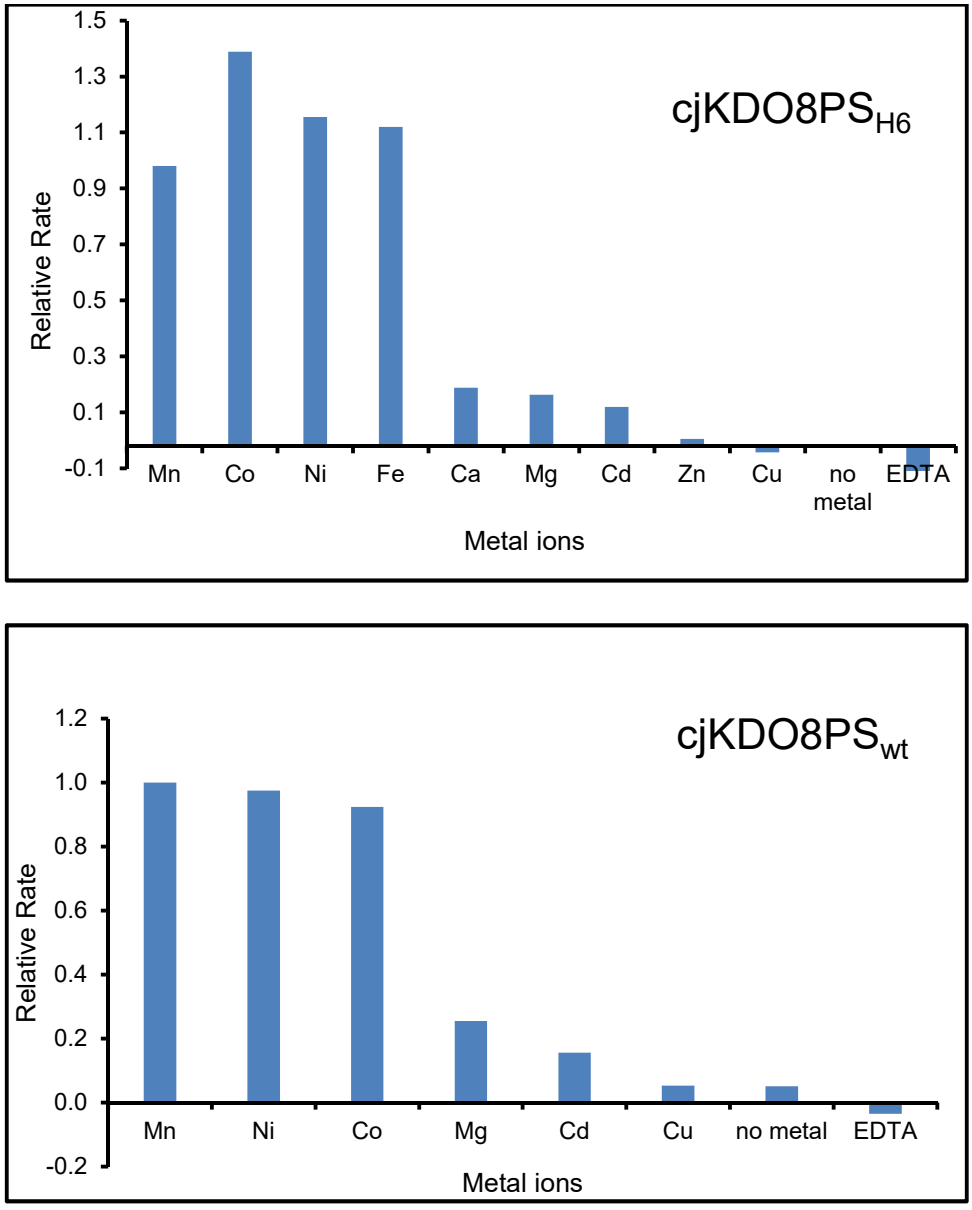

Figure 2.10. Divalent metal ion activation cjKDO8PS$_{H6}$ and cjKDO8PS$_{wt}$.

Both enzymes were exhaustively demetallated with EDTA before metals were added. Rates are reported relative to 1 mM Mn^{2+}.

2.3.9. Oligomeric structure

The native molecular weight, and therefore the oligomeric structure for cjKDO8PS was determined using a Superose 12 10/300 GL column with an elution buffer of 50 mM Tris·Cl, pH 7.0, 100 mM KCl. The enzyme injection volume and concentration were typically 50 μL and 40 μM, respectively. The column was run at 1 mL/min and protein elution was monitored by its A_{280}. A standard curve was produced by plotting log(mol. wt.) of standard proteins versus V_e/V_0, where V_e is the elution volume and V_o is the void volume, at which Blue Dextran eluted.

The molecular weights of cjKDO8PS$_{H6}$ and cjKDO8PS$_{wt}$ were interpolated from the standard curve (Figure 2.11), and were 120 ± 13 kDa for cjKDO8PS$_{H6}$ and 123 ± 3 kDa for cjKDO8PS$_{wt}$. Using the monomeric molecular weights from the amino acid sequences of 32 675 Da for cjKDO8PS$_{H6}$ and 29 392 Da for cjKDO8PS$_{wt}$, the number of subunits per oligomer were 3.7 ± 0.4 and 4.2 ± 0.1 for cjKDO8PS$_{H6}$ and cjKDO8PS$_{wt}$, respectively. Thus, both enzymes are homotetramers in solution. This is consistent with the fact that all bacterial KDO8P synthases characterized to date are homotetramers.[38–41]

Table 2.4. Oligomeric structure of cjKDO8PS.

Protein standards and cjKDO8PS molecular weights and elution volumes on a Superose 12 10/300 GL size exclusion column.

Protein ID	Molecular Weight (kDa)	V_e/V_0
Blue dextran 200	2000	1.00
Ferritin	440	1.27
catalase	232	1.43
Aldolase	158	1.47
$cjKDO8PS_{wt}$	123 ± 3	1.51
$cjKDO8PS_{H6}$	120 ± 13	1.52
Ovalbumin	45	1.64
Ribonuclease	13.7	1.94

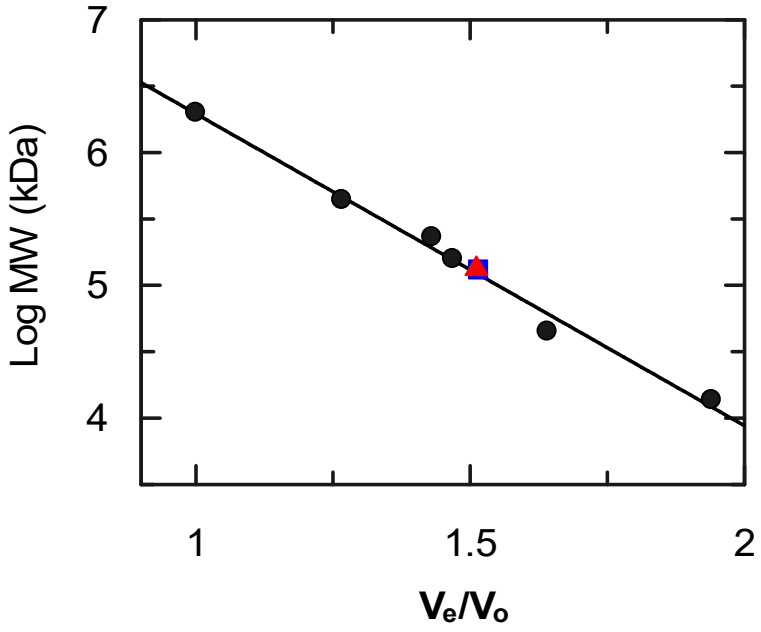

Figure 2.11. Standard curve of log(mol. wt.) versus elution volume for cjKDO8PS.

The molecular weight of cjKDO8PS was determined by plotting log(mol. wt.) of protein standards against V_e/V_o, the ratio of elution volume (V_e) to the void volume (V_o) at which Blue Dextran eluted (Table 2.4). The analysis was done in a Superose 12 10/300 GL column at 1 ml/min using 50 mM Tris·Cl pH 7.0, 100 mM KCl buffer as the mobile phase. $cjKDO8PS_{H6}$ (blue) and $cjKDO8PS_{wt}$ (red) eluted at V_e/V_0 = 1.52 and 1.51, respectively.

2.4. Discussion

2.4.1. cjKDO8PS expression and purification

cjKDO8PS$_{H6}$ was the first form of the protein to be prepared. When it was not possible to crystallize the His$_6$-tagged form, the cjKDO8PS$_{wt}$ form was also prepared. Its kinetic mechanism was analyzed in detail (see below). There were some modest differences in the kinetic parameters for cjKDO8PS$_{H6}$, but overall the proteins were very similar and cjKDO8PS$_{H6}$ was used more often because it was easier to purify. During purification, highly concentrated cjKDO8PS$_{H6}$ and cjKDO8PS$_{wt}$ aquired a pinkish colour, indicative of endogenously bound metal ion, presumably iron. Concentrated metal-dependent *A. aeolicus* KDO8PS purified from *E. coli* attained a pinkish coloured attributed to bound iron.[40,139] This suggests that, for metal-dependent KDO8PSs, a metal-bound enzyme form is stable.

2.4.2. cjKDO8PS kinetic mechanism

When discussing kinetic constants, it is important to recognize that the meaning of K_M is different when using the steady state approximation (ss) versus when the rapid equilibrium assumption (re) is used. K_M(ss) is the apparent K_M value for each substrate in the presence of infinitely high concentrations of the other two. The first substrates to bind can be "trapped" on the enzyme by the later binding substrates, which leads to K_M(ss) values that are much less than the

substrates' true K_d values. K_i(ss) is the substrate's (notional) inhibition constant for the reverse reaction, and is equivalent to the substrate's K_d value in most mechanisms.[98] Because the KDO8PS reaction is irreversible, K_i(ss) values are not directly experimentally accessible. In a rapid equilibrium mechanism, K_M(re) values reflect each substrate's K_d value. If the rapid equilibrium assumption is valid, then the K_i(ss) and K_M(re) values for each substrate should be equal, while the K_M(ss) values are less than either. The single substrate Michaelis-Menten equation has the same form regardless of whether the steady state approximation of the rapid equilibrium assumption is being made, so it is not possible to distinguish from the fitted K_M(1s) values which assumption holds true. Because initial velocities are determined in the presence of high fixed substrate concentrations, the early binding substrates (Mn^{2+} and PEP) can be "trapped" on the enzyme by later binding substrates. This leads to apparent K_M(1s) values that are lower than the true K_d values, even if the rapid equilibrium assumption is valid.

KDO8PS's kinetic mechanism was previously characterized as ordered sequential bi bi, with PEP binding first, followed by A5P, and then Pi dissociates before KDO8P.[40,43,97] For metal-dependent KDO8PSs the order of metal binding has not previously been described. In most studies, a metal is added at a single high concentration and not further investigated. However, both cjKDO8PS activity and inhibitor binding (see Chapter 3) are metal ion dependent. Therefore, complete characterization of activity and inhibition also requires complete

characterization of Mn^{2+}'s involvement in the kinetic mechanism. Mn^{2+} is, strictly, an essential activator rather than a substrate because it does not undergo a chemical reaction. However, essential activators can be treated as substrates in initial velocity calculations,[96] and this was done in our lab's previous study on *E. coli* DAHPS.[98]

Fitting the initial velocity data to different kinetic mechanisms demonstrated that cjKDO8PS$_{wt}$ follows a rapid equilibrium ordered sequential ter ter mechanism. While the order of PEP and A5P binding relative to each other had been established previously,[40,43,97] the orderedness of Mn^{2+} binding had to be established kinetically. The extremely poorly defined fits of the parameters for the "random A" kinetic mechanism (Figure 2.5) were a result of trying to fit parameters for steps that do not exist in reality.

Fitting to a steady state ordered mechanism gave better defined fitted parameters (Table 2.2). The fitted parameters demonstrated that the rapid equilibrium assumption was valid for cjKDO8PS$_{wt}$. Specifically, the K_M(ss) values for Mn^{2+} and PEP were much less than their K_i(ss) values, and the microscopic rate constants were much greater than k_{cat} (Table 2.2, Table S10.3). $K_{M,X}$(re) values represent the true dissociation constants for substrate X, while $K_{M,X}$(ss) values represent the *apparent* dissociation constant for X in the presence of infinite concentrations of the other two substrates. High [PEP] and [A5P] can "trap" Mn^{2+} on the enzyme, leading to low apparent $K_{M,Mn}$(ss) values. Similarly, high [A5P] can trap PEP. This was observed in the steady state kinetic

parameters, where K_M(ss) values were much less than the corresponding K_i(ss) values, which represent the true dissociation constants. When using the single substrate Michaelis-Menten equation (eq. **2.3**), $K_{M,X}$(1s) is the apparent dissociation constant at high, but not infinite concentrations of the other two substrates. As would be expected, the observed values for Mn^{2+} and PEP were K_M(ss) < K_M(1s) < K_M(re) ≈ K_i(ss) (Table 2.2). The same pattern was not observed with A5P; because it is the last substrate to bind, it cannot be "trapped" on the enzyme. As a result, $K_{M,A5P}$(ss) represents A5P's dissociation constant. This is reflected in the fact that $K_{M,A5P}$(ss) = $K_{M,A5P}$(re) ≈ $K_{M,A5P}$(1s) (Table 2.2). The implication of a rapid equilibrium kinetic model is that both substrate binding and dissociation are fast relative to catalysis, and therefore that every enzyme form between E and EABC (Figure 2.5) is in equilibrium throughout the reaction.

An ordered kinetic mechanism is further supported by ITC titrations (see Chapter 3). In brief, the ITC titrations suggest that the metal ion, Mn^{2+}, binds first, before PEP and A5P. For example, PEP bound poorly in the absence of Mn^{2+}, and A5P bound 9-fold worse in the presence of Mn^{2+} implying that a metal bound active site is only conformationally optimized for the most catalytically viable route, which is Mn^{2+} binding, then PEP, then A5P.

Kinetic constants for *A. aeolicus* KDO8PS determined at 40 °C under the steady state bi bi mechanism were k_{cat} = 0.5 s^{-1}, $K_{M,PEP}$ = 0.5 μM and $K_{M,A5P}$ = 7 μM.[43] While the difference in $K_{M,A5P}$ is modest, the k_{cat} and $K_{M,PEP}$ values are 5-fold lower than the corresponding values for cjKDO8PS$_{wt}$. In an independent

study, the kinetic parameters for *A. aeolicus* KDO8PS were determined in a similar way and similar results were obatianed.[68] Furthermore, the steady-state kinetic study of *E. coli* KDO8PS was analyzed via inhibition using KDO8P and inorganic phosphate products, and Rib5P as a dead-end inhibitor.[140] In that study, reaction mechanism analysis was done by examining the initial velocities by varying one substrate at different concentrations of the second substrate. Intersecting lines in double-reciprocal plots of initial-velocity data denoted a sequential mechanism for the enzyme-catalyzed reaction. The mode of inhibition of Rib5P, Pi and KDO8P with respect to PEP and A5P was also used to conclude that the reaction mechanism by *E. coli* KDO8PS was a steady state sequential bi bi mechanism. The study reported $K_{M,A5P}$ = 26 μM and k_{cat} = 7 s^{-1}, and these values are in the same order of magnitude with our $K_{M(ss)}$ values for cjKDO8PS$_{wt}$. In all the studies above, in which the order of substrate binding was determined, the kinetic parameters determined therein are considerably lower than our kinetic parameters under the rapid equilibrium assumption for both cjKDO8PS$_{wt}$ and cjKDO8PS$_{H6}$ (Table 2.2 and Table 2.3). Comparing this study to previous reports of KDO8PS kinetics, the fitted k_{cat} values are in reasonable agreement (see below), but the K_M(re) values (Table 2.2 and Table 2.3) did not match well with literature K_M values for other KDO8PSs (Table 2.5). These differences could be attributed to the fact that the KDO8PSs compared here originate from different sources and/or different reaction conditions. However, the more likely source of the differences is the fact that all the literature values in Table 2.5 only describe

the kinetic parameters as originating from fits to the "Michaelis-Menten" equation, meaning, presumably, the single substrate equation. In this context, comparing the single substrate kinetic constants for cjKDO8PS is a reasonable way to compare this enzyme with previously characterized ones.

The fitted values of k_{cat} are not significantly affected by the equations used for fitting, and all the k_{cat} values are broadly similar, ranging from 1.1 to 8.0 s^{-1}. The only K_Ms reported for any metal ion (Mn^{2+}, Co^{2+} and Cd^{2+}) were for *A. ferrooxidans* KDO8PS, at 2 μM, 6 μM and 5.6 μM for $K_{M,Mn}$, $K_{M,Co}$, and $K_{M,Cd}$, respectively.[70] These are similar to the values for cjKDO8PS$_{H6}$ and cjKDO8PS$_{wt}$, $K_{M,Mn}$(1s) = 2.8 and 16 μM, respectively. The $K_{M,PEP}$ (1s) values of 86 and 48 μM for cjKDO8PS$_{H6}$ and cjKDO8PS$_{wt}$, respectively, are in the middle of the range of reported $K_{M,PEP}$ values, of 6 to 290 μM. Similarly, $K_{M,A5P}$ (1s) values, at 19 and 36 μM, are in the middle of the reported range, of 6 to 74 μM. In this regard, cjKDO8PS appears to be a typical example of the enzyme.

Table 2.5: Kinetic parameters of cjKDO8PS compared to bacterial KDO8P synthases in literature.
The cjKDO8PS kinetic constants are for the single substrate Michaelis-Menten equation (eq. **2.3**).

Enzyme	Temp. (°C)	k_{cat} (s^{-1})	$K_{M,Metal}$ (μM)	$K_{M,PEP}$ (μM)	$K_{M,A5P}$ (μM)	Metal dependent?	Reference
$cjKDO8PS_{wt}$	37	2.1 ± 0.3	16 ± 3[c]	48 ± 7	36 ± 6	yes	This study. [a]
$cjKDO8PS_{H6}$	37	1.2 ± 0.1	2.8 ± 0.5[c]	86 ± 16	19 ± 6	yes	This study. [b]
Acidithiobacillus ferrooxidans	37	4.8 ± 0.07	2 ± 0.2[c] 6 ± 2[d] 5.6 ± 1.6[e]	12 ± 0.7	21 ± 2	yes	Allison et al.[70]
Aquifex aeolicus	60 – 90	0.4 – 2.0	n.d.[f]	43 – 28	8 – 74	yes	Duewel et at.[39]
Aquifex pyrophilus	60	4	n.d.[f]	290 ± 40	70 ± 8	yes	Shulami et al.[47]
Helicobacter pylori J99	Room temp.	1.1	n.d.[f]	6.5	5.9	yes	Krosky et al.[48]
Neisseria meningitidis	37	8.0 ± 0.1		2.5 ± 0.2	5.7 ± 0.5	no	Cochrane et al.[45]
Escherichia coli	37	2.5		5.9	20	no	Ray.[30]

[a] Eq. **2.3** is the single substrate kinetic mechanism (Table 2.2).

[b] Eq. **2.3** is the single substrate kinetic mechanism (Table 2.3).

[c] Metal = Mn^{2+}

[d] Metal = Co^{2+}

[e] Metal = Cd^{2+}

[f] n.d. – not determined

2.4.3. Metal-dependence

In contrast to DAHPS and NeuB enzymes, all examples of which are metal ion dependent, some KDO8PSs are metal ion independent. KDO8PSs are composed of two classes, I and II. Class I KDO8PS.[40,43,97] KDO8PSs such as from *Neisseria. meningitidis*[45], *E. coli*[30] and the plant *Arabidopsis thaliana,*[42] do not require metal ions for activity. Class II KDO8PSs do require a metal ion for catalysis. Crystal structure alignment of metal-binding residues in the metal-dependent *A. aeolicus* KDO8PS, the metal ion-independent *E. coli* KDO8PS, and *E. coli* DAHPS(Phe) show that at least two out of four metal binding residues, a His and Glu residue, are conserved in all three enzymes (Figure 2.12).[52] *A. aeolicu*s KDO8PS H185 and E222, *E. coli* KDO8PS H202 and E239 correspond to DAHPS(Phe) H268 and E302. The cysteine residue that also binds metal is present in metal dependent *A. aeolicu*s KDO8PS and DAHPS(Phe) but is replaced with an asparagine residue in metal-ion independent *E. coli* KDO8PS. To further investigate metal-binding in cjKDO8PS, a protein BLAST[141] search was conducted for cjKDO8PS$_{wt}$. cjKDO8PS$_{wt}$[142] was aligned with *Helicobacter pylori J99* KDO8PS, *A. aeolicus* KDO8PS, *E. coli* KDO8PS and *E. coli* DAHPS (Figure 2.13). Four residues that are responsible for metal binding in the active site are conserved in all enzymes (Figure 2.13, cyan shading). In cjKDO8PS the metal binding residues (C8, H192, E229, D240) are conserved and correspond to the metal-binding residues in *H. pylori J99* KDO8PS (C18, H204, E241, D252), *A.*

aeolicus KDO8PS (C11, H185, E222, D233) and in *E. coli* DAHPS(Phe) (C61, H268, E302, D326). In non-metal ion dependent *E. coli* KDO8PS, the Cys residue is replaced with Asn: *E. coli* (N29, H202, E239, D251). Considering the protein sequence analysis of cjKDO8PS in comparison to known KDO8P synthases and the structural alignment shown in Figure 2.12, it is likely that a metal bound structure of cjKDO8PS$_{wt}$ is structured in a similar way.

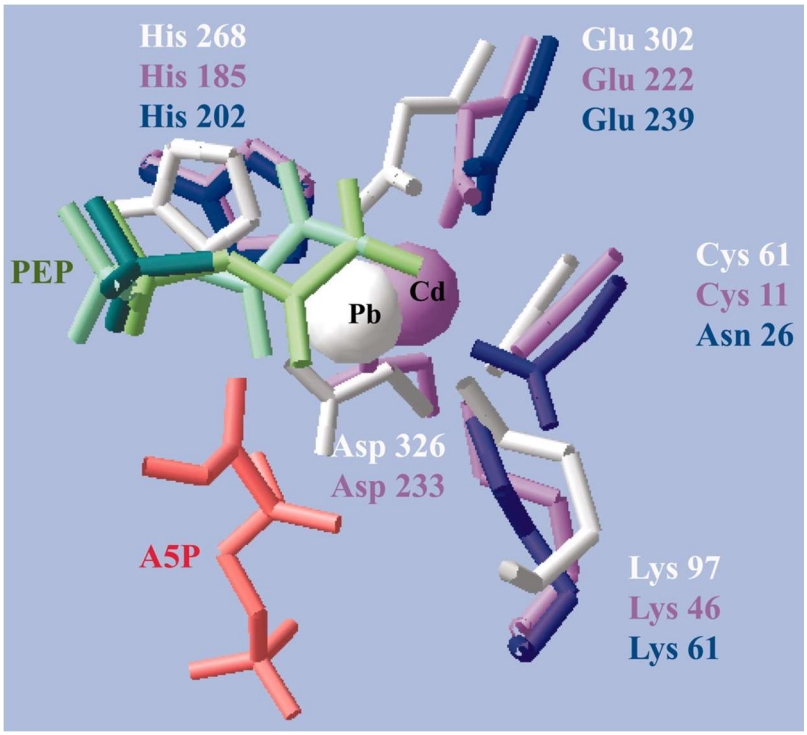

Figure 2.12. Structural alignment of the metal-binding residues in KDO8PS

E. coli DAH7PS (white), *A. aeolicus* KDO8PS (lilac) and the corresponding residues of *E. coli* KDO8PS (purple) are shown. The metal-binding residues shown here are conserved in cjKDO8PS (see Figure 2.13) and presumably form the same metal binding interactions as shown above. Figure taken directly from Oliynyk et al.[52], with permission via the Copyright Clearance Center's RightsLink (CCC- Danvers, Massachusetts).

```
C. jejuni KDO8PS          1     M----------ILIAGPCVIESKDLIFKVAEQLKNFNENPN--IEFYFKSSFDKANRTSINSFRGPGLEEGLKILQ  64
H. pylori KDO8PS          1     MKTSNTKTPKPVLIAGPCVIESLENLRSIAIKLQPLANNER--LDFYFKASFDKANRTSLESYRGPGLEKGLEMLQ  74
A. aeolicus KDO8PS        1     -------MEKFLVIAGPCAIESEELLLKVGEEIKRLSEKFK-eVEFVFKSSFDKANRSSIHSFRGHGLEYGVKALR  68
E. coli KDO8PS            1  [ 8]GDINVANDLPFVLFGGMCVLESRDLAMRICEHYVTVTQKLG--IPYVFKASFDKANRSSIHSYRGPGLEEGMKIFQ  82
E. coli DAHPS(Phe)        1  [43]HKILKGNDDRLLVVIGPCSIHDPVAAKEYATRLLALREELKdeLEIVMRVYFEKP--RTTVGWKGLINDPHMDNSF  117

C. jejuni KDO8PS         65  SVKDEF    GMKILTDIHESNQANPVSEVADVLQIPAFLCRQTDLLVAAAKTKAKINIKKGQF   LNPSDIKYSVKKV  137
H. pylori KDO8PS         75  TIKDEF    GYKILTDVHESYQASVAAKVADILQIPAFLCRQTDLIVEVSQTNAIVNIKKGQF   MNPKDMQYSVLKA  147
A. aeolicus KDO8PS       69  KVKEEF    GLKITTDIHESWQAEPVAEVADIIQIPAFLCRQTDLLLAAAKTGRAVNVKKGQF   LAPWDTKNVVEKL  141
E. coli KDO8PS           83  ELKQTF    GVKIITDVHEPSQAQPVADVVDVIQLPAFLARQTDLVEAMAKTGAVINVKKPQF   VSPGQMGNIVDKF  155
E. coli DAHPS(Phe)      118  QINDGL[13]GLPAAGEFLDMITPQYLADLMSWGAIGARTTESQVHRELASGLSCPVGFKNGTD[4]VAIDAINAAGAPH  207

C. jejuni KDO8PS        138  lqtR--GIEDEGYEAAQ-RNGVFVAERGASFGY--GNLVVDMRSLVIMREFAP   VIFDATHSVQMPGAAGGSSGGKSE  209
H. pylori KDO8PS        148  lktRDSSIQSPTYETAL-KNGVWLCERGSSFGY--GNLVVDMRSLKIMREFAP   VIFDATHSVQMPGGANGKSSGDSS  221
A. aeolicus KDO8PS      142  ---KFGGA-----------KEIYLTERGTTFGY--NNLVVDFRSLPIMKQWAK   VIYDATHSVQLPGGLGDKSGGMRE  202
E. coli KDO8PS          156  ---KEGG-----------NEKVILCDRGANFGY--DNLVVDMLGFSIMKKVSG[3]VIFDVTHALQCRDPFGAASGGRRA  219
E. coli DAHPS(Phe)      208  ---CFLSVTKWGHSAIVnTSGNGDCHIILRGGKepNYSAKHVAEVKEGLNKAG[4]VMIDFSHANSSKQ------FKKQM  279

C. jejuni KDO8PS        210  FVEPLARAAAAVG---IDGFFFETHINPCEALCDGPNMLNLTRLKNCVNTLLEIQNIIKENK------      268
H. pylori KDO8PS        222  FPPILPRAAAAVG---IDGLFAETHIDPKNALSDGANMLKPDELEHLVTDMLKIQNLF----------      27
A. aeolicus KDO8PS      203  FIFPLIRAAVAVG---CDGVFMETHPEPEKALSDASTQLPLSQLEGIIEAILEIREVASKYYETIPVK      267
E. coli KDO8PS          220  QVAELARAGMAVG---LAGLFIEAHPDPEHAKCDGPSALPLAKLEPFLKQMKAIDDLVKGFEELDTSK      284
E. coli DAHPS(Phe)      280  DVCADVCQQIAGGekaIIGVMVESHLVEGNQSLESGEPLAYGKSITDACIGWEDTDALLR-QLANAVK[4]  350
```

Figure 2.13. Amino acid sequence alignment of KDO8PSs.

Amino acid sequences of metal-dependent KDO8PSs from *C. jejuni*, *H. pylori*, *A. aeolicus,* and metal-independent *E. coli* KDO8PS are shown. The sequence of *E. coli* DAHPS(Phe) is also included. The conserved metal-binding residues shown in the structural alignment of *A. aeolicus* KDO8PS, *E. coli* KDO8PS and *E. coli* DAHPS(Phe) in Figure 2.12[52] are highlighted in cyan. The green-highlighted K is the Lys residue believed to act as a general acid catalyst in the breakdown of the THI. Numbers in brackets (e.g., [13]) indicate the number of amino acids left out of the alignment figure to save space. The Genbank accession numbers are: *C. jejuni* KDO8PS – EFV08406.1, *H. pylori* KDO8PS – AAD05587.1, *A. aeolicus* KDO8PS – O66496.1; *E. coli* KDO8PS – P0A715.1, *E. coli* DAHPS(Phe) – P0AB92.

2.4.4. Oligomeric structure of cjKDO8PS

Tetrameric and dimeric bacterial DAHP synthases has been reported.[57,143,144] All bacterial KDO8PSs, on the other hand, are tetramers in solution. The one known dimeric KDO8PS is from the plant *A. thaliana* KDO8PS.[42] Analysis of cjKDO8PS$_{wt}$ and cjKDO8PS$_{H6}$ by size exclusion chromatography showed that it was a tetramer in solution (see section 2.3.9), consistent with the other bacterial KDO8P synthases (Table 2.6).

Table 2.6. Comparison of oligomeric structural properties of KDO8PSs.

Enzyme	Calculated subunit MW (kDa)	Gel filtration	Reference
cjKDO8PS$_{wt}$	29	Tetramer	This study
cjKDO8PS$_{H6}$	33	Tetramer	This study
A. aeolicus KDO8PS	30	Tetramer	Duewel et al.[39]
E. coli KDO8PS	31	Tetramer	Ray.[30]
A. thaliana KDO8PS	32	Dimer	Wu et al.[42]

3. Ligand Binding by Isothermal Titration Calorimetry

3.1. Introduction

Isothermal titration calorimetry (ITC) is a tool used in studying biomolecular interactions to monitor non-covalent binding interactions.[145–147] Other techniques such as enzyme activity assays or NMR techniques require analytical techniques to detect probes or reporter molecules directly. Using ITC, it is the interaction itself that is detected in the form of heat that is released or absorbed during the binding event. Titrating a protein and ligand at a constant temperature produces a complete binding profile in ΔG, ΔH and ΔS, from which the equilibrium binding constant K_b ($1/K_b = K_d$) and the reaction stoichiometry (n) can be extracted in a single 2 h experiment.

The ITC calorimeter consists of a reference cell, which contains only water or buffer, and a sample cell, which contains the macromolecule. The ligand is incrementally injected onto the sample cell, and gives a signal as the power (in μJ/s) required to maintain a constant temperature in the sample cell.[145] The area under the signal peak which corresponds to the heat of binding in μJ is then integrated, normalized and fit to a binding model to calculate the affinity, enthalpy and stoichiometry of the interaction.[148] Examples of ITC applications in life sciences include; study of protein-protein, protein-peptide[149,150] and protein-drug interactions.[151,152] Our lab has previously used ITC to study interactions of the ligands Mn^{2+} and DAHP oxime with *E. coli* $DAHPS_{H6}$. The K_d values

obtained for Mn^{2+} and DAHP oxime were comparable to their respective K_M and K_i values.[98] ITC was also used to support the kinetic data that showed that DAHP oxime binds competitively with respect to Mn^{2+} at neutral pH. In the present study, ITC was also utilized to study the thermodynamic interactions of cjKDO8PS$_{H6}$ ligands; A5P, PEP, Mn^{2+} and KDO8P oxime inhibitor.

3.2. Experimental

cjKDO8PS$_{H6}$ was expressed and purified as described in Chapter 3. The purified enzyme was dialyzed against 2 mM EDTA overnight in 50 mM Tris·Cl pH 7.5, 200 mM KCl, 1 mM TCEP. The enzyme was then exchanged two times, by dialysis, into ITC buffer (20 mM Tris·Cl, pH 7.5, 200 mM KCl, 1 mM TCEP) to bring the EDTA concentration to sub-nanomolar concentrations. The enzyme was concentrated to 150 μM using 10 kDa molecular weight cut-off Amicon® Ultra centrifugal filter device (EMD Millipore Corporation). The ligands, namely $MnCl_2$, KDO8P oxime, PEP and A5P were dissolved to 3 mM concentrations in the ultrafiltrate and the pH was adjusted to 7.5. ITC titrations were performed on a NanoITC calorimeter (TA Instruments, Delaware, MD). The sample cell contained 300 μL of protein solution while the reference cell contained 300 μL of ultrafiltrate and the titrant syringe contained 50 μL of ligand. All solutions were vacuum degassed with stirring for 15 min at 20 °C, then equilibrated to 25 °C for approximately 45 min. Titrations were initiated with a

0.48 µL injection, followed by 19 × 2.5 µL injections. In some titrations, there was 500 µM $MnCl_2$ present in the enzyme solution along with the 150 µM cjKDO8PS$_{H6}$.

The thermodynamic parameters K_d, the equilibrium dissociation constant, and n, the reaction stoichiometry, were obtained by fitting the data to an independent one-site binding model integrated into the NanoAnalyze software suite. The cjKDO8PS$_{H6}$ concentration was the monomeric concentration, therefore n = 1 would indicate that the ligand binds to all four active sites per tetramer. The fitting model assumed that the macromolecule consists of identical binding sites with the same intrinsic affinity for the ligand.

3.3. Results

The ligand binding properties of cjKDO8PS$_{H6}$ with respect to Mn^{2+}, PEP, A5P and KDO8P oxime (a cjKDO8PS inhibitor) were investigated by ITC. Mn^{2+}, A5P and KDO8P oxime bound cjKDO8PS$_{H6}$ exothermically (Figure 3.5, Figure 3.3 , Figure 3.4, Figure 3.5). Mn^{2+} bound to cjKDO8PS$_{H6}$ with a $K_d = 17 \pm 2$ µM. At the end of the titration experiment, the protein sample was visibly cloudy, indicating that it was becoming denatured during the titration, or that the solubility of the cjKDO8PS$_{H6}$·Mn^{2+} complex was significantly lower than unliganded enzyme under the titration conditions. Due to the effects of high concentration on cjKDO8PS$_{H6}$ a sigmoidal curve could not be obtained for binding of Mn^{2+}. Therefore, the binding stoichiometry could not be accurately

calculated, but the fit gave an average n = 0.4 ± 0.3 for the three titration trials. Titrations of cjKDO8PS$_{H6}$ with PEP resulted in too weak signals to allow K_d to be determined (data not shown). Titrating cjKDO8PS$_{H6}$·Mn^{2+} with PEP produced weakly endothermic peaks, giving K_d = 122 ± 42 μM and n = 1 ± 1 (Figure 3.2). For A5P K_d = 34 ± 2 μM with binding stoichiometry number (n) of 2 ± 1. A5P binding only occurred in the absence of Mn^{2+}. KDO8P oxime, a potent slow-binding inhibitor of cjKDO8PS$_{H6}$ is described in detail in the following chapters. In this section, we report that KDO8P oxime bound cjKDO8PS$_{H6}$ with K_d = 18 ± 2 μM and n = 1.5 ± 0.7. KDO8P oxime bound more strongly in the presence of Mn^{2+}. In the absence of Mn^{2+} its binding was weaker, with K_d = 346 ± 37 μM (Figure 3.5). The number of binding sites (n) was 0.1. This could be an indication that only 10% of the enzyme bound the inhibitor, and that it was less stable in the absence of Mn^{2+}. This was observed with DAPHS, which routinely gave binding stoichiometries of approximately 10% in the absence of metal.[98] Finally, the heat of the KDO8P synthesis reaction was accidentally measured when the aim was to measure PEP binding in the presence of A5P in the absence of Mn^{2+}. Since contaminating metal ions could be available from the cell chamber, injection syringe or the degassing tubes, activation of the enzyme was not prevented in this method. As a result, a thermogram likely indicative of the conversion of PEP and A5P into KDO8P was obtained (Figure S10.6). Relevant parameters obtained here were the ΔG and ΔH of -9.9 and -21.6 kcal mol^{-1}, respectively. These values are close to the energies of activation obtained in Section 2.3.7 (20 kcal mol^{-1}).

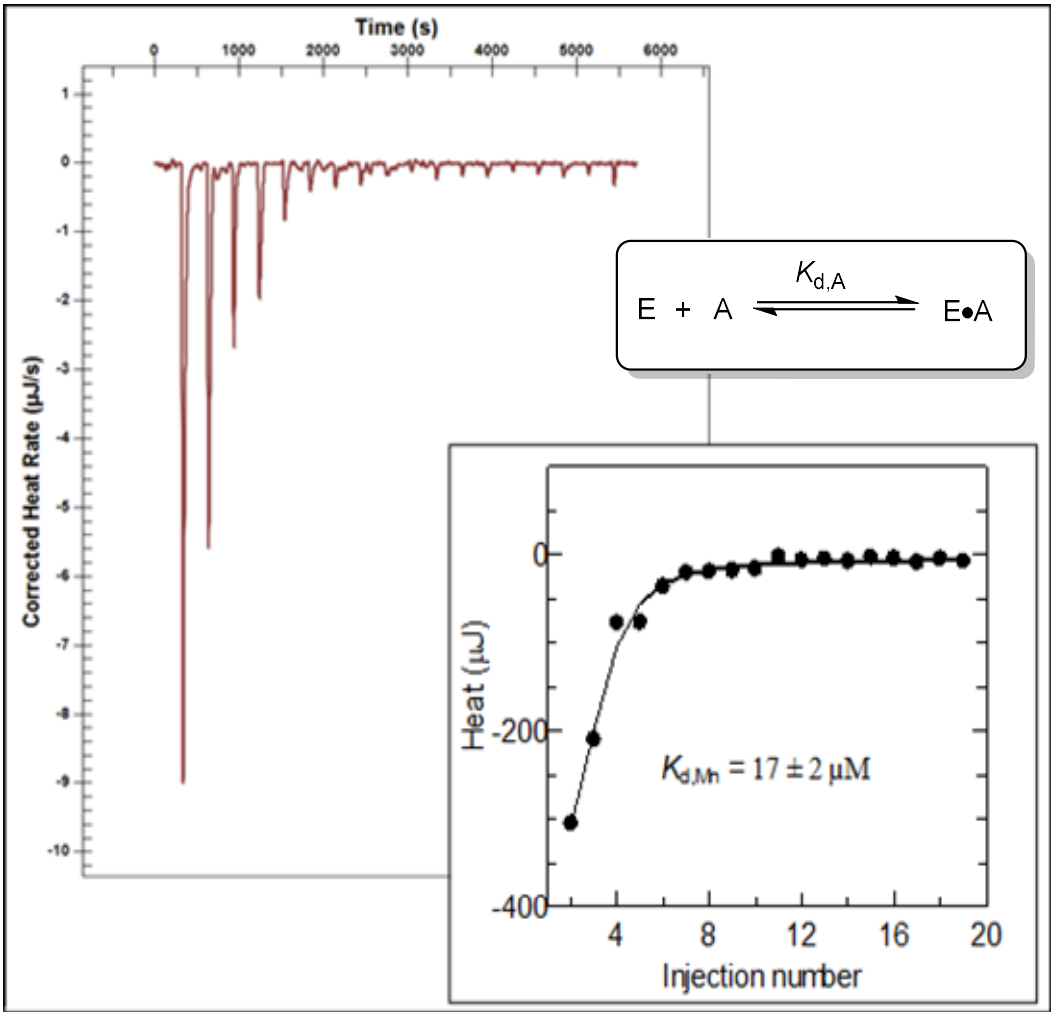

Figure 3.1. ITC titrations of cjKDO8PS$_{H6}$ with Mn^{2+}.

Binding of Mn^{2+} produced exothermic signals with parameters; K_d = 17 ± 2 µM, n = 0.4 ± 0.3.

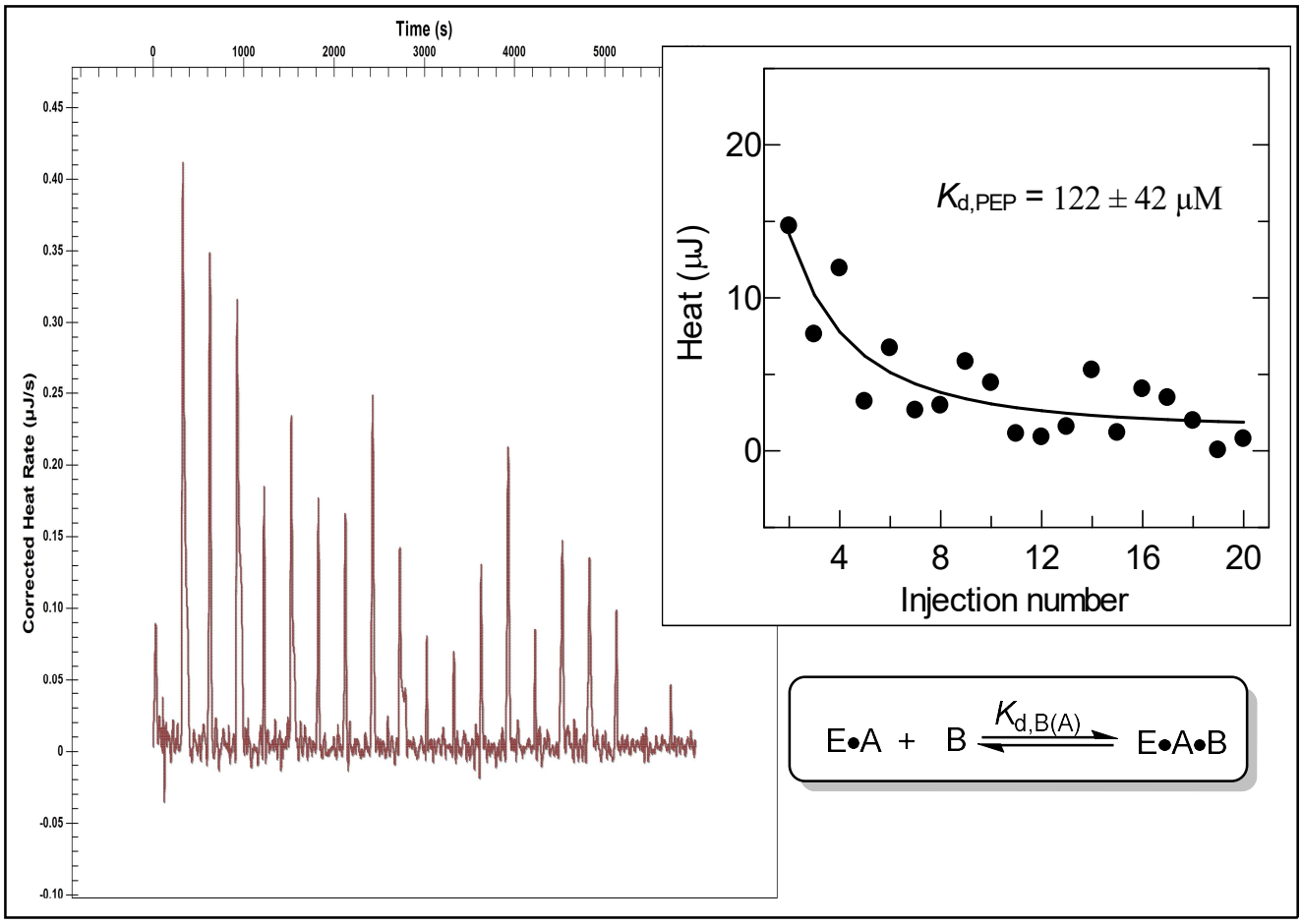

Figure 3.2. ITC titrations of cjKDO8PS$_{H6}$·Mn^{2+} with PEP.

Binding of PEP was only observed in the presence of Mn^{2+}. Titration of PEP to a cjKDO8PS$_{H6}$·Mn^{2+} complex produced an endothermic thermogram with K_d = 122 ± 42 µM, n = 1 ± 1.

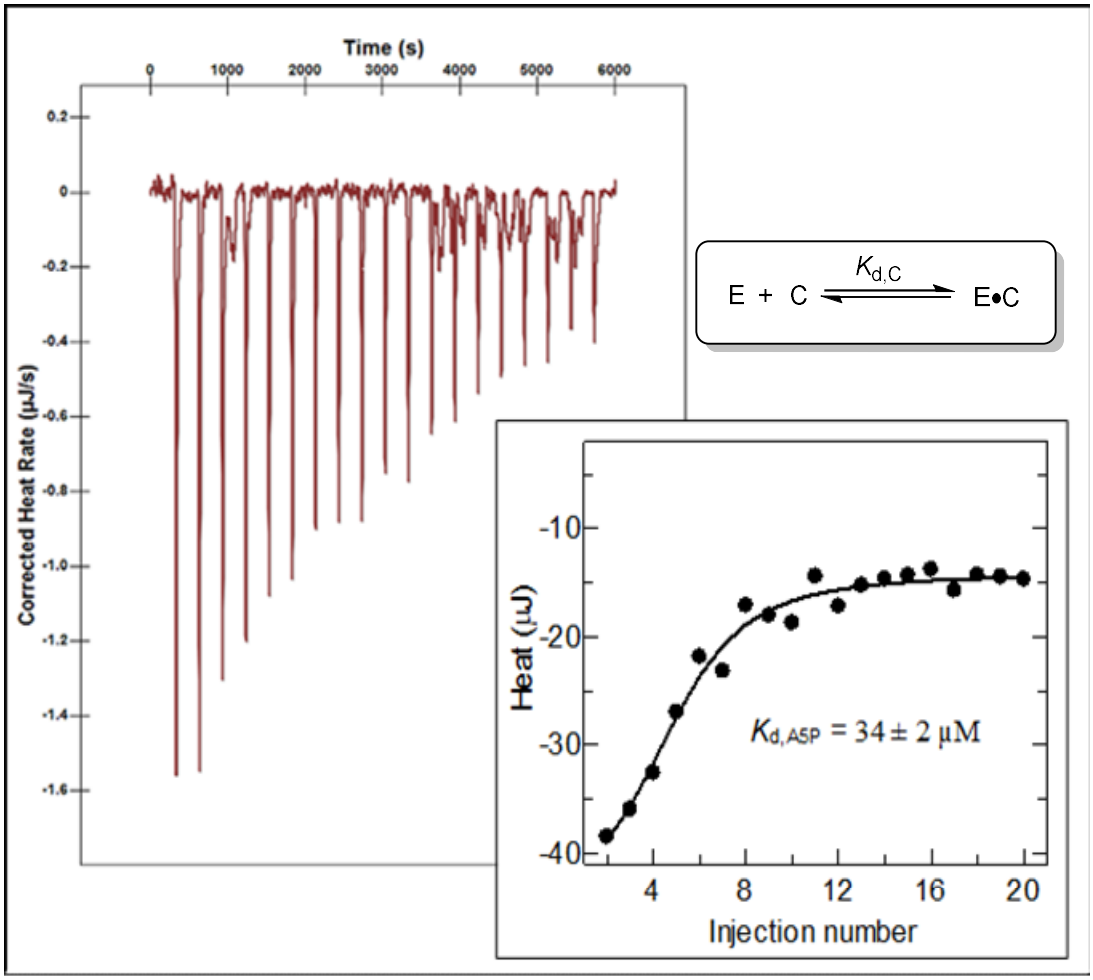

Figure 3.3. ITC titration of cjKDO8PS$_{H6}$ with A5P.

Binding of A5P only occurred against free cjKDO8PS (in the absence of Mn^{2+}); K_d = 34 ± 2 µM, n = 2 ± 1.

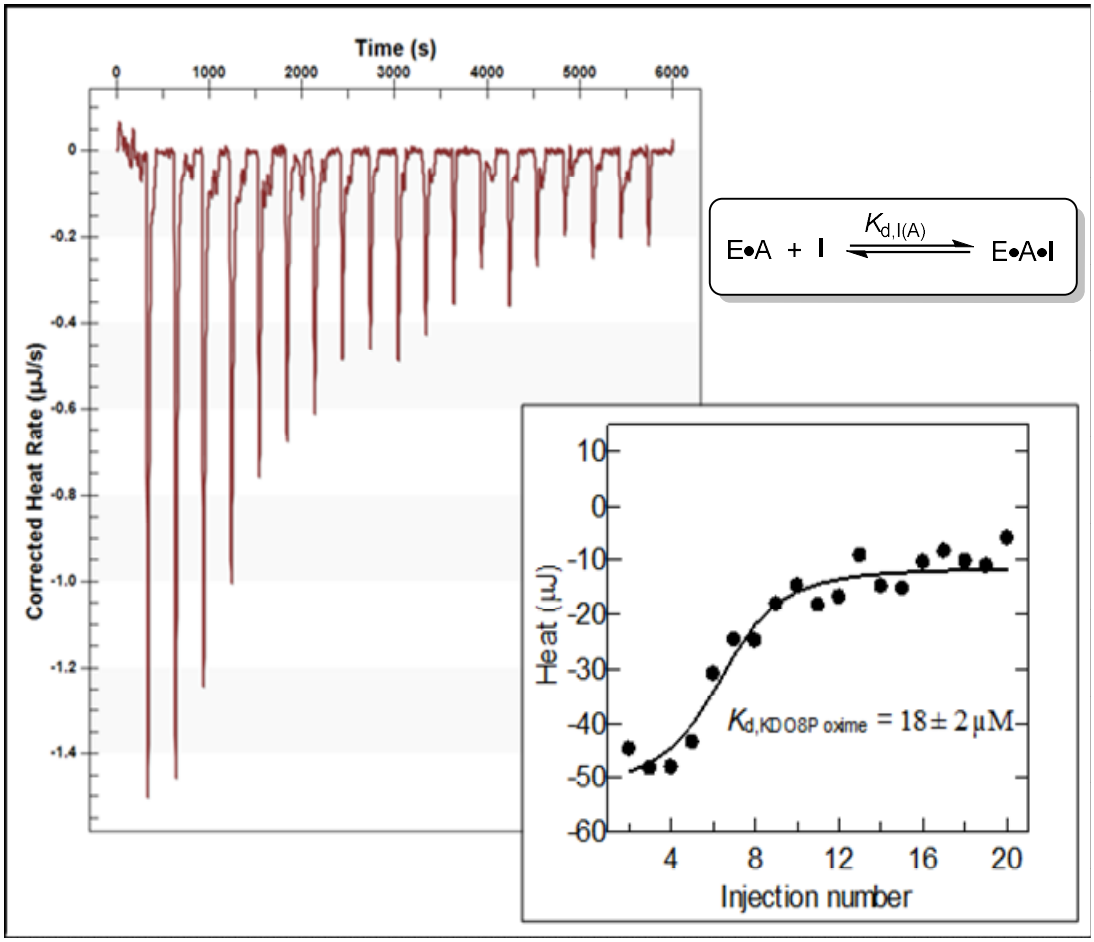

Figure 3.4. ITC titrations of cjKDO8PS$_{H6}$·Mn^{2+} with KDO8P oxime.

Binding of KDO8P oxime to cjKDO8PS$_{H6}$ was favourable in the presence of Mn^{2+} (cjKDO8PS$_{H6}$·Mn^{2+}); K_d = 18 ± 2 µM, n = 1.5 ± 0.7.

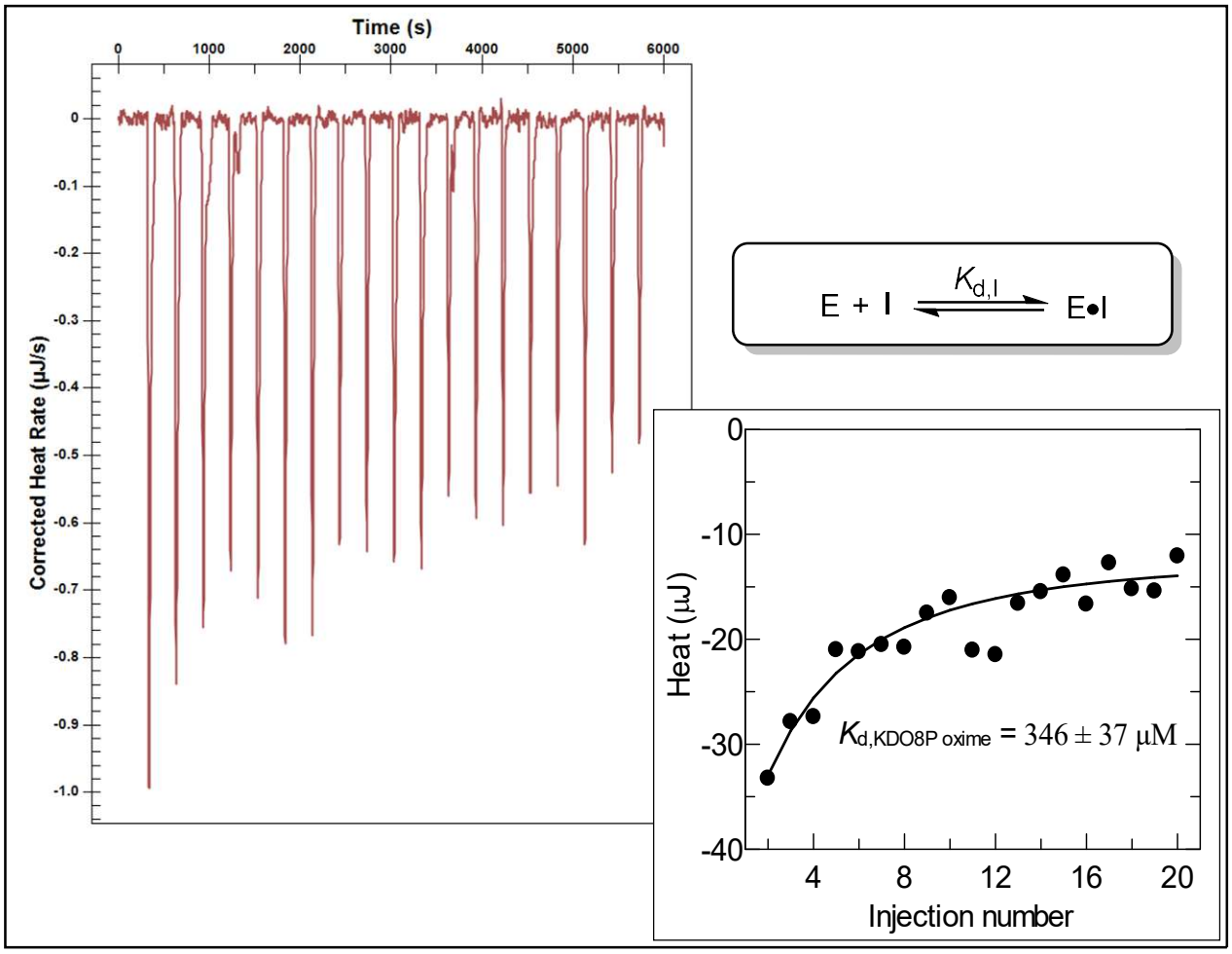

Figure 3.5. ITC titrations of cjKDO8PS$_{H6}$ KDO8P oxime.

KDO8P oxime binds to free cjKDO8PS$_{H6}$ with K_d = 346 ± 37 µM and n = 0.1.

3.4. Discussion

ITC provides a different view of enzyme·substrate interactions by allowing ligand binding to be measured independently of activity. This can be an advantage in that it allows ligand binding to be measured under conditions in which the enzyme is not active, or not optimally active. For example, the kinetic

assays were conducted at 37 °C while the ITC experiments were conducted at 25 °C because the enzyme was not stable long enough at 37 °C to allow full titrations before it denatured. Because ITC titrations are sensitive to solutes with significant heats of dissolution, the number of buffer components was minimized, and the enzyme was extensively dialyzed via ultrafiltration to remove unneeded buffer components. Ligands were dissolved in the ultrafiltrate to ensure a constant buffer composition and minimize background noise.

The stoichiometries of ligand binding (n) were not very reliable in these experiments, for reasons that are not clear. It was not well defined for Mn^{2+} binding to cjKDO8PS$_{H6}$ and KDO8P oxime binding to cjKDO8PS$_{H6}$ in the absence of Mn^{2+} because proper sigmoidal curves could not be obtained. The accuracy of n depends on many factors, including: the accuracy of the protein and ligand concentrations, the actual concentration of active binding sites in the protein and solubility at high protein concentrations.[153] Since the concentration of cjKDO8PS$_{H6}$ used is the monomeric concentration, a binding stoichiometry of 1 would imply that all four active sites in tetrameric cjKDO8PS$_{H6}$ were occupied. The apparent stoichiometry of Mn^{2+} binding was 0.4 ± 0.3. This could indicate, for example, half-of-sites metal binding, but it could also indicate that the metal-free enzyme was unstable, as observed with *E. coli* DAHPS(Phe)[98], and would be consistent with the presence of precipitate at the end of some cjKDO8PS$_{H6}$ titrations. The stoichiometries of A5P, PEP and KDO8P oxime binding were

higher but also variable, being 2 ± 1, 1 ± 1 and 1.5 ± 0.7, respectively. The reasons for this variability were not analyzed further.

KDO8PSs has been reported to follow an ordered sequential substrate binding mechanism, where PEP binds first followed by A5P, and that Pi dissociates first before KDO8P.[97] For metal-dependent KDO8PSs like cjKDO8PS, the order in which the metal binds was not previously known, though we show that the kinetic mechanism is ordered, with the Mn^{2+} binding first (see Chapter 2). Given that cjKDO8PS requires divalent metals for activity, with Mn^{2+} conferring the highest activity, it was imperative to further probe the Mn^{2+}'s binding to cjKDO8PS. $cjKDO8PS_{H6}$ was used because it was easier to purify.

$cjKDO8PS_{H6}$ (E) bound Mn^{2+} (substrate A) with $K_{d,A} = 17$ μM to form the E·A complex (Figure 3.6). PEP (substrate B) binding produced endothermic peaks and binding was only observed in the presence of Mn^{2+}, with a $K_{d,B(A)} = 122 \pm 42$ μM, implying that the sequence of substrate binding involves Mn^{2+} binding first, followed by PEP. This result further supported the kinetic mechanism in which cjKDO8PS follows an ordered mechanism where Mn^{2+} binds first, then PEP (Chapter 2). The presence of Mn^{2+} made KDO8P oxime inhibitor (I) bind better, with $K_{d,I(A)} = 18$ μM compared to $K_{d,I} = 346$ μM in the absence of Mn^{2+}. To complete the thermodynamic box involving A, B and I, the binding of A in the presence of I can be derived as $K_{d,A(I)} = \{K_{d,A} \times K_{d,I(A)}\}/K_{d,I} = 0.9$ μM, implying that the inhibitor binding would improve Mn^{2+} binding. Surprisingly, the dissociation constant for A5P (substrate C) was 9-fold lower in the absence of

Mn^{2+}, with $K_{d,C}$ = 34 μM, than with it present, $K_{d,C(A)}$ = 298 μM. Using the thermodynamic box, Mn^{2+} binding in presence of A5P was derived as $K_{d,A(C)}$ = $\{K_{d,A} \times K_{d,C(A)}\}/K_{d,C}$ = 149 μM. Thus Mn^{2+} binding in the presence of A5P would be similarly poorer.

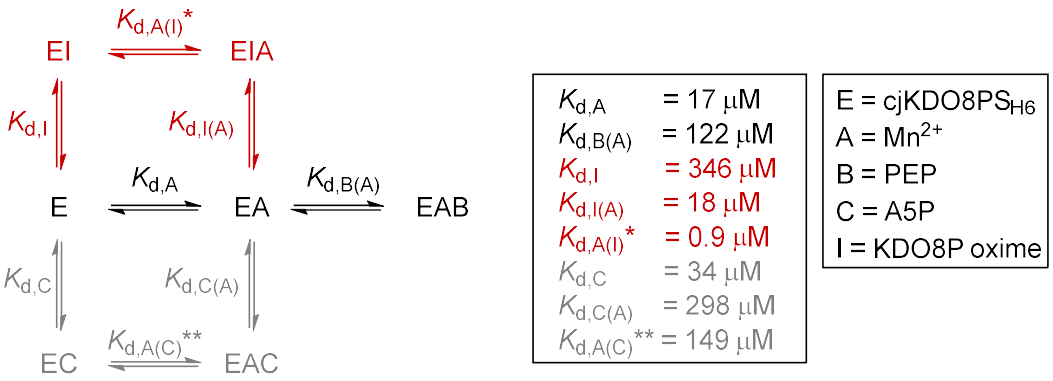

Figure 3.6. Thermodynamic box describing ITC-based dissociation constants with cjKDO8PS$_{H6}$.

Mn^{2+} bound to cjKDO8PS$_{H6}$ with $K_{d,A}$ = 17 μM, followed by PEP with a $K_{d,B(A)}$ = 122 μM. The inhibitor KDO8P oxime bound favorably to E·Mn^{2+} with $K_{d,I(A)}$ = 18 μM, 20-fold lower than $K_{d,I}$ = 346 μM in the absence of Mn^{2+}. $K_{d,A(I)}$* was the implied K_d of Mn^{2+} in the presence of I, expressed as: $K_{d,A(I)} = \{K_{d,A} \times K_{d,I(A)}\}/K_{d,I}$ = 0.9 μM. A5P binding in the absence of Mn^{2+} ($K_{d,C}$ = 34 μM) was more favorable than in the presence of Mn^{2+} ($K_{d,C(A)}$ = 298 μM). $K_{d,A(C)}$**, the dissociation constant for Mn^{2+} in the presence of A5P, was $K_{d,A(C)}** = \{K_{d,A} \times K_{d,C(A)}\}/K_{d,C}$ = 149 μM.

The dissociation constant for Mn^{2+} binding was $K_{d,A}$ = 17 μM, slightly higher than the rapid equilibrium $K_{M,Mn}$(re) value of 6.4 μM for cjKDO8PS$_{H6}$ (Chapter 2). This difference can be explained by the different conditions for ITC measurements versus activity assays. ITC titrations were conducted at 25 °C in 20 mM Tris·Cl, pH 7.5, 200 mM KCl, 1 mM TCEP, while activity assays were at 37 °C in 50 mM BTP·HCl, pH 7.5, 150 mM KCl, 1% glycerol, 100 μM TCEP. The dissociation constant for PEP was unmeasurable in the absence Mn^{2+}. This

could have been because it did not bind in the absence of Mn^{2+}, though it is also possible that it did bind but the heat of binding was very low. $K_{d,PEP}$ = 122 μM for binding to the E·Mn^{2+} complex was obtained. This compares with $K_{M,PEP}$(re) = 899 μM (Table 2.3), which should reflect the same dissociation constant. The reason for the large difference is not clear. Some of it may arise from the difference in conditions, as discussed above, though the almost 10-fold difference is larger than that observed for Mn^{2+} binding. The discrepancy could arise because of A5P binding competing with PEP binding. The fixed A5P concentrations in activity assays were >> $K_{d,A5P}$, which could have led A5P increasing PEP's apparent dissociation constant. The dissociation constants for A5P, $K_{d,C}$ = 34 μM, and $K_{d,C(A)}$ = 298 μM were higher than $K_{M,A5P}$(re) = 14 μM reported in Chapter 2. These dissociation constants all reflect A5P binding to different species, namely E for $K_{d,C}$, E·Mn^{2+} for $K_{d,C(A)}$, and E·Mn^{2+}·PEP for $K_{M,A5P}$(re). A5P binding to neither E or E·Mn^{2+} is functionally relevant, but the differences in K_d values point to the complicated interactions between enzyme and substrates throughout the catalytic cycle. It is also relevant that A5P will exist predominantly in the cyclic, hemiacetal form (99%) in solution,[154] but can react only in the linear, aldehyde form. The spontaneous ring-opening rate constants for the α- and β-furanose forms of A5P at pH 7.5, are 50 s^{-1} and 33 s^{-1}, respectively, greater than k_{cat} = 1.2 s^{-1}, implying that the conversion between acyclic and cyclic forms of A5P are in equilibrium and that this interconversion between the acyclic and cyclic forms of A5P is not the rate-limiting step. The k_{cat} values for 4-deoxy A5P

analogue (which cannot form a ring) and A5P were similar but $K_{M,A5P}$ was 10-fold lower than that of the 4-deoxy analogue tested on *E. coli* KDO8PS.[97] This implies that the enzyme binds the linear form and that the hydroxyl group at position 4 is important for binding. Although the proposition that the enzyme binds to linearized A5P is more likely, it is not known with certainty which form(s) bind to the enzyme, or when linearization occurs, but this could also have an effect on the observed dissociation constants.

The discrepancy between K_d and K_M values does not appear to be unique to cjKDO8PS. The $K_{d,PEP}$ and $K_{d,A5P}$ values for *A. aeolicus* KDO8PS were 5 μM and 152 μM, respectively even though the corresponding K_M(1s) values for this enzyme were 12 μM and 21 μM.[70] Because the single substrate Michaelis-Menten equation was used (inappropriately) for *A. aeolicus* KDO8PS, the reported $K_{M,PEP}$(1s) value should be less than $K_{d,PEP}$ since it will be trapped on the enzyme by high A5P concentrations. However, the opposite is observed. Because A5P is the last substrate to bind, the $K_{d,A5P}$ and $K_{M,A5P}$(1s) values should be comparable, but the former value is 7-fold higher. This could be a reflection of the presence of Mn^{2+} in the ITC titration if, like cjKDO8PS$_{H6}$, Mn^{2+} increases A5P's dissociation constant. Since we have determined that substrate binding is sequential for cjKDO8PS, with Mn^{2+} binding before PEP, we can presume that the active site in a cjKDO8PS·Mn^{2+} complex is only optimized for PEP binding, rather than for A5P. It has been found that if Cd^{2+} is present, a change in conformation in the crystal structure appears to originate in the active sites located on one face of *A.*

aeolicus KDO8PS.[40] This prevents binding of A5P in the active sites located on the opposite face whereas in the absence of metal the active sites on both faces of the enzyme act independently and bind A5P simultaneously.[40, 139] This might also explain the higher stoichiometry of binding that we obtain with A5P binding to cjKDO8PS$_{H6}$ in the absence of Mn^{2+}. It is likely that cjKDO8PS is catalytically productive when following the ordered sequential binding mechanism of Mn^{2+}, then PEP, then A5P. Thus, A5P could be a dead-end inhibitor of KDO8PS when it binds independently from PEP and/or Mn^{2+} if it binds in the PEP-binding site (Figure 3.7).

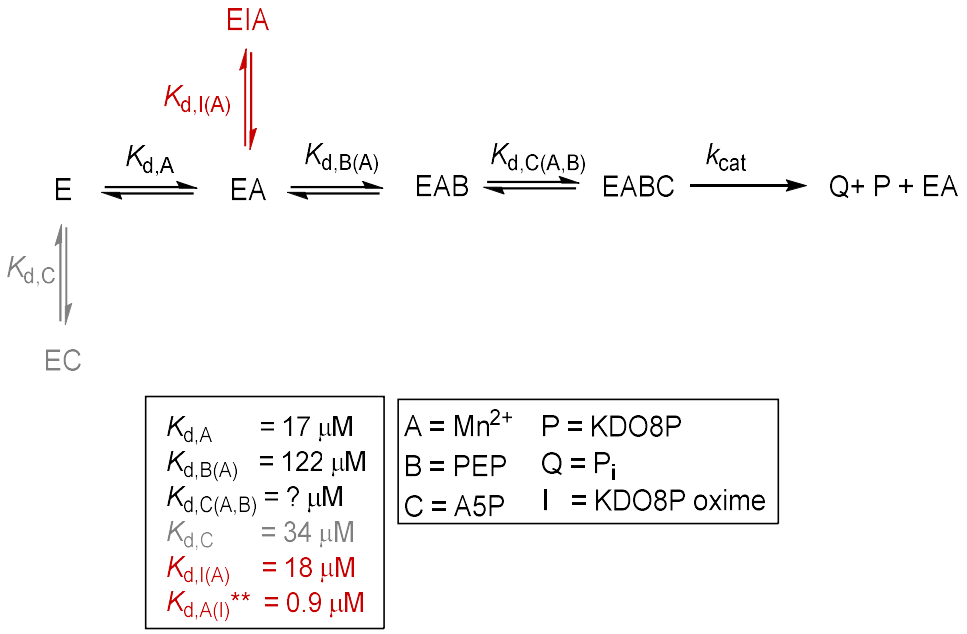

Figure 3.7. Possible substrate binding mechanism for cjKDO8PS$_{H6}$.

The sequence of substrate binding to cjKDO8PS$_{H6}$ is Mn^{2+} (A), PEP (B) then A5P (C) with experimentally determined K_d values of 17 and 122 μM, respectively. The binding of A5P in the presence of Mn^{2+} and PEP could not be measured without triggering a reaction. Since cjKDO8PS catalysis follows a rapid equilibrium mechanism where A5P binds after Mn^{2+} and PEP, we can assume that $K_{d,C(A,B)}$ will equal $K_{M,A5P}$(re) = 14 μM. The reaction products KDO8P (P) and Pi (Q) are produced via a k_{cat} of 1.2 s^{-1} for cjKDO8PS$_{H6}$. Since Mn^{2+} is not consumed in the reaction, the EA complex can be recycled for the next binding event.

From ITC experiments were learn that: (1) PEP and KDO8P oxime preferentially bind to the same enzyme species, namely E·Mn^{2+}, implying that KDO8P oxime is an uncompetitive inhibitor with respect to Mn^{2+}. (2) The E·Mn^{2+} complex binds A5P poorly. One drawback of DAHP oxime as a DAHPS inhibitor is the fact that it is competitive with respect to the metal ion, which means that *in vivo* it would be subject to being outcompeted by metal ions, rendering it ineffective.[98] In contrast, if KDO8P oxime binding is uncompetitive with respect

to metal binding, then increasing metal ion concentrations *in vivo* will improve inhibitor binding; this feature may offer some clinical advantage.[100]

4. *C. jejuni* KDO8PS inhibition by KDO8P oxime

4.1. Introduction

NeuNAc oxime is a potent slow-binding inhibitor of NeuB with an ultimate slow-binding K_i^* of 1.6 pM.[123] Only partial inhibition was achieved, even after prolonged incubation, if only enzyme + inhibitor were incubated together, or enzyme + inhibitor + any two of the three substrates (namely, Mn^{2+}, PEP, *N*-acetyl mannosamine). In the presence of all three substrates, while NeuB is actively catalyzing NeuNAc synthesis, complete inhibition by NeuNAc oxime was observed after 6 h. DAHP oxime is also a potent slow-binding inhibitor of DAHPS with a K_i of 1.5 μM, and like NeuNAc oxime, displays only partial inhibition.[98] Linear free energy relationship (LFER) analysis showed that DAHP oxime is a transition state mimic, presumably mimicking the transition state for phosphate departure during THI breakdown.[94] Since NeuB, DAHPS and KDO8PS are structurally and mechanistically similar, we hypothesized that KDO8P oxime would be a KDO8PS inhibitor.

Here we describe KDO8P oxime as a cjKDO8PS inhibitor. The inhibition characteristics of KDO8P oxime are described for both $cjKDO8PS_{H6}$ and $cjKDO8PS_{wt}$.

4.2. Experimental

4.2.1. KDO8P oxime synthesis and purification

KDO8P oxime was synthesized by first enzymatically making KDO8P using 3 μM cjKDO8PS$_{H6}$, 5 mM A5P, 4 mM PEP, and 1 mM $MnCl_2$ in 10 mM BTP·Cl, pH 7.5, and total reaction volume of 5 mL. The reaction progress was measured by the consumption of PEP, as monitored by anion exchange HPLC with a Mono Q 5/50 GL column (GE Healthcare). The HPLC run consisted of a 2 min (2 column volumes) wash with 100 mM ammonium formate (buffered with 10 mM ammonium bicarbonate, pH 6.2) at a flowrate of 1 mL/min, followed by a gradient of 100 to 800 mM ammonium formate over 28 min. PEP eluted at 22 min (590 mM ammonium formate). The reaction was complete after 6 h at 37 °C (Figure S10.7). KDO8P oxime synthesis was initiated by reacting KDO8P with 20 mM hydroxylamine hydrochloride. The pH of the reaction mixture was adjusted to 5.5 by adding a few drops of formic acid and the reaction was incubated at room temperature overnight. KDO8P oxime was purified by anion exchange chromatography through a 20-mL Q-Sepharose column (GE Healthcare). The purification protocol is described in Section 2.2.2. KDO8P oxime eluted over 4 column volumes, at ≈ 400 mM ammonium formate (Figure S10.8). The formate salt was removed through repeated lyophilization and KDO8P oxime was stored at -20 °C. HRMS (m/z): [M − 1]− calcd. for $C_8H_{15}NO_{11}P$, 332.0388; found, 332.0381 (Figure S10.12). ^{1}H NMR (700 MHz,

D_2O) δ: 2.89 (1H, dd, J = 13.4, 3.2, H3), 2.79 (1H, dd, J = 14.9, 2.7, H3′), 4.03 (1H, m, H4), 3.61 (1H, dd, J = 8.3, 8.2, H5), 3.79 (1H, m, H6), 3.76 (1H, ddd, J = 11.4, 2.4, 2.7, H7), 3.99 (1H, dd, J = 5.7, 2.1, H8), 3.99 (1H, dd, J = 8.4, 2.7, H8′) (Figure S10.9). ^{13}C NMR (700 MHz, D_2O) δ: 171.1 (C1), 156.8 (C2), 29.9 (C3), 69.9 (C4), 72.5 (C5), 71.9 (C6), 68.6 (C7), 66.4 (C8) (Figure S10.11).

4.2.2. cjKDO8PS$_{H6}$ and cjKDO8PS$_{wt}$ inhibition by KDO8P oxime

Kinetic assays to determine KDO8P oxime's K_i were carried out by varying its concentration from 0 to 9 mM with fixed substrate concentrations of 500 μM PEP, 200 μM A5P and 1 mM $MnCl_2$, in reaction buffer (50 mM BTP·Cl, pH 7.5, 150 mM KCl, 1% glycerol, 100 μM TCEP) at 37 °C. The enzyme was added to a final concentration of 125 – 450 nM to start the reaction. The reaction was monitored for 3 – 7 min using the Malachite Green/ammonium molybdate colorimetric assay for the release of Pi.[134] Based on the ITC results (Chapter 3) and the substrate dependence of inhibition (discussed later in this chapter), the data were better fitted to a three substrate, ordered binding uncompetitive (with respect to Mn^{2+}) and competitive (with respect to PEP and A5P) inhibition model (eq. **4.1**), using GraFit Version 5.0.13 software.[136]

$$\frac{v_0}{[E]_0} = \frac{k_{cat}\dfrac{[Mn][PEP][A5P]}{K_{M,Mn}K_{M,PEP}K_{M,A5P}}}{\left(1+\dfrac{[I]}{K_i}\right)\left(\dfrac{[Mn]}{K_{M,Mn}}\right)+\dfrac{[Mn][PEP]}{K_{M,Mn}K_{M,PEP}}+\dfrac{[Mn][PEP][A5P]}{K_{M,Mn}K_{M,PEP}K_{M,A5P}}} + r \quad (4.1)$$

where [Mn], [PEP] and [A5P] are the substrate concentrations, and the corresponding Michaelis-Menten constants (K_M) are $K_{M,Mn}$, $K_{M,PEP}$ and $K_{M,A5P}$. [I] is KDO8P oxime concentration, and its inhibition constant K_i. Parameter r is the nonzero residual rate at $[I]_\infty$. The kinetic parameters determined in Chapter 2 were used. The initial fitted value of r was then used as a constant to optimize K_i. This did not change the value of K_i, but did decrease the standard error in its value.

4.2.3. Substrate dependence of inhibition

KDO8P oxime's mode of inhibition with respect to PEP was determined by assaying cjKDO8PS$_{wt}$'s activity in the presence of fixed concentrations of KDO8P oxime (500 μM), A5P (200 μM) and $MnCl_2$ (1 mM) and varying PEP concentrations from 100 μM to 5 mM in reaction buffer at 37 °C, with 200 nM cjKDO8PS$_{wt}$ added to start the reaction. KDO8P oxime's mode of inhibition with respect to A5P was determined as above using 100 μM PEP, 1 mM $MnCl_2$ and 350 μM KDO8P oxime, and 100 to 600 μM A5P.

KDO8P oxime's mode of inhibition with respect to Mn^{2+} was fully characterized. This was done using fixed concentrations of 250 nM cjKDO8PS$_{wt}$, 200 μM A5P and 500 μM PEP and varying Mn^{2+} concentration from 0 to 1.2 mM

while the KDO8P oxime concentration was varied from 0 to 2 mM. The data was analyzed by fitting the data to competitive, noncompetitive and uncompetitive inhibition models using single substrate, rapid-equilibrium kinetic mechanisms and fitted using the software package Dynafit (BioKin Ltd.)[124] (Courtesy of Dr. Berti). Using a single-substrate kinetic mechanism means that fitted rate and equilibrium constants will not be accurate, but the patterns characteristic of each mode of inhibition will be. Given the residual rate, a rate for product formation from the E·S·I complex was included. The fitted data was visualized using Eadie-Hofstee plots[101] to determine the mode of inhibition.

4.2.4. Effect of substrates on KDO8P oxime binding by ITC

The effect of substrates on KDO8P oxime binding to cjKDO8PS was further examined directly with ITC. ITC binding of KDO8P oxime to cjKDO8PS$_{H6}$ was examined in the absence and presence of saturating Mn^{2+} concentrations. KDO8P oxime (3 mM) was titrated into 150 μM cjKDO8PS$_{H6}$ in the presence or absence of 500 μM $MnCl_2$. To determine the effect of PEP, 3 mM KDO8P oxime was titrated into 150 μM cjKDO8PS$_{H6}$ in the presence of 500 μM $MnCl_2$ and 500 μM PEP. The effect of A5P on inhibitor binding was determined by titrating 3 mM A5P into 150 μM cjKDO8PS$_{H6}$ in the presence of 500 μM KDOP oxime. The experimental procedure for ITC titrations are described in Section 3.2. All experiments were conducted at 25 °C in ITC buffer (20 mM

Tris·Cl, pH 7.5, 200 mM KCl, 1 mM TCEP). All heats of binding data were fitted to a one-site binding model as in Section 3.2.

4.3. Results

4.3.1. Inhibition

KDO8P oxime inhibited cjKDO8PS$_{H6}$ and cjKDO8PS$_{wt}$ with K_i values of 10 ± 2 μM and 10 ± 1 μM, respectively (Figure 4.1A, B). The K_i values are in agreement with the $K_{d,KDO8P\ oxime}$ of 18 ± 2 μM obtained by ITC in Chapter 3. Activity was not completely abolished with either version of the enzyme. The residual rate persisted even at KDO8P oxime concentrations of 5 mM, i.e., > 200 × K_i. Inhibition of NeuB by NeuNAc oxime and DAHPS by DAHP oxime also demonstrated residual rates.[98,123] X-ray crystallography showed that DAHP oxime only occupies two of the four active sites, hence the residual activity. These observations suggest that partial inhibition is common with the α-carboxyketose synthase family of enzymes.

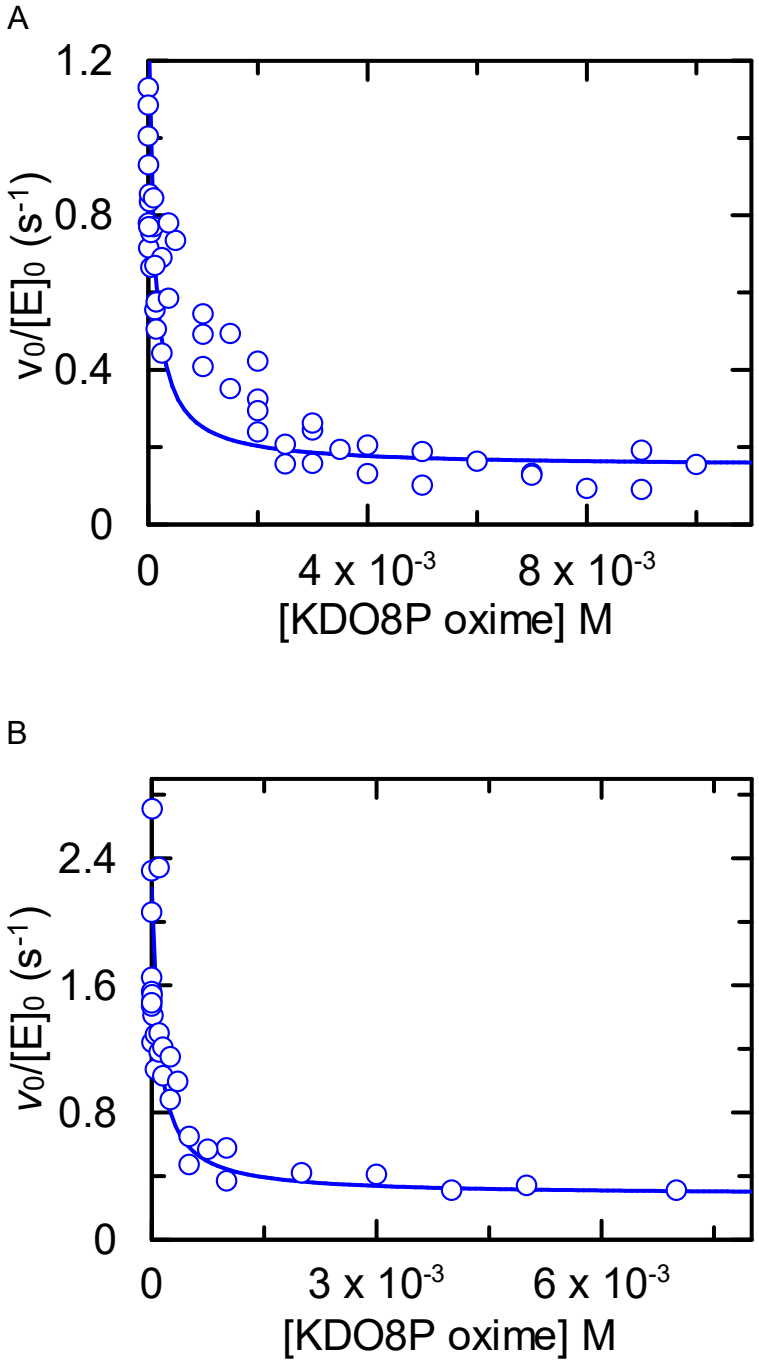

Figure 4.1. Fast-binding inhibition of cjKDO8PS by KDO8P oxime.

(A) cjKDO8PS$_{H6}$ is inhibited with a K_i = 10 ± 2 μM and residual rate of 9%. (B) KDO8P oxime inhibits cjKDO8PS$_{wt}$ with a K_i = 10 ± 1 μM and 14% residual rate.

4.3.2. Mode of binding of KDO8P oxime with respect to substrates

KDO8P oxime's mode of inhibition with respect to all three substrates was examined. Preliminary assays were conducted at room temperature with cjKDO8PS$_{H6}$. In that experiment, increasing the Mn^{2+} concentration at fixed KDO8P oxime concentration only restored 54% of the control rate of cjKDO8PS$_{H6}$ (Figure 4.2). This suggested that KDO8P oxime binding to cjKDO8PS$_{H6}$ was not competitive with respect to Mn^{2+}. To distinguish between non- versus uncompetitive inhibition, we used cjKDO8PS$_{wt}$ to fully characterize $K_{M,Mn}$ in the presence of varying KDO8P oxime concentrations. Rate data were fitted to competitive, noncompetitive and uncompetitive kinetic mechanisms (Figure 4.3, Table S10.1). The fitted data were visualized using Eadie-Hofstee plots[101] (Figure 4.4). A competitive inhibitor will give a series of lines that converge at a single point on the y-axis, which did not occur here. Noncompetitive inhibitors give parallel lines, while uncompetitive inhibitors give lines that converge at the x-axis. It was not obvious from the fitted data whether non- or uncompetitive inhibition fitted the data better. The experiments were limited by the accessible range of Mn^{2+} concentrations. Based on numerical simulations (data not shown), much lower [Mn^{2+}] would have been needed to clearly differentiate between noncompetitive and uncompetitive inhibition. However, in this range, residual EDTA, even after dialysis, would have made free Mn^{2+} concentrations unreliable. As such, these experiments only show that

KDO8P oxime inhibition was not competitive with respect to Mn^{2+}, but could not distinguish between noncompetitive and uncompetitive inhibition.

ITC experiments, which directly measure ligand binding independent of enzyme activity, was a suitable supplementary technique to the kinetic data. As such, titrations of KDO8P oxime against cjKDO8PS$_{H6}$ revealed that KDO8P oxime bound cjKDO8PS$_{H6}$ 20-fold better in the presence of Mn^{2+} than in its absence (Figure 4.5). The kinetic data and the ITC results taken together show that KDO8P oxime preferentially binds to the cjKDO8PS·Mn^{2+} complex, thus making KDO8P oxime an uncompetitive inhibitor with respect to Mn^{2+}.

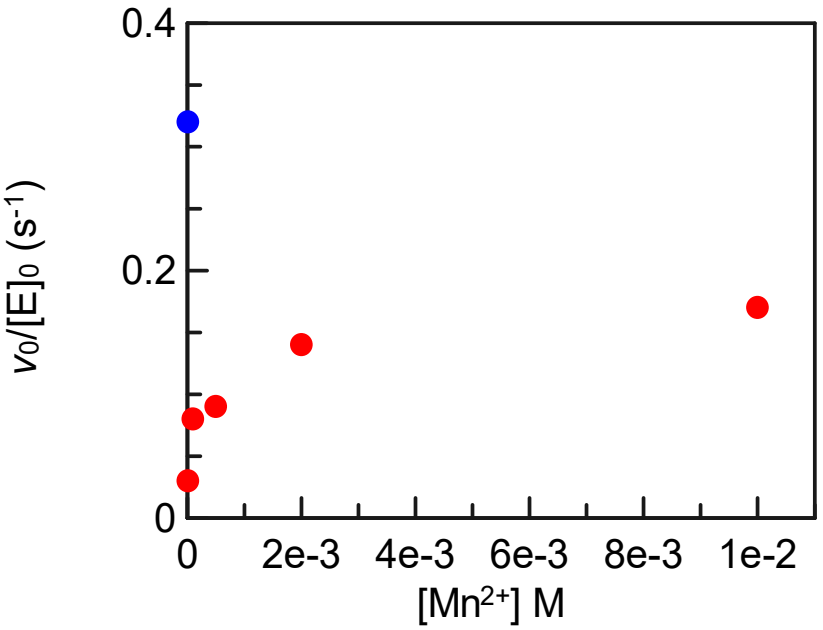

Figure 4.2. Recovery of cjKDO8PS$_{H6}$ activity in the presence of 1 mM KDO8P oxime and increasing [$MnCl_2$].

The control rate (no KDO8P oxime, blue dot) is not recovered in inhibited cjKDO8PS$_{H6}$ (red dots) even at 10 mM Mn^{2+}. Therefore, KDO8P oxime binding was not competitive with respect to Mn^{2+}. This experiment was conducted at room temperature.

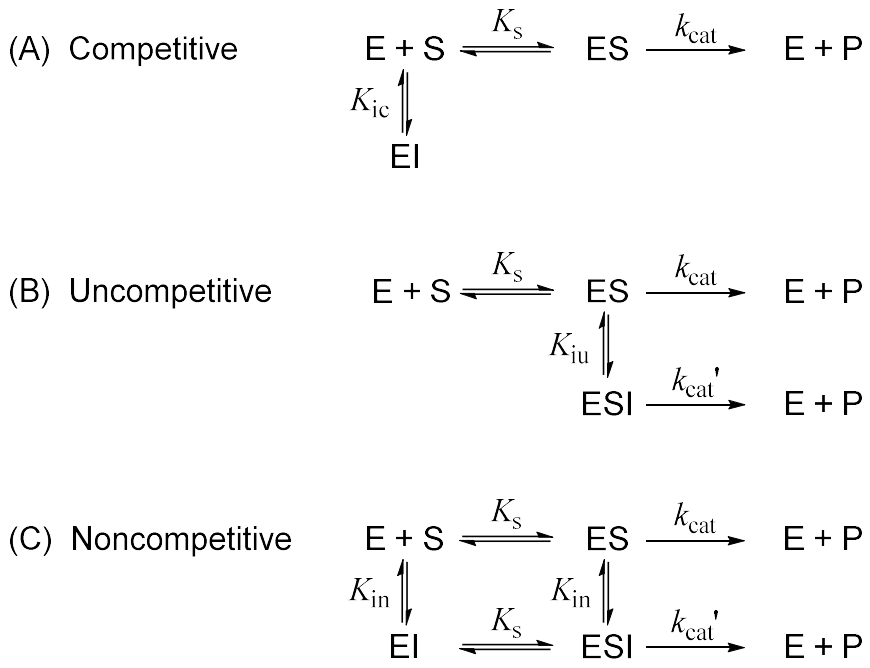

Figure 4.3. Modes of inhibition with respect to Mn^{2+} binding.
The modes of inhibition for a single substrate reaction are shown, with the inhibition constants for competitive (K_{ic}), uncompetitive (K_{iu}) and noncompetitive (K_{in}) inhibition shown. Based on the observed residual rate for KDO8P oxime, a second k_{cat} term for turnover of the ESI complex, k_{cat}', was added.

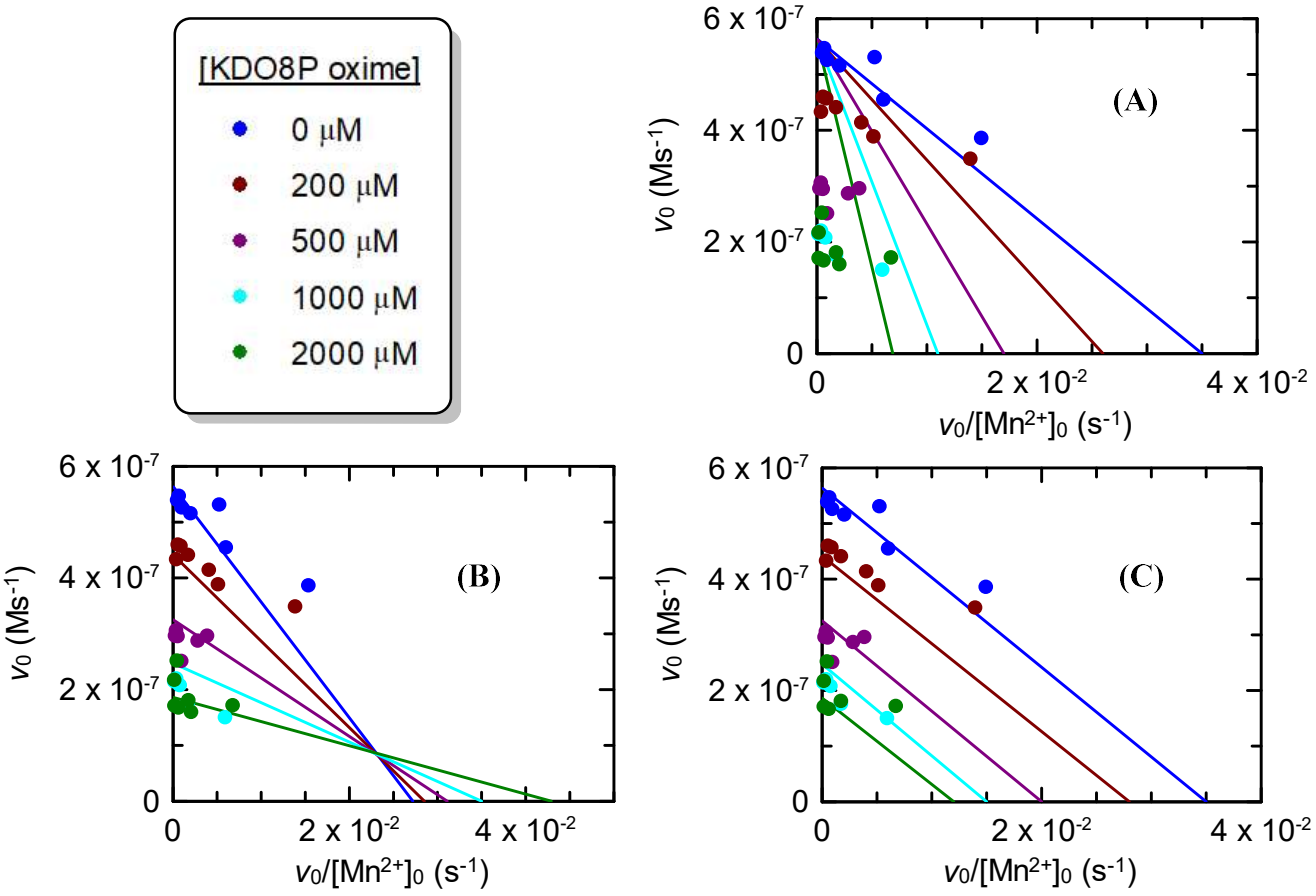

Figure 4.4. Eadie-Hoftsee plots of KDO8P oxime inhibition with respect to Mn^{2+}.

(**A**) Competitive inhibition model (see Table S10.5): k_{cat} = 1.8 ± 0.1 s^{-1}, K_{ic} = 61 ± 38 µM, $K_{M,Mn}$ = 10 ± 5 µM. (**B**) Uncompetitive inhibition model: k_{cat} = 2.3 ± 0.1 s^{-1}, k_{cat}' = 0.3 ± 0.1 s^{-1}, K_{iu} = 44 ± 12 µM, $K_{M,Mn}$ = 21 ± 4 µM. Normally uncompetitive inhibition gives lines that intersect at the x-axis; however, the presence of the k_{cat}' raise the intersection point above the x-axis. (**C**) Noncompetitive inhibition model: k_{cat} = 2.3 ± 0.1 s^{-1}, k_{cat}' = 0.4 ± 0.2 s^{-1}, K_{in} = 48 ± 15 µM, $K_{M,Mn}$ = 16 ± 3 µM. A single substrate kinetic model was used, meaning that the fitted parameters are not accurate, though the patterns in the Eadie-Hofstee plots are.

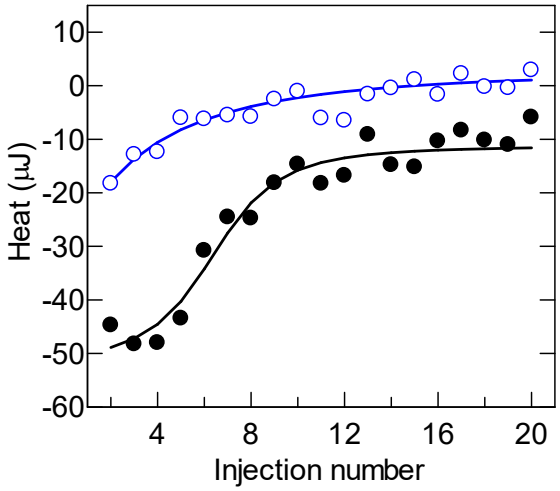

Figure 4.5. ITC titration of KDO8P oxime binding to cjKDO8PS$_{H6}$ in the absence or presence of Mn^{2+}.

ITC titrations of cjKDO8PS$_{H6}$ + KDO8P oxime (blue) and cjKDO8PS$_{H6}$·Mn^{2+} + KDO8P oxime (black) are shown. Fitting the data to a one-site binding model yielded a KDO8P binding K_d of 18 ± 2 μM in for the cjKDO8PS$_{H6}$·Mn^{2+} + KDO8P oxime titration and a K_d of 346 ± 37 μM for the cjKDO8PS$_{H6}$ + KDO8P oxime titration. The cjKDO8PS$_{H6}$ + KDO8P oxime titration data was shifted up by 15 μJ to improve visibility.

KDO8P oxime inhibition of cjKDO8PS was competitive with respect to PEP in that the control rate was recovered with increasing PEP concentration (Figure 4.6). This implies that KDO8P oxime and PEP occupy the same subsite in cjKDO8PS's binding site. The same was true for DAHPS inhibition by DAHP oxime, which was also competitive with respect to PEP.[120] KDO8P oxime's mode of inhibition with respect to PEP was also tested using ITC, where KDO8P oxime was titrated against the cjKDO8PS$_{H6}$·Mn·PEP complex. KDO8P oxime was added to 150 μM cjKDO8PS$_{H6}$ in the presence of $MnCl_2$ and 500 μM PEP. In line with the kinetics result, $K_{d,KDO8P\ oxime}$(apparent) = 144 ± 7 μM in the presence of PEP,

8-fold higher than in the absence of PEP (Figure 4.7). This experiment independently confirmed that KDO8P oxime binding was competitive with respect to PEP. ITC titrations of DAHP oxime against ecDAHPS(Phe) in the presence of PEP showed a similar trend. (Maren Heimhalt, personal communication).

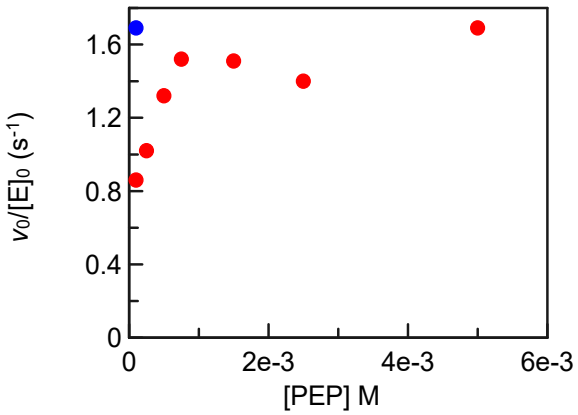

Figure 4.6. KDO8P oxime inhibition of cjKDO8PS$_{wt}$ activity is competitive with respect to PEP.

cjKDO8PS$_{wt}$ activity was measured in the presence of 500 μM KDO8P oxime and increasing concentrations of PEP. Increasing [PEP] outcompeted KDO8P oxime, as the activity of the inhibited cjKDO8PS$_{wt}$ (red dots) returned to the control activity (no KDO8P oxime, blue dot) at higher [PEP].

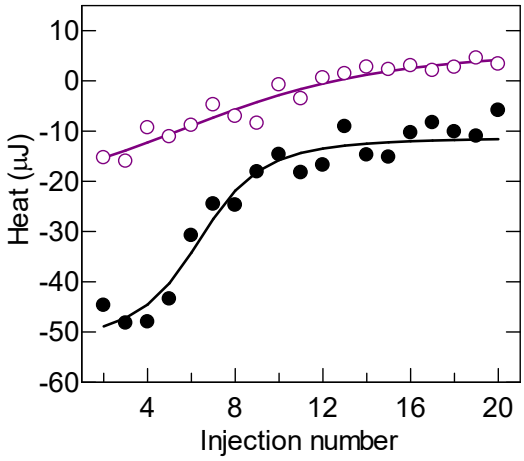

Figure 4.7. Competitive binding of cjKDO8PS$_{H6}$ by KDO8P oxime was competitive with respect to PEP by ITC titrations.

ITC titrations of KDO8PS$_{H6}$□Mn^{2+} + KDO8P oxime (black) compared to that of KDO8PS$_{H6}$□Mn^{2+}□PEP + KDO8P oxime (purple) are shown. The $K_{d,KDO8Poxime}$ = 144 ± 7 μM for the KDO8PS$_{H6}$·Mn^{2+}□PEP, versus 18 ± 2 μM for KDO8PS$_{H6}$·Mn^{2+}; that is 8-fold higher. The cjKDO8PS$_{H6}$·Mn^{2+}□PEP titration curve was shifted up by 15 μJ to improve visibility.

KDO8P oxime's mode of inhibition with respect to A5P was also probed. When the activity of the inhibited enzyme was measured at fixed [KDO8P oxime] and increasing [A5P], it was not possible under the assay conditions to make [A5P] high enough to completely restore the activity to the uninhibited controls. Instead, the mode of inhibition with respect to A5P was tested using ITC titrations. ITC titration of A5P against cjKDOP$_{H6}$ in the presence of 500 μM KDO8P oxime indicated that A5P did not bind in the presence of KDO8P oxime (Figure 4.8). The ITC result clearly indicated that KDO8P oxime prevented A5P binding. Thus, we can conclude that KDO8P oxime binds competitively with respect to A5P since it can be categorized as a bi-substrate inhibitor combining

the A5P and PEP moieties in one molecule. Therefore, KDO8P oxime binding should extend to the A5P binding subsite as well in cjKDO8PS.

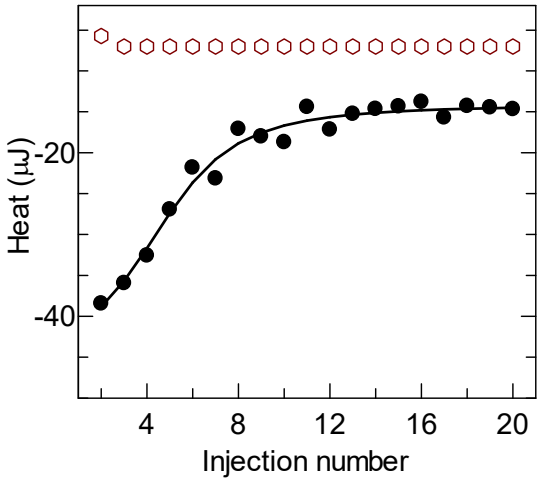

Figure 4.8. ITC titration of cjKDO8PS$_{H6}$ with A5P in presence and absence of KDO8P oxime.

ITC titrations of cjKDO8PS$_{H6}$·KDO8P oxime + A5P (maroon) and cjKDO8PS$_{H6}$ + A5P (black) are shown. Fitting the data to a one-site binding model yielded $K_{d,A5P}$ = 34 ± 2 μM.

4.3.3. Effect of metal ion on inhibition

KDO8P oxime binding was better in the presence of Mn^{2+} ion, as a result, we attempted to test % inhibition with different divalent metals. The percent inhibition was tested at a fixed 1 mM KDO8P oxime concentration with different metal ions, with 200 μM A5P, 500 μM PEP and 250 nM cjKDO8PS$_{wt}$. The concentrations for Mn^{2+}, Ni^{2+}, Co^{2+}, Cu^{2+} and Mg^{2+} were 1 mM, 1 mM, 200 μM, 200 μM and 2 mM, respectively. The assays were conducted in reaction buffer at 37 °C. The % inhibition by KDO8P oxime in the presence of each metal was

calculated relative to the control rate with each metal (**Error! Reference source not found.**). There was no apparent correlation between % inhibition and the ionic radius or solvated ionic radius. There may be a modest relationship between pK_{sp} and % inhibition for the transition metals, not including Mg^{2+}, however, it was difficult to draw a firm conclusion from only four data points (**Error! Reference source not found.**). pK_{sp} refers to the metal–sulfide solubility product, a measure of a metal's affinity for sulfur.[155] Finding a correlation between an ion's characteristics and % inhibition would be complicated by the fact that the metal is coordinated to O, N and S atoms from the sidechains of the metal binding residues C8, H192, E229, D240 in cjKDO8PS. Thus, the metal's hard/soft characteristics will have offsetting effects on its ability to bind different amino acid sidechains. Furthermore, there was also no correlation between individual metal ion's characteristics and its ability to activate the enzyme. With the inhibitor-free enzyme, transition metals were largely good activators of the enzyme except for Cu^{2+}, Cd^{2+} and Zn^{2+} which conferred lower enzyme activity (Section 2.3.8). Taken together this result indicates that inhibition of cjKDO8PS by KDO8P oxime was not significantly hindered by the majority of the metal ions tested but inhibition was modestly affected by each metal.

Table 4.1. Effect of metal ions on inhibition of cjKDO8PS$_{wt}$ by KDO8P oxime.

Activity of the control (no KDO8P oxime) and the inhibited enzyme was determined in the presence of different divalent metal ions.

Metal ion	% inhibition $(1 - v_{inhib}/v_0) \times 100$	pK_{sp}^{155}
Mn^{2+}	69	17.8
Cd^{2+}	64	33.3
Co^{2+}	59	24.6
Mg^{2+}	48	-0.3
Cu^{2+}	38	40.3

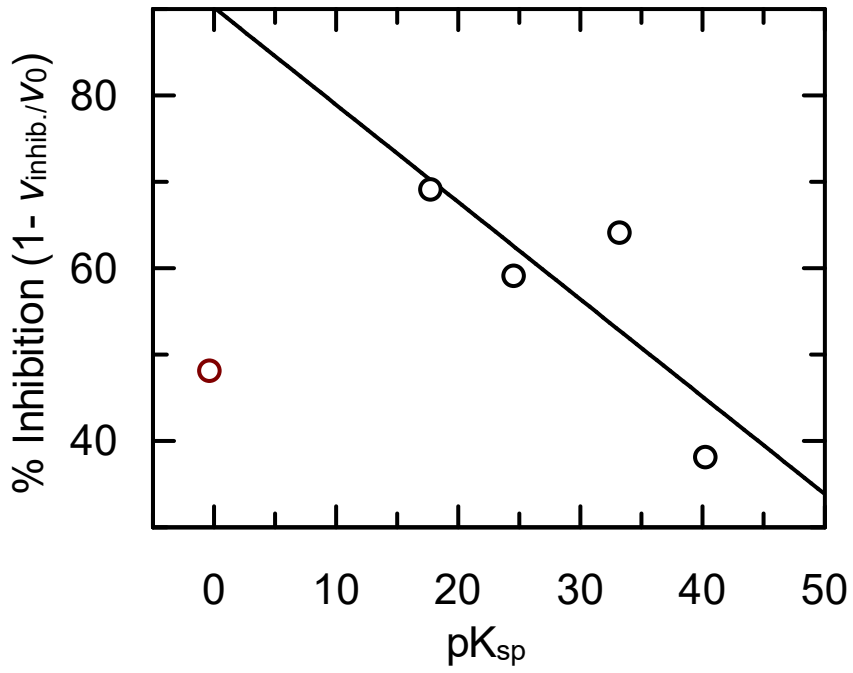

Figure 4.9. Effect of metal ions on inhibition.

The Mg^{2+} ion data (red) was clearly off the apparent linear correlation between % inhibition and pK_{sp}^{155}) for the transition metals.

4.4. Discussion

4.4.1. Mode of inhibition

We kinetically determined that KDO8P oxime inhibition of $cjKDO8PS_{wt}$ is relieved by increasing PEP concentrations, and ITC titrations showed that in the presence of PEP, the apparent KDO8P oxime binding affinity decreased. These two independent experimental findings, taken together, indicate that KDO8P oxime is competitive with respect to PEP. Both PEP and KDO8P oxime bind preferentially to the $E{\cdot}Mn^{2+}$ complex.

Kinetic analyses and ITC titrations demonstrated that the mode of inhibition was primarily uncompetitive with respect to Mn^{2+}. Eadie-Hofstee plots demonstrated that inhibition was not competitive; however, it could not unambiguously distinguish between noncompetitive and uncompetitive inhibition (Figure 4.4). Normally uncompetitive inhibition gives an Eadie-Hofstee plot where the lines intersect at the x-axis; however, the residual rate at high inhibitor concentrations raised the intersection point above the x-axis. A mixed inhibition model was also fitted (not shown). However, given the fact that the data could not distinguish between the extremes of noncompetitive (I binds equally to E and E·S) and uncompetitive (I binds only E·s, not E) inhibition, a mixed mode of inhibition (where I binds with different affinities to both E and E·S) did not shed any further light on the mode of inhibition. The ITC results unambiguously showed that KDO8P oxime could bind to both E and E·S, but 20-fold tighter to E·S (Figure

4.5). Thus, the mode of inhibition was primarily uncompetitive, favouring binding to E·S, but with some measurable binding to E. Unlike in DAHPSs, the metal ion in KDO8Ps plays a structural role by positioning the substrate A5P in the active site. This is facilitated by the coordination of the C2 hydroxyl group of A5P with a metal ion via a water molecule in metal-dependent KDOPSs.[40,56] In metal-dependent KDO8PSs this role is fulfilled by an asparagine side-chain. In KDO8P oxime binding to cjKDO8PS, the C4 hydroxyl in KDO8P oxime is likely coordinated to Mn^{2+} via a water molecule thus favouring uncompetitive-like mode of binding with respect to Mn^{2+}.

ITC titration of A5P to a weakly bound E·I complex did not result in binding, implying that A5P is prevented from binding to the enzyme. The ITC result argued that KDO8P oxime binding is competitive with respect to A5P.

4.4.2. Fast-binding inhibition

KDO8P oxime is a novel inhibitor of cjKDO8PS, with inhibitory constants of K_i = 10 ± 1 μM and 10 ± 2 μM against cjKDO8PS$_{H6}$ and cjKDO8PS$_{wt}$, respectively. The K_i values are within a factor of 2 of the $K_{d,KDO8P\ oxime}$ = 18 ± 2 μM obtained by ITC under somewhat different conditions. In both cases there is residual rate of 9% and 14% of k_{cat} for cjKDO8PS$_{H6}$ and cjKDO8PS$_{wt}$, respectively. The cause for the residual rate is not yet understood, but is likely due to half-of-sites binding to this homotetrameric enzyme. DAHPS inhibition by DAHP oxime also showed partial inhibition and the X-ray crystal structure

showed the inhibitor binding to only two out of four active sites, with subunits B and C containing inhibitor in their active sites, while subunits A and D were unbound.[98] H/D exchange experiments showed that binding of DAHP oxime to DAHPS caused stabilization of the otherwise highly dynamic enzyme. This decrease in protein dynamics might occur at the unbound subunits, causing a decrease in k_{cat} for inhibited DAHPS. Extensive kinetic analysis of DAHPS inhibition by DAHP oxime showed that the substrates, particularly erythrose 4-phophate (DAHPS's third substrate, analogous to A5P) bind better (decreased K_M) to the uninhibited subunits (A and D) when DAHP oxime binds to B and C. Given that KDO8PS and DAHPS are similar and inhibited by similar compounds, it is likely that the observation with DAHPS inhibition by DAHP oxime can be translated to cjKDO8PS inhibition pattern by KDO8P oxime.

KDO8P oxime inhibition is compared with reported KDO8PS inhibitors (Table 4.2). As discussed in Chapter 2, K_M values obtained using the single substrate Michaelis-Menten equation give artificially low K_M values, which leads, in turn, to artifactually low K_i values for competitive inhibitors. It is not possible to retroactively apply the three-substrate Michaelis-Menten equation to literature K_i values. However, applying the single substrate equation (eq. **2.3**) it is possible to estimate the effect of the equation on K_i. Using the K_M(1s) values in equation **4.1** gave apparent K_i values of 2.2 ± 0.5 μM for cjKDO8PS$_{wt}$ and 2.6 ± 0.5 μM for cjKDO8PS$_{H6}$ compared with the true value of 10 μM for both enzymes (Table 4.2) Based on the correct K_i values, KDO8P oxime is already among the most

potent inhibitors of KDO8PSs reported to date. The KDO8P oxime K_i values were comparable to K_i = 3.3 μM of compound **1**, a bi-substrate analogue designed to mimic the oxacarbenium ion intermediate,[156] and K_i = 7.9 μM for **8,** a THI mimic.[117] The reliability of literature K_i values is not always clear. For example, the K_i value for **1** was measured by varying [PEP] using the single-substrate Michaelis-Menten equation.[156] This means that the $K_{M,PEP}$ value used was most likely lower than the true value, which would lead to an artifactually low apparent K_i value. However, the assays were done in the presence of high [A5P], which was not considered in the equations. Assuming that **1** binds competitively with A5P, which is likely given its structure, neglecting [A5P] would lead to the apparent K_i being higher than the true value. As the size of these potential errors are of unknown magnitude and would have opposing effects on the apparent K_i, the reported K_is can be taken only as a rough guide to inhibitor binding.

Table 4.2. Literature dissociation constants of published KDO8PS inhibitors.

Inhibitor [a]	K_i (μM)	Target	Reference
KDO8P oxime	10 ± 1	cjKDO8PS$_{wt}$	This study.[b]
KDO8P oxime	10 ± 2	cjKDO8PS$_{H6}$	This study.[b]
1	3.3 ± 0.3	*E. coli* KDO8PS	Du et al.[156]
2	500	*E. coli* KDO8PS	Du et al.[115]
3	50 ± 5	*E. coli* KDO8PS	Belakhov et. al.[116]
5	260 ± 40	*N. meningitidis* KDO8PS	Harrison et al.[117]
	330 ± 40	*A. ferrooxidans* KDO8PS	
6	870 ± 90	*N. meningitidis* KDO8PS	
	390 ± 70	*A. ferrooxidans* KDO8PS	
7	1200 ± 50	*N. meningitidis* KDO8PS	
	1000 ± 220	*A. ferrooxidans* KDO8PS	
8	7.9 ± 1.6	*N. meningitidis* KDO8PS	
	20 ± 3	*A. ferrooxidans* KDO8PS	
9	1000 ± 80	*N. meningitidis* KDO8PS	
	540 ± 50	*A. ferrooxidans* KDO8PS	
10	270 ± 40	*N. meningitidis* KDO8PS	
	190 ± 40	*A. ferrooxidans* KDO8PS	

[a] The structures of compounds **1** – **9** are shown in Chapter 1.

[b] The K_i values are fitted using K_M(re) derived from the sequential ter ter rapid equilibrium eq. **2.1**.

5. Slow-binding inhibition

5.1. Introduction

The thermodynamic parameters for inhibitor binding to its target, namely K_i or K_d, are generally obtained under "fast-binding" conditions where the inhibitor and substrates are allowed to interact with the enzyme at the same time, and binding/dissociation are assumed to occur on the second or sub-second time scale. However, slow-binding inhibitors are not rare,[98,157–159] and full characterization of an inhibitor often requires taking slow-binding inhibition into account. Slow-binding inhibition often involves two steps; a fast-binding phase and an isomerization phase. In the fast phase inhibitor binding is described by K_i. The enzyme-inhibitor complex (E·I) then undergoes a slow conformational change to form a more tightly bound complex, E*·I. The dissociation rate of the tight complex is necessarily slower than its formation in slow-tight-binding inhibitors. A long residence time of an inhibitor on its target, where $t_R = 1/k_{off}$, is a desirable characteristic that has been shown to be correlated with *in vivo* efficacy.[109] The *in vitro* selection of compounds during preclinical stages of drug discovery must consider both the thermodynamic and kinetic aspects of inhibitor binding to its target. Considering this, oxime-based inhibition of the α-carboxyketose family was also investigated with respect to kinetics of inhibitor binding; that is, whether these inhibitors are slow-binding. Indeed, DAHP oxime is a slow-binding inhibitor of DAHPS, with maximum inhibition requiring 20 min

to develop, while the residence time was 83 min.[120] NeuNAc oxime is also a slow-binding inhibitor of NeuB where complete loss of activity was observed over 6 h when the enzyme was actively turning over, and no recovery of activity was observed in dilution experiments.[123] In this study, we demonstrate that KDO8P oxime is a slow-binding inhibitor of cjKDO8PS.

5.2. Experimental

5.2.1. Slow-binding inhibition of cjKDO8PS$_{wt}$ by KDO8P oxime

To investigate inhibitory properties of KDO8P oxime under slow-binding conditions, as well as to measure the rate of onset of slow-binding inhibition (k_{obs}), cjKDO8PS$_{wt}$ and KDO8P oxime were incubated together at room temperature, then the E·I complex was assayed for activity over time. cjKDO8PS$_{wt}$, 30 μM, was preincubated for 18 or 25 h with varying concentrations of KDO8P oxime (0 – 10 mM) in storage buffer (50 mM Tris·HCl, pH 7.5, 100 mM KCl, 5% glycerol, 1 mM TCEP). The initial velocity of pre-incubated samples was then measured after a 66-fold dilution in reaction buffer (50 mM BTP·Cl, pH 7.5, 150 mM, 1% glycerol, 100 μM TCEP) containing 1 mM $MnCl_2$, 500 μM PEP and 200 μM A5P. A dose-response curve was produced by fitting the data at 18 and 25 h of preincubation using eq. **5.1** adapted from Copeland.[100]

$$\frac{v_{0,I}}{v_{0,C}} = \frac{[\max - \min]\left(1 - I^{n}\right)}{1 + \left(\frac{I}{IC_{50}}\right)^{n}} + \min \qquad (5.1)$$

where, $v_{0,I}$ and $v_{0,C}$ are the initial velocities of the inhibited enzyme and control, respectively, max and min are $v_{0,I}/v_{0,C}$ at zero and infinite [I], respectively, [I] is the inhibitor concentration, IC_{50} is the inhibitor concentration that causes a 50% reduction in activity, and n is the Hill coefficient, often described as a measure of cooperativity.

5.2.2. Slow-binding association rate constant (k_{on})

The value of k_{on} was measured using two different methods: directly, reported as $k_{on,direct}$, and from the concentration dependence of slow-binding inhibition, reported as $k_{on,conc}$ (see below).

The rate of the onset of slow-binding inhibition, k_{obs}, is the sum of the slow-binding association rate constant, k_{on}, and the slow-binding dissociation rate constant, k_{off}, at very high inhibitor concentration. Thus, at very high inhibitor concentrations, assuming k_{off} is very small, k_{obs} is essentially equivalent to k_{on}. To determine $k_{on,direct}$, the time-dependent loss of activity was measured for cjKDO8PS$_{wt}$. To do this, 15 μM cjKDO8PS$_{wt}$ was incubated with 2 mM KDO8P oxime at room temperature in 50 mM BTP·Cl, pH 7.5, 100 mM KCl, 6% glycerol, 0.6 mM TCEP. The complex was assayed for activity over 20 h at 37 °C in reaction buffer containing 1 mM $MnCl_2$, 500 μM PEP and 200 μM A5P. The data were fitted to eq. **5.2**.

$$\frac{v_0}{[\mathrm{E}]_0} = e^{-k_{on,direct} \times t} + \mathrm{offset} \qquad (5.2)$$

where v_0 = initial velocity, $[E]_0$ = total enzyme concentration, $k_{on,direct}$ = slow-binding association rate constant, t = time, and offset = non-zero residual rate at infinitely high inhibitor concentration.

5.2.3. Slow-binding dissociation rate constant (k_{off})

The dissociation rate constant, k_{off}, was measured using three different methods, jump dilution, gel filtration, and by the concentration dependence. Each method gave a different value, so they are differentiated below as $k_{off,jump}$, $k_{off,gel}$, and $k_{off,conc}$.

The slow-binding dissociation rate constant, $k_{off,gel}$ was determined by first forming the E*·I complex with 15 μM cjKDO8PS$_{wt}$ and 2 mM KDO8P oxime in 50 mM BTP·Cl, pH 7.5, 100 mM KCl, 6% glycerol, 0.6 mM TCEP at room temperature over 20 h, purifying the complex from excess KDO8P oxime by desalting using a gel filtration MicroSpin G-25 column (GE healthcare) pre-equilibrated with 50 mM BTP·Cl, pH 7.5, 1 mM $MnCl_2$, 2 mM PEP, 6% glycerol, 0.25 mg/mL BSA, 100 mM KCl, and 600 μM TCEP. This was centrifuged at 700 ×g at 20 °C for 2 min. The eluate (250 μL) was diluted to 500 μL with the same buffer, leading to 7-fold dilution of the E*·I complex, to 2 μM, and was incubated at 20 °C for varying periods. Activity was monitored over time by adding an aliquot of the complex to a reaction buffer containing 50 mM BTP·Cl, pH 7.5, 690 μM PEP, 200 μM A5P, 1.1 mM $MnCl_2$, 157 μM TCEP, 0.024 mg/mL BSA, 1.57 % glycerol and 150 mM KCl at 37 °C.

Alternatively, the 'jump dilution' method was utilized to measure $k_{off,jump}$. Here, the E*·I complex that had been formed overnight was diluted 43-fold into incubation buffer (50 mM BTP·Cl pH 7.5, 1 mM $MnCl_2$, 2 mM PEP, 6% glycerol, 0.25 mg/mL BSA, 100 mM KCl, and 600 μM TCEP) such that the enzyme and inhibitor concentrations were 350 nM and 47 μM, respectively. The pre-incubation mixture was aliquoted into 200 μL portions and each aliquot was tested for activity at different time points. This was done by adding 10 μL of substrate mixture (4 mM A5P and 10 mM PEP) to start the reaction. The data in both cases were fitted to eq. **5.3**[98] to obtain $k_{off,jump}$.

$$v_{0,t} = v_{0,i} + \text{limit} \times \left(1 - e^{-k_{off,jump} \times t}\right) \tag{5.3}$$

where t is the preincubation time, $v_{0,t}$ is the initial velocity at time = t, $v_{0,i}$ is the initial velocity at t = 0, k_{off} is the slow-binding dissociation rate constant, , and limit is the maximum recovery of initial velocity at t = ∞.

5.2.4. Determination of the mode of slow-binding inhibition - k_{obs} vs [I]

For each inhibitor concentration, the ratio $v_{0,t}/v_{0,i}$ for the experiment described in Section 5.2.1 was fitted to eq. **5.4** to obtain k_{obs} at each KDO8P oxime concentration.

$$\frac{v_{0,t}}{v_{0,i}} = v_{0,i} \times e^{-k_{obs} \times t} + \text{offset} \tag{5.4}$$

where k_{obs} is rate of the onset of slow-binding inhibition and offset is the non-zero residual rate at t_∞. The k_{obs} determined at each inhibitor concentration was then plotted against KDO8P oxime concentration. The data was fitted to eq. **5.5** to estimate the slow-binding association rate constant $k_{on,conc}$ and dissociation rate constant $k_{off,conc}$.[100]

$$k_{obs} = \frac{k_{on,conc}}{\left(1 + \frac{IC_{50}}{[I]}\right)} + k_{off,conc} \quad (5.5)$$

5.2.5. Aggregation test for cjKDO8PS$_{wt}$·KDO8P oxime complex

The E*·I complex was made by mixing 15 µM of cjKDO8PS$_{wt}$ with 3 mM KDO8P oxime in storage buffer at room temperature overnight. The complex was assayed for activity, and was found to be 77 % inhibited. Next, 100 µL of the complex was injected onto a 24 mL Superose 12 10/300 GL size exclusion column equilibrated with storage buffer and run at 4° C with a flow rate of 1 mL/min and A_{280} detection. Two controls were also run; cjKDO8PS$_{wt}$ alone and KDO8P oxime alone. The partition coefficient (K_{av}) of each analyte was determined using eq. **5.6**:

$$K_{av} = \frac{V_e - V_0}{V_C - V_0} \quad (5.6)$$

where V_0 = column void volume (8.4 mL), V_e = elution volume, and V_C = geometric column volume (24 mL). The void volume was determined by running

Blue Dextran through the column. The molecular weight of cjKDO8PS$_{wt}$ was determined according to the calibration curve eq. **5.7**:

$$K_{av} = 0.2727 \times \log(MW) + 1.7183. \quad (5.7)$$

5.3. Results

5.3.1. Association (k_{on}) and dissociation (k_{off}) rate constants

For slow-binding inhibitors, inhibition occurs in two phases (Figure 5.1). The initial encounter of E and I to form an E·I complex is fast and governed by the equilibrium inhibition constant K_i. The rate of E·I isomerization to a tight-binding E*·I complex is dictated by the forward and reverse isomerization rate constants; k_{on} and k_{off}, respectively. Under the assumption that the reverse isomerization, or the dissociation of E*·I, is slower than k_{on}, the observed rate of slow-binding inhibition (k_{obs}) at very high inhibitor concentration is equivalent to k_{on}. (If E*·I reverse isomerization or dissociation is fast, then slow-binding inhibition will not be observed.)

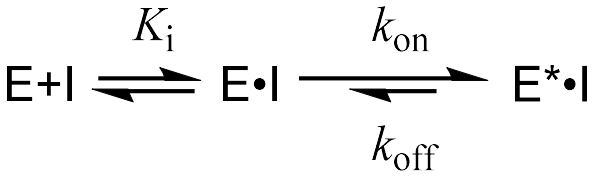

Figure 5.1. Schematic for slow-binding inhibition.

Fast-binding of E and I forms a weakly bound E·I complex with an inhibition constant of K_i. E·I isomerizes to a tight-binding E*·I complex governed by the forward and reverse isomerization constants k_{on} and k_{off}, respectively.

$k_{on,direct}$ determination

When cjKDO8PS$_{wt}$ was pre-incubated with KDO8P oxime, the initial velocity decreased with increasing pre-incubation time. The time-dependent loss of activity followed an apparent first order rate with a rate constant, $k_{on,direct}$, of 0.36 ± 0.06 h^{-1}, or $t_{1/2} = 1.9$ h. Maximum inhibition was observed by 12 h, with a residual rate of 13% (Figure 5.2).

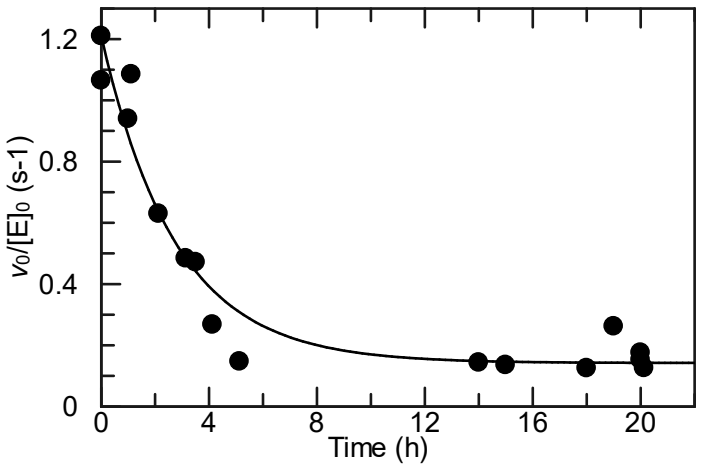

Figure 5.2. Time-dependent inhibition of cjKDO8PS$_{wt}$ by KDO8P oxime.

cjKDO8PS$_{wt}$ (15 μM) was pre-incubated with 2 mM KDO8P oxime for up to 20 h. The pre-incubated mixture was added to 200 μM A5P, 500 μM PEP and 1 mM $MnCl_2$ in reaction buffer to start the reaction, giving final concentrations of 200 nM cjKDO8PS$_{wt}$ and 27 μM KDO8P oxime. The kinetic assays to determine initial velocity ($v_0/[E]_0$) were conducted in under 3 min, and thus were fast relative to $k_{on,direct}$.

$k_{off,gel}$ determination

In order to measure the dissociation rate of the E*·I complex, it was pre-formed overnight in the presence of excess KDO8P oxime, then the excess KDO8P oxime was removed by gel filtration. The purified E*·I complex was incubated with large excesses of PEP and Mn^{2+}. PEP was used to prevent

rebinding of the inhibitor as E*·I complex dissociated. Mn^{2+} and BSA were added to stabilize the enzyme. Without BSA the enzyme rapidly lost activity. The control reaction of only cjKDO8PS$_{wt}$ retained over 80 % activity during the course of the experiment. When the gel filtration method to remove excess inhibitor was used in $k_{off,gel}$ determination, the return of activity gave $k_{off,gel}$ = 2.2 ± 0.2 h^{-1}, and a residence time, t_R, = 27 min (Figure 5.3). This was faster than $k_{on,direct}$, which implies that that slow-binding should not have been observed. This fast return of activity was also observed even in the absence of PEP and Mn^{2+}. Removing BSA destabilized the enzyme such that there was loss of activity immediately after the gel filtration step. The removal of the excess inhibitor was the cause of the unexpectedly fast dissociation of the E*·I complex.

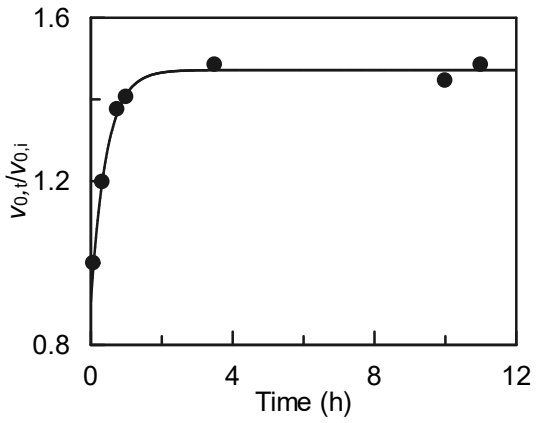

Figure 5.3. Determination of $k_{off,gel}$ of KDO8P oxime from cjKDO8PS$_{wt}$ – gel filtration method.

The E*·I complex was purified by gel filtration to remove excess inhibitor, then incubated in the presence of large excesses of PEP (2 mM) and $MnCl_2$ (1 mM). To this mix, A5P was added to start the reaction and determine initial velocity. The ratio of the initial velocity at time t ($v_{0,t}$) to the initial velocity at t = 0 ($v_{0,i}$) versus time is plotted.

An alternate method, jump dilution, was also used to measure the dissociation rate, $k_{off,jump}$. Here, the E*·I complex was pre-formed by incubating cjKDO8PS$_{wt}$ with excess KDO8P oxime at room temperature overnight. The mixture was then diluted 43-fold in incubation buffer containing 2 mM PEP, 1 mM $MnCl_2$ and 0.25 mg/ml BSA, such that the diluted concentration of KDO8P oxime was 47 μM, 100-fold higher than the E*·I concentration. Under these conditions fitting the rate of return of activity to eq. **5.3** yielded $k_{off,jump}$ = 0.09 ± 0.05 h^{-1}, with a t_R = 11 h (Figure 5.4). Thus, with the jump dilution method E*·I dissociation was 4 times slower than the association rate constant.

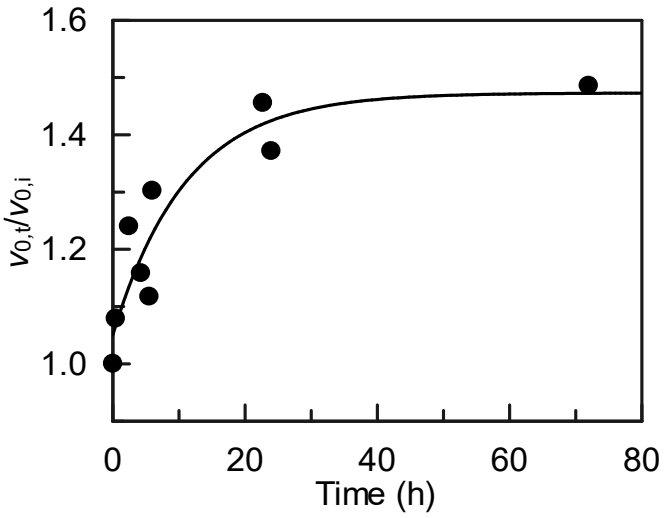

Figure 5.4. Determination of $k_{off,jump}$ –using the jump dilution method.

The E*·I complex was diluted 43-fold in the presence of large excesses of PEP (2 mM) and $MnCl_2$ (1 mM), so that any dissociated enzyme would be trapped as the E·Mn^{2+}·PEP complex. A5P was added to aliquots at different times to start the reaction and determine initial velocities. The ratio $v_{0,t}/v_{0,i}$, that is, the initial velocity at time t ($v_{0,t}$) to the initial velocity at t = 0 ($v_{0,i}$) was plotted versus time.

5.3.2. Concentration dependence of slow-binding inhibition

cjKDO8PS$_{wt}$ was preincubated with varying KDO8P oxime concentrations for 18 - 25 h, then the activity was assayed. The activity assay (3 min) was too fast for significant E*·I dissociation to occur during the assay, which means that the observed activity reflected the E*·I concentration in the preincubation mixture, rather than the reaction mixture. Therefore, the KDO8P oxime concentrations in the preincubation mixture were used in the dose-response curve. The ratio of the initial velocity of the inhibited enzyme ($v_{0,I}$) to the initial velocity of the control ($v_{0,C}$) were fitted to the Hill equation (eq.**5.1**), giving IC_{50} = 3.1 ± 0.1 mM, with a Hill coefficient n = 3.6 ± 0.3 (Figure 5.5). This implied that KDO8P oxime molecules must bind to all four subunits to trigger slow-binding inhibition, though that contradicts the finding from fast-binding inhibition that there is residual rate at high inhibitor concentrations, suggesting half-of-sites inhibitor binding. That being said, the IC_{50} value was over 300-fold higher than K_i. This was consistent with KDO8P oxime binding being less favorable in the absence of the metal, as seen with the ITC titrations (Chapter 3). It would also be consistent with inhibitor binding to all four subunits with a K_i value much higher than observed in the fast-binding inhibition experiments. Even under slow-binding conditions a 15% residual rate was observed, indicating that slow-binding inhibition was induced in only two of the four subunits, forming the E*·I_2 complex.

The concentration dependence of slow-binding inhibition of cjKDO8PS$_{H6}$ was determined under slightly different conditions, by preincubating 10 μM cjKDO8PS$_{H6}$ with varying KDO8P oxime concentrations (0 - 3 mM) at room temperature for over 21 h. Assays were conducted at room temperature. Preincubation of cjKDO8PS$_{H6}$ with KDO8P oxime also showed cooperativity of inhibitor binding, yielding IC_{50} = 600 ± 51 μM, and n = 1.6 ± 0.2 (Figure 5.5B). This suggested slightly higher affinity, but a lower degree of cooperativity in inhibitor binding than cjKDO8PS$_{wt}$. The IC_{50} of 600 μM obtained by preincubation of cjKDO8PS$_{H6}$ with KDO8P oxime was within a factor of two of the fitted $K_{d,KDO8P\ oxime}$ obtained with ITC titrations in the absence of Mn^{2+} (Chapter 3).

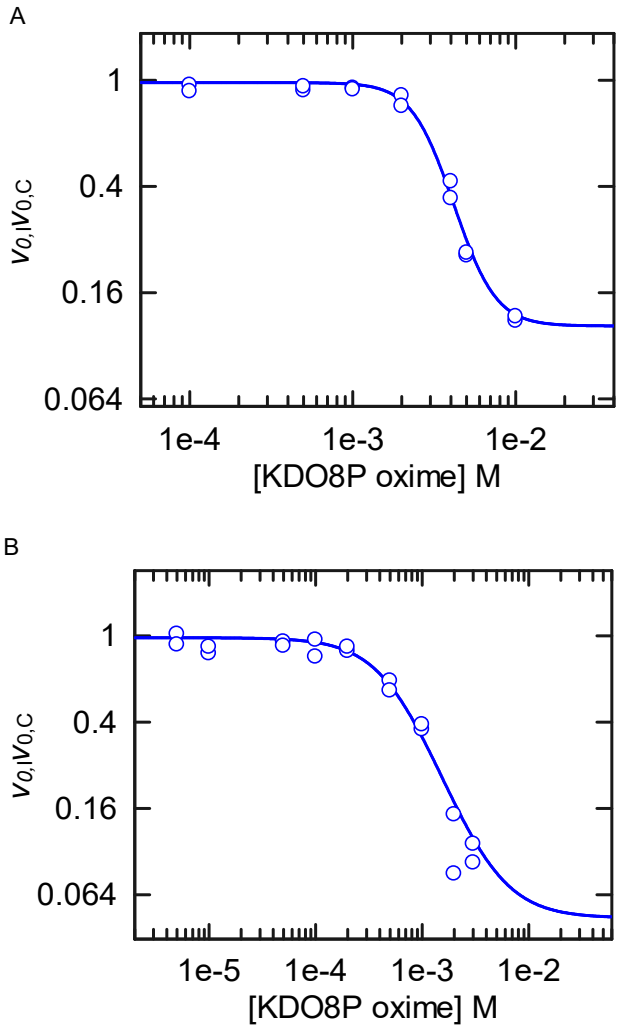

Figure 5.5. Slow-binding inhibition of cjKDO8PS$_{wt}$ and cjKDO8PS$_{H6}$ by KDO8P oxime.

Each enzyme was pre-incubated with varying [KDO8P oxime] for 18 - 25 h at room temperature before rate assays at 37 °C for cjKDO8PS$_{wt}$ and room temperature for cjKDO8PS$_{H6}$. The ratio $v_{0,I}/v_{0,C}$, that is, the initial velocity of the inhibited enzyme divided by the initial velocity of the control, decreased with increasing inhibitor concentration, producing a sigmoidal inhibition curve. The data was fitted to eq. **5.1**. (A) cjKDO8PS$_{wt}$. IC_{50} = 3.1 ± 0.1 mM, n = 3.6 ± 0.3. (B) cjKDO8PS$_{H6}$. IC_{50} = 600 ± 51 µM, n = 1.6 ± 0.2.

The apparent cooperativity in the dose-response curves could be indicative of protein aggregation and/or the inhibitor's solubility limit at high

concentrations.[100] cjKDO8PS$_{wt}$ was incubated at room temperature with KDO8P oxime overnight to form the E*·I complex, which was then subjected to size exclusion chromatography alongside free cjKDO8PS$_{wt}$ as a control. There was no evidence of higher oligomeric structures or protein aggregation (Figure S10.13), thus the cooperativity of inhibitor binding here was not a result of protein aggregation.

5.3.3. k_{obs} vs [I] – implications for the mode of slow-binding inhibition

Slow-binding inhibition can be characterized into three mechanisms (Figure 5.6).[100] (A) E·I formation in a simple single-step equilibrium binding mechanism in which the association (k_3) or dissociation (k_4) rate constants, or both, are slow. (B) Formation of E·I is simple, rapid equilibrium binding, followed by a slow enzyme isomerization (via k_5) to form a tighter complex E*·I with an even slower reverse isomerization or dissociation step (determined by k_6). (C) The formation of an irreversible E·I complex, such as in covalent modification of the enzyme by an affinity label or mechanism-based inhibitor.

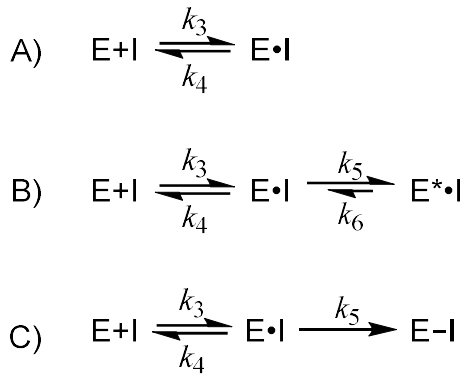

Figure 5.6. Mechanisms of slow-binding inhibition.
From reference [100].

Mechanism A is eliminated for KDO8P oxime because fast-binding inhibition was observed before the onset of slow-binding inhibition. Mechanism C is eliminated because inhibition was reversible, as shown by the return of activity when E*·I was diluted or purified away from excess KDO8P oxime by gel filtration. In mechanism B the first encounter of enzyme and inhibitor is fast, governed by k_3 and k_4. Next, the slow isomerization step to form a high affinity complex E*·I is determined by k_5 (or k_{on}). The reverse isomerization of E*·I to E·I is given by k_6 (or k_{off}). A plot of k_{obs} vs [I] is a Michaelis-Menten type rectangular hyperbolic curve where, at infinitely high inhibitor concentration, k_{obs} (or k_{max}) = $k_{on,conc} + k_{off,conc}$ and the y-intercept = $k_{off,conc}$ as shown in eq. **5.5**.

Indeed, the inactivation of cjKDO8PS was concentration dependent (Figure 5.7, left column). Using eq. **5.4**, a global analysis of the data at each inhibitor concentration for both $cjKDO8P_{wt}$ and $cjKDO8PS_{H6}$ was used to obtain k_{obs} at varying [KDO8P oxime]. Plotting k_{obs} versus [KDO8P oxime] produced a rectangular hyperbolic curve for both $cjKDO8PS_{wt}$ and $cjKDO8PS_{H6}$ (Figure 5.7,

right column). The shape of the curves conformed to mechanism B type slow-binding. From these plots, with cjKDO8PS$_{wt}$, $k_{on,conc}$ = 0.2642 ± 0.0004 h^{-1}, $k_{off,conc}$ = 0.0077 ± 0.0002 h^{-1} and IC_{50} = 3.20 ± 0.01 mM. In order words, under ideal conditions $t_{1/2}$ of inhibitor binding under slow-binding conditions was 2.6 h for cjKDO8PS$_{wt}$ and the residence time, t_R, was 130 h, or 5 days. The fitted $k_{on,conc}$ value was close to $k_{on,direct}$ obtained at high KDO8P oxime concentration in Section 5.3.1. The value of $k_{off,conc}$, however, was considerably lower than the values of $k_{off,gel}$ or $k_{off,jump}$ determined in Section 5.3.1. This reinforced the observation that the apparent k_{off} depended on [I], with $k_{off,gel}$ = 2.2 h^{-1} ([I] ≈ 0), $k_{off,jump}$ = 0.09 h^{-1} ([I] = 47 μM), and $k_{off,conc}$ = 0.008 h^{-1} ([I] = 100 μM – 10 mM). The IC_{50} values were identical, within error. The corresponding values for cjKDO8PS$_{H6}$ were k_{on} = 0.10 ± 0.01 h^{-1}, $k_{off,conc}$ = 0.032 ± 0.003 h^{-1} and IC_{50} = 1.1 ± 0.3 mM. Therefore, for cjKDO8PS$_{H6}$, t_R = 31 h. These constants were clearly, but modestly, different from cjKDO8PS$_{wt}$. Part of this could be due to the fact that cjKDO8PS$_{wt}$ was assayed at 37 °C while the cjKDO8PS$_{H6}$ was assayed at room temperature. Nonetheless, both enzyme versions displayed slow-binding inhibition by KDO8P oxime following mechanism B. The estimated long residence times of KDO8P oxime on the enzyme target are impressive and have implications for *in vivo* efficacy.

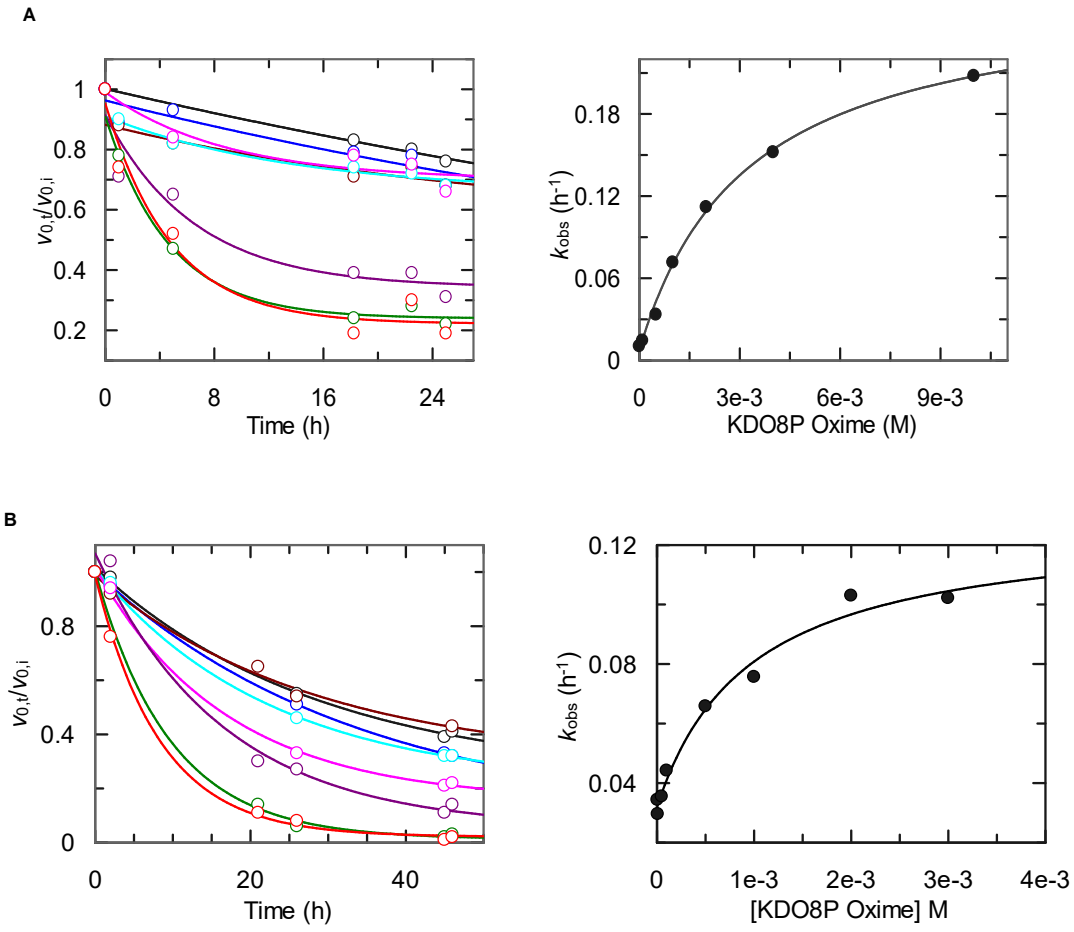

Figure 5.7. Slow-binding inhibition of cjKDO8PS by KDO8P oxime follows mechanism B slow-binding kinetics.

Left column: Residual rate ($v_{0,t}/v_{0,i}$) versus incubation time for varying [KDO8P oxime] with (A) cjKDO8PS$_{wt}$ and (B) cjKDO8PS$_{H6}$. For cjKDO8PS$_{wt}$, [KDO8P oxime] = 0 μM (black), 100 μM (blue), 500 μM (maroon), 1 mM (aqua), 2 mM (purple), 4 mM (magenta), 5 mM (green), 10 mM (red). For cjKDO8PS$_{H6}$, [KDO8P oxime] = 5 μM (black), 10 μM (blue), 50 μM (maroon), 100 μM (aqua), 500 μM (purple), 1 mM (magenta), 2 mM (green), 3 mM (red).
Right column: k_{obs} derived from global analysis of the data shown on the left column using eq. **5.4**. The k_{obs} is plotted against KDO8P oxime concentration and eq. **5.5** was used to fit for $k_{on,conc}$, $k_{off,conc}$ and IC_{50}.

5.4. Discussion

5.4.1. Slow-binding inhibition

KDO8P oxime exhibited slow-binding behavior against cjKDO8PS. KDO8P oxime's slow-binding behavior followed a type B mechanism (Figure 5.6), where the first encounter of E and I to form weakly bound E·I is fast, followed by a slow isomerization phase to a tight-binding E*·I complex. The first phase of inhibitor binding was measured under fast-binding conditions with a K_i = 10 ± 1 μM (Section 4.3.1) against cjKDO8PS$_{wt}$. The ultimate inhibition constant, K_i^*, takes into account the slow isomerization of E·I to a higher affinity complex, E*·I. K_i^* is determined by taking into account the forward and reverse isomerization rate constants k_{on} and k_{off}, respectively (eq. **5.8**):[100,160]

$$K_i^* = \frac{K_i}{1 + \frac{k_{on}}{k_{off}}} \quad (5.8).$$

Applying the measured values of K_i = 10 ± 1 μM (Section 4.3.1), $k_{on,conc}$ = 0.26 ± 0.06 h^{-1} and $k_{off,conc}$ = 0.0077 ± 0.0002 h^{-1} gives K_i^* = 0.28 ± 0.10 μM. This is the ultimate inhibition constant under the best possible conditions, when there is a large excess concentration of KDO8P oxime. As shown by the relative values of $k_{off,gel}$, $k_{off,jump}$, and $k_{off,conc}$, k_{off} depends on [KDO8P oxime]$_{free}$. The K_i^* value of 0.28 μM makes KDO8P oxime the tightest binding KDO8PS inhibitor characterized to date, though with the caveat that tight binding is maintained only

in the presence of excess KDO8P oxime. When $[\text{KDO8P oxime}]_{free} \approx 0$, as in the gel filtration experiment, $k_{off,gel}$ is higher, leading to $K_i^* = 8.9$ μM, only slightly lower than K_i. The previous best inhibitor had $K_i^* = 0.4$ μM (compound **1**, Table 5.1).[115] KDO8P oxime has the advantage over compound **1** that the phosphate group mimicking the tetrahedral intermediate phosphate group is replaced in KDO8P oxime by a neutral small oxime group. Even though the K_i^* is in the high nanomolar range, KDO8P oxime's long residence time (130 h) on the target is important. For example, some drugs have been developed that have micromolar K_i values, yet, because of their long residence times, have high *in vivo* efficacy. For example, 2-amino-5-mercapto-1,3,4-thiadiazole (AMT) is a slow-binding inhibitor of *E. coli* peptide deformylase with a K_i^* of 3.7 μM and residence time of 12.6 h that is indicated for bacterial infection.[159] Similarly, a cyclophostin analogue that targets human acetylcholinesterase indicated for Alzheimer's disease has $K_i^* = 1.4$ μM and a residence of 4.2 h.[157]

The difference in free energy between E·I and E*·I can be estimated from the ratio of inhibition constants for the two complexes, K_i and K_i^* (eq. **5.9**):[159,161]

$$\Delta\Delta G = -RT \ln\left(\frac{K_i^*}{K_i}\right) \qquad (\mathbf{5.9})$$

where R is the ideal gas constant and T is the temperature. Applying K_i = 10 μM and $K_i^* = 0.28$ μM, R = 0.00199 kcal K^{-1} mol^{-1} and T = 298 K, the free energy difference between E·I and E*·I was -2.1 kcal mol^{-1} at 25 °C. This is equivalent to one medium-strength hydrogen bond. Table 5.1 lists inhibition

parameters, including slow-binding parameters, for reported inhibitors in comparison to cjKDO8PS$_{wt}$ inhibition by KDOP oxime.

Table 5.1. Binding affinity and kinetics for cjKDO8PS$_{wt}$ in comparison to some inhibitors in literature.

Compound	Target	K_i (μM)	k_{on}	k_{off}	K_i^*(μM)	t_R (h)	ΔΔG (kcal mol^{-1})	Indication	Reference
KDO8P oxime	cjKDO8PS$_{wt}$	10[a]	0.0043 min^{-1} ($k_{on,conc}$)	1.3 × 10^{-4} min^{-1} ($k_{off,conc}$)	0.28	130	-2.1		This study
DAHP oxime	*E. coli* DAHPS	1.5	0.24 min^{-1}	0.012 min^{-1}	0.07	1.4	-1.8		98
Cyclophostin Analogue entry #9	Human AChE[c]	76	0.2 min^{-1}	0.01 min^{-1}	3.62	1.7	-1.8	Alzheimer's disease	157
Cyclophostin Analogue entry #15	Human AChE[c]	310	4.2 min^{-1}	0.13 min^{-1}	9.31	0.1	-2.1	Alzheimer's disease	157
Cyclophostin Analogue entry #2a	Human AChE[c]	24	0.3 min^{-1}	0.02 min^{-1}	1.50	0.8	-1.6	Alzheimer's disease	157
Cyclophostin Analogue entry #2b	Human AChE[c]	140	0.40 min^{-1}	4 × 10^3 min-^{1}	1.39	4.2	-2.7	Alzheimer's disease	157
Efavirenz	HIV-1 reverse transcriptase	5				4.1		HIV	158
Bis-AMT	*E. coli* Peptide deformylase	3.7				12.6		Bacterial infection	159

[a] K_i is obtained using eq. **4.1**.

[b] Converted to units of min^{-1} for comparison with literature values. $k_{on,conc}$ = 0.26 h^{-1}, $k_{off,conc}$ = 0.0077 h^{-1}.

[c] AChE = acetylcholinesterase.

The dissociation of KDO8P oxime from E*·I in the presence of excess inhibitor, $k_{off,conc}$, was 290-fold slower than in the absence of free inhibitor ($k_{off,gel}$). KDO8P oxime binding showed positive cooperativity under slow-binding conditions with cjKDO8PS$_{wt}$, but not under fast-binding conditions. The measure of cooperativity was n = 3.6 implying that the onset of slow-binding, that is, the transition from E·I to E*·I, is only induced when all four subunits are occupied by inhibitor (Figure 5.8). This is somewhat at odds with the observations of residual activity in both fast-binding and slow-binding inhibition assays (Sections 4.3.1, 5.3.1), which implies incomplete occupancy of the enzyme active sites. However, the IC_{50} value for slow-binding inhibition of cjKDO8PS$_{wt}$, 3.2 mM, compared with K_i = 10 μM, implies that there is negative cooperativity of inhibitor binding. That is, partial occupancy of the tetrameric enzyme's active sites leads to lower affinity in the unbound active sites. However, inhibitor binding in the lower affinity sites is needed for slower (and tighter) binding to occur. In other words, given the residual rate under slow-binding conditions, the slow isomerization presumably occurs in only two of the active sites while all four active sites are occupied to form the tightly bound E*·I_2 complex. The E·I_4 to E*·I_2 conversion rate was $k_{on,conc}$ = 0.26 h^{-1} for cjKDO8PS$_{wt}$. The remaining weakly bound active sites (A and D, blue circles) are presumably responsible for the residual rate even at extended incubation periods. If the presence of inhibitor on the weakly bound active sites stabilizes the tightly bound sites E*·I_2 (B and C, red squares), then the purification of the complex through a gel filtration column removes inhibitor

molecules from the weakly bound sites, which then induces relatively fast reverse isomerization of the tightly bound sites. This is likely what caused the rather high $k_{off,gel} = 2.2\ h^{-1}$. Because this value is greater than k_{on}, it cannot represent the off rate during the onset of slow-binding inhibition, otherwise no slow-binding inhibition would be observed. Using the jump dilution method to measure $k_{off,jump}$ maintained a modest concentration of free KDO8P oxime, which could bind to the low affinity sites, thus trapping it in the high affinity sites. At much higher KDO8P oxime concentrations, the reverse isomerization step was even slower, with $k_{off,conc} = 0.0077\ h^{-1}$. As a result, the dissociation rate is limited by the rate of relaxation of $E^*{\cdot}I_2$ to $E{\cdot}I_4$. Since the post-separation/post-dilution incubations for $k_{off,gel}$ and $k_{off,jump}$ measurements were done in the presence of excess PEP, the equilibrium is shifted from $E^*{\cdot}I$ towards E·PEP once the inhibitor had dissociated.

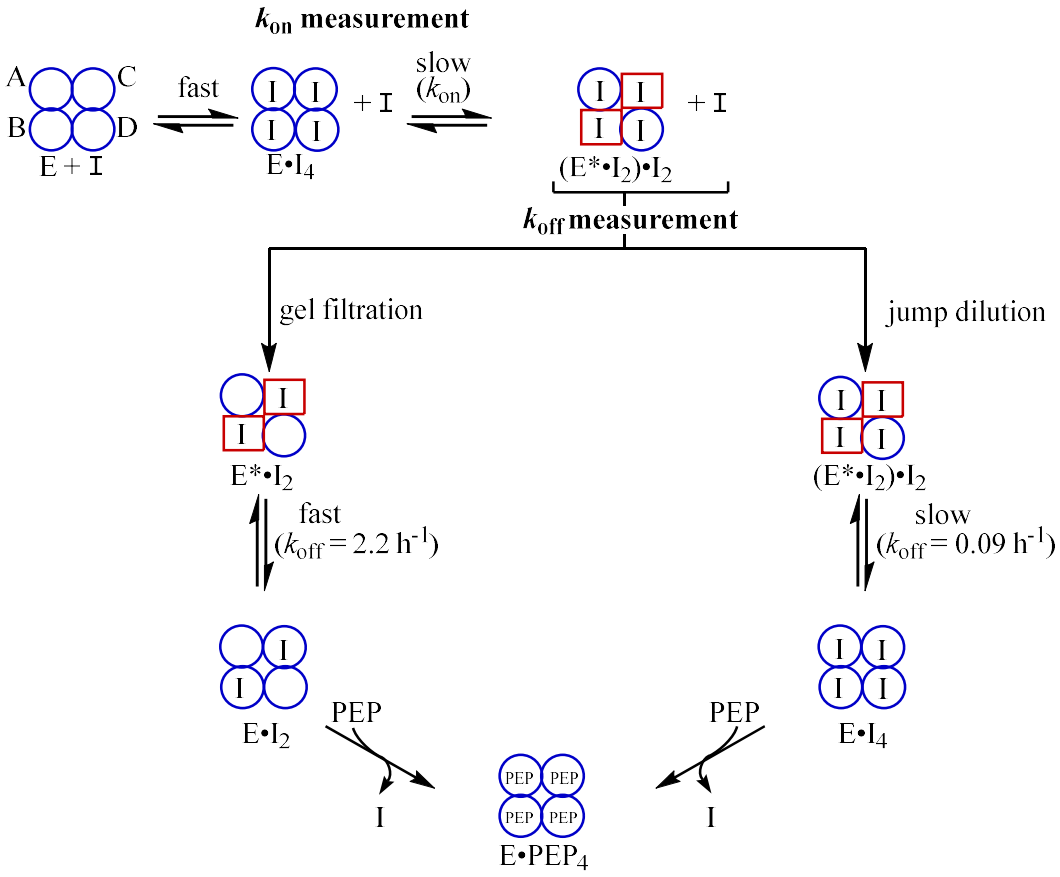

Figure 5.8. Slow-binding dissociation rates: jump dilution versus gel filtration methods.

Homotetrameric cjKDO8PS is composed of four active sites, A – D. Slow-binding is induced when all four active sites are bound, but isomerization to a tight complex occurs in only two active sites (red squares). The $E^*{\cdot}I_2$ complex is stabilized by inhibitor bound in the weakly bound active sites. Purification of the $E^*{\cdot}I$ complex by gel filtration removes inhibitor from the weakly bound sites, thus destabilizing the tightly bound sites and leading to a faster reverse isomerization rate, k_{off}. In the jump dilution method a slight excess of inhibitor is present, enough to bind the weakly bound active sites. This traps the tightly bound active sites $E^*{\cdot}I_2$. The reverse isomerization k_{off} of this complex is slow. The presence of excess PEP drives the equilibrium towards $E{\cdot}PEP_4$ complex and prevents inhibitor rebinding.

6. Radiolabelling of KDO8P oxime: method development and optimization

6.1. Introduction

We have kinetically established that KDO8P oxime is a slow binding inhibitor of cjKDO8PS$_{wt}$ with a residence time of up to 130 h, but there was quick dissociation when free inhibitor concentration was decreased. When [KDO8P oxime]$_{free} \approx 0$, the residence time decreased to 0.45 h. We attempted to confirm the activity-derived inhibitor binding kinetics with a radioactivity detection method.

6.2. Experimental

6.2.1. ^{33}P-Radiolabelling of KDO8P oxime

[^{33}P]KDO8P oxime was initially synthesized from [γ-^{33}P]ATP via [^{33}P]A5P (Figure 6.1).

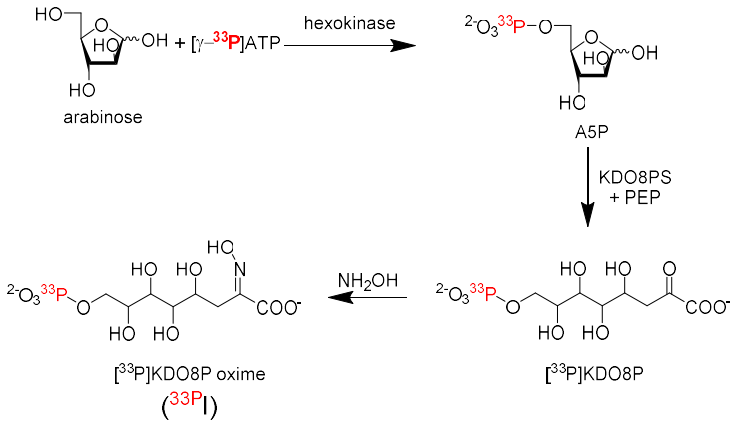

Figure 6.1. [^{33}P] KDO8P oxime synthesis

^{33}P-labelled A5P was synthesized from D-arabinose using 2 µL [γ–^{33}P]ATP (20 µCi), 1000 U hexokinase, 438 U pyruvate kinase, 12 mM unlabelled ATP, 103 mM PEP, 400 mM D-arabinose, 50 mM Tris·HCl, pH 7.6, 14.3 mM KCl, 300 mM $MgSO_4$, and 31 mM 2-mercaptoethnanol in a total volume of 5 mL and the reaction was carried out as described in Section 2.2.2.Reaction progress was monitored by ^{31}P NMR spectroscopy, and the reaction was complete in 5 to 9 days, as indicated by the disappearance of the PEP peak and the appearance of an A5P peak (Figure S10.14). [^{33}P]KDO8P oxime was synthesized as described in Section 4.2.1 except the synthesis began with [^{33}P]A5P. Radioactive KDO8P oxime was obtained with a specific radioactivity of 4.5×10^8 cpm/mmol.

Slow-binding experiments with [^{33}P]KDO8P oxime were conducted in an attempt to monitor the formation of the cjKDO8PS$_{H6}$·[^{33}P]KDO8P oxime complex (designated as E·^{33P}I). This was done by mixing 1.5 mM [^{33}P]KDO8P oxime/non-labelled KDO8P oxime mixture with 80 µM cjKDO8PS$_{H6}$ all in 50 mM BTP·Cl, pH 7.5, 50 mM KCl, 50 mM arginine and 50 mM glutamic acid. These are the conditions in which the enzyme was most stable. Slow-binding inhibition was monitored by assaying both the E·^{33P}I and control mixtures for activity using the general Malachite Green/ammonium molybdate colorimetric assay for Pi formation described in Chapter 2. To monitor binding by radioactivity, 50 µL aliquots of the mixture were injected onto 2 × 5-mL HiTrap desalting columns

connected in series. The column was run at 1 mL/min using AKTA FPLC system. Fractions, 1 mL each, were collected into scintillation vials and 5 mL of Bio-Safe II Scintillation fluid (Research products International Corp.) was added into each vial and mixed. The samples were counted for radioactivity using a Beckman Coulter LS 6500 Multi-purpose Liquid Scintillation Counter (Beckman Coulter). A chromatogram based on counts per min versus elution time was generated to monitor the transfer of radioactivity from the free small molecule, ^{33P}I, to the high molecular weight complex, E·^{33P}I.

6.2.2. ^{14}C-Radioactivity labelling

A method for synthesizing ^{14}C-labelled DAHP oxime method was developed. DAHP oxime slow binding to DAHPS was complete in 1 h, faster than KDO8P oxime binding to cjKDO8PS, therefore, it was reasonable to use the DAHPS/DAHP oxime system to develop and optimize ^{14}C-radiolabelling and monitoring method. [1−^{14}C]DAHP oxime was synthesized from [1−^{14}C]pyruvate via [1−^{14}C]PEP synthesis (Figure 6.2).

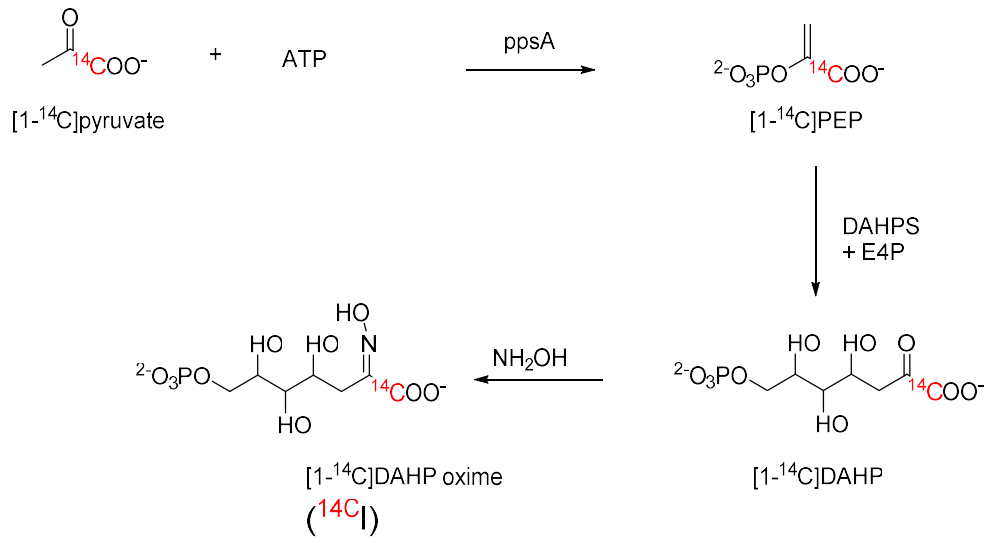

Figure 6.2. [1−^{14}C]DAHP oxime synthesis.

[1−^{14}C]PEP was enzymatically synthesized from [1−^{14}C]pyruvate and ATP using partially purified phosphoenolpyruvate synthase (ppsA).[162] The [1−^{14}C]PEP synthesis reaction mixture contained 20 mM non-labelled pyruvate, 2.5 µCi [1−^{14}C]pyruvate, 30 mM ATP, 1 mM DTT, 20 mM $MgCl_2$ and 16 % (v/v) of partially purified phosphoenolpyruvate synthase (ppsA) in 400 mM Tris·acetate, pH 8. The reaction was incubated at room temperature for 7 h. Reaction progress was monitored by following the incorporation of radioactivity into PEP by anion exchange chromatography, by injecting 5 µL of the 1 mL reaction onto a Mono Q anion exchange column. The column was washed with 2 column volumes of 100 mM ammonium formate, pH 6.2, and a gradient was run up to 800 mM ammonium formate over 30 column volumes. Fractions of 1 mL were collected and the radioactivity quantified to monitor for [1−^{14}C]PEP

formation, as indicated by a shift in the radioactivity's elution times from [1−^{14}C]pyruvate at 5 min to [1−^{14}C]PEP at 21 min.

[1−^{14}C]PEP synthesis was complete in 7 h, and it was purified from unreacted [1−^{14}C]pyruvate and side products using a preparative Q-Sepharose anion exchange column run at 2 mL/min. The purification protocol was the same as above, using ammonium formate as the eluting salt buffered with 10 mM ammonium formate, pH 6.2. All peaks were isolated and the [1−^{14}C]PEP peak eluting at 38 – 43 min (Figure 6.5) was used for the next step. Purified [1−^{14}C]PEP was lyophilized to remove the ammonium formate salt.

To make [1−^{14}C]DAHP, [1−^{14}C]PEP was dissolved in 9.5 mL of reaction buffer (50 mM Tris·HCl, pH 7.0, 100 mM KCl) to form 2 mM [1−^{14}C]PEP. This was mixed with 2 mM E4P (pH adjusted to 7.0 with 5 M KOH), and the mixture was pH adjusted to 7.0. $MnCl_2$ (100 μM) was added and 50 μL of this reaction was taken for a t = 0 HPLC injection. $DAHPS_{H6}$,[98] was added to a final concentration of 400 nM and this was incubated at room temperature for 3 h, at which point 50 μL was withdrawn for HPLC injection. The reaction progress was monitored using Mono Q column as described above. The reaction was complete within 3 h (Figure 6.6).

To make [1−^{14}C]DAHP oxime, 37 mM hydroxylamine hydrochloride was added to the mixture and the pH was adjusted to 5.5. The reaction mixture was left at room temperature overnight. The extent of the reaction was assessed by injection of a fraction of the mixture onto Mono Q column as described above. All

[1−^{14}C]DAHP has reacted to [1−^{14}C]DAHP oxime (Figure 6.7). The product was then purified using a Q-Sepharose column as described above and the pure product was collected between 25 and 38 min (Figure 6.8). The [1−^{14}C]DAHP oxime was lyophilized extensively to remove ammonium formate salt. Unfortunately, when the inhibitor was tested for slow binding there was no transfer of radioactivity. Nonetheless, the synthesis method has been developed and is straightforward while the slow binding experiments might need extensive optimization.

6.3. Results

Although the activity of the E·^{33P}I complex mixture dropped to 20% over 25 h of preincubation, there was no apparent radioactivity transfer from free ^{33}I to the E·^{33P}I complex (Figure 6.3). The two joined desalting columns were calibrated with cjKDO8PS$_{H6}$ to determine the enzyme elution time and with free inhibitor to determine the position at which free inhibitor elutes. The expected elution time for the E·^{33P}I complex was between 1 and 4 min while the free ^{33P}I eluted between 5 and 12 min (Figure 6.3). The relative activity of the E·^{33P}I complex, that is, the ratio of E·^{33P}I complex activity to the activity of the control is shown graphically (Figure 6.3, inset).

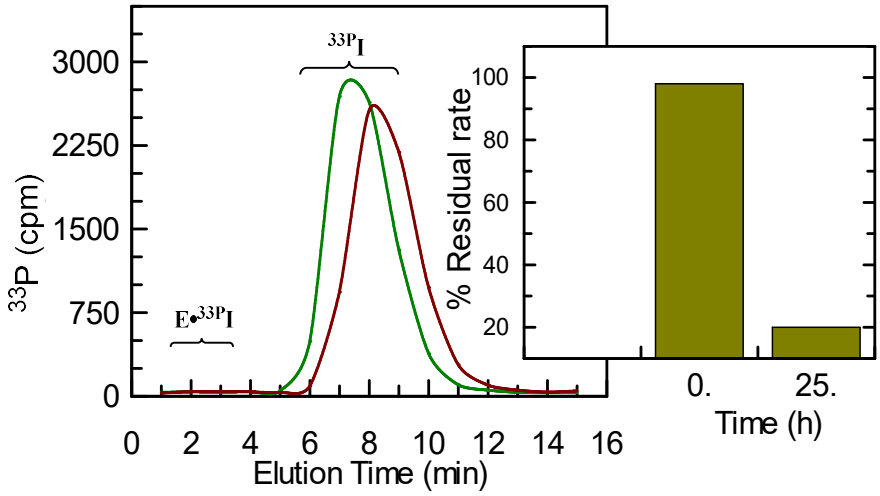

Figure 6.3. Monitoring E·^{33P}I formation by ^{33}P radioactivity.

^{33}P-radioactivity gel filtration chromatogram of the E·I complex at t = 0 (green) and 25 h (maroon) after preincubation. Aliquots were injected on to 2 × 5 mL HiTrap desalting columns connected in series and run at 1 mL/min, then 1 mL fractions were collected and ^{33}P measured by scintillation counting. The elution times for the E·^{33P}I complex and the free ^{33P}I are labeled. The inset shows the relative enzymatic activity (as determined by Pi production)[134] of the E·^{33P}I compared to the control at 0 and 25 h after preincubation. The relative rate decreased from 98% to 20% over 25 h but no corresponding radioactivity transfer into the E·^{33P}I complex.

6.3.1. [1−^{14}C]DAHP oxime synthesis – method development

Given, the low ^{33}P incorporation into KDO8P oxime, we hypothesized that the radioactive phosphate might be inherently unstable or prone to hydrolysis. As result we attempted to make a ^{14}C-labeled inhibitor from [1−^{14}C]pyruvate via [1−^{14}C]PEP synthesis from which [1−^{14}C]KDO8P oxime was made. The method was first developed using DAHPS/DAHP oxime system. DAHP oxime is a slow binding inhibitor of DAHPS and binding was complete in 1 h, compared with cjKDO8PS requiring overnight incubation to see significant slow-binding inhibition. The method development for this synthesis was successful and

[1−^{14}C]PEP synthesis was accomplished in 7 h as shown by the [1-^{14}C]PEP peak eluting between 19 and 24 min (Figure 6.4).

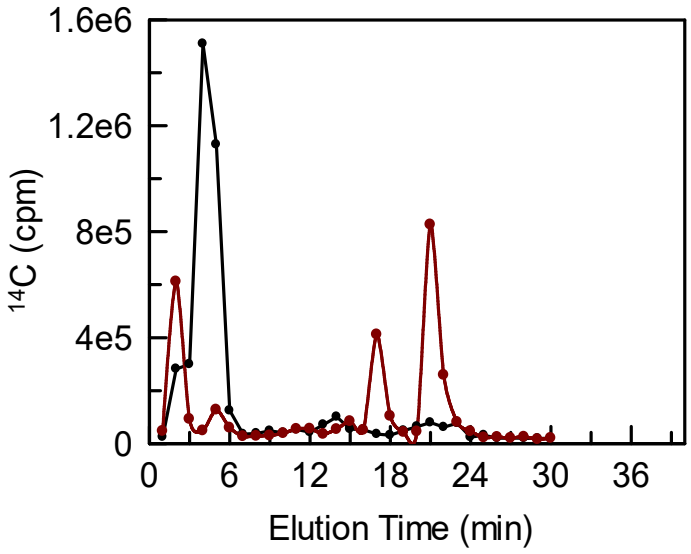

Figure 6.4. Monitoring [1-^{14}C]PEP synthesis by anion exchange chromatography.

Mono Q-anion exchange chromatogram monitoring [1-^{14}C]PEP synthesis. (black line), t = 0. (maroon line), t = 7 h after addition of ppSA. [1-^{14}C]PEP is eluted between 19 and 24 min (≈ 600 mM NH_4HCO_2).

Due to the presence of radioactive impurities eluting at 17 min (Figure 6.4), we decided to first purify PEP before DAHP synthesis. This was achieved by anion exchange chromatography using a Q-Sepharose preparative column. All the radioactive peaks were isolated, and the last eluting peak (38-43 min) was used for the next step (Figure 6.5).

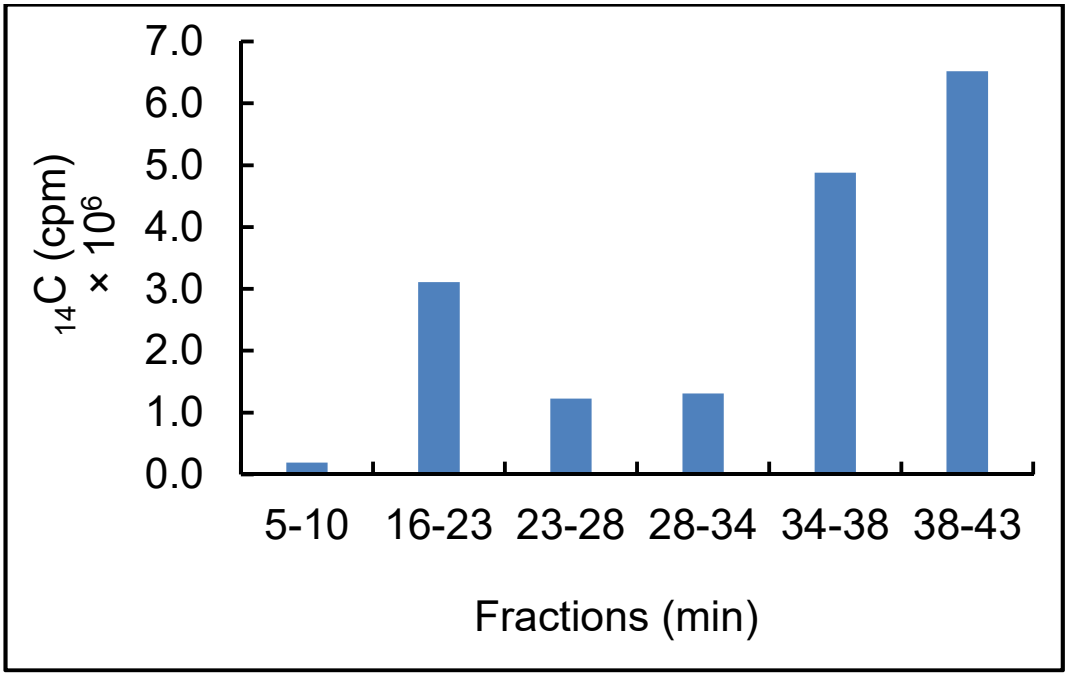

Figure 6.5. [1-^{14}C]PEP purification by anion exchange chromatography.

The fractions collected were peaks in the chromatogram as shown by absorbance at 230 nm. All the peaks were collected individually but the peak at 38-43 min (≈ 600 mM NH_4HCO_2) was assigned to [1-^{14}C]PEP.

[1-^{14}C]DAHP was synthesized from the 38 - 43 min fraction after lyophilization. The fraction was mixed with E4P, $MnCl_2$ and DAHPS in reaction buffer. [1-^{14}C]DAHP synthesis was complete in 3 h since the [1-^{14}C]PEP peak at 21 min was completely transformed into [1-^{14}C]DAHP (15 min) (Figure 6.6). [1-^{14}C]DAHP oxime was made by mixing the [1-^{14}C]DAHP reaction mixture with hydroxylamine hydrochloride at pH 5.5 to form [1-^{14}C]DAHP oxime (Figure 6.7).

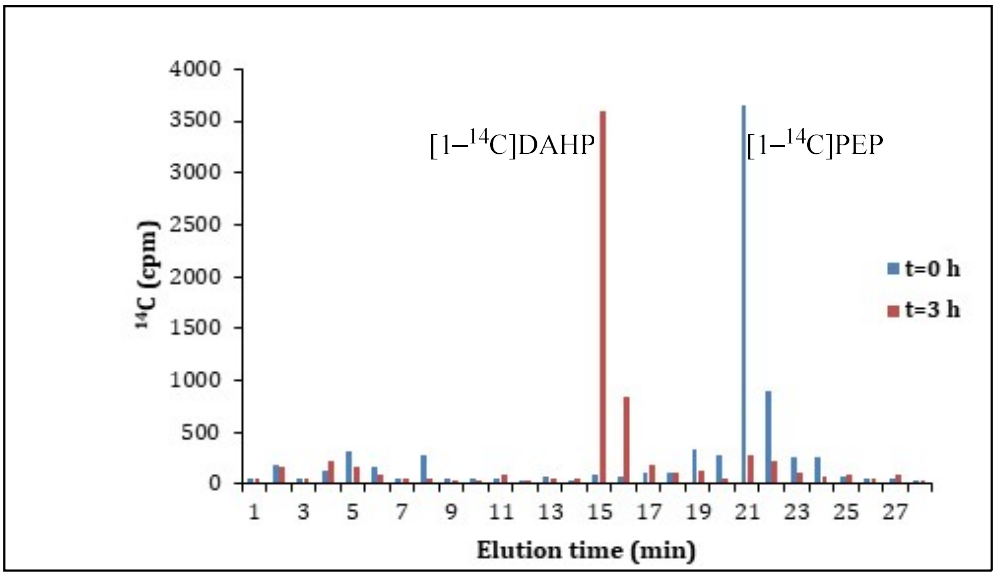

Figure 6.6. Synthesis of [1–^{14}C]DAHP from [1–^{14}C]PEP using DAHPS.

Mono-Q anion exchange chromatogram of 2 µL of the synthesis mixture. cpm = counts per minute.

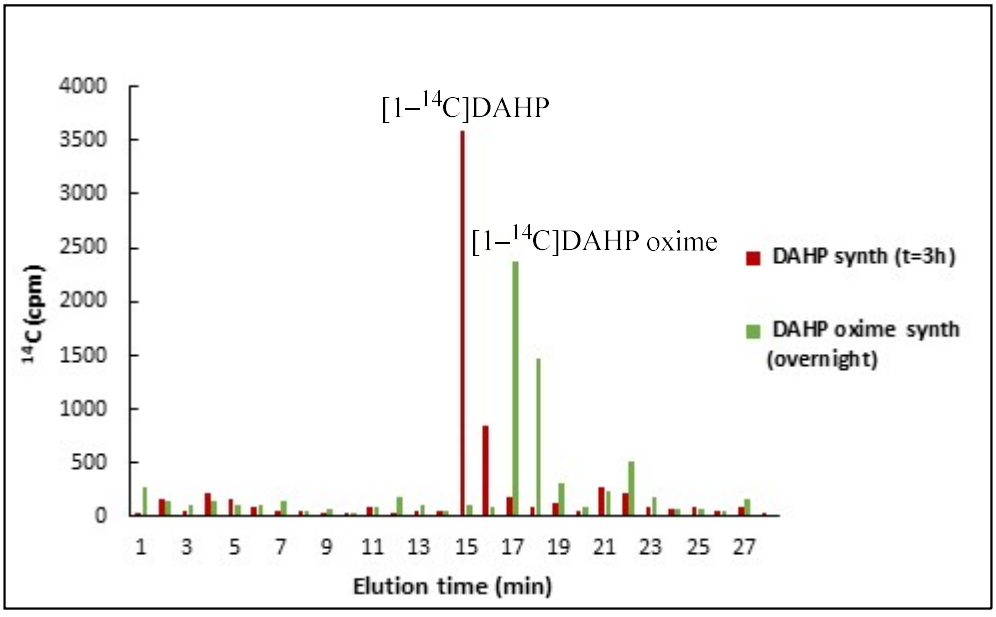

Figure 6.7. Synthesis of [1–^{14}C]DAHP oxime from [1–^{14}C]DAHP using $NH_2OH{\cdot}HCl$.

Mono-Q anion exchange chromatogram of 2 µL of the synthesis mixture. [1-^{14}C]DAHP oxime eluted at 17 and 18 min. cpm = counts per minute.

[1−^{14}C]DAHP oxime was purified using a Q-Sepharose anion exchange column and eluted as an isolated peak at about 400 mM ammonium formate (between 28 - 35 min) (Figure 6.8). The slow-binding experiments with [1−^{14}C]DAHP oxime and DAHPS required extensive optimization. For example, it appeared that slow binding of DHAP oxime to DAHPS occurred in the presence of $MnCl_2$ which conflicts with the findings that DAHP oxime is a competitive inhibitor with respect to $MnCl_2$ under fast binding conditions. Nonetheless, a method of synthesizing and purifying [1−^{14}C]DAHP oxime has been developed.

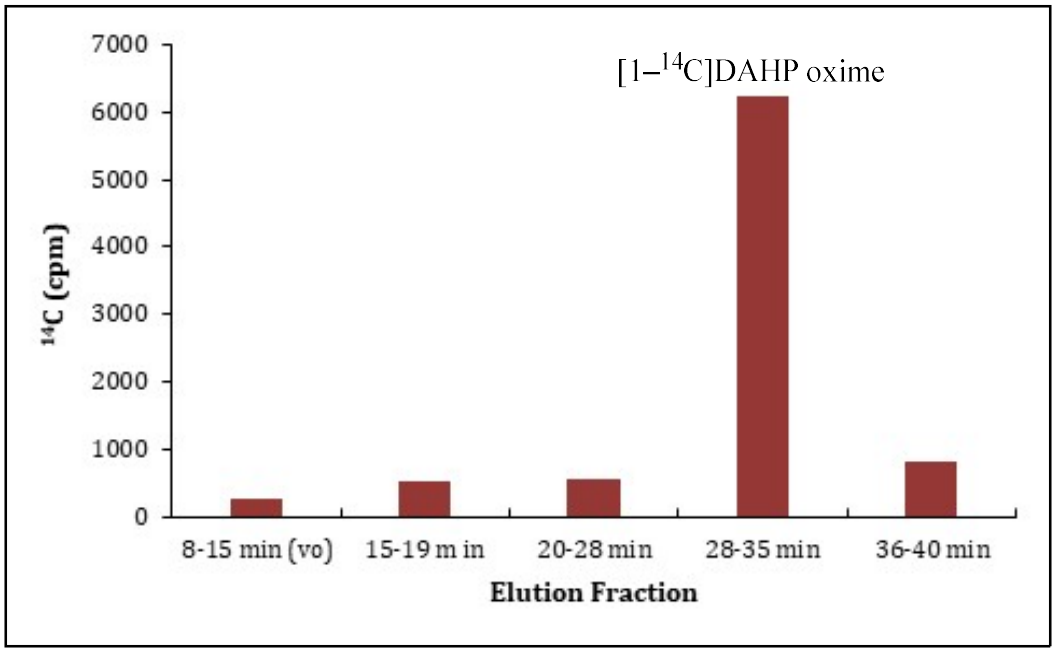

Figure 6.8. Purification of [1−^{14}C]DAHP oxime by anion exchange chromatograph.

The Q-Sepharose column was run at 2 mL/min for 60 min with the gradient: 100 mM ammonium formate for 2 min, 100-800 mM ammonium formate for 30 min. [1−^{14}C]DAHP oxime eluted at 28-35 min (≈ 400 mM ammonium formate).

6.4. Discussion

Tracking the binding of radioactively labelled KDO8P oxime or DAHP oxime to their respective enzymes to form slow-binding E*·I complexes was not successful. These experiments were performed before those described in Chapter 5. Based on the E*·I dissociation experiments in Chapter 5, it is likely that passing the E*·I complex through the desalting column removed excess free inhibitor, plus inhibitor from the weakly bound subunits. This could then destabilize the tightly bound subunits, causing rapid dissociation of the E*·I complex. Nonetheless, the method to radiolabel the oxime-based inhibitors with ^{14}C was developed and, with optimization, has the potential to be utilized to track inhibitor binding. This method is applicable to all three of the α-carboxyketose family of enzymes. If the oxime-based inhibitors were to be derivatized for antimicrobial activity, the radioactivity method can be used to track binding *in vivo* of these derivatives.

7. Crystallography

7.1. Introduction

cjKDO8PS is a newly characterized enzyme, and thus a crystal structure would be useful in helping to characterize it. A crystal structure of the DAHPS·DAHP oxime complex showed the oxime inhibitor binding to two of the four subunits and thus explained the residual rate observed at high inhibitor concentrations.[98] There is also a residual rate for KDO8P oxime inhibition of cjKDO8PS, even at 8 mM (800 × K_i). We were interested to see how the inhibitor is bound in the active sites. In the *A. aeolicus* KDO8PS crystal structure, only two subunits, located on one face of the enzyme, bind both PEP and A5P simultaneously.[40] This implies that even though the enzyme is a homotetramer composed of four identical active sites, they are functionally distinct in that only half of the active sites on one face are committed to catalysis at a time, and this feature was only apparent once ligands are introduced. It would be interesting to see if KDO8P oxime showed the same half-of-sites occupancy. The *A. aeolicus* KDO8PS structure further showed that the L7 loop is ordered and closes the active site off from solvent when both PEP and A5P are bound, but remains disordered when only one substrate is bound.[40] Although residues in this loop bind to the phosphate of A5P, the loop also remains disordered when only A5P is bound. This suggests that the loop closure is triggered when both A5P and PEP are bound. Given that KDO8P oxime combines both the PEP and A5P motifs in one molecule, one could expect that binding of KDP8P oxime would have similar

effects on cjKDO8PS active site loops. Unlike DAHPS, where DAHP oxime was competitive with respect to Mn^{2+}, KDO8P oxime binding was primarily uncompetitive with respect to Mn^{2+}, binding much more strongly to the cjKDO8PS·Mn^{2+} complex than cjKDO8PS alone. It would be interesting also to see how the metal interacts with the enzyme and inhibitor in the active site.

7.2. Experimental

The initial crystallographic screens were conducted using the hanging-drop vapor diffusion method with a drop made of 1 μL protein sample plus 1 μL of screening solution. Crystallization screens used included: MCSG screens I to IV (Anatrace), Nextal the classic suite lite, Nextal SM5, Nextal-anions (Qiagen), low ionic strength kit (Sigma), and the Wizard screen (Rigaku). The reservoir contained 1 M ammonium sulphate. In the initial screening process, the protein concentration was typically 10 mg/mL in complex with 5 mM PEP and 1 mM $MnCl_2$, and the crystal plates were prepared at 4 °C. cjKDO8PS_{wt} was used due to its higher solubility than cjKDO8PS_{H6}. In these trials, precipitation or clear drops were prevalent, with no crystals visible. These conditions were also tried at 20 °C, with no success. cjKDO8PS_{H6} was then tried. We wanted to try the crystallization with the JCSG I screen (Qiagen) with the conditions: 0.2 M tri-lithium citrate, 20% (w/v) PEG 3350. This condition produced crystals for DAHPS·DAHP oxime,[120] and with DAHPS in complex with other inhibitors (Maren Heimhalt, personal communication). Given the ITC results that indicated that KDO8P oxime

preferentially binds to the cjKDO8PS·Mn^{2+} complex, we set crystals with the cjKDO8PS·Mn^{2+}·KDO8P oxime complex. The concentrations were 400 µM (13 mg/mL) cjKDO8PS_{H6}, 500 µM $MnCl_2$ and 3 mM KDO8P oxime in crystallography/ITC buffer (20 mM Tris·HCl, pH 7.5, 200 mM KCl, 1 mM TCEP). The drops set up was 1 µL protein solution: 1 µL screen: 0.2 µL additive screen. The additive screen package contained 96 conditions from Hampton Research. The reservoir contained 500 µL of 1 M ammonium sulphate. The crystals were set at 4 °C.

7.3. Results

The initial crystallization trials with cjKDO8PS_{wt} produced no crystals. Results included precipitation, oily and clear drops. Switching to the JCSG I screen produced positive results. Crystals were obtained with the additive screen containing 20% (w/v) benzamidine hydrochloride with cjKDO8PS_{H6}. This condition produced small thin diamond-shaped plate crystals within two weeks (Figure 7.1). Unfortunately, these crystals did not diffract.

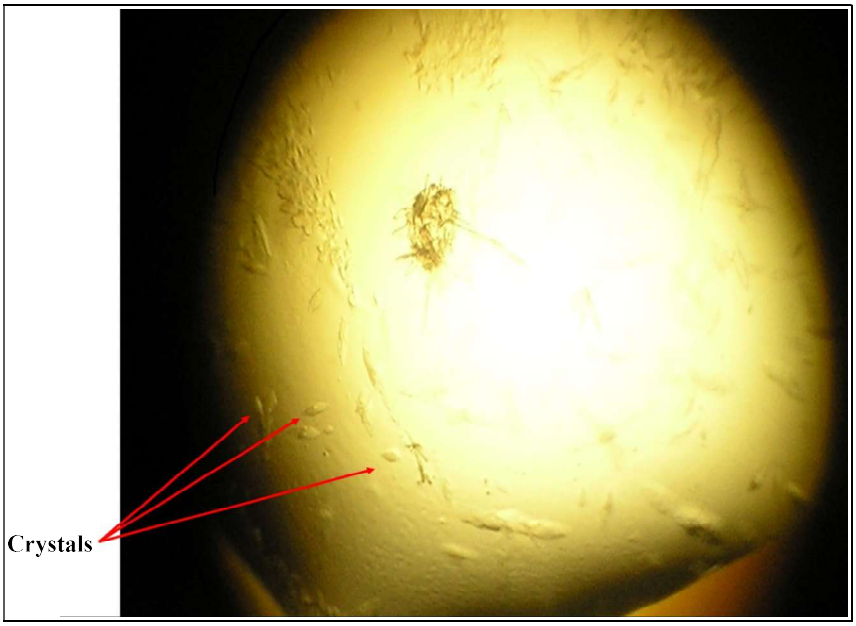

Figure 7.1. A picture of cjKDO8PS$_{H6}$·Mn^{2+}·KDO8P oxime crystals.

7.4. Discussion

Preliminary crystallization trials indicated that cjKDO8PS in complex with Mn^{2+} and KDO8P oxime can form crystals, but in a very narrow range of conditions. Crystals of cjKDO8PS$_{H6}$·Mn^{2+}·KDO8P oxime complex, in crystallization buffer (20 mM Tris·HCl, pH 7.5, 200 mM KCl, 1 mM TCEP), were formed using JCSG I screen containing 0.2 M tri-lithium citrate, 20% (w/v) PEG 3350 and Hampton additive screen containing 20% (w/v) benzamidine hydrochloride and 1 M ammonium sulphate in the reservoir. These did not diffract. Even though many trials were done with no success, this result is promising. Further optimization such as varying the enzyme and ligands concentrations and drop sizes using automated screening could be done. One radical optimization step would be to attempt to form the cjKDO8PS crystals

without ligands bound and then soak the formed crystals with the desired ligand. This method was successfully used elsewhere.[163,164] For example, *A. aeolicus* KDO8PS crystals in complex with substrates were obtained by first forming crystals of the enzyme and then the formed crystals were soaked in the reservoir buffer containing the substrates.[163] The same method was applied in *E. coli* KDO8PS crystallization. Crystals of *E. coli* KDO8PS degraded rapidly when incubated with many ligands[164]. In that study, they proposed that this is likely that conformational changes to the protein upon ligand binding triggered the collapse of the crystal lattice. Application of this method manually or by automated screening and further refinement of the conditions obtained above, may assist in obtaining crystals and lead to the determination of the structure of cjKDO8PS.

8. Concluding Remarks

8.1. Conclusions

In this work, we have successfully cloned and expressed the *kdsA* gene from *Campylobacter jejuni* in an *E. coli* expression system. A BLAST search with the cjKDO8PS$_{wt}$ amino acid sequence suggested that cjKDO8PS would be a metal-dependent KDO8PS and the sequence aligned well with other metal-dependent KDO8PSs (see Chapter 2). We kinetically demonstrated that cjKDO8PS is a Class II KDO8PS that is highly activated by Mn^{2+}, Co^{2+}, Fe^{2+} and Ni^{2+}. Using Mn^{2+}, we determined that cjKDO8PS$_{H6}$ is optimally active at a pH and temperature of 7.5 and 60 °C, respectively. The enzyme was unstable at pH < 7, so the apparent decrease in activity in the acid limb of the pH profile could have been due to some combination of denaturation and/or a true decrease in its activity. A pK_a value of 9.8 was obtained, which is close to the unperturbed pK_a value of a Lys sidechain (10.6). The residue K120 in cjKDO8PS (Figure 2.13) is a good candidate for being the residue responsible for the pH dependence of cjKDO8PS$_{H6}$'s activity, and may act as a general acid catalyst in promoting phosphate group departure during breakdown of the tetrahedral intermediate. Using size exclusion chromatography, we demonstrated that cjKDO8PS$_{wt}$ and cjKDO8PS$_{H6}$ were tetramers in solution. We have developed a purification method for cjKDO8PS$_{wt}$, namely: ammonium sulphate fractionation, hydrophobic integration chromatography, anion exchange chromatography and size exclusion chromatography.

We determined the microscopic rate constants that describe substrate binding under the steady state assumption (Chapter 2). The results showed that cjKDO8PS$_{wt}$ had a sequential ordered ter ter kinetic mechanism in which Mn^{2+} binds first, followed by PEP, then A5P (Figure 2.5). However, off-pathway (unproductive) substrate binding is possible. In fact, ITC titration assays showed that A5P bound to free cjKDO8PS$_{H6}$ (Chapter 3). We further showed that cjKDO8PS's kinetic mechanism could be further simplified with the rapid equilibrium assumption, with kinetic parameters: k_{cat} = 2.4 s^{-1}, $K_{M,Mn(re)}$ = 130 μM $K_{M,PEP(re)}$ = 650 μM and $K_{M,A5P(re)}$ = 21 μM for cjKDO8PS$_{wt}$ (Table 2.2). The kinetic constants for cjKDO8PS$_{H6}$ were k_{cat} = 1.2 s^{-1}, $K_{M,Mn(re)}$ = 6.4 μM $K_{M,PEP(re)}$ = 899 μM and $K_{M,A5P(re)}$ = 14 μM, implying that there are modest differences between the kinetics of cjKDO8PS$_{wt}$ and cjKDO8PS$_{H6}$. Using the incorrect single substrate equation normally used in literature, cjKDO8PS's kinetic parameters were similar to kinetic parameters reported for other KDO8PSs (see Table 2.5).

We also measured direct binding of Mn^{2+}, PEP and A5P to cjKDO8PS$_{H6}$ by ITC (Chapter 3). The thermodynamic parameters obtained were: $K_{d,Mn}$ = 17 μM, $K_{d,PEP}$ = 122 μM $K_{d,A5P}$ = 34 μM. Detectable PEP binding occurred only in presence of Mn^{2+}, in good agreement with the kinetic mechanism that PEP binds after Mn^{2+}. A5P binding, on the other hand, did not occur in the presence of Mn^{2+} without PEP. This showed that a cjKDO8PS$_{H6}$·Mn^{2+} complex is optimized to bind PEP first before A5P.

We characterized cjKDO8PS$_{wt}$ and cjKDO8PS$_{H6}$ in terms of inhibition by KDO8P oxime, a novel inhibitor of cjKDO8PS. For cjKD8PS$_{wt}$ there was fast-binding inhibition with K_i = 10 μM, and slow-binding inhibition. Slow-binding inhibition exhibited cooperativity, n = 3.6, implying that the onset of slow binding occurred when all four active sites are bound. We also showed that the inhibitor dissociation rate (k_{off}) under slow binding conditions was dependent on the free KDO8P oxime concentration. Using gel filtration, where [I] ≈ 0, $k_{off,gel}$ = 2.2 h^{-1}, 24 times faster than $k_{off,jump}$ = 0.09 h^{-1} when using the jump dilution method, where [I]$_{free}$ = 47 μM. The concentration dependence of slow-binding inhibition gave $k_{off,conc}$ = 0.0077 h^{-1} when [I] = 100 μM to 10 mM. The residence time under the best conditions derived from $k_{off,conc}$ was 130 h. KDO8P oxime is thus the only inhibitor against KDO8PSs ever reported to have such a long residence time on the target. The ultimate inhibition constant, K_i^*, was 0.28 μM, the tightest binding KDO8PS inhibitor reported to date. This K_i^* value has a caveat, though, that such tight binding only occurs in the presence of excess free inhibitor. A plot of k_{obs} versus KDO8P oxime concentration produced an [I] saturable rectangular hyperbolic curve. This shape is indicative of slow binding inhibition that follows a two-step mechanism B (Figure 5.6). The first step produces a weakly bound complex E·I which, in the second step, isomerizes to form a much tighter complex E*·I.

We developed a method to radiolabel KDO8P oxime with ^{14}C using DAHPS/DAHP oxime system. This method has the potential to be used to track

KDO8P oxime *in vitro*, and could even be utilized in bacterial cells with appropriately derivatized KDO8P oxime.

We showed that KDO8P oxime binding is competitive with respect to PEP through kinetic assays and by ITC. ITC titrations showed that KDO8P oxime prevents A5P binding, making KDO8P oxime binding competitive with A5P. KDO8P oxime binding with respect to Mn^{2+} was kinetically found to be not competitive, but it was not possible to distinguish between noncompetitive and uncompetitive binding. ITC experiments showed that KDO8P oxime bound to cjKDO8PS$_{H6}$·Mn^{2+} 20-fold more tightly than free cjKDO8PS$_{H6}$. Thus, KDO8P oxime displayed more uncompetitive binding-like character with respect to Mn^{2+}. It is therefore not surprising that crystal formation only occurred with the cjKDO8PS·Mn^{2+}·KDO8P oxime complex.

8.2. Future work

KDO8P oxime binding to cjKDO8PS$_{wt}$ and cjKDO8PS$_{H6}$ did not lead to full inhibition under fast-binding conditions even at higher KDO8P oxime concentrations. Slow binding inhibition exhibited cooperativity with n = 3.6 implying that slow binding is induced once all four active sites are occupied, yet the residual rate persisted under these conditions. Even though slow-binding was induced when all four active sites are occupied in cjKDO8PS$_{wt,}$ the IC_{50} of 3.2 mM, compared with K_i = 10 μM, implies that there is negative cooperativity of inhibitor binding. That is, partial occupancy of the tetrameric enzyme's active

sites leads to lower affinity in the unbound active sites. It is unclear how the partial inhibitor occupancy occurs. Crystallization conditions for the cjKDO8PS·Mn^{2+}·KDO8P oxime complex have been found and can be optimized to obtain a crystal structure that shows how KDO8P oxime interacts with the active sites, and potentially provide a structural basis to interpret the functional results. Since KDO8P oxime binding is uncompetitive with respect to Mn^{2+}, it would be interesting also to see how the metal interacts with the enzyme and inhibitor in the active site. The crystal has the potential to also show whether there is active site loop closure upon KDO8P oxime binding as was shown in structure of *A. aeolicus* KDO8PS with bound A5P and PEP.[40] Residue R106 of *A. aeolicus* KDO8PS, a residue conserved in both Class I and II KDO8PSs (Figure 2.13), has been implicated in regulating the L7 loop opening and closing in different subunits.[40] Mutation of arginine R106 to Gly in *A. aeolicus* KDO8PS resulted in impairment of the L7 loop closure even when both PEP and A5P were bound. The R106's sidechain extends from one subunit into the active site of the other subunit.[43] Based on the results of cjKDO8PS crystallization, the role of R102 in cjKDO8PS on loop closure, if any, and on KDO8P oxime occupancy and residual rate could be investigated with a corresponding R102G substitution.

Kinetic parameters at high KDO8P oxime concentrations, that is, the binding profile for the remaining unoccupied binding sites responsible for the observed residual activity, could be determined. This experiment has the potential to kinetically explain the observed residual rate in cjKDO8PS. This experiment

was conducted in our lab with DAHPS at high DAHP oxime concentrations. In that study, the apparent $K_{M,E4P}$ at high DAHP oxime concentrations was 10-fold lower than in the absence of inhibitor, suggesting that the binding of DAHP oxime in two active sites (B and C) in the tetramer made E4P binding in the unoccupied sites (A and D) tighter preventing full inhibition.[98]

Since KDO8P oxime has a very long residence time (5 days) on the target, it has the potential to be effective *in vivo*. However, the negative charge on the primary phosphate in KDO8P oxime would make it cell impermeant.[165] Thus, this phosphate would have to be replaced by a small neutral group. Preliminary experiments have indicated that KDO oxime, with the primary phosphate replaced with a hydroxyl group, inhibited cjKDO8PS$_{H6}$ but with poor affinity. Replacing the phosphate with an oxime group instead might help retain affinity and aid in absorption by bacterial cells.

DAHP hydrazone, another potent novel α-carboxyketose synthase inhibitor, has been synthesized in our lab and has shown to fully inhibit DAHPS with K_i = 12 nM. An attempt to make KDO8P hydrazone was not successful because the compound was not stable enough to survive the lyophilization step. Substituted hydrazones such as KDO8P phenylhydrazone and KDO8P trifluoroethylhydrazones could be stable alternatives and potentially new cjKDO8PS inhibitors.

9. References

(1) Levin, D. H., and Racker, E. (1959) Condensation of Arabinose 5-Phosphate and Phosphorylenol Pyruvate by 2-Keto-3-deoxy-8-phosphooctonic Acid Synthetase. *J. Biol. Chem. 234*, 2532–2539.

(2) Bravo, I. G., García-Vallvé, S., Romeu, A., and Reglero, Á. (2004) Prokaryotic origin of cytidylyltransferases and α-ketoacid synthases. *Trends Microbiol. 12*, 120–128.

(3) World Health Organization. (2014) Antimicrobial resistance: global report on surveillance 2014. *World Heal. Organ.*

(4) Frieden, T. (2013) Antibiotic resistance threats in the United States, 2013. *CDC*.

(5) World Health Organization. (2010) Multidrug and extensively drug-resistant TB (M/XDR-TB): 2010 global report on surveillance and response. *Geneva World Heal. Organ.*

(6) Johnston, A. M. (2001) Animals and antibiotics. *Int. J. Antimicrob. Agents 18*, 291–294.

(7) Economou, V., and Gousia, P. (2015) Agriculture and food animals as a source of antimicrobial-resistant bacteria. *Infect. Drug Resist. 8*, 49–61.

(8) Hawkey, P. M. (1998) The origins and molecular basis of antibiotic resistance. *BMJ 317*, 657–660.

(9) Chopra, I., Hawkey, P. M., and Hinton, M. (1992) Tetracyclines, molecular and clinical aspects. *J. Antimicrob. Chemother. 29*, 245–77.

(10) Spratt, B. G. (1988) Hybrid penicillin-binding proteins in penicillin-resistant strains of Neisseria gonorrhoeae. *Nature 332*, 173–176.

(11) Łeski, T. A., and Tomasz, A. (2005) Role of penicillin-binding protein 2 (PBP2) in the antibiotic susceptibility and cell wall cross-linking of Staphylococcus aureus: evidence for the cooperative functioning of PBP2, PBP4, and PBP2A. *J. Bacteriol. 187*, 1815–24.

(12) Michel, M., and Gutmann, L. (1996) Methicillin-resistant Staphylococus aureus and vancomycin-resistant enterococci: Therapeutic realities and possibilities. *Lancet 349*, 1901–1906.

(13) Pinho, M. G., Filipe, S. R., De Lencastre, H., and Tomasz, A. (2001) Complementation of the essential peptidoglycan transpeptidase function of penicillin-binding protein 2 (PBP2) by the drug resistance protein PBP2A in Staphylococcus aureus. *J. Bacteriol. 183*, 6525–6531.

(14) Rice, L. B. (2008) Federal Funding for the Study of Antimicrobial Resistance in Nosocomial Pathogens: No ESKAPE. *J. Infect. Dis. 197*, 1079–1081.

(15) Boucher, H. W., Talbot, G. H., Bradley, J. S., Edwards, J. E., Gilbert, D., Rice, L. B., Scheld, M., Spellberg, B., and Bartlett, J. (2009) Bad bugs, no drugs: no ESKAPE! An update from the Infectious Diseases Society of America. *Clin. Infect. Dis. 48*, 1–12.

(16) Gould, I. M., and Bal, A. M. (2013) New antibiotic agents in the pipeline and how they can help overcome microbial resistance. *Virulence 4*, 185–

91.

(17) Spellberg, B., Bartlett, J. G., and Gilbert, D. N. (2013) The Future of Antibiotics and Resistance. *N. Engl. J. Med. 368*, 299–302.

(18) Ventola, C. L. (2015) The antibiotic resistance crisis: part 1: causes and threats. *P T A peer-reviewed J. Formul. Manag. 40*, 277–83.

(19) Boucher, H. W., Talbot, G. H., Benjamin, D. K., Bradley, J., Guidos, R. J., Jones, R. N., Murray, B. E., Bonomo, R. a., and Gilbert, D. (2013) 10 x ’20 Progress--Development of New Drugs Active Against Gram-Negative Bacilli: An Update From the Infectious Diseases Society of America. *Clin. Infect. Dis.* 1–10.

(20) Food and Drug Administration. (2017) Approved Drug Products with Therapeutic Equivalence Evaluations. *Dep. Heal. Hum. Serv.* 37th ed. Department of Health and Human Services, Rockville, MD.

(21) Raetz, C. R. (1990) Biochemistry of endotoxins. *Annu. Rev. Biochem. 59*, 129–70.

(22) Meredith, T. C., Aggarwal, P., Mamat, U., Lindner, B., and Woodard, R. W. (2006) Redefining the requisite lipopolysaccharide structure in Escherichia coli. *ACS Chem. Biol. 1*, 33–42.

(23) Takeuchi, O., and Akira, S. (2010) Pattern Recognition Receptors and Inflammation. *Cell 140*, 805–820.

(24) Lin, L., Tan, B., Pantapalangkoor, P., Ho, T., Baquir, B., Tomaras, A., Montgomery, J. I., Reilly, U., Barbacci, E. G., Hujer, K., Bonomo, R. A., Fernandez, L., Hancock, R. E. W., Adams, M. D., French, S. W., Buslon, V. S.,

and Spellberg, B. (2012) Inhibition of LpxC protects mice from resistant Acinetobacter baumannii by modulating inflammation and enhancing phagocytosis. *MBio 3*, 312–12.

(25) Dowhan, W. (1997) Molecular basis for membrane phospholipid diversity: why are there so many lipids? *Annu. Rev. Biochem. 66*, 199–232.

(26) Raetz, C. R. H., and Whitfield, C. (2002) Lipopolysaccharide Endotoxins. *Annu. Rev. Biochem. 71*, 635–700.

(27) Brozek, K. A., and Raetz, C. R. H. (1990) Biosynthesis of lipid A in Escherichia coli: Acyl carrier protein-dependent incorporation of laurate and myristate. *J. Biol. Chem. 265*, 15410–15417.

(28) García-Quintanilla, M., Caro-Vega, J. M., Pulido, M. R., Moreno-Martínez, P., Pachón, J., and McConnell, M. J. (2016) Inhibition of LpxC increases antibiotic susceptibility in Acinetobacter baumannii. *Antimicrob. Agents Chemother. 60*, 5076–5079.

(29) Meredith, T. C., and Woodard, R. W. (2003) Escherichia coli YrbH is a D-arabinose 5-phosphate isomerase. *J. Biol. Chem. 278*, 32771–32777.

(30) Ray, P. H. (1980) Purification and characterization of 3-deoxy-D-manno-octulosonate 8-phosphate synthetase from Escherichia coli. *J. Bacteriol. 141*, 635–644.

(31) Asojo, O., Friedman, J., Adir, N., Belakhov, V., Shoham, Y., and Baasov, T. (2001) Crystal structures of KDOP synthase in its binary complexes with the substrate phosphoenolpyruvate and with a mechanism-based inhibitor.

Biochemistry 40, 6326–34.

(32) Bigham, E. C., Gragg, C. E., Hall, W. R., Kelsey, J. E., Mallory, W. R., Richardson, D. C., Benedict, C., and Ray, P. H. (1984) Inhibition of arabinose 5-phosphate isomerase. An approach to the inhibition of bacterial lipopolysaccharide biosynthesis. *J. Med. Chem. 27*, 717–726.

(33) Claesson, A., Luthman, K., Gustafsson, K., and Bondesson, G. (1987) A 2-deoxy analogue of KDO as the first inhibitor of the enzyme CMP-KDO synthetase. *Biochem. Biophys. Res. Commun. 143*, 1063–1068.

(34) Goldman, R., Kohlbrenner, W., Lartey, P., and Pernet, A. (1987) Antibacterial agents specifically inhibiting lipopolysaccharide synthesis. *Nature 329*, 162–164.

(35) Rick, P. D., and Osborn, M. J. (1972) Isolation of a Mutant of Salmonella typhimurium Dependent on D-Arabinose-5-phosphate for Growth and Synthesis of 3-Deoxy-D-mannoctulosonate (Ketodeoxyoctonate). *Proc. Natl. Acad. Sci. 69*, 3756–3760.

(36) Rick, P. D., and Osborn, M. J. (1977) Lipid A mutants of Salmonella typhimurium. Characterization of a conditional lethal mutant in 3-deoxy-D-mannooctulosonate-8-phosphate synthetase. *J. Biol. Chem. 252*, 4895–4903.

(37) Grison, C., Petek, S., Finance, C., and Coutrot, P. (2005) Synthesis and antibacterial activity of mechanism-based inhibitors of KDO8P synthase and DAH7P synthase. *Carbohydr. Res. 340*, 529–537.

(38) Birck, M. R., and Woodard, R. W. (2001) Aquifex aeolicus 3-deoxy-

D-manno-2-octulosonic acid 8-phosphate synthase: a new class of KDO 8-P synthase? *J. Mol. Evol. 52*, 205–14.

(39) Duewel, H. S., Sheflyan, G. Y., and Woodard, R. W. (1999) Functional and Biochemical Characterization of a Recombinant 3-Deoxy-d-manno-octulosonic Acid 8-Phosphate Synthase from the Hyperthermophilic Bacterium Aquifex aeolicus. *Biochem. Biophys. Res. Commun. 263*, 346–351.

(40) Duewel, H. S., Radaev, S., Wang, J., Woodard, R. W., and Gatti, D. L. (2001) Substrate and metal complexes of 3-deoxy-D-manno-octulosonate-8-phosphate synthase from Aquifex aeolicus at 1.9-Å Resolution: Implications for the condensation mechanism. *J. Biol. Chem. 276*, 8393–8402.

(41) Wagner, T., Kretsinger, R. H., Bauerle, R., and Tolbert, W. D. (2000) 3-Deoxy-D-manno-octulosonate-8-phosphate synthase from Escherichia coli. Model of binding of phosphoenolpyruvate and D-arabinose-5-phosphate. *J. Mol. Biol. 301*, 233–8.

(42) Wu, J., Patel, M. a, Sundaram, A. K., and Woodard, R. W. (2004) Functional and biochemical characterization of a recombinant Arabidopsis thaliana 3-deoxy-D-manno-octulosonate 8-phosphate synthase. *Biochem. J. 381*, 185–93.

(43) Xu, X., Kona, F., Wang, J., Lu, J., Stemmler, T., and Gatti, D. L. (2005) The catalytic and conformational cycle of Aquifex aeolicus KDO8P synthase: role of the L7 loop. *Biochemistry 44*, 12434–44.

(44) Dotson, G. D., Nanjappan, P., Reily, M. D., and Woodard, R. W.

(1993) Stereochemistry of 3-deoxyoctulosonate 8-phosphate synthase. *Biochemistry 32*, 12392–7.

(45) Cochrane, F. C., Cookson, T. V. M., Jameson, G. B., and Parker, E. J. (2009) Reversing evolution: re-establishing obligate metal ion dependence in a metal-independent KDO8P synthase. *J. Mol. Biol. 390*, 646–661.

(46) Yeoman, J. A. (2007) Biochemical Characterization of Metal-Dependent 3-Deoxy- D - manno -Octulosonate 8- Phosphate Synthases from Chlorobium tepidum & Acidithiobacillus ferrooxidans. Master of Science, Massey University, 120 p.

(47) Shulami, S., Yaniv, O., Rabkin, E., Shoham, Y., and Baasov, T. (2003) Cloning, expression, and biochemical characterization of 3-deoxy-D-manno-2-octulosonate-8-phosphate (KDO8P) synthase from the hyperthermophilic bacterium Aquifex pyrophilus. *Extremophiles 7*, 471–481.

(48) Krosky, D. J., Alm, R., Berg, M., Carmel, G., Tummino, P. J., Xu, B., and Yang, W. (2002) Helicobacter pylori 3-deoxy-D-manno-octulosonate-8-phosphate (KDO-8-P) synthase is a zinc-metalloenzyme. *Biochim. Biophys. Acta - Protein Struct. Mol. Enzymol. 1594*, 297–306.

(49) Subramaniam, P. S., Xie, G., Xia, T., and Jensen, R. a. (1998) Substrate Ambiguity of 3-Deoxy-d-manno-Octulosonate 8-Phosphate Synthase from Neisseria gonorrhoeae in the Context of Its Membership in a Protein Family Containing a Subset of 3-Deoxy-d-arabino-Heptulosonate 7-Phosphate Synthases. *J. Bacteriol. 180*, 119–127.

(50) Jensen, R. A., Xie, G., Calhoun, D. H., and Bonner, C. A. (2002) The Correct Phylogenetic Relationship of KdsA (3-Deoxy-D-manno-octulosonate 8-Phosphate Synthase) with One of Two Independently Evolved Classes of AroA (3-Deoxy-D-arabino-heptulosonate 7-Phosphate Synthase). *J. Mol. Evol. 54*, 416–423.

(51) Duewel, H. S., and Woodard, R. W. (2000) A metal bridge between two enzyme families. 3-deoxy-D-manno-octulosonate-8-phosphate synthase from Aquifex aeolicus requires a divalent metal for activity. *J. Biol. Chem. 275*, 22824–22831.

(52) Oliynyk, Z., Briseño-Roa, L., Janowitz, T., Sondergeld, P., and Fersht, a R. (2004) Designing a metal-binding site in the scaffold of Escherichia coli KDO8PS. *Protein Eng. Des. Sel. 17*, 383–90.

(53) Shulami, S., Furdui, C., Adir, N., Shoham, Y., Anderson, K. S., and Baasov, T. (2004) A reciprocal single mutation affects the metal requirement of 3-deoxy-D-manno-2-octulosonate-8-phosphate (KDO8P) synthases from Aquifex pyrophilus and Escherichia coli. *J. Biol. Chem. 279*, 45110–20.

(54) Li, J., Wu, J., Fleischhacker, A. S., and Woodard, R. W. (2004) Conversion of Aquifex aeolicus 3-deoxy-D-manno-octulosonate 8-phosphate synthase, a metalloenzyme, into a nonmetalloenzyme. *J. Am. Chem. Soc. 126*, 7448–7449.

(55) Ahn, M., Pietersma, A. L., Schofield, L. R., and Parker, E. J. (2005) Mechanistic divergence of two closely related aldol-like enzyme-catalysed

reactions. *Org. Biomol. Chem. 3*, 4046.

(56) Ahn, M., Cochrane, F. C., Patchett, M. L., and Parker, E. J. (2008) Arabinose 5-phosphate analogues as mechanistic probes for Neisseria meningitidis 3-deoxy-D-manno-octulosonate 8-phosphate synthase. *Bioorg. Med. Chem. 16*, 9830–6.

(57) König, V., Pfeil, A., Braus, G. H., and Schneider, T. R. (2004) Substrate and metal complexes of 3-deoxy-D-arabino-heptulosonate-7-phosphate synthase from Saccharomyces cerevisiae provide new insights into the catalytic mechanism. *J. Mol. Biol. 337*, 675–690.

(58) Howe, D. L., Sundaram, A. K., Wu, J., Gatti, D. L., and Woodard, R. W. (2003) Mechanistic insight into 3-deoxy-D-manno-octulosonate-8-phosphate synthase and 3-deoxy-D-arabino-heptulosonate-7-phosphate synthase utilizing phosphorylated monosaccharide analogues. *Biochemistry 42*, 4843–54.

(59) Schofield, L. R., Anderson, B. F., Patchett, M. L., Norris, G. E., Jameson, G. B., and Parker, E. J. (2005) Substrate Ambiguity and Crystal Structure of Pyrococcus furiosus 3-Deoxy-d-arabino-heptulosonate-7-phosphate Synthase: An Ancestral 3-Deoxyald-2-ulosonate-phosphate Synthase?,. *Biochemistry 44*, 11950–11962.

(60) Sheflyan, G. Y., Howe, D. L., Wilson, T. L., and Woodard, R. W. (1998) Enzymatic Synthesis of 3-Deoxy- D - manno -octulosonate 8-Phosphate , 3-Deoxy- D - arabino -heptulosonate 7-Phosphate Synthase. *JACS 120*, 11027–11032.

(61) DeLeo, A. B., Dayan, J., and Sprinson, D. B. (1973) Purification and Kinetics of Tyrosine-sensitive 3-Deoxy-d-arabino-heptulosonic Acid 7-Phosphate Synthetase from Salmonella. *J. Biol. Chem. 248*, 2344–2353.

(62) Comb, D. G., and Roseman, S. (1960) The Sialic Acids: I. THE STRUCTURE AND ENZYMATIC SYNTHESIS OF N-ACETYLNEURAMINIC ACID. *J. Biol. Chem. 235*, 2529–2537.

(63) Brown, K. D., and Doy, C. H. (1966) Control of three isoenzymic 7-phospho-2-oxo-3-deoxy-d-arabino-heptonate-d-erythrose-4-phosphate lyases of Escherichia coli W and derived mutants by repressive and "inductive" effects of the aromatic amino acids. *Biochim. Biophys. Acta - Enzymol. Biol. Oxid. 118*, 157–172.

(64) Bentley, R., and Haslam, E. (1990) The Shikimate Pathway — A Metabolic Tree with Many Branche. *Crit. Rev. Biochem. Mol. Biol. 25*, 307–384.

(65) Garner, C. C., and Herrmann, K. M. (1984) Structural analysis of 3-deoxy-d-arabino-heptulosonate 7-phosphate by 1H-and natural-abundance 13C-n.m.r. spectroscopy. *Carbohydr. Res. 132*, 317–322.

(66) Herrmann, K. M., and Weaver, L. M. (1999) the Shikimate Pathway. *Annu. Rev. Plant Physiol. Plant Mol. Biol. 50*, 473–503.

(67) Gosset, G., Bonner, C. A., and Jensen, R. A. (2001) Microbial origin of plant-type 2-keto-3-deoxy-D-arabino-heptulosonate 7-phosphate synthases, exemplified by the chorismate- and tryptophan-regulated enzyme from Xanthomonas campestris. *J. Bacteriol. 183*, 4061–70.

(68) Kona, F., Xu, X., Martin, P., Kuzmic, P., and Gatti, D. L. (2007) Structural and mechanistic changes along an engineered path from metallo to nonmetallo 3-deoxy-D-manno-octulosonate 8-phosphate synthases. *Biochemistry 46*, 4532–44.

(69) Duewel, H. S., Sheflyan, G. Y., and Woodard, R. W. (1999) Functional and Biochemical Characterization of a Recombinant 3-Deoxy-d-manno-octulosonic Acid 8-Phosphate Synthase from the Hyperthermophilic Bacterium Aquifex aeolicus. *Biochem. Biophys. Res. Commun. 263*, 346–351.

(70) Allison, T. M., Yeoman, J. A., Hutton, R. D., Cochrane, F. C., Jameson, G. B., and Parker, E. J. (2010) Specificity and mutational analysis of the metal-dependent 3-deoxy-d-manno-octulosonate 8-phosphate synthase from Acidithiobacillus ferrooxidans. *Biochim. Biophys. Acta - Proteins Proteomics 1804*, 1526–1536.

(71) Ray, J. M., and Bauerle, R. (1991) Purification and properties of tryptophan-sensitive 3-deoxy-D-arabino-heptulosonate-7-phosphate synthase from Escherichia coli. *J. Bacteriol. 173*, 1894–901.

(72) Schoner, R., and Herrmann, K. M. (1976) 3-Deoxy-D-arabino-heptulosonate 7-phosphate synthase. Purification, properties, and kinetics of the tyrosine-sensitive isoenzyme from Escherichia coli. *J. Biol. Chem.*

(73) Akowski, J. P., and Bauerle, R. (1997) Steady-state kinetics and inhibitor binding of 3-deoxy-D-arabino-heptulosonate-7-phosphate synthase (tryptophan sensitive) from Escherichia coli. *Biochemistry 36*, 15817–22.

(74) McCandliss, R. J., Poling, M. D., and Herrmann, K. M. (1978) 3-Deoxy-D-arabino-heptulosonate-7-phosphate synthase. Purification and molecular characterization of the phenylalanine-sensitive isoenzyme from Escherichia coli. *J. Biol. Chem. 253*, 4259–4265.

(75) Tanner, M. E. (2005) The enzymes of sialic acid biosynthesis. *Bioorg. Chem. 33*, 216–228.

(76) Traving, C., Schauer, R., and Institut, B. (1998) Structure , function and metabolism of sialic acids. *Cell. Mol. Life Sci. 54*, 1330–1349.

(77) Vestweber, D., and Blanks, J. E. (1999) Mechanisms that regulate the function of the selectins and their ligands. *Physiol. Rev. 79*, 181–213.

(78) Varki, A. (1997) Sialic acids as ligands in recognition phenomena. *FASEB J. 11*, 248–255.

(79) Jarvis, G. A. (1995) Recognition and control of neisserial infection by antibody and complement. *Trends Microbiol. 3*, 198–201.

(80) Gunawan, J., Simard, D., Gilbert, M., Lovering, A. L., Wakarchuk, W. W., Tanner, M. E., and Strynadka, N. C. J. (2005) Structural and mechanistic analysis of sialic acid synthase NeuB from Neisseria meningitidis in complex with Mn2+, phosphoenolpyruvate, and N-acetylmannosaminitol. *J. Biol. Chem. 280*, 3555–3563.

(81) Hao, J., Balagurumoorthy, P., Sarilla, S., and Sundaramoorthy, M. (2005) Cloning, expression, and characterization of sialic acid synthases. *Biochem Biophys Res Commun 338*, 1507–1514.

(82) Huang, H. H., Liao, H. K., Chen, Y. J., Hwang, T. S., Lin, Y. H., and Lin, C. H. (2005) Structural characterization of sialic acid synthase by electrospray mass spectrometry - A tetrameric enzyme composed of dimeric dimers. *J. Am. Soc. Mass Spectrom. 16*, 324–332.

(83) Sundaram, A. K., Pitts, L., Muhammad, K., Wu, J., Betenbaugh, M., Woodard, R. W., and Vann, W. F. (2004) Characterization of N-acetylneuraminic acid synthase isoenzyme 1 from Campylobacter jejuni. *Biochem. J. 383*, 83–89.

(84) DeLano, W. L. (2014) The PyMOL Molecular Graphics System, Version 1.8. *Schrödinger LLC* http://www.pymol.org.

(85) Liang, P. H., Lewis, J., Anderson, K. S., Kohen, a, D'Souza, F. W., Benenson, Y., and Baasov, T. (1998) Catalytic mechanism of Kdo8P synthase: transient kinetic studies and evaluation of a putative reaction intermediate. *Biochemistry 37*, 16390–9.

(86) Hedstrom, L., and Abeles, R. (1988) 3-Deoxy-D-manno-octulosonate-8-phosphate synthase catalyzes the C-O bond cleavage of phosphoenolpyruvate. *Biochem. Biophys. Res. Commun. 157*, 816–820.

(87) Radaev, S., Dastidar, P., Patel, M., Woodard, R. W., and Gatti, D. L. (2000) Structure and mechanism of 3-deoxy-D-manno-octulosonate 8-phosphate synthase. *J. Biol. Chem. 275*, 9476–9484.

(88) Shumilin, I. A., Bauerle, R., Wu, J., Woodard, R. W., and Kretsinger, R. H. (2004) Crystal Structure of the Reaction Complex of 3-Deoxy-d-arabino-heptulosonate-7-phosphate Synthase from Thermotoga maritima Refines the

Catalytic Mechanism and Indicates a New Mechanism of Allosteric Regulation. *J. Mol. Biol. 341*, 455–466.

(89) Stephens, C. M., and Bauerle, R. (1991) Analysis of the metal requirement of 3-deoxy-D-arabino-heptulosonate-7-phosphate synthase from Escherichia coli. *J. Biol. Chem. 266*, 20810–20817.

(90) Tao, P., Gatti, Domenico (1) Tao, P., Gatti, D. L., and Bernhard Schlegel, H. (2009) The energy landscape of 3-deoxy-D-manno-octulosonate 8-phosphate synthase. Biochemistry 48, 11706–11714.L., and Bernhard Schlegel, H. (2009) The energy landscape of 3-deoxy-D-manno-octulosonate 8-phosphate synthase. *Biochemistry 48*, 11706–11714.

(91) Li, Z., Sau, A. K., Shen, S., Whitehouse, C., Baasov, T., and Anderson, K. S. (2003) A snapshot of enzyme catalysis using electrospray ionization mass spectrometry. *J Am Chem Soc 125*, 9938–9939.

(92) Allison, T. M., Hutton, R. D., Cochrane, F. C., Yeoman, J. A., Jameson, G. B., and Parker, E. J. (2011) Targeting the role of a key conserved motif for substrate selection and catalysis by 3-deoxy-D-manno-octulosonate 8-phosphate synthase. *Biochemistry 50*, 3686–95.

(93) Clark, M. E., and Berti, P. J. (2007) Enolpyruvyl activation by enolpyruvylshikimate-3-phosphate synthase. *Biochemistry 46*, 1933–1940.

(94) Balachandran, N., To, F., and Berti, P. J. (2017) Linear Free Energy Relationship Analysis of Transition State Mimicry by 3-Deoxy- D - arabino heptulosonate-7-phosphate (DAHP) Oxime , a DAHP Synthase Inhibitor and

Phosphate Mimic. *Biochemistry 56*, 592–601.

(95) Loncke, P. G., and Berti, P. J. (2006) Implications of protonation and substituent effects for C-O and O-P bond cleavage in phosphate monoesters. *J. Am. Chem. Soc. 128*, 6132–6140.

(96) Segel, I. H. (1975) Enzyme Kinetics-Behavior and Analysis of Rapid Equilibrium and Steady-State Enzyme Systems. *John Wiley Sons New York*.

(97) Kohen, A., Jakob, A., and Baasov, T. (1992) Mechanistic studies of 3-deoxy-D-manno-2-octulosonate-8-phosphate synthase from Escherichia coli. *Eur. J. Biochem. 208*, 443–449.

(98) Balachandran, N., Heimhalt, M., Liuni, P., To, F., Wilson, D. J., Junop, M. S., and Berti, P. J. (2016) Potent Inhibition of 3-Deoxy- d -arabinoheptulosonate-7-phosphate (DAHP) Synthase by DAHP Oxime, a Phosphate Group Mimic. *Biochemistry 55*, 6617–6629.

(99) Hopkins, A. L., and Groom, C. R. (2002) The druggable genome. *Nat Rev Drug Discov 1*, 727–730.

(100) Copeland, R. A. (2005) Evaluation of enzyme inhibitors in drug discovery. A guide for medicinal chemists and pharmacologists. *Methods Biochem. Anal. 46*, 1–265.

(101) Fersht, A. (1985) Enzyme Structure and Mechanism 2, illustr ed. W.H. Freeman.

(102) Segel, I. H. (1993) Enzyme kinetics: behavior and analysis of rapid equilibrium and steady-state enzyme systems. *John Wiley Sons New York*.

(103) Wolfenden, R., and Snider, M. J. (2001) The depth of chemical time and the power of enzymes as catalysts. *Acc. Chem. Res. 34*, 938–945.

(104) Noonan, R. C., Carter, C. W. J., and Bagdassarian, C. K. (2002) Enzymatic conformational fluctuations along the reaction coordinate of cytidine deaminase. *Protein Sci. 11*, 1424–1434.

(105) Radzicka, A., and Wolfenden, R. (1995) Transition state and multisubstrate analog inhibitors. *Methods Enzymol. 249*, 284–312.

(106) Berti, P. J., and McCann, J. A. B. (2006) Toward a detailed understanding of base excision repair enzymes: transition state and mechanistic analyses of N-glycoside hydrolysis and N-glycoside transfer. *Chem. Rev. 106*, 506–55.

(107) Schramm, V. L. (1998) Enzymatic transition states and transition state analog design. *Annu. Rev. Biochem. 67*, 693–720.

(108) Morrison, J. F. (1982) The slow-binding and slow, tight-binding inhibition of enzyme-catalysed reactions. *Trends Biochem. Sci. 7*, 102–105.

(109) Walkup, G. K., You, Z., Ross, P. L., Allen, E. K. H., Daryaee, F., Hale, M. R., O'Donnell, J., Ehmann, D. E., Schuck, V. J. A., Buurman, E. T., Choy, A. L., Hajec, L., Murphy-Benenato, K., Marone, V., Patey, S. A., Grosser, L. A., Johnstone, M., Walker, S. G., Tonge, P. J., and Fisher, S. L. (2015) Translating slow-binding inhibition kinetics into cellular and in vivo effects. *Nat. Chem. Biol. 11*, 416–423.

(110) Guo, D., Mulder-Krieger, T., IJzerman, A. P., and Heitman, L. H.

(2012) Functional efficacy of adenosine A 2A receptor agonists is positively correlated to their receptor residence time. *Br. J. Pharmacol. 166*, 1846–1859.

(111) Lu, H., and Tonge, P. J. (2010) Drug-target residence time: Critical information for lead optimization. *Curr. Opin. Chem. Biol. 14*, 467–474.

(112) Luckner, S. R., Liu, N., Am Ende, C. W., Tonge, P. J., and Kisker, C. (2010) A slow, tight binding inhibitor of InhA, the enoyl-acyl carrier protein reductase from Mycobacterium tuberculosis. *J. Biol. Chem. 285*, 14330–14337.

(113) Pan, A. C., Borhani, D. W., Dror, R. O., and Shaw, D. E. (2013) Molecular determinants of drug-receptor binding kinetics. *Drug Discov. Today 18*, 667–673.

(114) Du, S., Tsipori, H., and Baasov, T. (1997) Synthesis and evaluation of putative oxocarbenium intermediate mimic in the KDO8P synthase-catalyzed reaction as a tool for the design of potent inhibitors for lipopolysaccharide biosynthesis. *Bioorg. Med. Chem. Lett. 7*, 2469–2472.

(115) Du, S., Faiger, H., Belakhov, V., and Baasov, T. (1999) Towards the development of novel antibiotics: synthesis and evaluation of a mechanism-based inhibitor of Kdo8P synthase. *Bioorg. Med. Chem. 7*, 2671–82.

(116) Belakhov, V., Dovgolevsky, E., Rabkin, E., Shulami, S., Shoham, Y., and Baasov, T. (2004) Synthesis and evaluation of a mechanism-based inhibitor of KDO8P synthase. *Carbohydr. Res. 339*, 385–392.

(117) Harrison, A. N., Reichau, S., and Parker, E. J. (2012) Synthesis and evaluation of tetrahedral intermediate mimic inhibitors of 3-deoxy-D-manno-

octulosonate 8-phosphate synthase. *Bioorganic Med. Chem. Lett. 22*, 907–911.

(118) Walker, S. R., and Parker, E. J. (2006) Synthesis and evaluation of a mechanism-based inhibitor of a 3-deoxy-D-arabino heptulosonate 7-phosphate synthase. *Bioorg. Med. Chem. Lett. 16*, 2951–4.

(119) Walker, S. R., Jiao, W., and Parker, E. J. (2011) Synthesis and evaluation of dual site inhibitors of 3-deoxy-D-arabino-heptulosonate 7-phosphate synthase. *Bioorg. Med. Chem. Lett. 21*, 5092–7.

(120) Balachandran, N. (2014) DAHP Oxime : A Transition State Mimic Inhibitor Of DAHP Synthase. Ph.D. Dissertation, McMaster University, 183 p.

(121) Reichau, S., Jiao, W., Walker, S. R., Hutton, R. D., Baker, E. N., and Parker, E. J. (2011) Potent inhibitors of a shikimate pathway enzyme from Mycobacterium tuberculosis: combining mechanism- and modeling-based design. *J. Biol. Chem. 286*, 16197–16207.

(122) Liu, F., Lee, H. J., Strynadka, N. C. J., and Tanner, M. E. (2009) Inhibition of Neisseria meningitidis sialic acid synthase by a tetrahedral intermediate analogue. *Biochemistry 48*, 9194–201.

(123) Popovic, V. (2012) Inhibition of the bacterial sialic acid synthase, NeuB. Master of Science, McMaster University, 62 p.

(124) Kuzmič, P. (2009) DynaFit-A Software Package for Enzymology. *Methods Enzymol. 467*, 247–280.

(125) Shumilin, I. A., Bauerle, R., and Kretsinger, R. H. (2003) The high-resolution structure of 3-Deoxy-D-arabino-heptulosonate-7-phosphate synthase

reveals a twist in the plane of bound phosphoenolpyruvate. *Biochemistry 42*, 3766–3776.

(126) Linton, D., Karlyshev, a V, Hitchen, P. G., Morris, H. R., Dell, a, Gregson, N. a, and Wren, B. W. (2000) Multiple N-acetyl neuraminic acid synthetase (neuB) genes in Campylobacter jejuni: identification and characterization of the gene involved in sialylation of lipo-oligosaccharide. *Mol. Microbiol. 35*, 1120–34.

(127) Allos, B. M. (2001) Campylobacter jejuni Infections: update on emerging issues and trends. *Clin. Infect. Dis. 32*, 1201–6.

(128) Engberg, J., Aarestrup, F. M., Taylor, D. E., Gerner-Smidt, P., and Nachamkin, I. Quinolone and macrolide resistance in Campylobacter jejuni and C. coli: resistance mechanisms and trends in human isolates. *Emerg. Infect. Dis. 7*, 24–34.

(129) Yuki, N., Sato, S., Tsuji, S., Ohsawa, T., and Miyatake, T. (1993) Frequent presence of anti-GQ1b antibody in Fisher's syndrome. *Neurology 43*, 414–417.

(130) Houliston, R. S., Vinogradov, E., Dzieciatkowska, M., Li, J., St Michael, F., Karwaski, M.-F., Brochu, D., Jarrell, H. C., Parker, C. T., Yuki, N., Mandrell, R. E., and Gilbert, M. (2011) Lipooligosaccharide of Campylobacter jejuni: similarity with multiple types of mammalian glycans beyond gangliosides. *J. Biol. Chem. 286*, 12361–70.

(131) Ausubel, F.M., Smith, J.A., Moore, D.D., Brent, R., Seidman, J. G.,

Struhl, K., Kingston, R. E. (1999) Short Protocols in Molecular Biology: A Compendium of Methods from Current Protocols in Molecular Biology 4th ed. Wiley, New York.

(132) Pace, C. N., Vajdos, F., Fee, L., Grimsley, G., and Gray, T. (1995) How to measure and predict the molar absorption coefficient of a protein. *Protein Sci. 4*, 2411–2423.

(133) Bednarski, M. D., Crans, D. C., Slmon, E. S., Steins, D., and Whitesides, G. M. (1988) Synthesis od 3-Deoy-D-manns-2-octulosonate-8-phosphate (KDO-8-P) from D-arabinose: Generation od D-arabinose-5-phosphate using Heokinase. *Tetrahedron Lett. 29*, 427–430.

(134) Lanzetta, P. a, Alvarez, L. J., Reinach, P. S., and Candia, O. a. (1979) An improved assay for nanomole amounts of inorganic phosphate. *Anal. Biochem. 100*, 95–7.

(135) Jiang, S., Gilpin, M. E., Attia, M., Ting, Y.-L., and Berti, P. J. (2011) Lyme disease enolpyruvyl-UDP-GlcNAc synthase: fosfomycin-resistant MurA from Borrelia burgdorferi, a fosfomycin-sensitive mutant, and the catalytic role of the active site Asp. *Biochemistry 50*, 2205–12.

(136) Leatherbarrow, R. J. (2009) GraFit Version 5, Erithacus. Erithacus Software Ltd., Horley, U.K.

(137) Selwyn, M. J. (1965) A simple test for inactivation of an enzyme during assay. *Biochim. Biophys. Acta (BBA)-Enzymology Biol. Oxid. 105*, 193–195.

(138) Wang, J., Duewel, H. S., Stuckey, J. a, Woodard, R. W., and Gatti, D. L. (2002) Function of His185 in Aquifex aeolicus 3-deoxy-D-manno-octulosonate 8-phosphate synthase. *J. Mol. Biol. 324*, 205–214.

(139) Kona, F., Tao, P., Martin, P., Xu, X., and Gatti, D. L. (2009) Electronic structure of the metal center in the Cd(2+), Zn(2+), and Cu(2+) substituted forms of KDO8P synthase: implications for catalysis. *Biochemistry 48*, 3610–30.

(140) Kohen, A., Jakob, A., and Baasov, T. (1992) Mechanistic studies of 3-deoxy-D-manno-2-octulosonate-8-phosphate synthase from Escherichia coli. *Eur. J. Biochem. 208*, 443–449.

(141) Papadopoulos, J. S., and Agarwala, R. (2007) COBALT: Constraint-based alignment tool for multiple protein sequences. *Bioinformatics 23*, 1073–1079.

(142) Takamiya, M., Ozen, A., Rasmussen, M., Alter, T., Gilbert, T., Ussery, D. W., and Knøchel, S. (2011) Genome sequences of two stress-tolerant Campylobacter jejuni poultry strains, 305 and DFVF1099. *J. Bacteriol. 193*, 5546–5547.

(143) Webby, C. J., Jiao, W., Hutton, R. D., Blackmore, N. J., Baker, H. M., Baker, E. N., Jameson, G. B., and Parker, E. J. (2010) Synergistic allostery, a sophisticated regulatory network for the control of aromatic amino acid biosynthesis in Mycobacterium tuberculosis. *J. Biol. Chem. 285*, 30567–30576.

(144) Shumilin, I. A., Kretsinger, R. H., and Bauerle, R. H. (1999) Crystal

structure of phenylalanine-regulated 3-deoxy-D-arabino-heptulosonate-7-phosphate synthase from Escherichia coli. *Structure 7*, 865–875.

(145) O'Brien, R., and Haq, I. (2004) Applications of Biocalorimetry: Binding, Stability and Enzyme Kinetics. *Biocalorimetry 2* 32.

(146) Doyle, M. L. (1997) Characterization of binding interactions by isothermal titration calorimetry. *Curr Opin Biotechnol 8*, 31–35.

(147) Graham, J., Cancer, B., Louisville, S. H. S., Garbett, N. C., and Chaires, J. B. (2012) Thermodynamic Studies for Drug Design and Screening. *Expert Opin. Drug Discov. 7*, 299–314.

(148) Garbett, N., Deleeuw, L., and Chaires, J. B. (2010) TA Instruments – Determination of a protein ligand interaction via continuous isothermal titration calorimetry 1–8.

(149) Bradshaw, J. M., Grucza, R. A., Ladbury, J. E., and Waksman, G. (1998) Probing the "two-pronged plug two-holed socket" model for the mechanism of binding of the Src SH2 domain to phosphotyrosyl peptides: A thermodynamic study. *Biochemistry 37*, 9083–9090.

(150) Renzoni, D. A., Pugh, D. J. R., Siligardi, G., Das, P., Morton, C. J., Rossi, C., Waterfield, M. D., Campbell, I. D., and Ladbury, J. E. (1996) Structural and thermodynamic characterization of the interaction of the SH3 domain from Fyn with the proline-rich binding site on the p85 subunit of PI3-kinase. *Biochemistry 35*, 15646–15653.

(151) Weber, P. C., and Salemme, F. R. (2003) Applications of

calorimetric methods to drug discovery and the study of protein interactions. *Curr. Opin. Struct. Biol. 13*, 115–121.

(152) Ward, W. H. J., and Holdgate, G. A. (2001) 7 Isothermal Titration Calorimetry in Drug Discovery. *Prog. Med. Chem. 38*, 309–376.

(153) Perozzo, R., Folkers, G., and Scapozza, L. (2004) Thermodynamics of Protein–Ligand Interactions: History, Presence, and Future Aspects. *J. Recept. Signal Transduct. 24*, 1–52.

(154) Pierce, J., Serianni, A. S., and Barker, R. (1985) Anomerization of furanose sugars and sugar phosphates. *J. Am. Chem. Soc. 107*, 2448–2456.

(155) Workentine, M. L., Harrison, J. J., Stenroos, P. U., Ceri, H., and Turner, R. J. (2008) Pseudomonas fluorescens' view of the periodic table. *Environ. Microbiol. 10*, 238–250.

(156) Du, S., Tsipori, H., and Baasov, T. (1997) Synthesis and Evaluation of Putative Oxocarbenium Intermediate Mimic in the Kdosp Synthase-Catalyzed Reaci'Ion As a Tool for the Design of Potent Inhibitors for Lipopolysaccharide Biosynthesis. *Bioorg. Med. Chem. Lett. 7*, 2469–2472.

(157) Dutta, S., Malla, R. K., Bandyopadhyay, S., Spilling, C. D., and Dupureur, C. M. (2010) Synthesis and kinetic analysis of some phosphonate analogs of cyclophostin as inhibitors of human acetylcholinesterase. *Bioorg. Med. Chem. 18*, 2265–2274.

(158) Braz, V. A., Holladay, L. A., and Barkley, M. D. (2010) Efavirenz binding to HIV-1 reverse transcriptase monomers and dimers. *Biochemistry 49*,

601–610.

(159) Berg, A. K., Yu, Q., Qian, S. Y., Haldar, M. K., and Srivastava, D. K. (2010) Solvent-assisted slow conversion of a dithiazole derivative produces a competitive inhibitor of peptide deformylase. *Biochim. Biophys. Acta - Proteins Proteomics 1804*, 704–713.

(160) Morrison, J. F. (1969) Kinetics of the reversible inhibition of enzyme-catalysed reactions by tight-binding inhibitors. *Biochim. Biophys. Acta 185*, 269–286.

(161) Van Aller, G. S., Nandigama, R., Petit, C. M., DeWolf, W. E., Quinn, C. J., Aubart, K. M., Zalacain, M., Christensen, S. B., Copeland, R. A., and Lai, Z. (2005) Mechanism of time-dependent inhibition of polypeptide deformylase by actinonin. *Biochemistry 44*, 253–260.

(162) Jakeman, D. L., and Evans, J. N. S. (1998) Overexpression, Purification, and Use of Phosphoenol Pyruvate Synthetase in the Synthesis of PEP Analogues. *Bioorg. Chem. 26*, 245–253.

(163) Wang, J., Duewel, H. S., Woodard, R. W., and Gatti, D. L. (2001) Structures of Aquifex aeolicus KDO8P synthase in complex with R5P and PEP, and with a bisubstrate inhibitor: Role of active site water in catalysis. *Biochemistry 40*, 15676–15683.

(164) Vainer, R., Belakhov, V., Rabkin, E., Baasov, T., and Adir, N. (2005) Crystal structures of Escherichia coli KDO8P synthase complexes reveal the source of catalytic irreversibility. *J. Mol. Biol. 351*, 641–652.

(165) Meanwell, N. A. (2011) Synopsis of some recent tactical application of bioisosteres in drug design. *J. Med. Chem. 54*, 2529–2591.

10. Supplementary Materials

10.1. Purification of cjKDO8PS$_{wt}$

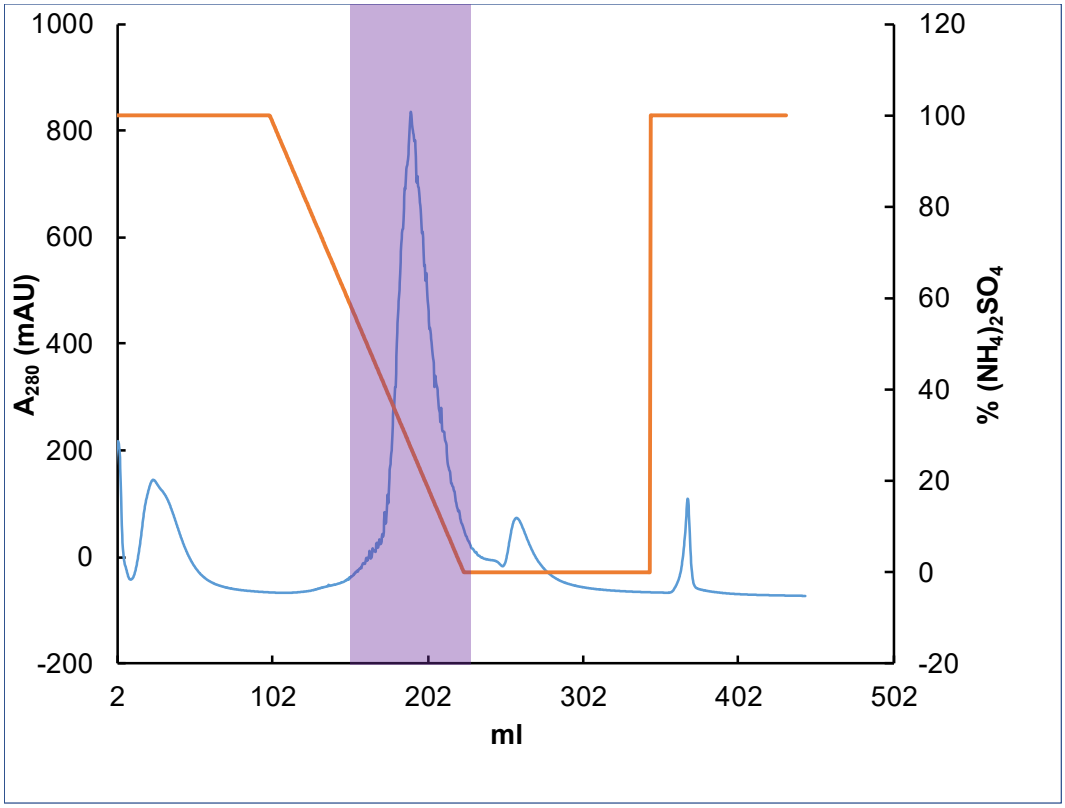

Figure S10.1. Hydrophobic interaction chromatography purification of cjKDO8PS$_{wt}$.

The 80% ammonium sulphate fraction was dissolved in a minimal amount of buffer F (50 mM Tris·Cl, pH 7.00, 1 M ammonium sulphate) and loaded onto a Phenyl-Sepharose Fast Flow XK 16/20 column (GE Healthcare) pre-equilibrated with buffer F. The bound protein was washed with 10 column volumes of buffer F, then eluted by decreasing the ammonium sulphate concentration (1 – 0 M) over 12 column volumes, i.e. 100 - 0 % $(NH_4)_2SO_4$ (orange curve). cjKDO8PS$_{wt}$ eluted at 30% $(NH_4)_2SO_4$ (purple-shaded peak).

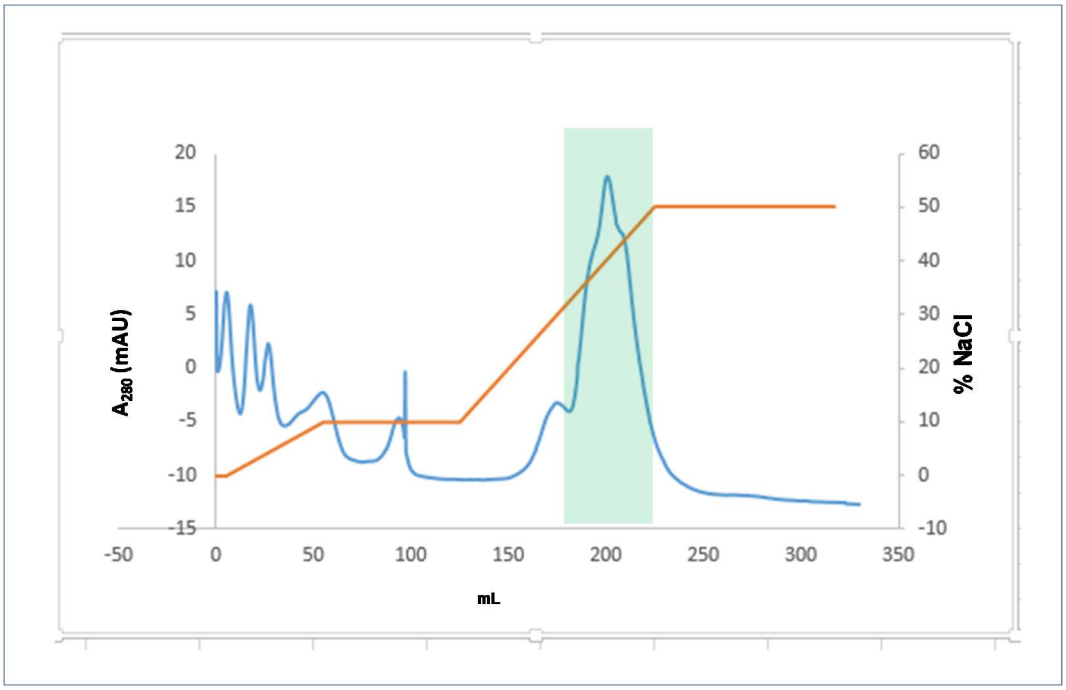

Figure S10.2. Anion exchange chromatography purification of cjKDO8PS$_{wt}$.

Fractions from the hydrophobic interaction chromatography step were pooled and dialyzed into anion exchange chromatography buffer G (50 mM Tris·Cl, pH 8.5) and loaded onto a preparative Q-Sepharose Fast Flow XK 16/20 column (GE Healthcare) pre-equilibrated with buffer G (or 0 % NaCl). A gradient was run from 0 – 10 % NaCl in buffer G, followed by a 3-column volume wash (orange curve). cjKDO8PS$_{wt}$ was eluted with a gradient to 50% NaCl over 4-column volumes. The target protein eluted at 30% NaCl (or 300 mM) in buffer G (green-shaded peak).

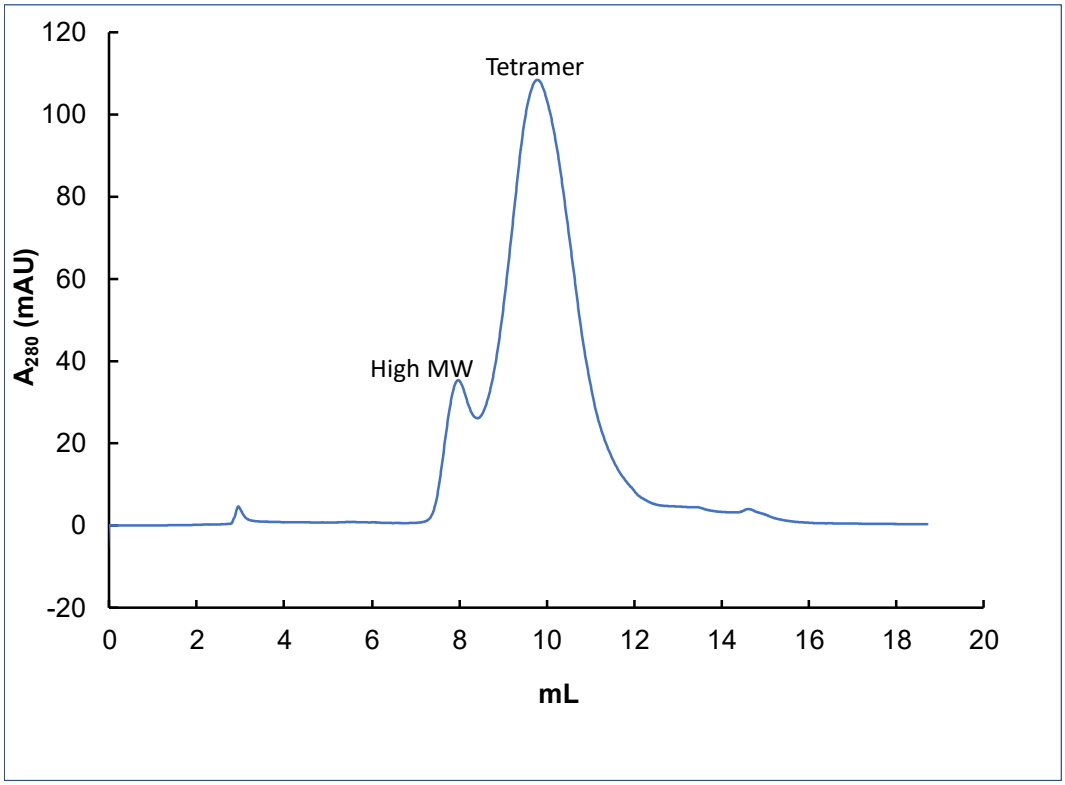

Figure S10.3. Size exclusion chromatography purification of cjKDO8PS$_{wt}$.

Fractions from the anion exchange chromatographic step were pooled and buffer exchanged into buffer G. These fractions were then concentrated and loaded onto a Superose 12 10/300 GL (GE Healthcare) column and run isocratically at 1 mL/min using buffer G.

10.2. A5P synthesis and purification

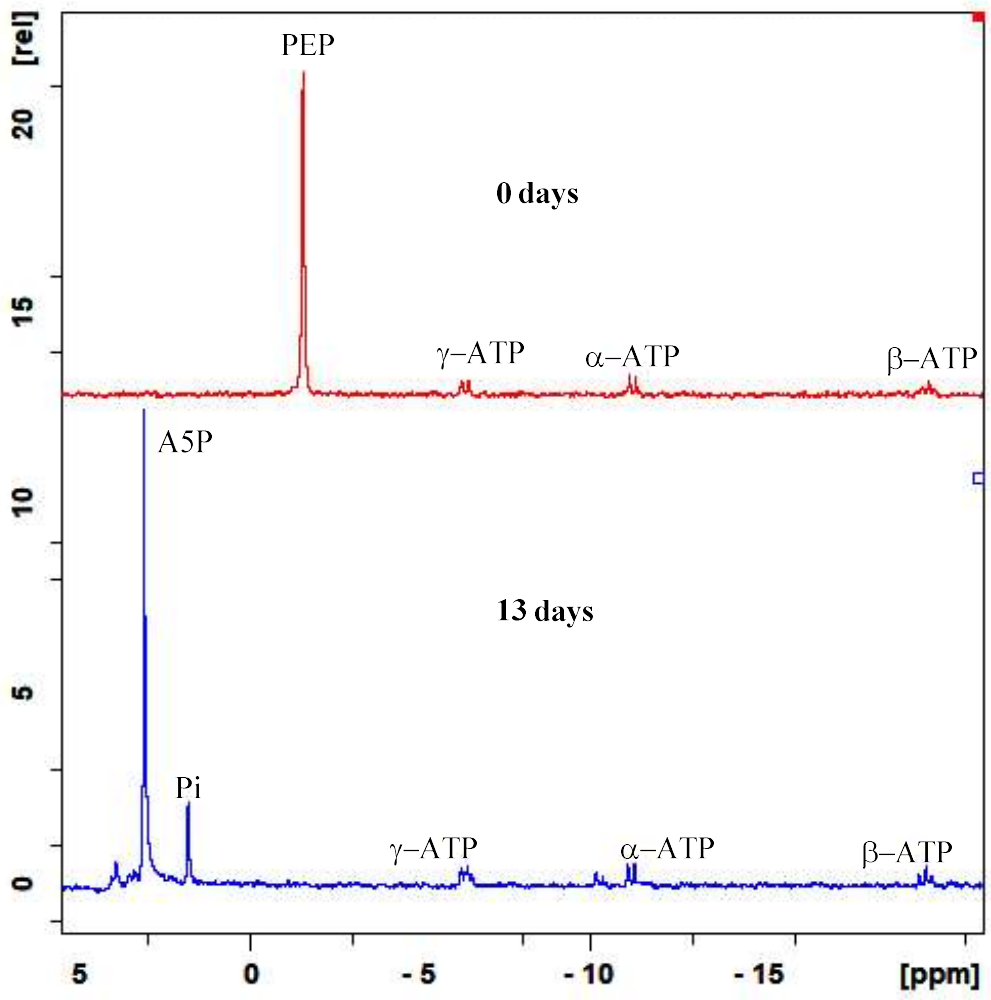

Figure S10.4. A5P synthesis monitored by ^{31}P NMR.
A5P synthesis was complete in 13 days, as shown by the disappearance of the PEP peak and the appearance of A5P.

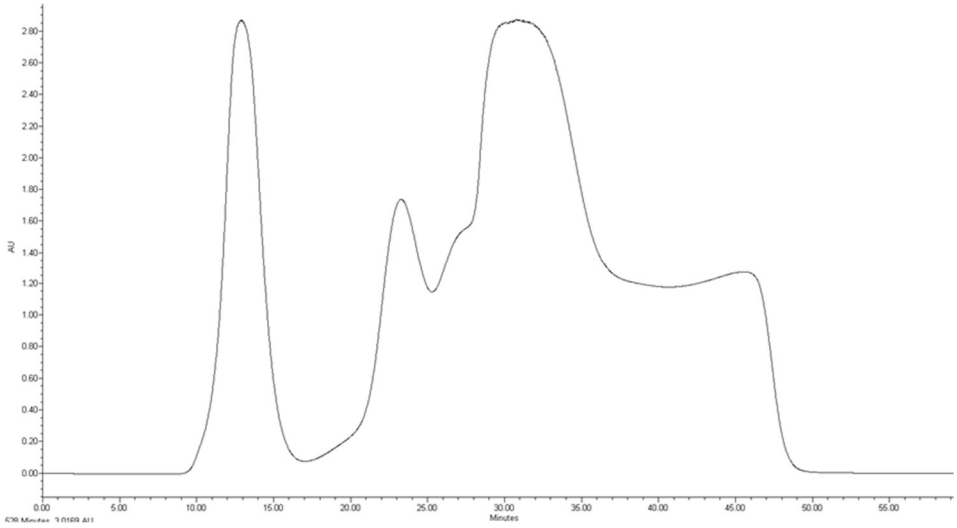

Figure 10.5. A5P purification by Q- Sepharose anion exchange chromatography.

A5P peak (20 – 24 min) at ≈ 300 mM ammonium formate.

10.3. Kinetic parameters

Table S10.1. Dynafit models of the steady state kinetic mechanisms.
A = Mn^{2+}, B = PEP, C = A5P, P = KDO8P, Q = P_i. All concentration units are μM and time units are s^{-1}. Association rate constants have units of μM^{-1} s^{-1}.

"Random A" kinetic mechanism

```
[task]
      task = fit
      data = rates
      approximation = king-altman
model random A, ordered B, C

[reaction]

A + B + C ==> APQ

[mechanism]

reaction A + B + C ==> APQ

E + A     <==>  EA           :     k1    k-1
EA + B    <==>  EAB          :     k2    k-2
EAB + C   <==>  EABC         :     k3    k-3
EABC       ==>  E + APQ      :     k4

E + B     <-->  EB           :     k5    k-5
EB + A    <-->  EAB          :     k6    k-6
EB + C    <-->  EBC          :     k7    k-7
```

```
EBC + A  <-->  EABC          :      k8     k-8

[constants]
k1     = 10
k-1    = 3162  ?
k2     = 0.1
k-2    = 5.2  ?
k3     = 10
k-3    = 435  ?
k4     = 2.5  ?
k5     = 0.1
k-5    = (k5 k-2 k-1 k6) / (k2 k1 k-6)
k6     = 1
k-6    = 6.5  ?
k7     = 1000
k-7    = (k7 k-3 k-6 k8) /  (k6 k-8 k3)
k8     = 1000
k-8    = 4910  ?
```

Ordered kinetic mechanism

```
[task]
      task = fit
      data = rates
      approximation = king-altman
model sequential ordered steady-state ter ter

[reaction]

A + B + C ==> APQ

[mechanism]

reaction A + B + C ==> APQ

;modifiers A

  E + A <==> EA              :      k1     k-1
  EA + B <==> EAB            :      k2     k-2
  EAB + C <==> EABC          :      k3     k-3
  EABC ==> E + APQ           :      k4

[constants]
k1     = 10
k-1    = 1323.89  ?
k2     = 1
k-2    = 574.843  ?
k3     = 1000
k-3    = 21038.1  ?
k4     = 2.37612  ?
```

Table S10.2. Microscopic rate constants for the steady state "random A" sequential ter ter kinetic mechanism for cjKDO8PS$_{wt}$.

After two rounds of initial scans and optimization, the five best sets of initial estimates were optimized (Figure 2.5). The initial estimates of the association rate constants (k_1, $k_{2,}$…) were fixed, while the dissociation rate constants (k_{-1}, $k_{-2,}$…), and k_{cat} (k_4) were optimized. A = Mn^{2+}, B = PEP, C = A5P.

Model #	Random A	Random A	Random A	Random A	Random A	Random A
	195	146	367	373	234	212
k_1 ($\mu M^{-1}s^{-1}$)	10	10	10	10	10	
k_{-1} (s^{-1})	$(0.03 \pm 9.90) \times 10^5$	$(0.012 \pm 127) \times 10^4$	$(0.012 \pm 130) \times 10^4$	$(0.3 \pm 252) \times 10^4$	$(0.01 \pm 134) \times 10^4$	$(0.1 \pm 47) \times 10^2$
k_2 ($\mu M^{-1}s^{-1}$)	0.1	0.1	0.1	0.1	0.1	0.1
k_{-2} (s^{-1})	5 ± 439	7 ± 1016	7 ± 1029	5 ± 1198	7 ± 1079	7 ± 14
k_3 ($\mu M^{-1}s^{-1}$)	10	10	10	10	1000	10
k_{-3} (s^{-1})	$(0.4 \pm 3.9) \times 10^3$	$(0.4 \pm 8.5) \times 10^3$	$(0.4 \pm 8.6) \times 103$	$(0.04 \pm 1.10) \times 10^4$	$(0.4 \pm 9.1) \times 10^5$	419 ± 163
k_4 (s^{-1})	2.5 ± 0.5	2.5 ± 1.1	2.5 ± 1.2	2.5 ± 1.4	2.5 ± 1.2	2.5 ± 0.1
k_5 ($\mu M^{-1}s^{-1}$)	0.1	0.1	0.1	0.1	0.1	0.01
k_{-5} (s^{-1})[a]	252	1.9	2	142	1.3	0.0089
k_6 ($\mu M^{-1}s^{-1}$)	1	1	0.1	0.1	1	1
k_{-6} (s^{-1})	7 ± 8797	$(0.04 \pm 21) \times 10^3$	4 ± 2100	1 ± 2332	$(0.04 \pm 22) \times 10^3$	45 ± 159
k_7 ($\mu M^{-1}s^{-1}$)	1000	10	10	1000	1000	10
k_{-7} (s^{-1})[b]	5.8×10^4	4.4×10^3	4.4×10^3	9.3×10^4	4.5×10^5	4.9×10^3
k_8 ($\mu M^{-1}s^{-1}$)	1000	1000	1000	1000	1000	1000
k_{-8} (s^{-1})	$(0.05 \pm 2) \times 10^5$	$(0.4 \pm 5) \times 10^5$	$(0.4 \pm 5) \times 10^5$	$(0.5 \pm 6) \times 10^5$	$(0.4 \pm 5) \times 10^5$	$(3.8 \pm 4.4) \times 10^3$
Derived kinetic constants						
k_{cat} (s^{-1}) (= k_4)	2.5 ± 0.5	2.5 ± 1.1	2.5 ± 1.2	2.5 ± 1.4	2.5 ± 1.2	2.5 ± 0.1

K_d,A (μM) (= k_{-1}/k_1)	(0.03 ± 9.9) × 10^5	(0.001 ± 1.3) × 10^5	(0.001 ± 1.3) × 10^5	(0.03 ± 2.5) × 10^5	(0.03 ± 2.5) × 10^5	8 ± (1.5 × 10^5)
K_d,B (μM) (= k_{-2}/k_2)	52 ± 4388	(0.07± 10) × 10^3	(0.07± 10) × 10^3	(0.05± 12) × 10^3	(0.07± 11) × 10^3	70 ± 137
K_d,C (μM) (= k_{-3}/k_3)	44 ± 395	42 ± 848	42 ± 862	43± 1097	42± 908	42 ±16
(k_{-5}/k_5) (μM)	2515	19	20	1425	13	0.89
(k_{-6}/k_6) (μM)	(0.1± 88) × 10^2	(0.4± 207) × 10^2	(0.1± 233) × 10^2	(0.4± 220) × 10^2	(0.4± 218) × 10^2	45 ± 159
k_{-7}/k_7) (μM)	58	444	444	93	452	488
k_{-8}/k_8) (μM)	5 ± 212	4 ± 460	4 ± 468	5 ± 578	4 ± 490	3.8 ± 4.4

[a] Redundant parameter, calculated as $k_{-5} = (k_5\ k_{-2}\ k_{-1}\ k_6) / (k_2\ k_1\ k_{-6})$. The standard error was not calculated.

[b] Redundant parameter, calculated as $k_{-7} = (k_7\ k_{-3}\ k_{-6}\ k_8) / (k_6\ k_{-8}\ k_3)$. The standard error was not calculated.

Table S10.3. Microscopic rate constants and King-Altman parameters for the steady state ordered sequential ter ter kinetic mechanism for cjKDO8PS$_{wt}$.

The best sets of initial estimates were optimized as described in the main text (Figure 2.5, Table S10.1). A = Mn^{2+}, B = PEP, C = A5P.

Solution set number	#1	#2	#3	#4	#5	#6
k_1 ($\mu M^{-1}s^{-1}$)	1000	10	1	1	1	1
k_{-1} (s^{-1})	$(2.5 \pm 0.8) \times 10^5$	$(2.4 \pm 0.8) \times 10^3$	170 ± 70	80 ± 42	70 ± 40	70 ± 40
k_2 ($\mu M^{-1}s^{-1}$)	0.1	0.1	0.1	1	10	1000
k_{-2} (s^{-1})	1 ± 4	1.2 ± 4.0	3 ± 5	660 ± 520	7 ± 6	7 ± 6
k_3 ($\mu M^{-1}s^{-1}$)	0.1	1000	1000	1000	1	1
k_{-3} (s^{-1})	2 ± 1	$(4.8 \pm 1.1) \times 10^4$	$(4.7 \pm 1.1) \times 10^4$	$(2.1 \pm 1.2) \times 10^4$	15 ± 12	15 ± 12
k_4 (s^{-1})	2.5 ± 0.1	2.5 ± 0.1	2.5 ± 0.1	2.4 ± 0.1	2.4 ± 0.1	2.4 ± 0.1
Derived kinetic constants [a]						
k_{cat} (s^{-1})	2.5 ± 0.1	2.5 ± 0.1	2.5 ± 0.1	2.4 ± 0.1	2.4 ± 0.1	2.4 ± 0.1
$K_{M,A}$(ss) (μM)	$(3 \pm 0.1) \times 10^{-3}$	0.3 ± 0.01	3 ± 0.1	0.2 ± 0.1	0.2 ± 0.1	0.2 ± 0.1
$K_{M,B}$(ss) (μM)	25 ± 1	25 ± 1	25 ± 1	2.0 ± 0.1	2.00 ± 0.01	$(2 \pm 0.1) \times 10^{-3}$
$K_{M,C}$(ss) (μM)	49 ± 10	48 ± 11	47 ± 11	21 ± 12	17 ± 12	17 ± 12
$K_{i,A}$(ss) (μM)	250 ± 80	240 ± 80	170 ± 70	17 ± 12	140 ± 40	70 ± 40
$K_{i,B}$(ss) (μM)	10 ± 40	10 ± 40	30 ± 50	580 ± 520	930 ± 820	970 ± 870
$K_{i,C}$(ss) (μM)	20 ± 9	24 ± 11	60 ± 11	5090 ± 12	67560 ± 12	686310 ± 12

[a] The derived kinetic constants are calculated as:[124] $k_{cat} = k_4$, $K_{M,A} = k_4/k_1$, $K_{M,B} = k_4/k_2$, $K_{M,C} = (k_4 + k_{-3})/k_3$, $K_{i,A} = k_{-1}/k_1$, $K_{i,B} = k_{-2}/k_2$.

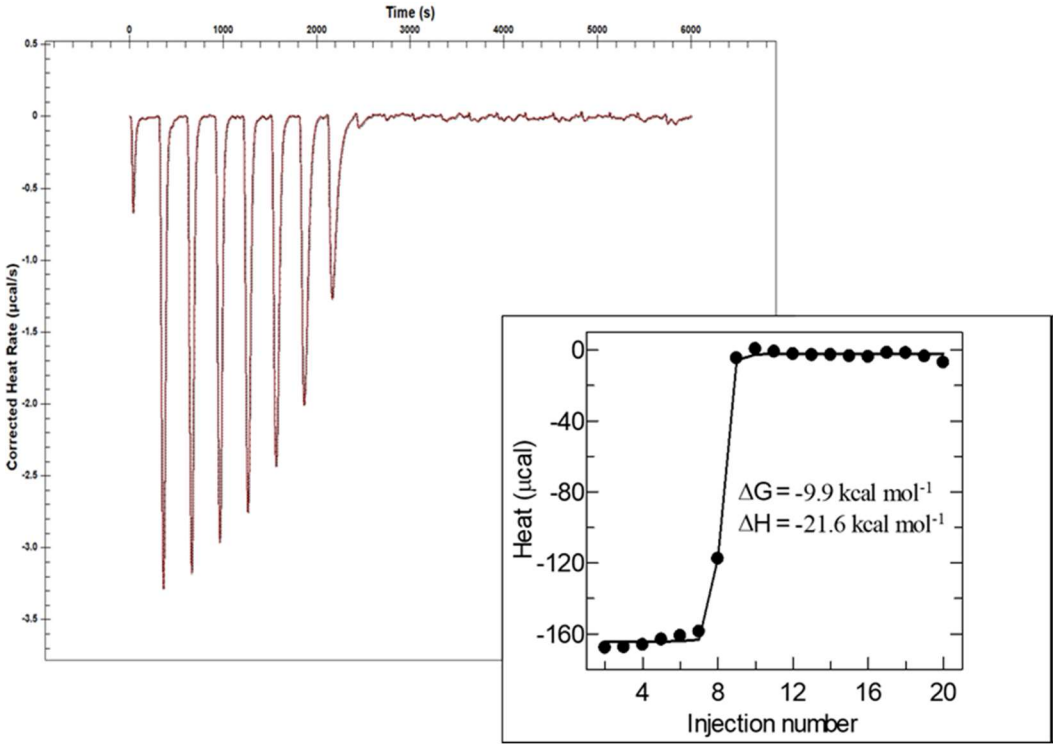

Figure S10.6 Heats of reaction: 150 µM cjKDO8PS$_{H6}$ + 350 µM A5P + 3 mM PEP.

The heat of reaction is observed presumably because metal ion contaminants were available in the cell chamber, syringe or degassing tubes. ΔG = -9.9 kcal/mol, ΔH = -21.6 kcal/mol.

10.4. KDO8P oxime synthesis and Purification

10.4.1. KDO8P synthesis

KDO8PS synthesis and monitoring was conducted as described in the text (Section 4.2.1) and the reaction was complete in 6 h (Figure S10.7).

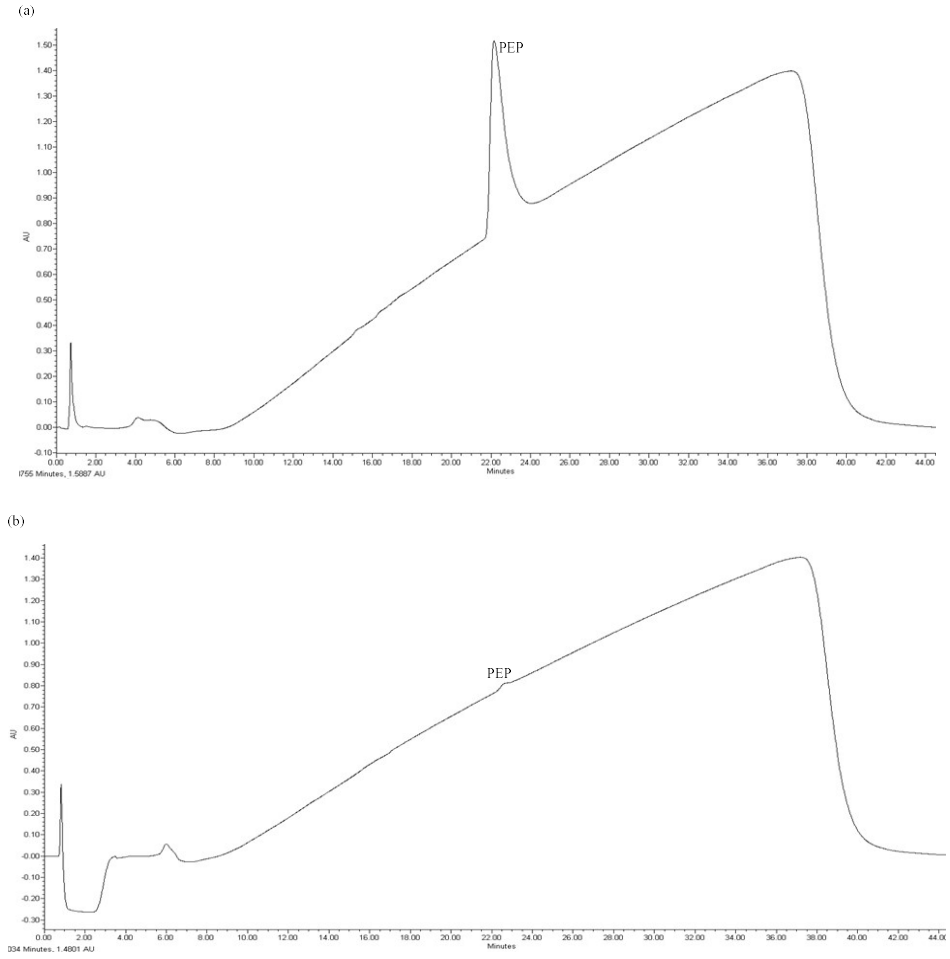

Figure S10.7. KDO8P synthesis monitored by Mono Q anion exchange chromatography.

Reaction progress is monitored by the disappearance of the PEP peak. PEP elutes at 22 min or 590 mM ammonium formate. (a) Injection of the reaction mixture before addition of cjKDO8PS. (b) Injection of the reaction mixture 6 h after addition of cjKDO8PS.

10.4.2. KDO8P oxime purification

The KDO8P oxime synthesis and purification procedure was described in Section 4.2.1. KDO8P oxime eluted as an isolated peak between 27 and 34 min (Figure S10.8).

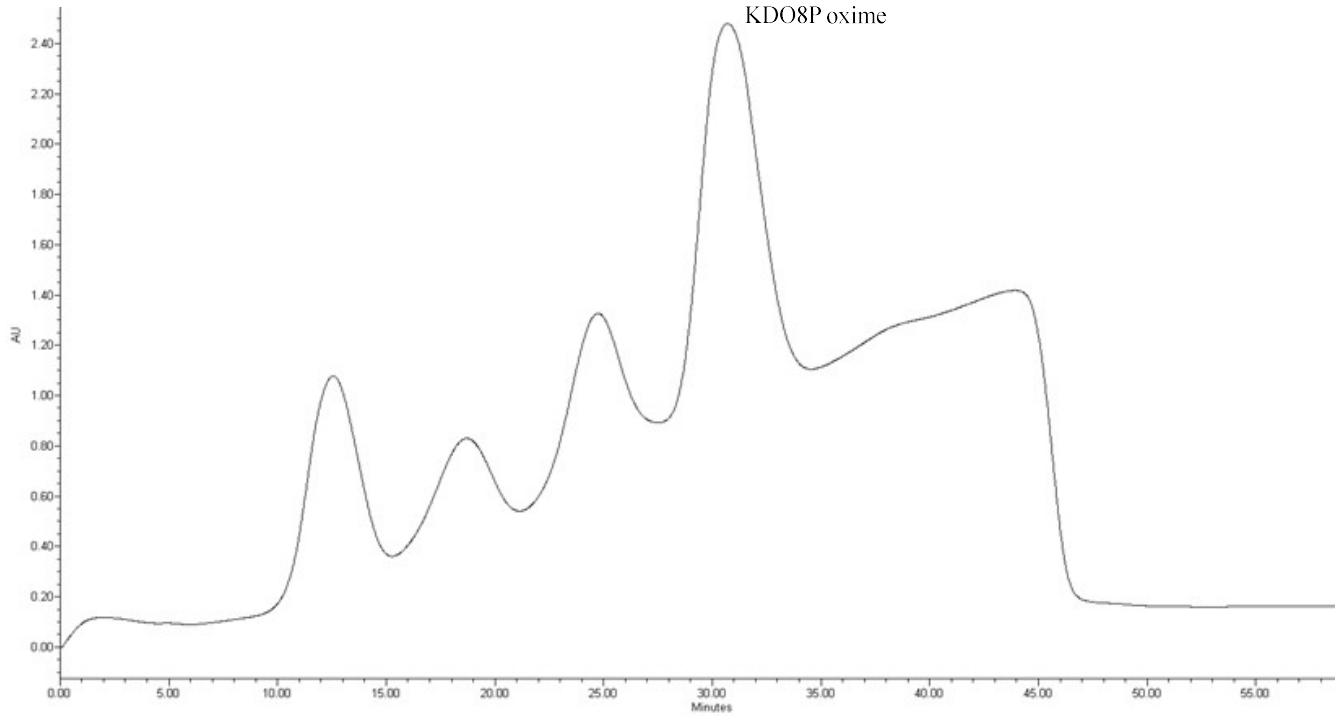

Figure S10.8. KDO8P oxime purification by Q-Sepharose anion exchange chromatography.

KDO8P oxime eluted over 4 column volumes, between 27 and 34 min, at ≈ 400 mM ammonium formate.

Table S10.4. KDO8P oxime ^{1}H and UDEFT-^{13}C NMR peak assignment

Proton	^{1}H δ (ppm)	J_{H-H}	Carbon	^{13}C δ (ppm)
H3	2.89	dd (13.4, 3.2)	C1	171.1
H3’	2.79	dd (14.9, 2.7)	C2	156.8
H4	4.03	m	C3	29.9
H5	3.61	dd (8.3, 8.2)	C4	69.9
H6	3.79	m	C5	72.4
H7	3.76	ddd (11.4, 2.4, 2.7)	C6	71.9
H8	3.99	dd (5.7, 2.1)	C7	68.6
H8’	3.99	dd (8., 2.7)	C8	66.4

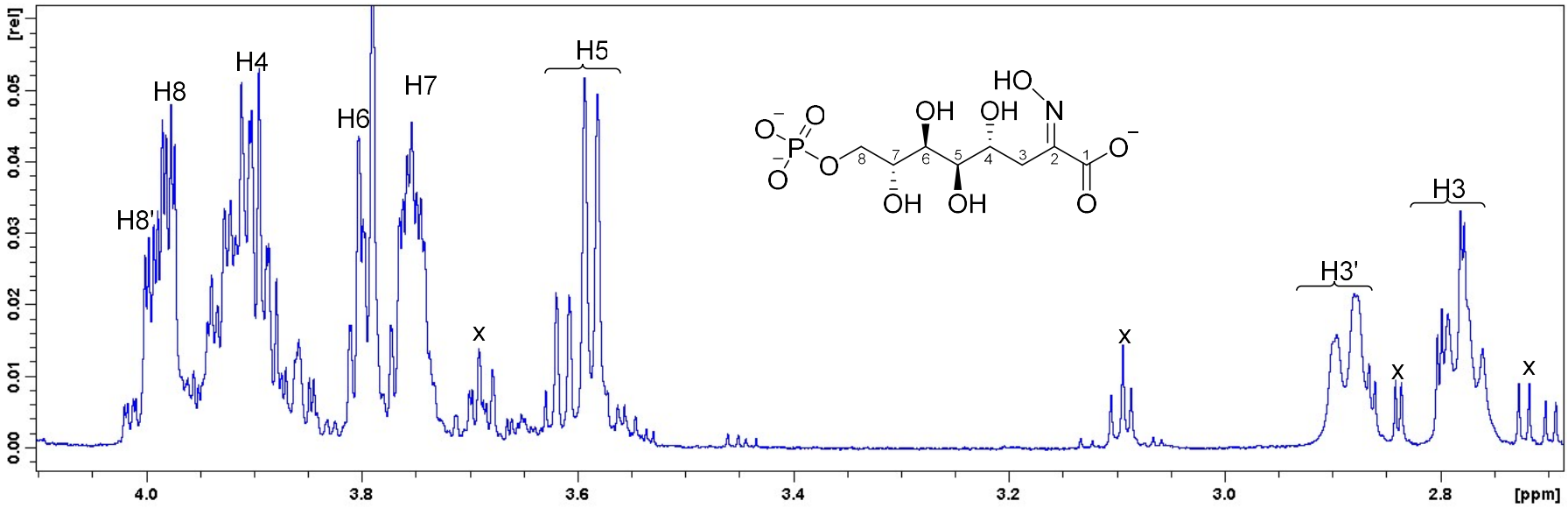

Figure S10.9. KDO8P oxime 1H NMR Spectra.

Impurity peaks are marked (x) in the 1H spectrum

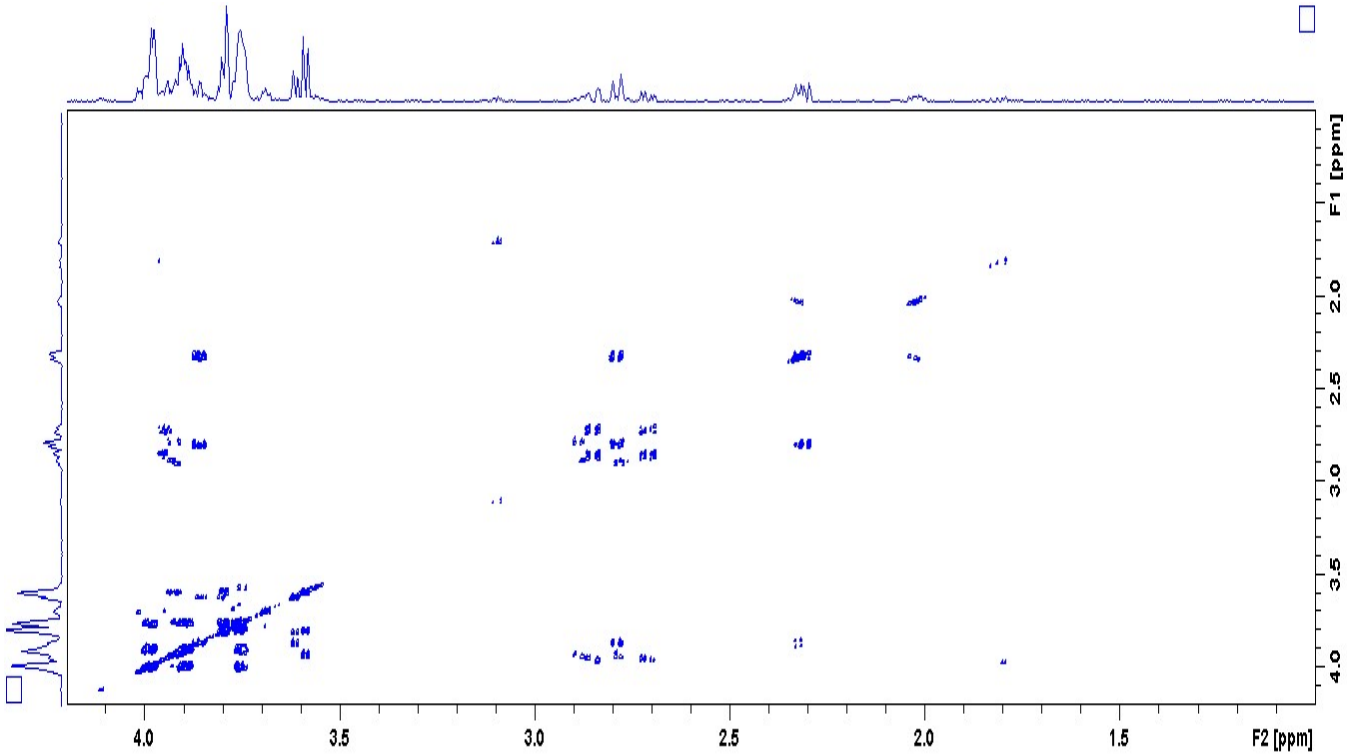

Figure S 10.10. COSY NMR spectrum of KDO8P oxime.

Spectrum was obtained on a 700 MHz spectrometer in D_2O.

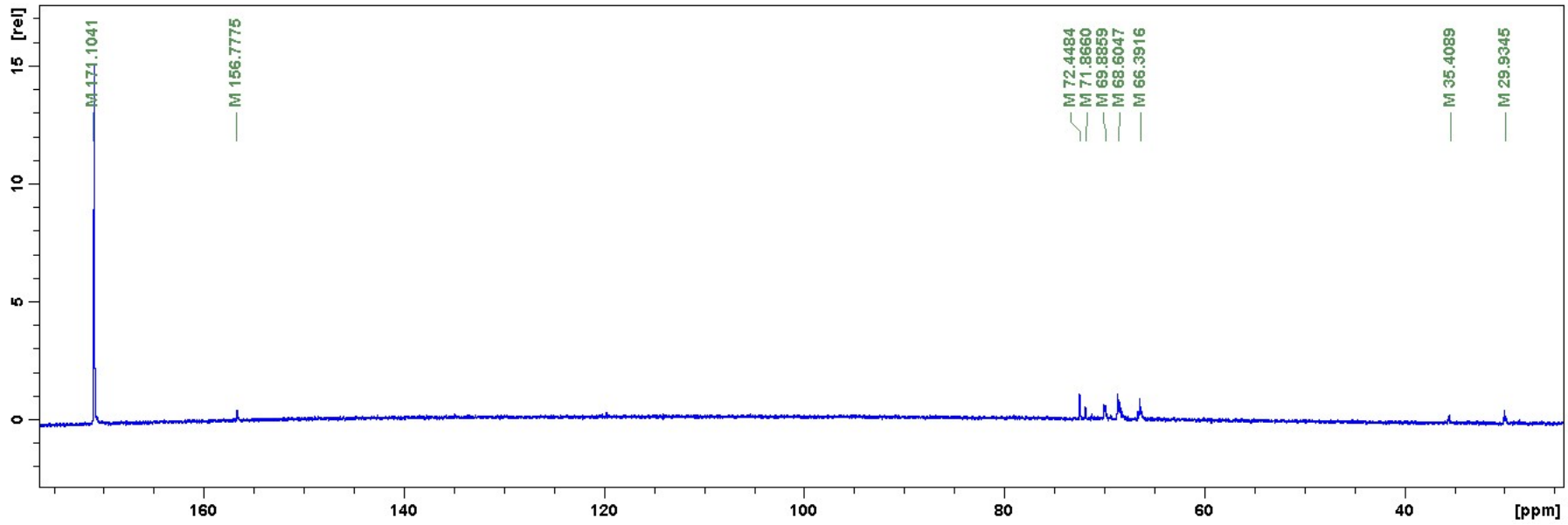

Figure S10.11. UDEFT-^{13}C NMR spectrum of KDO8P oxime.

The spectrum was obtained from a 700 MHz spectrometer.

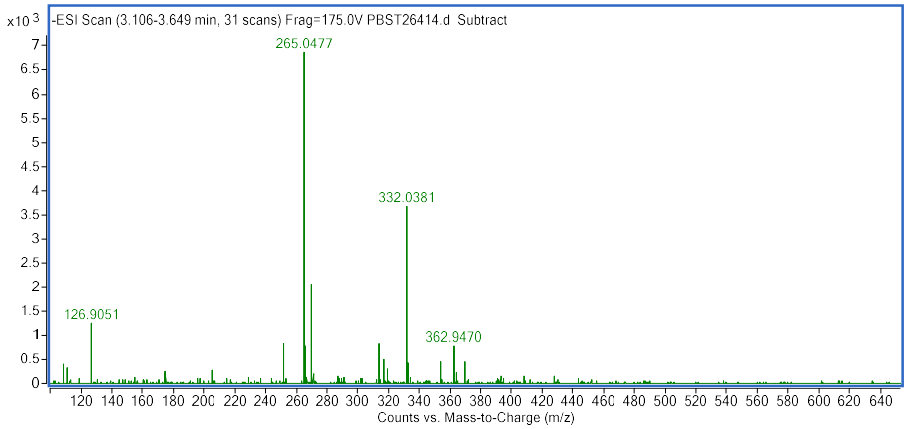

Figure S10.12. High resolution mass spectrum of KDO8P oxime.

Calculated mass of the M-1 peak was 332.0388 Da and the identified peak was 332.0381 Da.

10.5. Kinetic parameters

Table S10.5. Dynafit models for KDO8P oxime's mode of inhibition
E = cjKDO8PS$_{wt}$, S = Mn^{2+}, I = KDO8P oxime, P = KDO8P + Pi, K_s = $K_{d,Mn}$, K_{ic} = competitive K_i value, K_{iu} = uncompetitive K_i value, K_{in} = noncompetitive K_i value, k_{cat2} = residual rate at high [I].

```
[task]
   task = fit
   data = rates
   approximation = rapid-equilibrium
   model = competitive ?
[mechanism]
   E + S <==> E.S       :   Ks      dissociation
   E.S ---> E + P       :   kcat
   E + I <==> E.I       :   Kic     dissociation


[task]
   task = fit
   data = rates
   approximation = rapid-equilibrium
   model = uncompetitive partial ?
[mechanism]
   E + S <==> E.S       :   Ks      dissociation
   E.S ---> E + P       :   kcat
   E.S + I <==> E.S.I   :   Kiu     dissociation
   E.S.I ---> E.I + P   :   kcat2


[task]
   task = fit
   data = rates
   approximation = rapid-equilibrium
   model = noncompetitive partial ?
[mechanism]
   E + S <==> E.S       :   Ks      dissociation
   E.S ---> E + P       :   kcat
   E + I <==> E.I       :   Kin     dissociation
   E.S + I <==> E.S.I   :   Kin     dissociation
   E.S.I ---> E.I + P   :   kcat2
```

10.6. Slow-binding Inhibition

The concentration dependence of slow-binding for cjKDO8PSwt and cjKDO8PSH6 showed cooperativity. Size exclusion chromatography was used to test possible protein aggregation which might otherwise manifest as cooperativity.

The method is described in Section 5.2.5. There is no detectable aggregation in both the control and inhibited cjKDO8PS$_{wt}$ (Figure S10.13).

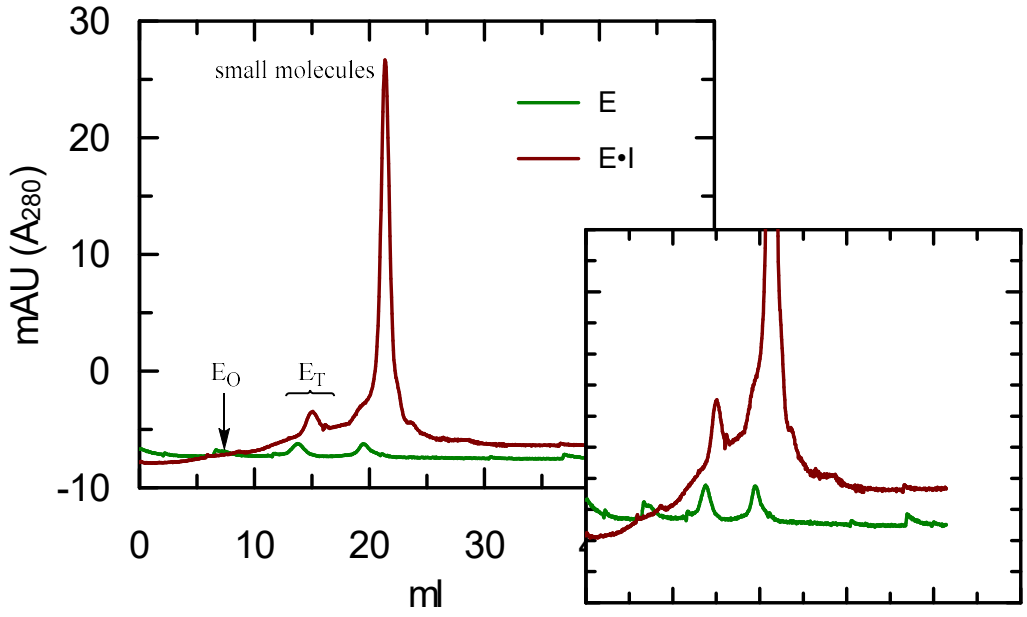

Figure S10.13. Aggregation test for cjKDO8PS$_{wt}$·KDO8P oxime complex.

The E*·I complex was made by mixing 15 μM of cjKDO8PS$_{wt}$ with 3 mM KDO8P oxime in storage buffer at room temperature overnight. The complex was injected onto 24 mL Superose 12 10/300 GL size exclusion column equilibrated with storage buffer and run at 4° C. The flow rate was 1 mL/min, with absorbance detection 280 nm. Maroon = E*·I complex, green = control E, E_O = aggregated oligomer position ≈ column void volume, E_T = tetramer position. The molecular weight of E_T was 111 Da for cjKDO8PS$_{wt}$ and using the molecular weight = 29 392 Da from the amino acid sequence gave 3.7 number of subunits per oligomer.

10.7. ^{33}P-radiolabelling of A5P

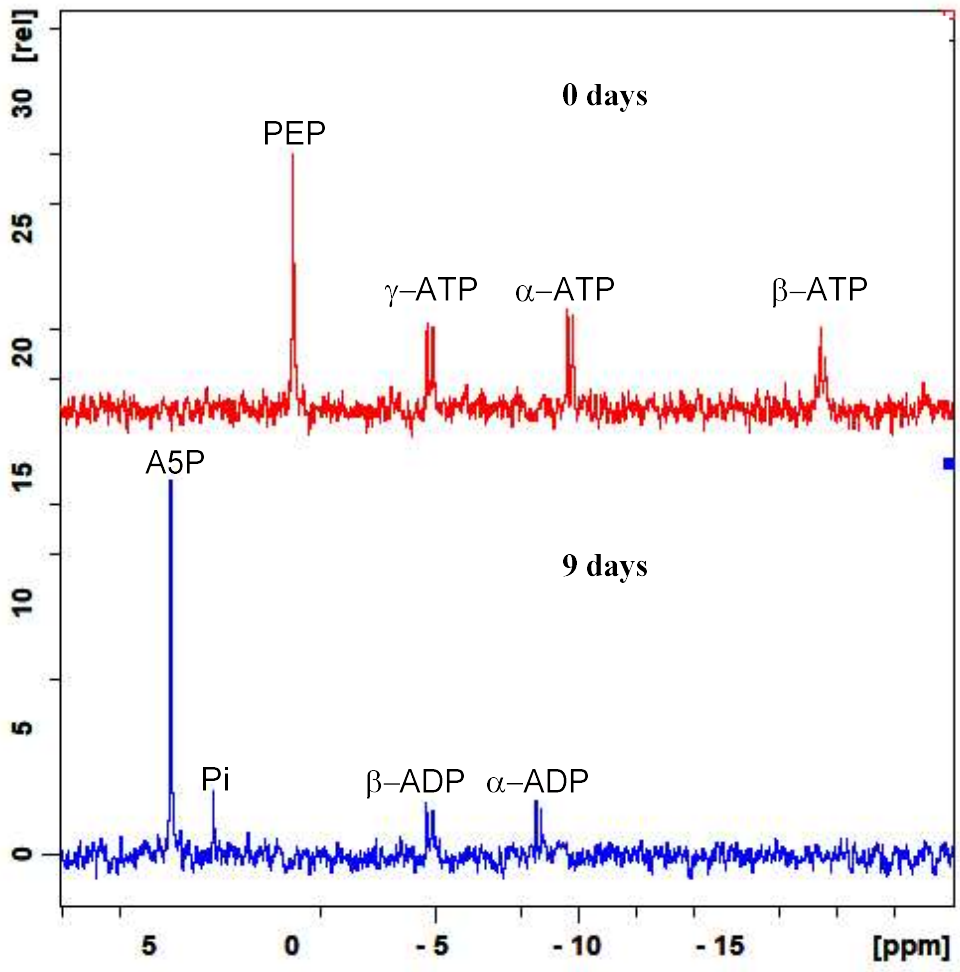

Figure S10.14. [^{33}P]A5P synthesis monitored by ^{31}P NMR.

[^{33}P]A5P synthesis was complete in 5 to 9 days, as shown by the disappearance of the PEP peak and the appearance of A5P.